5-2015

SRC HOMOLOGY 2 DOMAIN-CONTAINING 5'-INOSITOL PHOSPHATASE-2 (SHIP2) IS AN EFFECTOR OF LYMPHATIC DYSFUNCTION

Germaine D. Agollah

SRC HOMOLOGY 2 DOMAIN-CONTAINING 5'-INOSITOL PHOSPHATASE-2 (SHIP2)

IS AN EFFECTOR OF LYMPHATIC DYSFUNCTION

by

Germaine Dorah Agollah, B.S.

APPROVED:

_____

Eva. M. Sevick-Muraca, Ph.D.
Supervisory Professor.

_____

R. Eric Davis, M.D.

_____

Jeffrey E. Gershenwald, M.D.

_____

Philip D. King, Ph.D.

_____

Bradley W. McIntyre, Ph.D.

APPROVED:

_____

Dean, The University of Texas
Graduate School of Biomedical Sciences at Houston

SRC HOMOLOGY 2 DOMAIN-CONTAINING 5'-INOSITOL PHOSPHATASE-2 (SHIP2) IS AN EFFECTOR OF LYMPHATIC DYSFUNCTION

A

DISSERTATION

Presented to the Faculty of

The University of Texas

Health Science Center at Houston

and

The University of Texas

M.D. Anderson Cancer Center

Graduate School of Biomedical Sciences

in Partial Fulfillment

of the Requirements

for the Degree of

DOCTOR OF PHILOSOPHY

By

Germaine Dorah Agollah, B.S.

Houston, Texas

May, 2015

DEDICATION

To my mother: Evelyn Chebet Ruto. A woman of unwavering faith, my true north, my biggest cheerleader and confidant.

ACKNOWLEDGEMENTS

I would like to express my sincerest gratitude to the multitude of people who have helped and supported me through this journey. To my mentor Dr. Eva Sevick-Muraca, thank you for your guidance, scientific and non-scientific advice, and for allowing me to develop into an independent scientist. To my other advisors and committee members throughout my graduate career: Dr. Scott Drouin, Dr. Gabor Balazsi, Dr. R. Eric Davis, Dr. Brad McIntyre, Dr. Jeff Gershenwald, Dr. Phil King, Dr. Gary Gallick, Dr. Kim Schluns and Dr. Wei Cao, thank you for your invaluable advice on my research, challenging me during my candidacy exam and for investing your time in my success.

To my friends at the Center of Molecular Imaging, thank you for your collective support of my work and for the collegiality of this department. Thank you to Manuel, SunKuk, Melissa, John, Ali, Barrett, Ken, Tan, Banghe, Yujie, Chinmay, Amy, Karen, Otis, Nat, Holly, Rodney, Gabe, Peng and Sukhen. To Grace, I would like to especially thank you for your advice, friendship, and for always being available with technical assistance especially when I faced difficulties with my project. To Eva Morschl, thank you for taking the time to train me and for your advice over the years. To Dana and Alainna, thank you for your friendship and for always taking care of my needs, yours' is indeed a thankless job. To current and past CMI students: Emily, Cynthia and Pier-Anne, thank you for your support over the years. To Amber and Rina, thank you for the sisterhood and camaraderie, you truly made graduate school worthwhile. I look forward to your defenses!

Thank you to the GSBS Dean's office for your support, financial and otherwise, throughout my studies. My deepest gratitude to The Schissler Family Foundation for their continued support of GSBS that has enabled my fellowship for the past year. Thank you to other organizations that have funded my research and have allowed me to travel to conferences over the years: GSBS Immunology Program, Carl Storm Underrepresented Minority Fellowship,

University of Texas Medical School Dean's Research Scholarship, and Tzu Chi Foundation. Thank you to the GSBS Immunology program for providing an environment conducive for our growth as scientists. I am grateful to our clinical collaborators at Memorial Hermann Hospital and St. Luke's Episcopal Hospital. I thank Drs. Barry Potter and Stephen Wells at University of Bath, U.K for their assistance in the computational analysis portion of this project. Very importantly, I'm grateful to the multitude of anonymous families that have travelled to Houston and have partaken in our clinical studies. You have been very generous with your time, and are indeed our partners as we all continue in our endeavor to understand what is going on with this disease.

To my family: Mummy, words can never begin to describe my gratitude for your love, the sacrifices you made for us and for your unshakeable belief in me. You gave up so much so that I can live life on my own terms, thank you! To my late Daddy, thank you for instilling the importance of education in me, I pray that I have made you proud. To my brothers Dayan and Owen, thank you for always taking care of me, for your love and your support. To my extended family: Sheneka, DJ, Bev, Cady, Ochi, Cynthia, Scott, Asa and Aloma, thank you for your support and cheering me along the way. To my closest friend, Mare, you have been with me throughout this journey, I'm forever grateful to you. To my immediate family: Francisco, you truly are the better part of me, you have my deepest love and appreciation; and to Paco, thank you for choosing me, you have lit up my life. Thank you!

Finally, and most importantly, I'm grateful to God for having led and guided me through this journey. Throughout, He has remained faithful even as I have strayed. I'm deeply indebted to all whom have stood in the gap and prayed for me. Thank you for your mercies and grace.

SRC HOMOLOGY 2 DOMAIN-CONTAINING 5'-INOSITOL PHOSPHATASE-2 (SHIP2) IS AN EFFECTOR OF LYMPHATIC DYSFUNCTION

by

Germaine Dorah Agollah, B.S.

Supervisory Professor: Eva M. Sevick-Muraca, Ph.D.

The lymphatic system is essential for the transport of excess fluid, protein, and foreign materials from interstitial tissues to lymph nodes; for immune surveillance, and to maintain fluid homeostasis. Dysregulated lymphatics can be attributed to pathological conditions including tumor metastasis, inflammation, chronic wounds, obesity, blood vascular disorders, and lymphedema. Of these, lymphedema is the most extreme of lymphatic disorders and is represented by a spectrum of symptoms ranging from mild, subtle presentation to severe, disfiguring, overt presentation. Lymphedema is more manageable in the early stages of disease but severely reduces quality of life with progression. Due to lack of molecular knowledge and inadequate imaging techniques to safely, rapidly and non-invasively visualize the lymphatics, lymphedema remains under diagnosed and progresses to the irreversible stage if not diagnosed early.

Candidate gene studies have identified a myriad of genes responsible for lymphedema, however, majority of patients do not harbor mutations in these putative genes, indicating many more unknown genes contribute to the pathology of this disease. In an effort to identify new polymorphisms that possibly effect lymphatic dysfunction, we combined investigational, non-invasive near-infrared fluorescence lymphatic imaging (NIRFLI) and next generation sequencing (NGS), to phenotype and genotype human subjects with familial lymphedema. We discovered that mutations in src homology 2-domain containing 5'-inositol phosphatase-2 (SHIP2), encoded by *INPPL1*, are associated with lymphatic abnormalities. SHIP2 is a phosphatidyIinositol (3,4,5)

triphosphate (PIP3) 5'-phosphatase that negatively controls PIP3 levels thereby inhibiting the PI3K/AKT signaling, a pathway implicated in various lymphatic disorders. Our studies confirm this inhibitory role of SHIP2 against PI3K/AKT in lymphatic endothelial cells, and identify SHIP2 as a potential regulator of MAPK/ERK signaling, another pathway also recently identified as important in lymphatic malformations. Pharmacological inhibition of SHIP2 impedes lymphatic contractility and impairs the normal wound healing processes of lymphangiogenesis and angiogenesis in mice. These studies suggest that SHIP2 could have a previously unidentified effector role in lymphatic dysfunction.

In elucidating the roles of SHIP2 in lymphatic dysfunction, the work presented herein expands our understanding of molecular basis of lymphatic failure which could have clinical implications affecting populations with lymphatic disorders, including the ever increasing population of cancer survivors who experience the chronic, disfiguring and incurable lymphedema.

TABLE OF CONTENTS

LIST OF FIGURES

CHAPTER 0

CHAPTER 1

CHAPTER 2

CHAPTER 3

LIST OF TABLES

CHAPTER 1

CHAPTER 2

CHAPTER 3

CHAPTER 5

ABBREVIATIONS

AKT	Protein Kinase B
APC	Antigen Presenting Cell
ANOVA	Analysis of Variance
AAALAC	Association for Assessment and Accreditation of Laboratory Animal Care
BCA	Bicinchoninic Acid
BCRL	Breast Cancer-Related Lymphedema
BEC	Blood Endothelial Cell
BMI	Body Mass Index
CCD	Charge Coupled Device
CD	Cluster of Differentiation
CLAMC	Center for Laboratory Animal Medicine and Care
CML	Chronic Myelogenous Leukemia
CMS	United States Centers for Medicare and Medicaid Services
CNV	Copy Number Variation
CRL	Cancer-Related Lymphedema
CV	Cardinal Vein
CVD	Cardiovascular Disease

DC	Dendritic Cell
EGFR	Epidermal Growth Factor Receptor
ERK	Extracellular signal Regulated Kinase
FDA	Food and Drug Administration
FLT4	Fms-related/Like Tyrosine kinase 4
GFP	Green Fluorescent Protein
GIST	Gastrointestinal Stromal Tumors
HDL	High-Density Lipoprotein
HDLEC	Human Dermal Lymphatic Endothelial Cell
HGF	Hepatocyte Growth Factor
HUVEC	Human Umbilical Vein/Vascular Endothelial Cell
IBC	Inflammatory Breast Cancer
ICG	Indocyanine Green
ID	Intradermal
IFN	Interferon
IL	Interleukin
INPPL1	Inositol Polyphosphate Phosphatase-Like 1
iRFP	InfraRed Fluorescent Protein

ISV	Intersomitic vessels
IV	Intravenous
LDL	Low-Density Lipoprotein
LE	Lymphedema
LEC	Lymphatic Endothelial Cell
LN	Lymph Node
LND	Lymph Node Dissection
MAPK	Mitogen-Activated Protein Kinase
MEK	Mitogen/Extracellular signal-regulated Kinase
MFI	Mean Fluorescence Intensity
MLD	Manual Lymphatic Drainage
NGS	Next Generation Sequencing
NIR	Near Infra-Red
NIRF	Near Infra-Red Fluorescence
NIRFLI	Near Infra-Red Fluorescence Lymphatic Imaging
OMIM	Online Mendelian Inheritance In Man
PDGFR	Platelet-Derived Growth Factor Receptor
PI3K	Phosphatidyl-Inositol-3-Kinase

PIP2	Phosphatidyl-Inositol-3,4-trisphosphate
PIP2	Phosphatidyl-Inositol-4,5-trisphosphate
PIP3	Phosphatidyl-Inositol-3,4,5-triphosphate
PO	Per os
PP2A	Protein phosphatase 2A
PROX1	Prospero Homeobox 1
PTEN	Phosphatase and Tensin homolog deleted on chromosome 10
ROI	Region of Interest
SDS-PAGE	Sodium Dodecyl Sulfate-Polyacrilamide Gel Electrophoresis
SHIP1	Src homology 2 (SH2) domain containing 5'-Inositol-Phosphatase-1
SHIP2	Src homology 2 (SH2) domain containing 5'-Inositol-Phosphatase-2
SMC	Smooth Muscle Cell
SNP	Single Nucleotide Polymorphism
TIME	Telomerase-Immortalized Microvascular Endothelial cell
TNF	Tumor Necrosis Factor
T reg	T regulatory cell
US	United States of America
UV	Ultra Violet

VEC	Venous Endothelial Cell
VEGFC	Vascular Endothelial Growth Factor C
VEGFR3	Vascular Endothelial Growth Factor Receptor 3
VSMC	Vascular Smooth Muscle Cell
WES	Whole Exome Sequencing
WGS	Whole Genome Sequencing

CHAPTER 0

ORGANIZATION OF THE DISSERTATION

0.1: The Lymphatic System: Role in Many Costly Disorders

The lymphatic system is an extensive network that is widely distributed within the human body, found in nearly all tissues and organs with the exception of the central nervous system and bone marrow. The lymphatics run parallel to, yet are intricately associated with the blood vasculature (**Figure 0.1A**); however, unlike the blood system, lymphatic research has lagged behind partly owing to limited methods to safely, rapidly and non-invasively image lymphatic architecture and function. Mainly responsible for regulating fluid balance, lipid metabolism and immune cell trafficking, lymphatics are a double-edged sword that can be either beneficial or disastrous to the immune system depending on physiological and pathological context. Given their ubiquitous tissue presentation and paradoxical function, it is not surprising that dysfunctional lymphatics are associated with a multitude of diseases.

Lymphatic failure or insufficiency manifests in lymphedema, a progressive, disfiguring and incurable disease, due to either genetic causes (primary lymphedema) or physical damage (secondary or acquired lymphedema). Moreover, disordered lymphatics are also associated with inflammation, cancer metastasis, peripheral venous disease, chronic wounds, hypertension and cardiovascular disease, inflammatory bowel diseases including colitis and Crohn's disease, autoimmune diseases such as rheumatoid arthritis, asthma; obesity and other adipose diseases. Combined, these disorders, summarized in **Figure 0.1B**, affect over 150 million U.S patients and present a huge economic burden to the U.S healthcare system, with current estimates over $250 billion. *Therefore the involvement of lymphatics in multiple debilitating pathologies necessitates the need for understanding molecular mechanisms that belie its function and dysregulation.* Herein, we focus on studying the molecular events associated with lymphedema with the belief that knowledge of the molecular mechanisms at play in this

seemingly rare disease will allow better understanding of more common diseases that are also associated with the lymphatics.

Figure 0.1. The lymphatic system: role in many costly disorders. (**A**) Schematic showing the ubiquitous involvement of the lymphatic system in the body with the direction of lymphatic flow depicted in green and blood flow depicted in red. Shown in the inset is the intricate association between lymphatic (green, stained with LYVE1 antibody) and blood vessels (red, stained with CD31 antibody) from a mouse ear. (**B**) The cost of pathological conditions associated with aberrant lymphatics showing direct markets in which lymphatics play a primary role in disease causation, progression, and severity; and indirect markets in which lymphatics does not play a causative role, but rather a secondary role in disease progression. CMS; Centers for Medicare and Medicaid Services.

Modified and reproduced with permission from Sevick-Muraca, E.M., Kwon, S., and Rasmussen, J.C., *Emerging lymphatic imaging technologies for mouse and man.* J Clin Invest, 2014. **124**(3): p. 905-14. [1].

Figure 0.1. The lymphatic system: role in many costly disorders

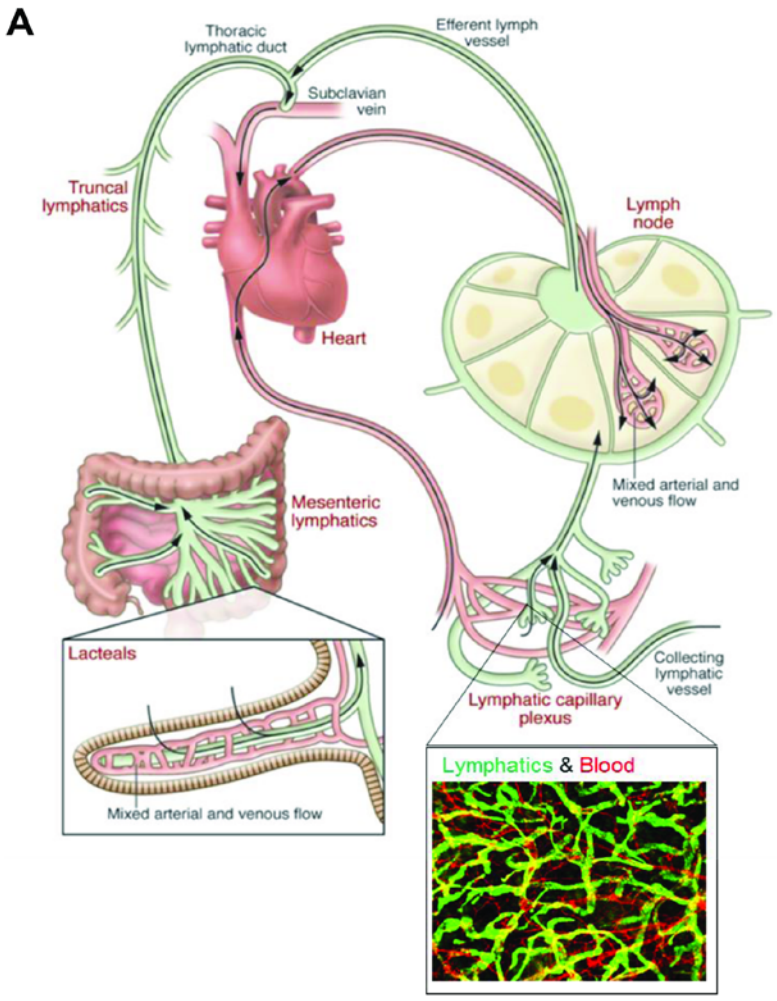

B

Disorders associated with Lymphatics

Direct markets	*Indirect markets*
Primary Lymphedema 1.15/0.1 million U.S children *$???*	**Refractory Hypertension** 35 million U.S. patients *$47.5 billion*
Cancer Related Lymphedema >3-5 million U.S. patients *13th most costly treatment to CMS*	**Inflammatory Bowel Disease** 2.4 million U.S. patients *$12-18 billion*
Peripheral Vascular Diseases >10 million U.S. patients *$3 billion*	**Autoimmune Disorders** 1.3 million U.S. patients *$3 billion*
Chronic Wounds 7 million U.S. patients *$20 billion*	**Obesity & Adipose Disorders** 100 million U.S. patients *$147 billion*
Lymph Node Cancer Staging 0.5million U.S. patients/year *$???*	**Asthma** 20 million U.S. patients *$56 billion*

0.2: Dissertation organization

The overall strategy employed in this work is threefold: (i) clinical studies that use non-invasive near infrared fluorescence lymphatic imaging (NIRFLI) to assess lymphatic phenotypes, (ii) next generation sequencing (NGS) in persons with lymphedema to identify disease-causing variants and (iii) biological validation of these variants in cell culture and mouse studies.

This dissertation aims to address two major gaps in lymphatic dysfunction research: (i) accurate phenotyping in patients with subtle disease and (ii) gene discovery to identify novel candidates that contribute to lymphatic failure. In **Chapter 1**, we introduce the lymphatic system including developmental events that occur during embryogenesis to give rise to the lymphatic system in a process known as lymphangiogenesis. In **Sections 1.2** and **1.3** we discuss the pathology of lymphedema including currently known genes responsible for this disease, and current strategies used in imaging the lymphatics. **Section 1.4** we discuss the principles of non-invasive NIRFLI and why it is a dynamic and superior imaging modality that provides sensitive lymphatic imaging that can discern varied lymphatic phenotypes even in asymptomatic patients without overt clinical symptoms, a linchpin in accurate phenotyping of lymphedema. We present evidence that current candidate genes can only explain one third of hereditary lymphedema and only one tenth of non-hereditary lymphedema, underpinning the need for broader, unbiased genetic techniques such as NGS for novel genetic discoveries.

In **Chapter 2**, we present our clinical findings that led to our discovery of one such gene, *INPPL1*, that encodes src homology 2-domain containing 5'-inositol phosphatase-2 (SHIP2), identified using this imaging and genetic sequencing approach

in two families with lymphedema. Our studies argue that novel gene discovery is only possible as a result of accurate phenotyping, such as that from NIRFLI.

The experimental studies' chapters of this dissertation investigate the potential role of SHIP2 as an effector of lymphatic dysfunction in humans. Thusly, in **Chapter 3**, we conduct experimental studies in lymphatic endothelial cells (LECs) to assess functional and phenotypical response to SHIP2 knockdown and upon overexpression of SHIP2 mutants, identified in the aforementioned families, in LECs. In **Chapter 4**, we further investigate the role of SHIP2 in lymphovascular pathology in mouse studies upon pharmacological inhibition of SHIP2. Our *in vitro* and *in vivo* studies reveal previously unknown, yet important maintenance roles that SHIP2 plays in lymphatic biology. In **Chapter 5**, we summarize our major findings; discuss the clinical impact that this project will have on the population of cancer survivors who suffer from, and are at risk for lymphedema; and discuss future strategies that can improve lymphedema diagnosis and treatment. Experimental methodology employed in this dissertation are outlined in **Chapter 6**, and Appendix presents summaries of secondary preclinical, NIRFLI projects that were published and undertaken during the course of this dissertation project.

Figure 0.2 provides the organization of this dissertation.

Figure 0.2. Dissertation organization

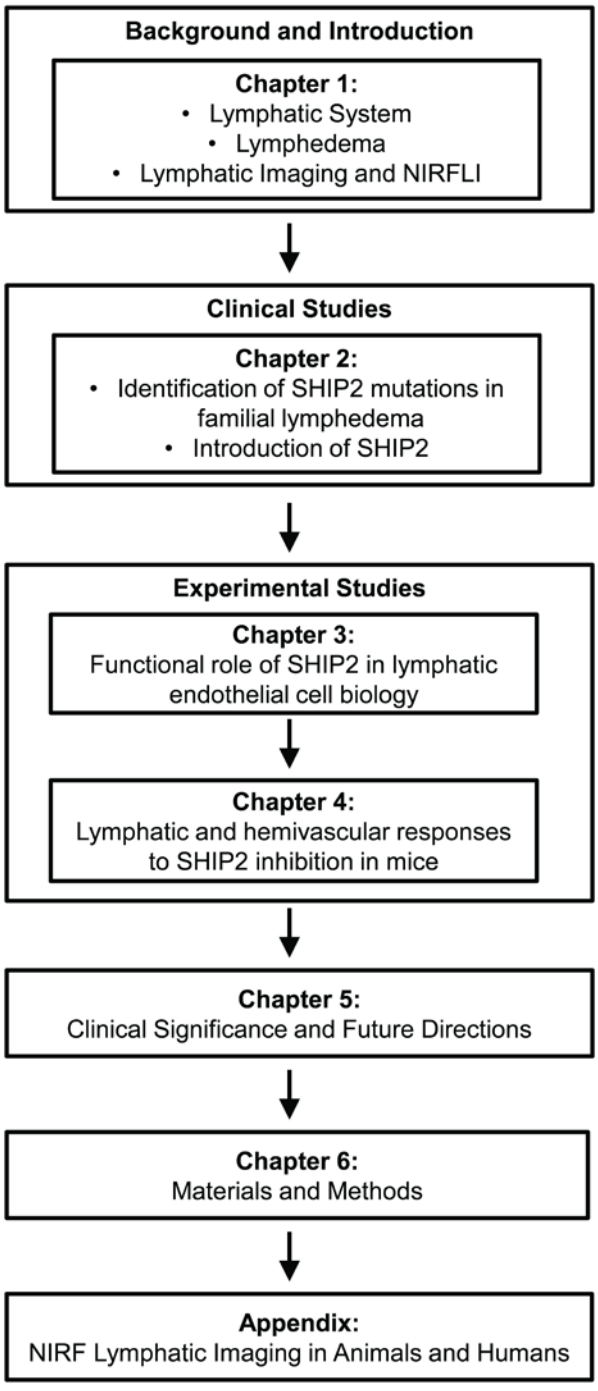

CHAPTER 1

LYMPHATIC SYSTEM

1.1: Lymphatic Development and Function

1.1.1: Embryonic Development

Origin of the lymphatics: The human body has two vascular systems, namely the blood (hemivascular) and lymphatic systems. While the existence of the lymphatics has been known since the 17th century, research in this field has lagged behind that of the blood system, mainly due to lack of knowledge of the molecular characteristics and processes that govern the development and maintenance of the lymphatics as well as the inability to visualize the lymphatics. In 1902, Florence Sabin suggested that during embryonic development, lymphatic vessels arise from preexisting blood vessels, specifically the cardinal vein (CV) [2], a hypothesis that has since been proven true [3-6]. Developmentally, the mammalian lymphatic system arises in the following four sequential steps (**Figure 1.1**):

(i). Lymphatic specification: Over the last 15 years, key molecular regulators of lymphatic development have been identified. Among them is the lymphatic endothelial hyaluronan receptor-1 (LYVE1), the earliest lymphatic marker and the prospero homeobox transcription factor PROX1, the master regulator of lymphatic endothelial differentiation [7, 8]. LYVE1 is expressed at embryonic day (E) 9 in a polarized manner in a portion of venous endothelial cells (VECs or LEC progenitors) within the CV, and represents the first sign of lymphatic competence. These LYVE1+ LEC progenitors begin to express PROX1 at E9.5, an event that indicates the beginning of LEC specification (**Figure 1.1A**). Expression and activation of PROX1 within LEC progenitors are regulated by two other transcription factors COUP-TFII and SOX18 [9, 10]. The expression of vascular endothelial growth factor receptor 3 (VEGFR3), a receptor

tyrosine kinase (RTK) initially expressed in blood endothelium, becomes restricted to the LYVE1+/PROX1+ LEC progenitors at E10.5 [11].

(ii). Lymphatic budding: Following their specification, LEC progenitors begin to bud from the CV into the mesenchyme, a process that requires VEGFR3 signaling in response to its ligand, VEGFC [12]. While not required for LEC commitment, VEGFC is necessary for sprouting, migration and maintenance of LEC during embryogenesis. LEC budding also results in the expression of the transmembrane mucin-type glycoprotein, podoplanin, at E11 in LEC progenitors that have fully exited the CV. While the molecular regulation of podoplanin expression in LEC progenitors currently remains unknown [13], podoplanin is essential for LEC adhesion and migration. VEGFC also binds a non-tyrosine kinase coreceptor neuropilin-2 (NRP2), which interacts with VEGFR3 to mediate LEC sprouting [14]. At this stage, LEC differentiation is progressing with combined LEC expression as LYVE1+/PROX1+/VEGFR3+/Podoplanin+/NRP2+.

(iii). Lymph sac formation: At E11.5, the primary lymphatic plexus develops into lymph sacs that give rise to the whole lymphatic vasculature. To achieve this, the differentiated LECs bud off and migrate in an interconnected manner and assemble into capillary-like structures which further organize and form lymph sacs (**Figure 1.1A**). Separation of the newly forming lymphatic sacs from the blood endothelial is critical at this juncture to prevent blood flow into the lymphatic vessels. The lymphovenous separation is achieved by valves (**Figure 1.1B**). While the majority of PROX1+ LEC progenitors bud off the CV, a small portion remains and downregulates VEGFR3 and podoplanin expression, to form lymphovenous valves [13]. Additionally, the lymphocyte cytosolic protein 2 (SLP76) and kinase protein SYK are necessary for separation of the lymphatic and blood systems, and mice deficient in any of these signaling factors develop blood-filled lymphatics [15]. Recent evidence suggests that platelets play an

essential role in the lymphovenous separation, and podoplanin activates the platelet receptor CLEC2 to activate SLP76 and SYK signaling [13, 16, 17].

(iv). Lymphatic maturation and differentiation: As the lymphatic plexus begins to mature, LECs undergo further differentiation to eventually form three distinctly hierarchal vessel subtypes of the lymphatic system (**Figure 1.2**). The initial capillaries comprise of LECs with high podoplanin expression that secrete the chemokine CCL21 which attract CCR7+ regulatory T cells (Tregs) and antigen presenting cells (APCs) such as dendritic cells (DCs). These initial LECs are blind-ended and thin-walled with endothelial junctions that allow fluid and protein absorption [18]. Precollector lymphatic vessels have decreased podoplanin expression, sparse pericyte or smooth muscle cell (SMC) coverage and secrete CCL27 which attracts CCR10+ inflammatory cells upon insult. However, beyond inflammatory cell recruitment, the functions of precollector vessels are currently unknown [13, 18]. Collector lymphatic vessels have a complete SMC layer, basement membrane, and valves. Intrinsic contractility of the SMCs aid in propulsion of lymph and lymphatic valves prevent retrograde flow or backflow of lymph [19]. As the lymphatic system lacks a central pumping organ, the collector vessels have a series of functional pumping units known as lymphangions (**Figure 1.3**). Collector vessels and valves develop at approximately E14.5 and E16, respectively, and key in this process is the forkhead transcription factor FOXC2. Mice deficient in *Foxc2* lack lymphatic valves, with normal initial vessels but later mispatterned lymphatic vasculature indicating the requirement of FOXC2 in lymphatic maturation [20].

Embryonic development of the lymphatic system is a dynamic process, and while not all genes, proteins or transcription factors that contribute to this intricate process have been mentioned above, loss-of-function phenotype of animal models of genes associated with lymphatic development is summarized in **Table 1.1**.

Figure 1.1. Embryonic development of the murine lymphatic system. (**A**) Sagittal schematic of developmental events at the cardinal vein (CV), from E9.0 to E11.5. **(i)** Expression of transcription factors COUP-TFII and SOX18 by blood ECs in the CV and intersomitic vessels (ISV). **(ii)** At E9.5, PROX1 expression is induced by SOX18 and COUP-TFII, indicating start of LEC specification. **(iii)** LEC progenitors start to bud from the CV and ISVs at E10.5, which requires the graded expression of VEGFC in the surrounding mesenchyme. LECs maintain their VEGFR3 expression and start expressing podoplanin (PDPN) once outside of the CV. The combined expression of these genes indicates that lymphatic differentiation is progressing. Transverse representation of the LEC budding process of PROX1+/PDPN+/VEGFR3+-differentiating LECs bud from the CV and ISVs at E10.5 is shown as well. **(iv)** By E11.5, LECs bud off in an interconnected manner and assemble together to form different lymph sacs, from which the lymphatic network arises following LEC proliferation and sprouting. **(B)** Diagrammatic representation of the lymphovenous valves. A small unique subpopulation of PROX1+/PDPN-/VEGFR3- LECs do not bud off from the CV and remain to form the lymphovenous valves at the junction of the jugular and subclavian veins (SCV). Each of the valve's two leaflets has two layers of PROX1+ ECs: an inner PROX1+/PDPN+ layer continuous with the lymph sac and an outer PROX1+/PDPN– layer continuous with the veins. Left: The region of an E13.5 embryo in which the jugular and subclavian veins join to form the lymphovenous valves. Right: A frontal view of the boxed region shown at left. EJV, external jugular vein; IJV, internal jugular vein; LS, lymph sac; LV, lymphovenous valve; SVC, superior vena cava.

Reproduced with permission from Yang, Y. and Oliver, G., *Development of the mammalian lymphatic vasculature*. J Clin Invest, 2014. 124(3): p. 888-97. [13].

Figure 1.1. Embryonic development of the murine lymphatic system.

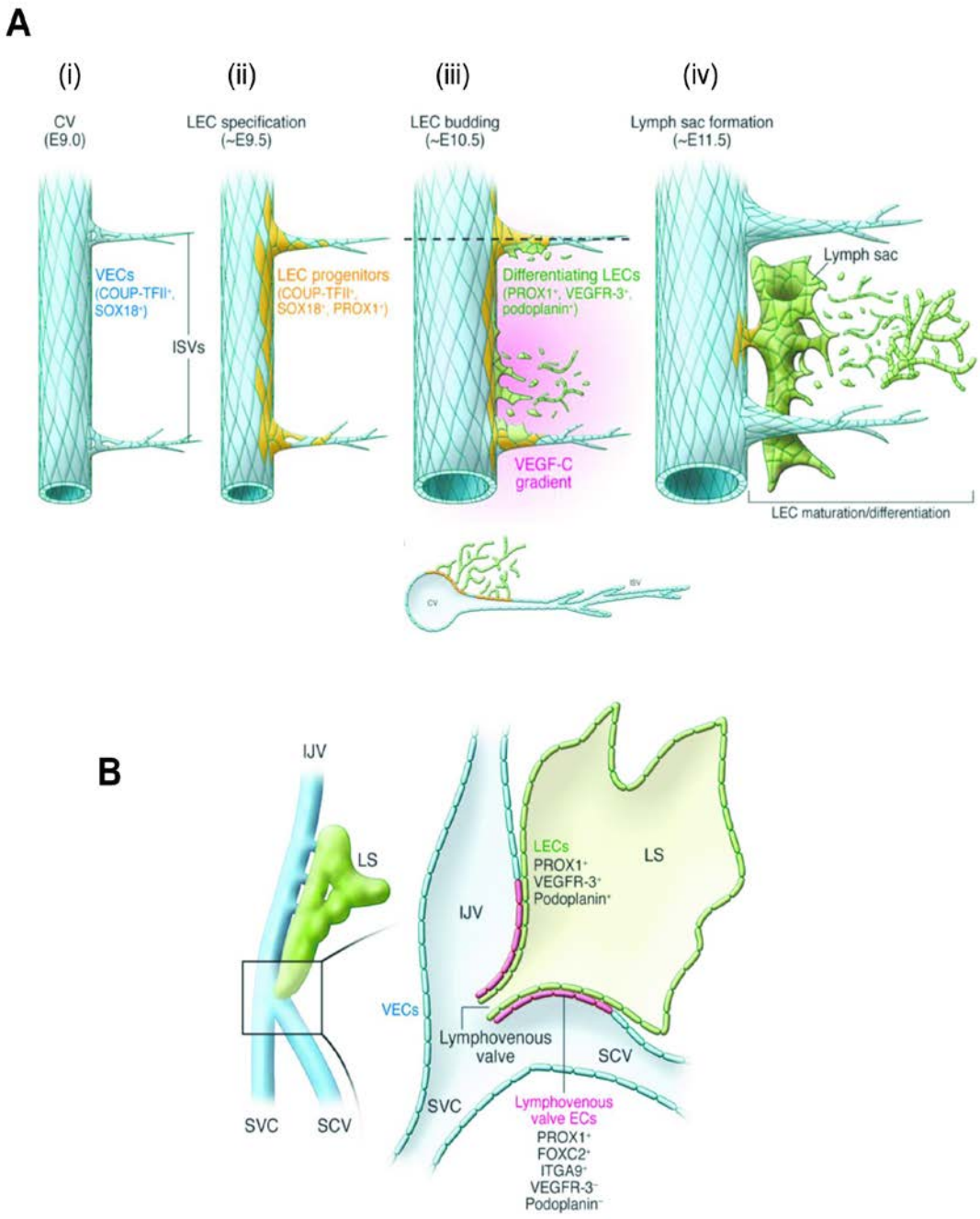

Figure 1.2. Hierarchy of the lymphatic vessels in the dermis. Initial lymphatic capillaries start as blind sacs (**Figure 1.1A**). Their LECs form overlapping junctions, express large amounts of the membrane mucoprotein podoplanin (green), and release the chemokine CCL21. This attracts CCR7+ immune cells, such as dendritic cells (DCs) and regulatory T cells (Tregs). The LECs of the precollector lymphatic vessel express low amounts of podoplanin and high CCL27, which attracts inflammatory CCR10+ T lymphocytes. The precollector vessels open into the collecting lymphatic vessels that are podoplanin-low and have lymphatic valves. Pericytes partially cover the precollectors and completely ensheath collecting vessels.

Reproduced with permission from Kerjaschki, D., *The lymphatic vasculature revisited.* J Clin Invest, 2014. **124**(3): p. 874-7. [18].

Figure 1.2. Hierarchy of the lymphatic vessels in the dermis.

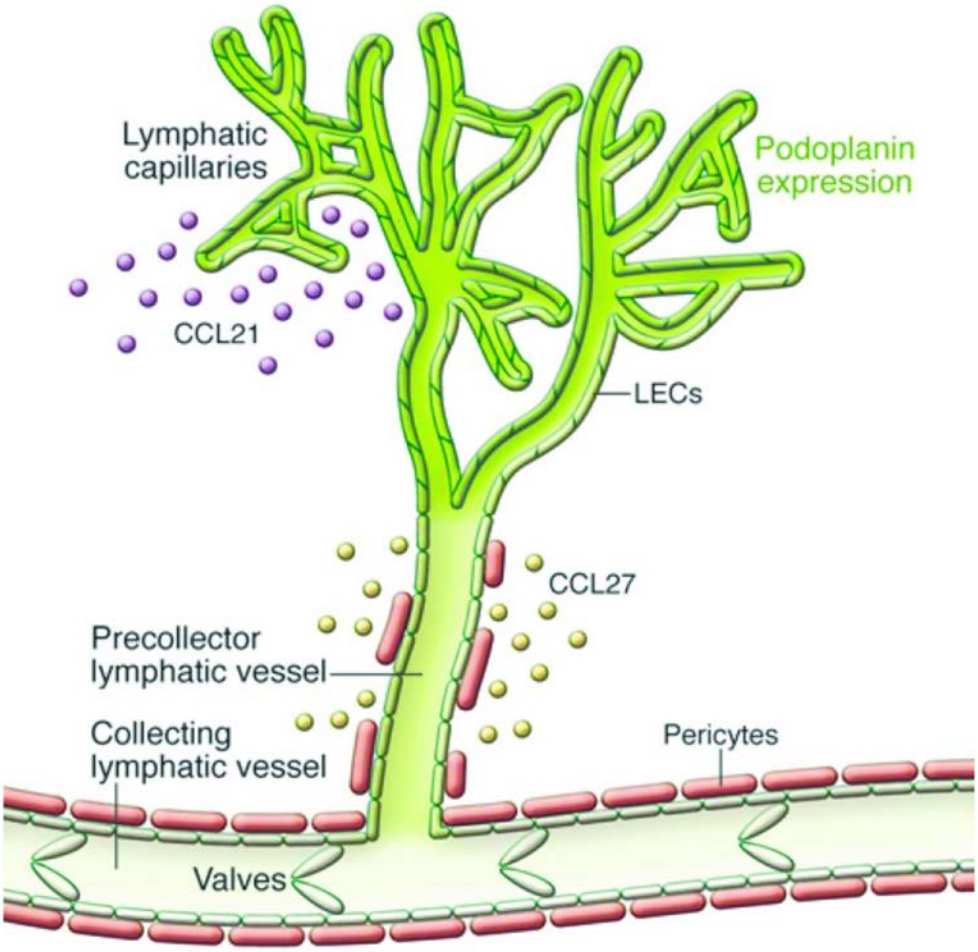

Figure 1.3. Organization of the lymphatic vasculature. Protein-rich interstitial fluid, collected by the initial lymphatic capillaries (green), is transported by precollector lymphatic vessels to larger collecting lymphatic vessels onto the lymph nodes for filtration and immune surveillance. Along the collector vessels are perciytes (red) which allow (i) lymphatic contraction and, (ii) functional luminal valve subunits known as lymphangions that prevent backflow of fluid. From the lymph nodes, fluid ultimately returns to the blood vasculature through the thoracic duct and to the subclavian vein (blue). Deep lymphatic vessels run along blood arteries and veins.

Reproduced with permission from Alitalo, K., Tammela, T., and Petrova, T.V., *Lymphangiogenesis in development and human disease*. Nature, 2005. 438(7070): p. 946-53. [19].

Figure 1.3. Organization of the lymphatic vasculature

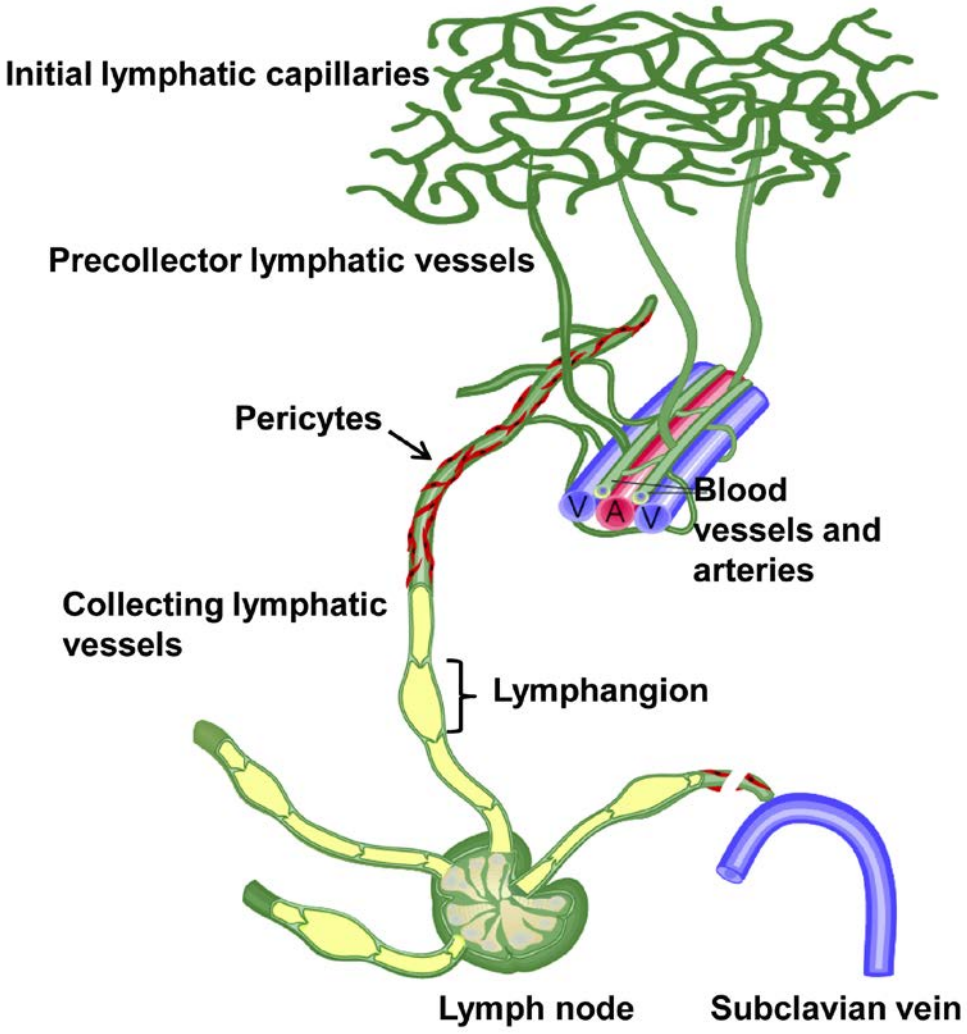

Table 1.1. Loss-of-function phenotypes of genes associated with lymphatic vasculature development. Reproduced with permission from Yang, Y. and Oliver, G., *Development of the mammalian lymphatic vasculature.* J Clin Invest, 2014. **124**(3): p. 888-97. [13].

Gene	Loss-of-function phenotype in animal models	Related human vascular disease
	Defective LEC progenitor specification	
Coup-TFII	Severe subcutaneous edema; embryos lack LECs and lymphatic vasculature due to failure in LEC progenitor specification	
Notch1	Loss of Notch1 results in an increased number of $PROX1^+$ LEC progenitors in the veins and outside the CV with significant lymphatic overgrowth, incomplete separation of veins, and formation of lymphatics	
Prox1	Severe subcutaneous edema; embryonic lethality at E14.5; embryos lack LECs and lymphatic vasculature due to failure in LEC progenitor specification; in most genetic backgrounds, *Prox1* haploinsufficiency results in defects in LEC fate maintenance, perinatal death with chylothorax, and chylous ascites; in the NMRI strain, surviving *Prox1* heterozygous mice exhibit adult onset obesity, leaky lymphatics, and lack of lymphovenous valves	
Sox18	Severe subcutaneous edema; embryonic lethal at E14.5; embryos lack LECs and lymphatic vasculature due to failure in LEC progenitor specification in certain genetic backgrounds	Hypotrichosis-lymphedema-telangiectasia syndrome
	Defective budding of LEC progenitors and lymph sac formation	
AM	*AM*-null embryos die at mid-gestation with interstitial edema and abnormal jugular lymphatics due to defective LEC proliferation	
Calcrl	Severe interstitial edema, embryonic lethal, hypoplastic lymph sacs	
Ccbe1	Severe subcutaneous edema, budding of LEC progenitors arrested in the CV, lack of lymphatic vasculature	Hennekam syndrome
Gata2	Hypoplastic lymph sacs and abnormal separation of venous and lymphatic vessels	Emberger syndrome
Nfatc1	Enlarged lymph sacs	
PU.1	Hypoplastic lymph sacs, hyperplastic lymphatic vessels	
Ramp2	Severe interstitial edema, embryonic lethal, hypoplastic lymph sacs	
Tie1	Reduction in TIE1 levels results in abnormal lymphatic patterning and dilated and disorganized lymphatics; homozygous null embryos are lethal at E14.5 and exhibit nuchal edema, hemorrhages, enlarged lymph sacs, dilated lymphatic vessels and impaired lymphatic drainage	
Vegfc	Embryonic lethal at E14.5; severe subcutaneous edema, budding of LEC progenitors arrested in the CV, lack of lymphatic vasculature	Milroy-like disease
Vegfr3	Primary receptor for VEGF-C, blood vasculature malfunction in loss of function embryos, required for survival and migration of LECs	Milroy disease
	Defective lymphatic vessel maturation and valve formation	
Akt1	Reduced diameter and EC number in lymphatic capillaries; loss of valves in the smaller collecting lymphatic vessels in the superficial dermal layer of the ear skin	
Bmp9	Mutant pups exhibit hyperplastic mesenteric collecting vessels with abnormally high LYVE1 expression, reduction in the number and in the maturation of mesenteric lymphatic valves	
Celsr1	Disorganized cell-cell junction, defects in cell reorientation during lymphatic valve formation, lack of lymphatic valves	
Cnb1	Defects in the demarcation of the valve territory	
Cx37	Mutant mice exhibit lymphedema and chylothorax and have defective valve formation in collecting lymphatics; regulates jugular lymph sacs size	
Cx43	Loss of lymphatic vessels in the diaphragm, absence of lymphatic valves in mesenteric collecting lymphatic vessels	
Cx47	Expressed in lymphatic valves, currently uncharacterized developmental function	Primary lymphedema

Emilin1	Defective lymphatic valve structure and lymph flow	
Ephrin B2	Hyperplastic collecting lymphatic vessels, lack of valves, abnormally high level of expression of LYVE1 in the lymphatic vessels	
Fn1	Defects in the formation and extension of the valve leaflets	
Foxc2	Embryonic lethal perinatally; unusual mural cell recruitment on the collecting lymphatic vessels with abnormal high level of LYVE1 expression, lack of lymphatic valves, and lymph backflow	Lymphedema-distichiasis syndrome
Integrin-α9	Reduced number of valves leads to failure in the formation of the matrix core of the valves (leaky, lymph backflow)	Congenital chylothorax
Nrp1	A mutation in the SEMA3A binding site of NRP1 leads to smaller lymphatic valves and ectopic SMC coverage on the valve region	
Plxna1	Smaller lymphatic valves	
Reelin	Reduced SMC coverage on the collecting lymphatic vessels with abnormally high level of LYVE1 expression, dilated and leaky collecting lymphatic vessels, and reduction in the rate of lymph flow	
Sema3a	Smaller lymphatic valves; ectopic SMC coverage on the valve region; aberrant lymph drainage	

Defective blood and lymphatic vessel separation

Clec2	Inactivation of this PDPN receptor results in defects similar to those reported for *Pdpn* and *SLP76*; mutant embryos show blood-filled intestinal and mesenteric lymphatic vessels	
Fiaf	Dilated and blood-filled lymphatic vessels in the intestine	
Plcg2	Blood-filled lymphatic vessels	
Pdpn	Embryonic lethal at birth; lymphedema and dilated and blood-filled lymphatic vessels	
Rac1	Conditional deletion results in embryonic lethality before birth, edema, and blood-filled lymphatic vessels	
SLP76	Severe subcutaneous edema, peritoneal hemorrhage, and chylous ascites	
Syk	Severe subcutaneous edema and blood-filled lymphatic vessels.	

Defective lymphatic vessel growth

Afadin	Modulates RhoA; severe subcutaneous edema with severe disruption of VE-cadherin–mediated cell-cell junctions in lymphatic vessels of the skin	
Ang2	Subcutaneous edema, chylous ascites, lymphatic vessel hypoplasia, and mispatterned lymphatic vessels in the mesentery	
Aspp1	Null embryos exhibit subcutaneous edema, defective lymphatic drainage, and mispatterned collecting lymphatic vessels	
Cxadr	Conditional deletion at E12.5 results in subcutaneous edema, hemorrhage, and embryonic death with dilated subcutaneous lymphatic vessels that appear structurally abnormal, exhibiting gaps and holes in LEC cell-cell junctions; blood-filled lymphatics show defects in the separation of the blood and lymphatic vasculatures	
Cx26	Conditional deletion in the ectoderm results in embryonic death before birth, severe subcutaneous edema, and reduced dermal lymphatic capillary network	
Integrin-β1	Edema and hemorrhages; embryonic lethality; reduced LEC numbers and LEC proliferation; smaller lymph sacs; complete lack of dermal and mesenteric lymphatic vasculature at E15.5	
Nrp2	Absence or severe reduction of small lymphatic vessels and capillaries	
Ptpn14	Lymphedema; lymphatic hyperplasia; interacts with VEGFR-3	Lymphedema-choanal atresia syndrome
Rasa1	Hyperplasia, dilation, and leakage of lymphatic vessels and chylothorax	Capillary and arteriovenous malformation
Tbx1	Regulates VEGFR3; conditional deletion in ECs results in embryonic edema and postnatal lethality between 2 and 4 days after birth; mice exhibit chylous ascites and lack of mesenteric lymphatic vessels	DiGeorge syndrome
TGFBRI or TGFBRII	Severe edema; blood-filled lymphatic vessels; reduced lymphatic branching; aberrant lymphatic vessel network	
Vezf1	Lymphatic hypervascularization, edema, and hemorrhaging the jugular region of heterozygous embryos	

1.1.2: Functions of the Lymphatics

Organization of lymphatic vasculature and lymphatic drainage: The main role of the lymphatic system is to return proteins and fluids back to the blood circulation system [19]. To achieve this key transport function, interstitial fluids, macromolecules and APCs are taken up by the blind-ended lymphatic capillaries, transported through the precollector vessels and to the collector vessels which are ensheathed with SMCs that aid in contractility. Once within the lymphatic plexus, intravasated fluid is defined as lymph, which is then filtered through lymph nodes before returning to the blood circulation via the subclavian vein (**Figure 1.3**) [19]. The largest lymphatic collector vessel is the thoracic lymphatic duct which drains lymph collected from all organs for drainage into the subclavian vein. To propel lymph, intrinsic SMC contractility is aided by extrinsic contractions from normal respiration, arterial heartbeat, and local skeletal muscles. In the lymph nodes (LNs), foreign particles taken up by APCs are presented to lymphocytes for initiation of immune responses, as further discussed below. The structures of the lymphatics allows for better remodeling of capillaries, which in lymphatics are thin-walled, lack tight junctions and either lack or have incomplete basement membrane, and can therefore quickly respond to physical changes within the local interstitial milieu. Increased interstitial flow and hydrostatic pressure within adjacent tissue results in pulling of anchoring filaments, which connect lymphatic capillary ECs to the surrounding stroma, to open the overlapping, zipper-like ECs and allow fluid flow into the capillaries [21]. As previously mentioned, collector vessels contain valves, which permit unidirectional lymph flow towards the subclavian vein, a direction that is favored because of decreased blood pressure and increased tissue osmotic pressure. This classic role of lymphatics in transport maintains vascular fluid homeostasis, and

disruption of this process leads to accumulation of proteins and fluid within the interstitial space, resulting in lymphedema, a chronic and progressive swelling of affected tissues.

Lymphatics in lipid absorption: The intestines are the main sites of lipid absorption by the lymphatics. Intestinal lymphatic vessels, known as lacteals, within intestinal villi take up dietary lipids such as chylomicrons for transportation back to the blood vasculature [22]. Chylomicrons are large lipoproteins structures (200nm-1000nm diameter) which transport ingested fat and fat-soluble vitamins from the intestine to peripheral tissues [23]. Chylomicrons are absorbed in a size exclusion manner through pores within lacteals for subsequent filtration through mesenteric LNs. This chylomicron-rich lymph is then transported by the thoracic duct and ultimately to the subclavian vein, in a similar manner as lymph drained from the lymphatic plexus of peripheral skin. Chylomicrons give lymph a milky appearance and aberrant lymphatic absorption leads to accumulation of chylous fluid within intestinal cavity. Mice with heterozygous mutation in *Vegfr3*, also known as *Chy* mice, have lymphedema, abnormal fat accumulation and accumulation of milky chylous fluid in the abdomen [24]; phenotypes that are also frequently seen in human lymphedema. Given the role of lymphatics in lipid transport and that lymphatic vessels and LNs are typically embedded within visceral fat where they can respond to interstitial changes, it is not surprising that dysfunctional lymphatics have been implicated in obesity-related diseases such as diabetes, insulin resistance and hypercholesterolemia [23, 25, 26].

Lymphatics in immune function: The lymphatics are the main component linking peripheral tissues, the usual site of infection, to the central immune system. Foreign antigens are carried within lymph by APCs, including DCs and macrophages, to LNs for presentation to lymphocytes and subsequent mounting of immune responses. Developmentally, LNs are induced approximately E12.5 when IL-17 and the tumor

necrosis factor family cytokine, TRANCE, stimulate lymphoid tissue inducer (LTi) cells to accumulate near LECs and produce lymphotoxin (LT)-α1β2 signals that produce chemokines, adhesion receptors, and cytokines that attract naïve lymphocytes into the developing LN [22, 27]. Afferent lymphatic vessels drain lymph from the tissues into the LNs where antigens are trapped for presentation. Within LNs, B lymphocytes are localized in follicles while T cells are diffused within the paracortical regions. Upon antigen presentation, naïve T cells proliferate and differentiate into antigen-specific effector cells while B cells proliferate and differentiate into antibody-secreting effector (plasma) cells. These effector cells leave the LNs *via* efferent lymphatic vessels. As previously mentioned, lymphatic capillary LECs secrete CCL21, which attracts and guides CCR7+ DCs and regulatory T cells (Tregs) while precollector vessels LECs secrete CCL27, which attract inflammatory CCR10+ and neoplastic T cells [18] (**Figure 1.2**). Beyond the traditional views that the lymphatics regulate fluid balance, lipid metabolism, and leukocyte trafficking, recent evidence shows that the lymphatics play active roles in both innate and adaptive immunity including modulating inflammation, autoimmune disease and tolerance, pro- and anti-tumor immune responses, and in transplant rejection [27-30]. For example, the response of CCR7+ Tregs to LEC- and LN-derived CCL21 activates Tregs to inhibit T effector cell proliferation and accumulation thus maintaining immune tolerance. Macrophages are chemotactically attracted by LECs and in turn macrophages contribute to lymphangiogenesis in two major ways: secrete pro-lymphangiogenic growth factors such as VEGFC in response to inflammation and by their capacity to transdifferentiate into LECs by incorporating into sprouting lymphatic vessels [18, 28, 31, 32]. Additionally, LECs express MHC class I and MHC class II molecules therefore can present antigen for T cell regulation [30, 33]. Collectively, these physiological and immune modulatory functions of the lymphatics highlight an emerging

intricate concept that the lymphatics are not just passive conduits but are also active participants in immune surveillance.

1.1.3: Differentiating blood and lymphatic endothelial cells (BECs and LECs)

While the lymphatic system is an open, linear system without a centralized organ, the hemivascular (blood) system is a close circulatory system with blood leaving and returning to the heart. Even though the lymphatics arise from the venous system, there are structural differences between the lymphatic and blood microvasculature, thus some molecular differences in the cells that line both endothelia [34]. Blood capillaries, lined by BECs, are covered by basement membranes and completely surrounded by SMCs [21]. As described above, lymphatic capillaries lack a basement membrane and SMC coverage. Another key structural difference is that lymphatic capillaries are anchored to the extracellular matrix (ECM) by filament bundles, which pull LECs open during increased fluid accumulation and increased pressure to allow flow into the lymphatics. In comparison to blood vessels, lymphatic vessels have thin walls and wide lumens. Summarized in **Table 1.2** are key structural and functional differences between the endothelial cells of the blood and lymphatic vascular systems.

Table 1.2. Comparison of blood vascular endothelial cells (BECs) and lymphatic endothelial cells (LECs). Reproduced with permission from Choi, I., Lee, S., and Hong, Y.K., *The new era of the lymphatic system: no longer secondary to the blood vascular system.* Cold Spring Harb Perspect Med, 2012. **2**(4): p. a006445. [35].

Feature	Blood vessels/BEC	Lymphatics/LEC
Constituents	Blood, blood cells	Lymph (interstitial fluid rich in protein, fat, and lipids, extravasated immune cells, and large extracellular molecules)
Gross structure	Closed, circular	Open, linear
Start/end	Heart/heart	Tissue/lymph-vein connection of the thoracic duct
Hierarchical division	Arteries, arterioles, capillaries, venules, veins	Capillaries, precollectors, collecting vessels, thoracic duct, lymph nodes
Vessel wall	Adherens and tight junctions, continuous basement membrane, pericytes, or vascular smooth muscle cells	Overlapping LECs, no tight junctions, anchoring filaments, discontinuous basement membrane, few pericytes (collecting lymphatic vessels have both continuous membranes and mural cells)
Development	Vasculogenesis and angiogenesis	Lymphangiogenesis (budding from cardinal vein)
Origin	Mesoderm, endothelial stem/precursor cells from bone marrow for adults	Mesoderm (vein) during development, lymphatic progenitor cells from bone marrow for adults
Cell markers	CD34, CD105/endoglin	PROX1, LYVE1, VEGFR3, and podoplanin
Absence	Cartilage, cornea	Cartilage, brain, bone, spinal cord, and the retina
Functions	Hemostasis, inflammation, leukocyte trafficking, barrier function, delivery for oxygen, nutrients, and tissue wastes	Tissue fluid homeostasis, absorption of large molecules and lipids in the digestive systems, trafficking of lymphocytes and antigen-presenting cells to regional lymph nodes, transport of degraded extracellular molecules, cell debris, and lymph fluid
Heterogeneity	Well-established phenotypic heterogeneity	Comparable LEC heterogeneity was reported. LEC fate is highly plastic in response to genetic and environmental stimuli

1.2: Lymphatic Disease and Lymphedema

Lymphatic dysfunction: Deficiency in any aspect of lymphatic transport is the etiological basis of lymphedema (LE), a chronic progressive swelling of affected tissues. Abnormal vessel development or damage to lymphatic vessels leads to accumulation of interstitial fluid, protein and cellular debris, which triggers an inflammatory response leading to tissue fibrosis, subcutaneous accumulation of fat, impaired immune responses and susceptibility to infections [19, 36, 37]. Lymphatic vessel damage can also cause lymph leakage back into interstitial space while damaged lymphatic valves lead to backflow of lymph and swelling of extremities. LE is a spectrum disease, which while not life-threatening, severely reduces quality-of-life with no current curative treatments available.

1.2.1: Lymphedema

Clinical presentation and staging: Peripheral edema (lymphedema) occurs when capillary and venous (microvascular) filtration rate exceeds lymph drainage for an extended period of time due to either increased filtration rate and/or lymph flow is decreased. While the most common site for peripheral edema is subcutaneous tissue, edema also occurs in the lungs (pulmonary edema), abdominal cavity (chylous ascites) and other body cavities (synovial, pericardial and pleural effusions) [38]. Clinical classification of LE is defined by the International Society of Lymphology on a scale of 0-III [36].

- Stage 0, also known as the latency stage, is preclinical disease where there is underlying impaired lymph transport but without overt edema.

- Stage I (reversible lymphedema) represents the early accumulation of fluid and when pressed, swollen area leaves a dent (“pitting” edema), which is resolved with limb elevation.
- Stage II (spontaneously irreversible lymphedema) shows development of fibrosis, pitting may or may not occur and limb elevation alone does not reduce swelling.
- Stage III (lymphostatic elephantiasis) is characterized by non-pitting severe edema with irreversible tissue damage, severe fibrosis, fat deposits and warty overgrowths.

These stages are depicted in **Figure 1.4**.

Early diagnosis at Stage 0 or I improves patient outcome as disease is more easily managed with appropriate therapies. However, diagnostic tools especially those that can detect subtle lymphedema before overt clinical presentation are lacking, as will be discussed later in this chapter.

Figure 1.4. Clinical staging of lymphedema. Images depicting increasing severity of lymphedema in the left arm of a patient at Stage 0, Stage I, Stage II and Stage III following axillary lymph node dissection (ALND) treatment for breast cancer.

Reproduced with permission from Columbia University Department of Surgery (http://columbiasurgery.org/news/healthpoints/2011_spring/p2.html)

Figure 1.4. Clinical staging of lymphedema.

1.2.2: Forms of Lymphedema

Lymphedema is classified based on the cause of lymphatic defect, either intrinsic or extrinsic factors, as either primary or secondary (acquired), respectively. Primary lymphedema arises from genetic defects that perturb normal lymphatic development and while variable in presentation, is further subdivided into three groups depending on age of onset: congenital lymphedema (at or shortly after birth), *praecox* (early stage of life, typically teenage years or early adulthood) and *en tarda* (after 35 years of age) [38]. On the other hand, secondary or acquired lymphedema is caused by external stimulus that damages the lymphatics for example following an infection, trauma or surgery.

Primary lymphedema:

1). Congenital lymphedema accounts for approximately 10-25% of all primary lymphedema, affecting more females than males [35]. Congenital lymphedema also manifests more in lower than upper extremities and presents unilaterally as opposed to bilaterally. Genetic studies have identified some causal mutations responsible for congenital lymphedema, with examples provided below.

Milroy's disease and Milroy-like disease: Heterozygous mutations in VEGFR3, encoded by *FLT4*, have been identified in a subgroup of congenital lymphedema known as Milroy's disease [39, 40] after initially being linked to the VEGFR3 locus on distal chromosome 5q [41-43]. Of the mutations reported thus far, all have been in the tyrosine kinase domain of VEGFR3 and disrupt downstream signaling. While Milroy's lymphedema typically exhibits an autosomal dominant inheritance, *de novo* mutations have also been identified, thus family history of lymphedema is not required for diagnosis [44]. Milroy's disease is often characterized by unilateral lower extremity lymphedema and a lack of initial lymphatic capillaries (**Figure 1.2**). Recently, a rare

mutation in VEGFC, the ligand for VEGFR3 was identified in a Milroy-like lymphedema patient [45]. As discussed in **Section 1.1.2**, *Chy* mice, which have a *Vefgr3* heterozygous mutation, develop lymphedema. A second animal model, *Chy3* mice, has a full deletion of the *Vegfc* gene also develop chylous ascites and lymphedema [46].

2). Lymphedema *praecox*, also known as Meige's disease, typically presents during puberty and exhibits an autosomal dominant pattern of inheritance [47]. *Praecox* covers all lymphedema with onset between 1-35 years of age, represents the majority of primary lymphedema cases (60-80%), and affects females four times more compared to males [35]. Because primary lymphedema is classified based on age of onset, rather than genetics, pathophysiology or etiology, there is often confusion between the terms *praecox* and Meige's disease [35]. Thusly, a variety of other anomalies including vertebral defects, cerebrovascular malformations, developmental defects, hearing loss and distichiasis (double rows of eyelashes) are seen in *praecox* [36]. Examples of *praecox* lymphedema are as follows:

Lymphedema distichasis (LD) syndrome: The most unique phenotype seen in LD patients is distichiasis, the presence of a second set of eyelashes at birth, which results in corneal irritation. LD is an autosomal dominant disorder and mutations in the transcription factor *FOXC2* have been identified in patients [48, 49]. Patients also develop bilateral lower extremity lymphedema at puberty and while they have normal number of lymphatic vessels, they exhibit impaired lymphatic drainage due to defective valves [50]. Mice deficient in *Foxc2* also have abnormal lymphatic patterning and defective valves [20].

Hypotrichosis-lymphedema-telangiectasia (HLTS): This is a rare form of *praecox* lymphedema characterized by absence of eyebrows and eyelashes, and presence of

eye edema and blood vessel dilations [51]. Mutations in the SRY-related transcription factor, SOX18, which is upstream of PROX1, have been identified in both recessive and dominant forms of HLTS. Mice deficient in *Sox18* are embryonically lethal but mutant embryos lack lymphatic vasculature and have edema [9].

Hennekam syndrome: This is another rare form of *praecox* disease characterized by lymphedema, lymphangiectasia (vessel dilation) and developmental delays. Lymphedema is typically present at birth and in the face or in the limbs and gradually progressive, while lymphangiectasias are present in the intestines [52]. Mutations in collagen and calcium binding EGF-domain 1 (*CCBE1*) have been identified as causative for Hennekam syndrome [53]. Zebrafish deficient in *ccbe1* show defective embryonic lymphangiogenesis and lymphatic sprouting from the venous endothelium [54].

3). Lymphedema *en tarda* manifests after 35 years of age and accounts for approximately 10% of all primary lymphedema [55-59]. Lymphedema *en tarda* exhibits hyperplastic, tortuous vessels which are often dilated and lack functional valves.

Other genes that have been identified to be causal for lymphedema include *ITGA9* that encodes integrin α9 in fetuses with congenital chylothorax [60]; *RELN* in congenital lymphedema [61]; *GJC2* that encodes connexin 47 in primary and secondary lymphedema subjects [62]; and *HGF* and *cMET* genes that encode hepatocyte growth factor and its receptor in both primary and secondary lymphedema subjects [63]. Lymphedema can be nonsyndromic (isolated) and also occur in conjunction with other blood vascular symptoms as part of a syndrome. **Table 1.3** summarizes the lymphedema spectrum that extends from nonsyndromic to syndromic disease, associated causal genes, mutation type, and pattern of inheritance and phenotypes of associated animal models, if available.

Table 1.3. Genes involved in lymphatic anomalies. Reproduced with permission from Brouillard, P., Boon, L., and Vikkula, M., *Genetics of lymphatic anomalies.* J Clin Invest, 2014. **124**(3): p. 898-904. [44].

Lymphatic anomalies/additional signs	Gene (protein)	Mutation type	Animal models
Isolated lymphedema			
Primary congenital lymphedema/ Nonne-Milroy	*FLT4* (VEGFR3)	Inactivating	**Chy**, *Flt4*$^{-/-}$
Milroy-like disease	*VEGFC*	LOF	**Chy-3**, *Vegfc*$^{-/-}$
Syndromic lymphedema			
Hennekam lymphangiectasia-lymphedema syndrome/mental retardation	*CCBE1*	LOF	**fof**
Lymphedema-distichiasis and yellow nail syndromes/ptosis	*FOXC2*	LOF	***Foxc2***$^{-/-}$
Hereditary lymphedema II (Meige disease)	*GJC2* (CX47)	Missense	(*Gjc2*$^{-/-}$)
Oculodentodigital dysplasia/lymphedema	*GJA1* (CX43)	Missense	(*Gja1*$^{-/-}$)
Choanal atresia/lymphedema	*PTPN14*	LOF	***Ptpn14***$^{-/-}$
Hypotrichosis-lymphedema-telangiectasia syndrome	*SOX18*	LOF?/D-N	**Ragged**,(*Sox18*$^{-/-}$)
Lymphedema-lymphangiectasia	*HGF*	LOF?	(*Met*$^{-/-}$)
MCLMR	*KIF11*	LOF	(*Kif11*$^{-/-}$)
Noonan syndrome 1(54% with lymphedema)	*PTPN11* (SHP2)	GOF	***Shp2***$^{-/-}$
Noonan syndrome 1 (63% with lymphedema)	*SOS1*	GOF	–
Primary lymphedema, myelodysplasia (Emberger syndrome)	*GATA2*	LOF	(*Gata2*$^{-/-}$)
OLEDAID	*IKBKG* (NEMO)	Hypomorphic	(*Ikbkg*$^{-/-}$)
CM-AVM/lymphedema	*RASA1*	LOF	***Rasa1***$^{-/-*}$
Cholestasis-lymphedema syndrome (Aagenaes syndrome)	*locus in 15q*	–	–
Syndromic chylothorax/chylous ascites, lymphangiectasia			
Fetal chylothorax	*ITGA9*	Missense	***Itga9***$^{-/-}$
Noonan syndrome, cardiofaciocutaneous syndrome/chylothorax	*KRAS*	GOF	***Kras***$^{-/-}$
Noonan syndrome 1/lymphangiectasia	*RAF1*	AD	
Costello syndrome/chylous ascites, chylothorax	*HRAS*	AD	
Syndromes with lymphatic malformations			
Turner syndrome/nuchal translucency	*Monosomy X*	–	(X0 mice)
Proteus syndrome, Pten hamartoma tumor syndrome	*PTEN*	LOF	(*Pten*$^{-/-}$)
CLOVES, Klipple-Trenaunay-Weber syndrome	*PIK3CA*	GOF	**pα100-KI**
Proteus syndrome	*AKT1*	GOF	***Akt1***$^{-/-}$

MCMLR, microcephaly with or without chorio- retinopathy, lymphedema, or mental retardation; OLEDAID, X-linked syndrome anhydrotic ectodermal dysplasia with immunodeficiency, osteopetrosis, and lymphedema; CV-AVM Capillary malformation-arteriovenous malformation; Parentheses indicate the absence of lymphatic anomaly, and bolded text indicates that the model partially mimics the human phenotype. *Inactivation in adults. AD, autosomal dominant; AR, autosomal recessive; D-N, dominant negative; GOF, gain of function; KI, knockin; LOF, loss of function; –, not applicable. Question marks indicate that mutation type and/or inheritance is unclear.

Secondary lymphedema:

Secondary, or acquired, lymphedema arises when there is damage to the lymphatics owing to infection, surgery, radiation, compression. Secondary lymphedema can occur within weeks or decades following lymphatic insult, the cause for this discrepancy is currently unknown. Examples of secondary lymphedema are as follows:

1). *Filariasis:* Worldwide, filariasis also known as elephantiasis, is the most common type of lymphedema affecting more than 120 million people, mostly in the tropical areas, with highest incidences seen in Africa and Asia [64, 65]. Filariasis is caused by a parasitic infection by mosquito-borne worm parasites including, *Wuchereria bancrofti*, *Brugia malayi* or *Brugia timori*, which invade and reproduce within the lymphatic system. Individuals bitten by an infected mosquito initially do not realize they have an infection even though lymphatic damage is already in progress. The infection triggers an inflammatory reaction that results in increased VEGFA, VEGFC and VEGFD leading to lymphatic vessel hyperplasia, obstruction and eventually blockage of lymph drainage, resulting in swelling of the extremities [37]. Other complications include tissue fibrosis, fat accumulation, secondary infections, genital lymphedema and permanent disability especially with progression to severe elephantiasis. Treatment options for filariasis include drugs that target the microfilarie larval offspring and those that target the intracellular bacterial symbiont of filarial parasites.

2). *Cancer-related lymphedema (CRL):* In the Western world, the most common cause of secondary lymphedema is due to cancer treatment, which occurs following lymph node dissection or radiation therapy that damages the lymphatics. CRL is often seen in breast, melanoma, pelvic, and head and neck cancer survivors. Currently, there are approximately 3-5 million individuals with lymphedema and these numbers are

expected to rise as the cancer survivorship increases accordingly. It is estimated that lymphedema affects ~15-20% of women undergoing breast cancer treatment and ~15% of all cancer survivors [66, 67]. As discussed in **Section 1.2.2**, mutations in *GJC2, HGF* and *cMET* genes have been identified in subjects with secondary lymphedema following breast cancer treatment, and primary lymphedema, which gives further credence to the hypothesis that there may be a genetic susceptibility for secondary lymphedema [68, 69]. Recently, additional mutations in *VEGFR2, VEGFR3* and *RORC* have also been identified in breast cancer survivors with lymphedema [70]. As CRL can develop decades into survivorship, understanding of genetic susceptibility will require prospective studies and associated molecular studies, some of which are currently underway [71], which will lead to identification of targeted therapies against CRL.

1.2.3: Lymphedema Diagnosis and Treatment

Diagnosis: Clinical diagnosis of lymphedema is usually done *via* bedside observations. Differentiating lymphedema from other forms interstitial edema depends on other unique sequelae of lymphedema. These physical characteristics include edema, *peau d'orange* (orange peel appearance), cutaneous fibrosis and positive "Stemmer sign" (inability to grasp the skin at base of the digit in the affected extremity) [72]. Limb measurements such as circumference and/or volumetric analysis, are also made between the affected and unaffected extremity, typically estimated ≥20%. More accurate than limb volume analysis are techniques including bioimpedance analysis that measures differences in edema volume relative to body composition [36]. Additional confirmation of diagnosis can be done using imaging techniques, which will be discussed in **Section 1.3**

Treatment: Physiotherapeutic interventions are the mainstay of lymphedema treatment. Complex decongestive physiotherapy (CDPT) involves massage or manual lymphatic drainage (MLD) and compression garments which aim to increase lymphatic contractility and flow; reduce accumulated fluid and direct stagnated lymph to functional lymphatics. However, CDPT techniques have not changed over the last century and therapy is often expensive, labor-intensive, time consuming and most importantly depends on patient compliance to be beneficial [36, 72, 73]. Debulking surgical procedures such as liposuction show initial postoperative success but continuous compression treatments are still necessary for limb volume maintenance; otherwise edema can recur at a much more rapid rate and often more severe than initial disease. All current treatments target lymphedema symptoms, not the underlying causes of disease, therefore are not curative, and thus there is high risk of recidivism especially in non-compliant patients. There are no pharmacological therapies currently available for lymphedema, but pre-clinical studies have shown activation of VEGFR3 by VEGFC as a promising gene therapy in murine model of primary lymphedema [24]. As lymphedema-causative genetic mutations are still being unraveled, current research efforts focuses on investigating known gene candidates, determine whether they are efficacious molecular targets, and if so, it is expected their use in therapy will stimulate regrowth of damaged and/or nonfunctional lymphatics, and overcome vascular insufficiency in order to improve or treat lymphedema.

1.3: Lymphatic Imaging

Unlike the blood circulatory system, research into the lymphatic system has often lagged behind, owing in part to limited imaging modalities that can easily and sensitively visualize the lymphatics. Angiographic techniques such as magnetic resonance (MR) and computed tomography (CT) allow for non-invasive visualization of the blood

vascular system following intravenous (i.v) injections of contrast agents [1]. Early in the 20th century, invasive isolation and cannulation of lymph vessels allowed for the first structural characterization of the lymphatics but these techniques often led to dysfunctional lymph transport and are therefore no longer used. Non-invasive methods are preferred. Lymph is a clear fluid and invisible to the naked eye; therefore the use of contrast agents is necessary for lymphatic imaging.

Lymphangiography. Angiography refers to the visualization of vessel lumen. Lymphangiography is the oldest imaging technique for investigating lymphatic architecture. Administration of an exogenous x-ray or MR contrast agent is done either directly into cannulated lymphatic vessel or indirectly by intradermal (i.d) injection into the lymphatic capillary plexus, the entry point for peripheral lymphatics for uptake into lymphatic vessels. Whether done *via* direct or indirect methods, an x-ray or MR imaging system is necessary for the detection of contrast agent transversing through the lymphatic vessels. Owing to its cumbersome nature and difficulty in cannulating mouse lymphatic vessels, direct lymphangiography is not performed in animal studies [1]. Indirect MR lymphangiography has recently been used to image lower extremity lymphedema in cancer survivors with great resolution (**Figure 1.5A**) [74]. Recent advances have been made in MR contrast agents such as albumin-binding gadolinium-based agents, which have enabled visualization of morphological features of lymph vessel abnormalities [75].

Lymphoscintigraphy. Currently, lymphoscintigraphy is the clinically accepted modality for imaging lymphedema. Lymphoscintigraphy, also known as isolated lymphography, involves the i.d injection of a radiolabelled colloid, usually ^{99m}technecium, into the affected extremity for uptake, and subsequent imaging of the lymphatics [36]. As the radiocolloid decays, it releases high energy photons, which exit the tissue and are

captured by a gamma camera. Within the camera is a sodium iodide crystal plane that absorbs the released photons and in turn releases an electron and a flash of light is produced as the electron returns to its ground state. This process is known as scintillation. Imaging is often performed hours after radiocolloid injection and the resulting images are often grainy (**Figure 1.5B**). Lymphatic function can be assessed which usually includes delayed or lack of radiocolloid uptake, dermal backflow or infusion, poor visualization of lymphatic vessels and lymph nodes [1, 36]. Lymphoscintigraphy takes approximately 30 minutes for each image to be acquired and since the subject is exposed to ionizing radiation, repeated imaging sessions are limited. Additionally, while lymphoscintigraphy is considered the gold standard for diagnosing and imaging lymphedema, it has limited photon count rate and poor resolution in comparison to MR lymphangiography. The acquired images are often of poor resolution thus the extent of lymphatic damage is harder to assess especially during diagnosis.

Fluorescence microlymphangiography (FML). This technique employs intradermal administration of fluorescein isothiocyanate (FITC)-conjugated dextran and is the first non-invasive fluorescence imaging technique that provides high resolution images [1]. FML uses video fluorescence microscopy for image capture. However the inherent spectral properties of a fluorophore like FITC in the visible wavelength only allows visualization of the initial lymphatic capillaries that are <200μm deep due to limited light penetration and tissue scattering in humans, although with high resolution (**Figure 1.5C,D**). Therefore the use of tissue-penetrating near-infrared (NIR) dyes that are excited >750nm, such as indocyanine green (ICG), could improve FML techniques.

Near-Infrared Fluorescence Lymphatic Imaging (NIRFLI). This technique pioneered by our research group, makes use of ICG, a fluorescent dye that has been approved for human use for intravenous (i.v) administration in hepatic and

cardiovascular testing and retinal angiography [1]. NIRFLI is also known as ICG lymphography and is not microscopy-based. Following ICG i.d administration, tissues as deep as 3-4cm are illuminated with NIR excitation light and ICG fluorescence is collected using charge-couples device (CCD) cameras. NIRFLI allows visualization of initial lymphatic capillaries, collecting vessels and lymph nodes (**Figure 1.5E, F**). However, FML provides a higher resolution of initial capillaries compared to NIRF imaging. NIRFLI is discussed further in **Section 1.4**

Summarized in **Table 1.4** are various non-invasive lymphatic imaging techniques used in mice and man.

Of all these techniques, NIRF lymphatic imaging is the only modality that can truly assess lymphatic function as images are acquired within milliseconds and lymphatic pumping assessed in real time. NIRFLI offers a rapid, high resolution, dynamic lymphatic imaging and currently is the only Food and Drug Administration (FDA)-approved investigational technique that employs ICG-administration for lymphatic imaging.

Figure 1.5. Examples of lymphatic imaging techniques. **(A)** Magnetic resonance (MR) lymphangiography (indirect) of normal (left) and diseased (right) lymphatic structure (thin arrows) following administration of gadopentate dimeglumine. Some enhanced veins are also shown (thick arrows). **(B)** Lymphoscintigram of lymphatic drainage in the lower extremities (anterior view) following bipedal administration of ^{99m}Technicium sulfur colloid. **(C** and **D)** Fluorescence microlymphangiography (FML) of FITC-dextran in initial lymphatic capillaries of medial ankle of human normal control subject **(C)** and subject with primary lymphedema **(D).(E** and **F)** NIRF imaging of the lymphatic drainage of an asymptomatic leg **(E)** and a symptomatic leg **(F)** following administration of indocyanine green (ICG). Scale bars: 1 mm **(C** and **D)**; 1 cm **(E** and **F)**.

Reproduced with permission from Sevick-Muraca, E.M., Kwon, S., and Rasmussen, J.C., *Emerging lymphatic imaging technologies for mouse and man.* J Clin Invest, 2014. **124**(3): p. 905-14. [1].

Figure 1.5. Examples of lymphatic imaging techniques

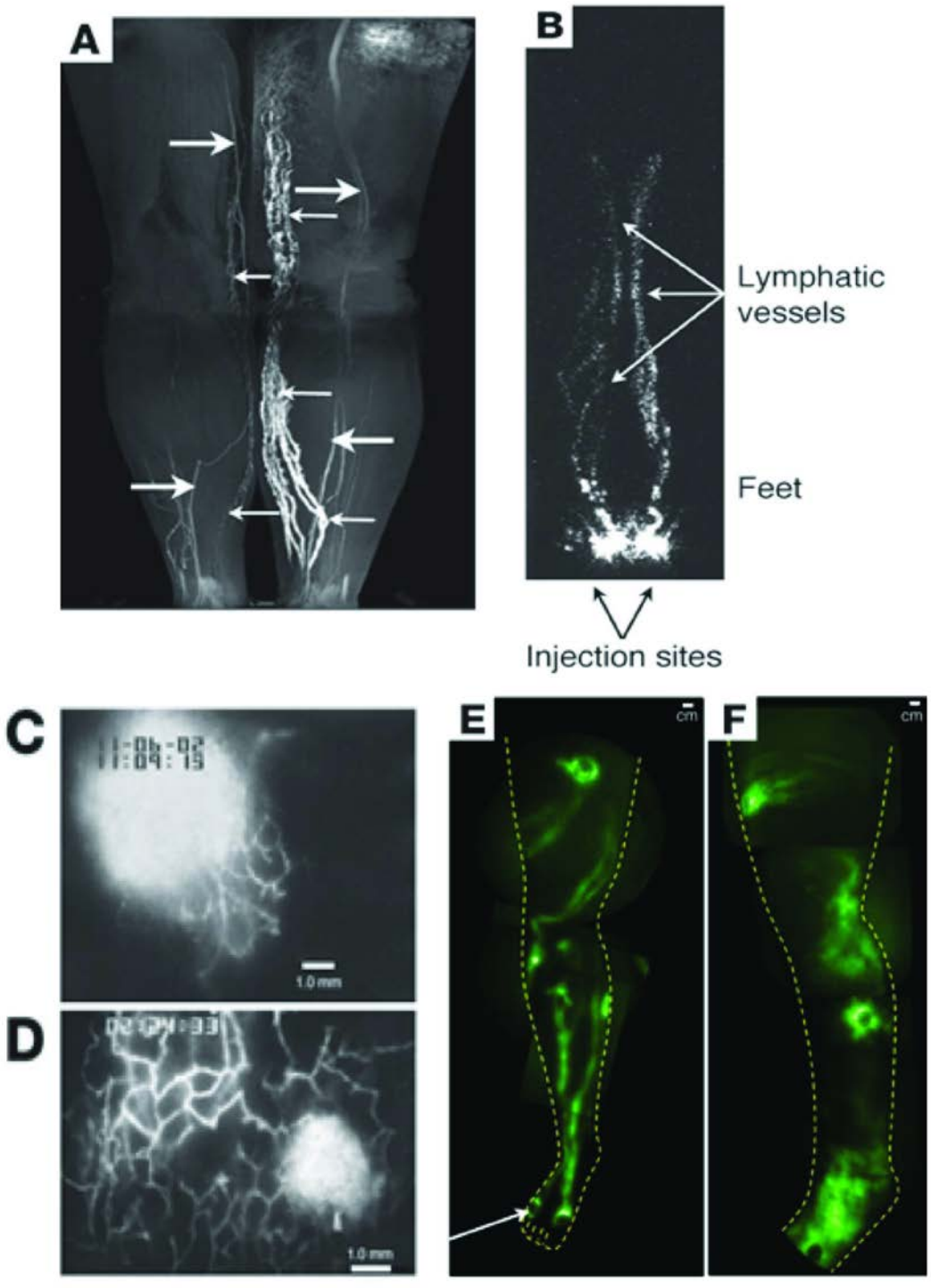

Table 1.4 Summary of imaging modalities for visualizing the lymphatic vasculature *in vivo* within small and large animals and humans. Reproduced with permission from Sevick-Muraca, E.M., Kwon, S., and Rasmussen, J.C., *Emerging lymphatic imaging technologies for mouse and man.* J Clin Invest, 2014. **124**(3): p. 905-14. [1].

Modality	Temporal Resolution (acquisition times)	Spatial Resolution	Depth Resolution	Small Animals	Large Animals	Humans	Contrast Agents	Comments
X-ray lymphangiography (direct)	ms/exposure; Requires surgical intervention to cannulate lymphatic vessel	<1 mm	Whole Body	No	Yes	Yes	Oily, iodinated agents such as Ethidol and Lipiodol	Used on a limited basis due to incidence of clinical complications and technical skill required to locate and cannulate lymphatic vessel
X-ray lymphangiography (indirect)	ms/exposure	<1 mm	Whole Body	No	Yes	Yes	Water-soluble iodinated agents such as Iotasul	
X-ray Computed Tomography	>20 sec, dependent on region of interest and desired resolution	1-3 mm	Whole body	Limited	Yes	Yes	Water-soluble iodinated agents such as Iopamidal	Visualizes lymph nodes and some larger lymphatic vessels
MRI Lymphangiography	>2 min, dependent on region of interest and desired resolution	0.1–0.3 mm in mice 1 mm in human	Whole Body	Yes	Yes	Yes	Gadolinium or iron oxide based agents; dendrimer based macromolecules	Difficult to resolve healthy, intact lymphatic vessels

MRI (non-contrast)	minutes	1 mm	Whole body	No	Yes	Yes	Unknown	Can only resolve dilated lymphatics filled with stagnate lymph
Lymphoscintigraphy	20-60 min	~1 cm	Whole body	No	Yes	Yes	Radiolabeled sulfur colloid, radiolabeled dextran, Technitium most commonly used isotope	Visualizes large lymphatic vessels and nodes only
FML	Video rates	50 µm	200 µm	Yes	Yes	Yes	FITC-dextran	Visualizes the initial lymphatics near the injection site
NIRF	Typically 50-800 ms per image	~200 µm at tissue surface, resolution decreases as depth increases due to photon scatter however larger, and deeper vessels are visualized	Varies with vessel diameter; larger nodes can be visualized up to 3-4 cm deep	Yes	Yes	Yes	NIRF dyes; Qdots; gene reporters	Initial lymphatics as well as collecting nd conducting vessels observed. Active lymphatic propulsion observed in small and large animals as well as in humans; Photon scattering limits spatial resolution, only off-label use of ICG is allowed in humans

1.4: NIRF Lymphatic Imaging in Mouse and Man

1.4.1: Principles of fluorescence

Fluorescence is the ability of molecules to absorb and emit light at certain wavelengths. When a fluorophore is excited at a certain wavelength, it emits light in a right (red) shifted light, for example ICG is excited at ~780nm and emits at ~830nm. During fluorescence, energy is lost therefore the emitted light has a longer wavelength and at a lower energy than the excitation wavelength; the difference between the two wavelengths is known as Stoke's shift. The principles of fluorescence are explained by the Jablonski's Energy Diagram (**Figure 1.6A**). The excitation of a fluorophore causes it to move from the ground state (S0) to a higher, second energy state (S2). From S2, the fluorophore undergoes internal conversion as it relaxes during a process known as vibrational relaxation where there is loss of energy but an absence of light emission, and then falls to the lowest vibrational energy level of the first excited state (S1). From S1, the fluorophore undergoes more relaxation and falls back to ground state S0 and emitting fluorescence in the process. The change in energy from S1 to S0 results in the emission of a unit of energy known as photon. Absorption of a fluorophore and subsequent fluorescent emission occurs in 1 nanosecond and the fluorophore is excited again. In one second there can be as many as $1x10^8$ photons emitted, making fluorescence a powerful and rapid imaging modality for collection and image formation [76-79]. This is in contrast to lymphoscintigraphy, the current clinical gold standard that requires approximately 30 minutes for acquisition of one image.

Optical properties of a fluorophore are based on three characteristics: extinction coefficient, quantum yield, and lifetime. Extinction coefficient (Є) is the capacity of light

absorption at a particular wavelength. Therefore a fluorophore with a high extinction coefficient will absorb more light. Quantum yield (ϕ) is a measure of fluorescence output and defined as a ratio of emitted photons per absorbed photons which is important in obtaining fluorescence signal, therefore a high quantum yield means the fluorophore is more efficient. The fluorescence output of a fluorophore, or its "brightness", is directly proportional to the product of its extinction coefficient and its quantum yield. Lifetime (τ) is an intrinsic property of a fluorophore and is the required time the fluorophore stays in the excited state before returning to the ground state. Lifetime is independent of experimental conditions such as excitation wavelength, method of excitation, duration of light exposure, or fluorophore concentration [78, 80].

1.4.2: Near-infrared fluorescence (NIRF) imaging system

Near-infrared (NIR) light lies beyond the visible light on the electromagnetic spectrum in the ~750-2500nm wavelength range (**Figure 1.6B**). NIRF imaging requires four essential elements: (a) excitation light from laser diodes or lasers capable of penetrating deep tissues and selectively excite contrast agents; (b) NIRF imaging agents that can be safely administered and sensitively imaged; (c) optical lenses and filters that can sensitively detect desired fluorescent light while blocking the scattered excitation light from the tissue; and (d) the detector, usually a charged coupled device (CCD) for fluorescent light collection [79]. The basic design for the imaging system is outlined in **Figure 1.7**.

NIR fluorescence contrast agents should be capable of *in situ* activation with tissue-penetrating light. The excitation light must have wavelengths >780nm to avoid autofluorescence. At wavelengths <780nm, endogenous chromophores are also excited

therefore increasing the likelihood of high background signal. The contrast agent also needs to be stable and fluoresce efficiently when excited. At >780nm, tissue penetration is high therefore excitation of NIRF contrast agents is achieved.

The NIRF imaging process comprises the following: The NIRF contrast agent is intradermally injected superficially below the skin into the lymphatic capillary plexus from where it is quickly taken up by the initial lymphatic capillaries. The contrast agent is excited by tissue penetrating light from a laser diode and in turn emits a fluorescent signal. The scattered signal from the tissue passes through optical filters that rejects other wavelengths and collects the emission at 830nm. The collected signal is detected and amplified by an NIR-sensitive intensifier and collected by the CCD camera and processed by a computer for visualization of collected images. Typical images are acquired every 200 milliseconds, which can be sequentially compiled and analyzed using imaging software such as ImageJ.

Figure 1.6. Basic principles of fluorescence. (A) Jablonski's diagram showing the energy transitions following absorption of a photon that produces fluorescence emission. Reproduced with permission from (http://www.piercenet.com/method/fluorescent-probes). **(B)** Near infrared (NIR) region of the electromagnetic spectrum is located just beyond visible light. Reproduced with permission from (http://www.scimed.co.uk/nir-spectrometers/).

Figure 1.6 Basic principles of fluorescence

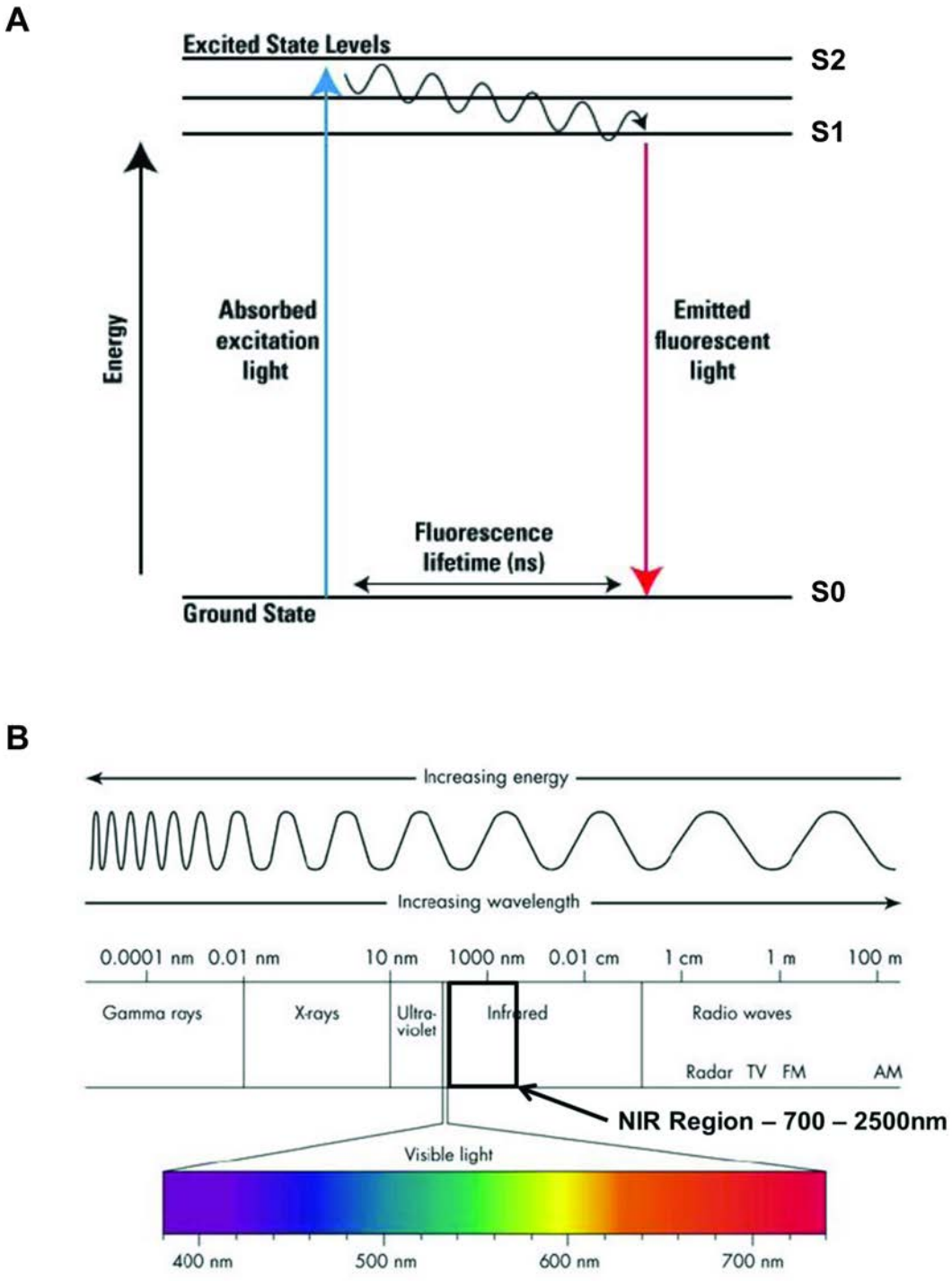

Figure 1.7. Near-infrared fluorescence lymphatic imaging (NIRFLI) system.

Schematic of near infrared imaging system used for lymphatic imaging. 785nm laser diode illumination provides the source for the excitation of the NIRF contrast agent after intradermal injection of indocyanine green (ICG) in mice (i) or humans (ii). A charged couple device (CCD) camera captures ICG fluorescence emission at 830nm while filters reject the scattered light from the tissue. Shown are examples of (i) basic mouse lymphatic architecture and (ii) human hand of a subject with lymphedema exhibiting abnormal retrograde lymph flow towards the fingers that can be visualized in computer.

Figure 1.7 Near-infrared fluorescence lymphatic imaging (NIRFLI) system

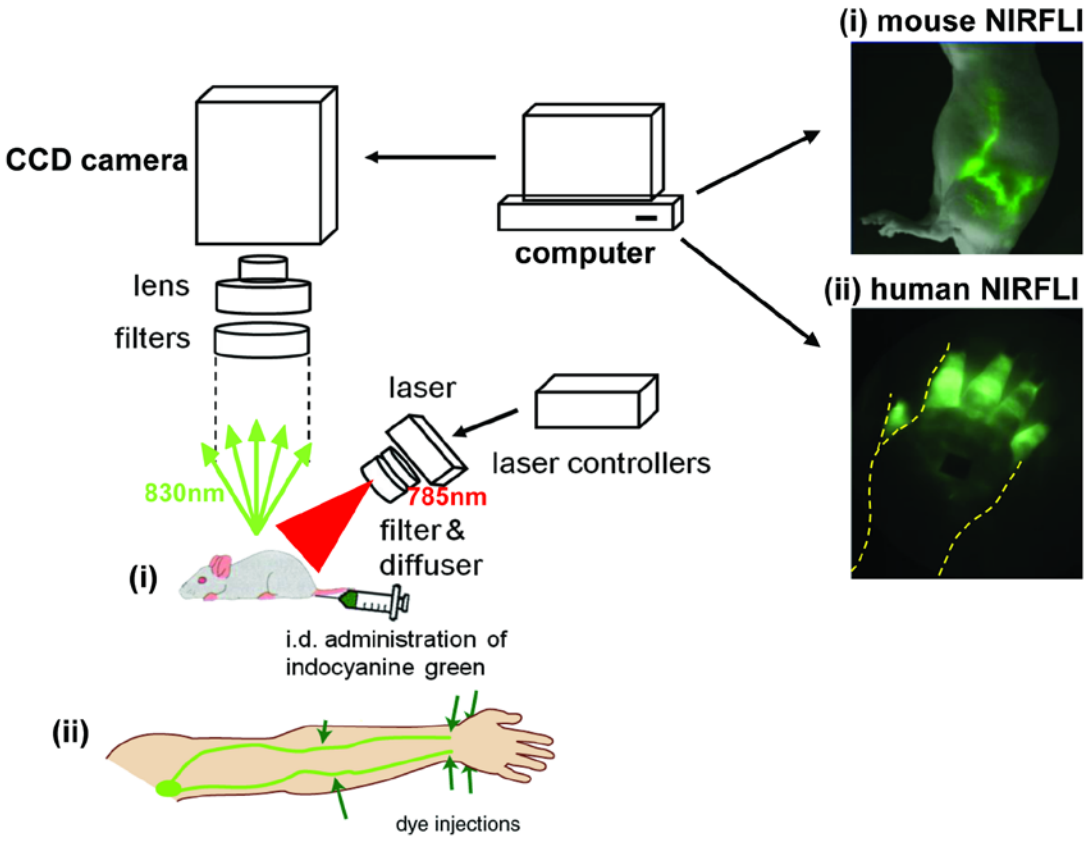

1.4.3: NIRF as a tool for phenotyping human lymphatic disorders in mouse and man

Fluorescence-based imaging techniques such as FML and NIRF provide the unique advantage of directly relating human lymphatic phenotypes to mouse models of lymphatic dysfunction. Currently, there are no fluorescence optical imaging modalities that are used in the clinic as part of standard-of-care to image the lymphatics. However, preclinical and clinical studies using ICG-based non-invasive NIRF imaging are underway. Two examples of the utility of NIRF in associating human and mouse lymphatic phenotypes are outlined below:

a) *Capillary malformation-arterial venous malformations (CM-AVM) and Rasa1 mouse*: CV-AVM is a syndromic vascular disorder in which there are enlarged cutaneous capillaries that increase blood flow near the skin surface. The clinical presentation of CV-AVM includes lymphedema, chylous ascites, chylothorax, lymphangiectasia and lymphatic vessel hyperplasia [81]. Genetic mutations in *RASA1* that encodes p120 RasGAP have been identified as responsible for CV-AVM [82, 83]. Using NIRF imaging, we identified abnormal lymphatic architecture and function in a patient with CM-AVM which was similar to that in an inducible *Rasa1* knockout mouse model [84, 85] (**Figure 1.8A**). In that mouse study, we confirmed that loss of p120 RasGAP, a negative regulator of the MAPK/ERK pathway, was directly responsible for aberrant, dysregulated lymphangiogenesis.
b) *Primary Lymphedema and Chy mouse*: As mentioned previously, mutations in *FLT4*, that encodes VEGFR3, have been identified in a portion of subjects with primary lymphedema. *Chy* mice have a loss-of-function mutation within the kinase domain of *Vegfr3*. Using NIRF imaging, we have characterized the hypolastic lymphatic phenotype of the *Chy* mouse, which is strikingly similar to

subjects with lymphedema who also possesses mutation in *VEGFR3* (**Figure 1.8B**) [1].

Significance: *NIRF is a powerful imaging modality that delineates lymphatic architecture including initial capillaries, vessels and lymph nodes. Furthermore, NIRF is the only lymphatic imaging modality that can truly assess the lymphatic functions of contractility and lymph pumping and propulsion. Thus NIRF is a critically useful clinical tool that can be used in early diagnosis of lymphedema as NIRF can detect underlying lymphatic architectural and functional abnormalities before the disease progresses to the irreversible stage when it is also unfortunately, incurable. Assessment of frequency and velocity of lymph pumping in the collecting and conducting vessels has been performed in rodent, swine and human studies in normal and disease models which have shown the utility of near infrared fluorescence as an emerging cutting edge technique of lymphatic imaging* [79, 86-95].

Figure 1.8. NIRF phenotypes of human disease in mouse and man. **(A)** The drainage of ICG from the lower extremity lymphatics into the abdomen in a subject diagnosed with capillary malformation-arterial venous malformations (CM-AVM) syndrome, associated with an inactivating mutation in *RASA1*. **(B)** The drainage of ICG into the abdominal cavity of a *Rasa1* knockout mouse (*Rasa1*$^{fl/fl/ubErt2\text{-}cre}$) exhibiting lymphatic hyperplasia. **(C** and **D)** Lymphatic drainage in a wild type (WT) C3H mouse **(C)** and a *Chy* mouse **(D)** with a *Vegfr3* loss-of-function mutation. **(E** and **F)** Similar phenotypes are observed in a normal human foot **(E)** and the foot of a human subject with a *VEGFR3* mutation with primary lymphedema **(F)**.

Reproduced with permission from Sevick-Muraca, E.M., Kwon, S., and Rasmussen, J.C., *Emerging lymphatic imaging technologies for mouse and man.* J Clin Invest, 2014. **124**(3): p. 905-14. [1].

Figure 1.8 NIRF phenotypes of human disease in mouse and man

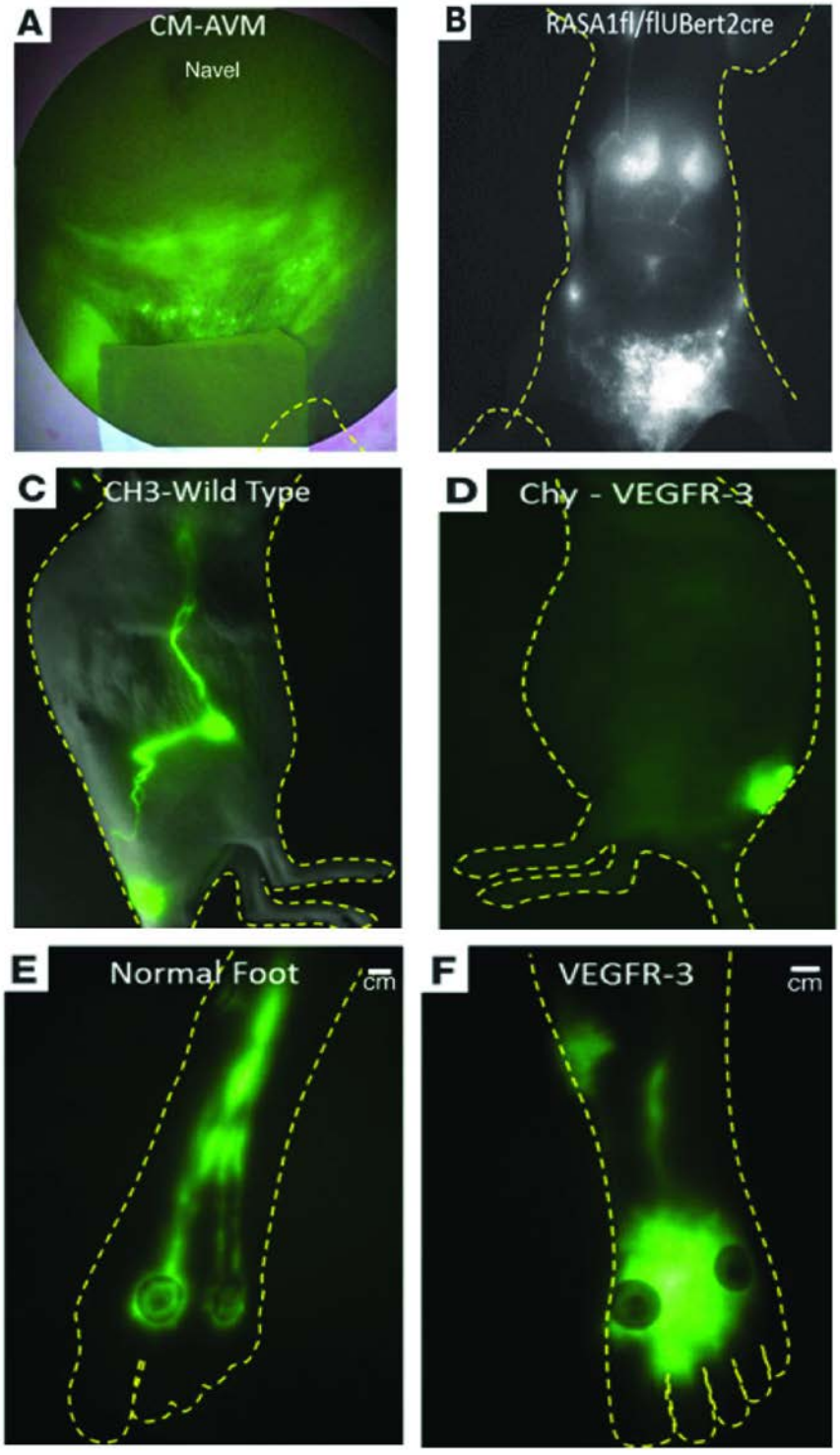

1.5 Motivation and rationale of this dissertation

Genetic studies of rare congenital lymphatic disorders provide an opportunity to identify key molecular mechanisms that may be contributory to more common conditions and disorders. From candidate gene studies, causal genes including *FOXC2, FLT4, SOX18, CCBE1, GJC2, GATA2, KIF11, PTPN14* and *RASA1* (**Table 1.3**) have thus far been associated with lymphatic malformations and lymphedema that generally presents with variable penetrance and expressivity, often late in life. *Yet the majority of patients diagnosed with lymphatic abnormalities do not possess mutations in these genes.* Current estimates show that these putative candidate genes are responsible for only 36% of familial primary lymphedema and only 8% of sporadic lymphedema [96]. This underscores the need to rapidly identify unknown genes that cause or contribute to lymphedema. With the advent of unbiased next generation sequencing (NGS) and associated bioinformatics analyses, key molecular pathways can be discovered in families harboring rare hereditary lymphatic disorders with as little as four family members [97], *provided accurate phenotyping is performed*.

The diagnoses of rare lymphatic disorders are not generally made on the basis of abnormal lymphatic architecture or function, but rather on the late-stage sequelae of fluid imbalances, such as irresolvable edema, chylothorax, or chylous ascites. For example, diagnosis of primary lymphedema is based upon edematous symptoms that appear at birth (congenital), at puberty (*praecox*), or late in life, usually following a minor challenge to the immune system (*en tarda*). As a consequence of the variable expressivity, the inaccuracy of phenotyping based upon overt symptoms can limit the association with genotype and therefore impede discovery of gene variants. While computed tomography (CT) or magnetic resonance (MR) lymphangiography can assess lymphatic abnormalities in symptomatic patients in rare cases, the radiographic procedure is

contraindicated in asymptomatic subjects owing to procedural risks. The current clinical gold standard technique of lymphoscintigraphy is commonly used to assess deficiency in lymph transport, but entails the use of a radioisotope to produce images that have limited temporal and spatial resolution, and can fail to identify architectural and functional abnormalities. On the other hand, near infrared fluorescence lymphatic imaging (NIRFLI) is a rapid, sensitive lymphatic imaging modality with high spatial and temporal resolution that can discern subtle phenotypes and has been used in clinical studies to assess human lymphatic phenotypes in normal and diseased subjects. Early detection of aberrant lymphatic function in asymptomatic patients at Stage 0 or I (**Figure 1.4**) would allow early diagnoses and allow for more effective treatment when lymphedema can be managed much more easily.

The overall objective of my dissertation project has been to uncover gene variants in persons with lymphatic disease that could point to the molecular basis of lymphatic failure. We hypothesized that the unique combination of accurate phenotyping using NIRF imaging with unbiased genotyping using NGS of families that harbor lymphatic defects would provide new molecular insights to lymphatic disorders, including lymphedema, a chronic, highly disfiguring and currently incurable disease. Discussed in ***Chapter 2*** *is the discovery one such novel gene, INPPL1, that encodes src homology 2-domain containing 5'-inositol phosphatase-2 (SHIP2), that was identified using this multidisciplinary approach.*

CHAPTER 2

INPPL1 MUTATIONS IDENTIFIED IN FAMILIAL LYMPHEDEMA *via* ASSOCIATION OF NIRF LYMPHATIC IMAGING AND WHOLE EXOME SEQUENCING

Portions of this chapter are based on “Agollah G.D., Gonzalez-Garay M.L, Rasmussen JC., Tan I-C., Aldrich M.B., Darne C., Fife C.E., Guilliod R., Maus, E.A., King P.D., Sevick-Muraca E.M., *“Evidence for SH2 domain-containing 5-inositol phosphatase-2 (SHIP2) contributing to a lymphatic dysfunction”* PLoS ONE (2014) 9(11): e112548. doi:10.1371/journal.pone.0112548 [98]. *PLOS applies Creative Commons Attribution License (CCAL) and Open-Access License, wherein no permission is required from authors or publishers for reprints or reproduction of published works, except proper citation of original work. Collaborator efforts are outlined in Figure legends, wherever necessary*.

2.1: Rationale

Pathophysiological processes that exhibit loss of fluid homeostasis, disrupted lipid absorption and transport, and compromised immune surveillance/response generally have some abnormal involvement of the lymphatic circulatory system [22]. Discovery of genetic variants responsible for inherited lymphatic abnormalities has been limited by candidate gene searches and inaccurate phenotyping based upon late-stage, overt symptomatic presentation. Recently, we used near-infrared fluorescence lymphatic imaging (NIRFLI) in investigational studies to (i) characterize normal lymphatic architecture and function in normal control subjects [79, 99]; (ii) characterize abnormal lymphatic architecture and function in subjects with lymphatic disorders including reduced lymphatic contractile function and lymphatic reflux [95]; (iii) detect early lymphatic abnormalities in a breast cancer survivor asymptomatic for cancer-acquired lymphedema [92] and (iv) identify abnormal lymphatic architecture and function in a patient with capillary-malformation arterial venous malformations (CM-AVM) (OMIM: 608354) and Parkes Weber Syndrome (OMIM: 608355) associated with an inactivating *RASA1* mutation which was similar to that in an inducible *Rasa1* knockout mouse model [84, 85].

In this study, we employed NIRF lymphatic imaging to accurately identify abnormal lymphatic phenotypes in two families with members who were diagnosed with congenital, *praecox*, *en tarda*, and secondary (acquired) lymphedema. In these families, we sought to discover gene variants, through unbiased whole exome sequencing (NGS) and analysis of rare single nucleotide polymorphisms (SNPs) with co-segregation analysis based on NIRFLI phenotyping. Using this approach, mutations in the inositol polyphosphate phosphatase-like 1 (*INPPL1*) gene that encodes the src homology 2 domain containing 5'-inositol-phosphatase-2 (SHIP2) were identified in both families.

2.2: NIRFL imaging subjects within two families with variable lymphedema phenotypes

2.2.1: NIRF phenotype in first nucleus family

Investigational NIRFLI consists of 0.1 cc intradermal injections of 25µg indocyanine green (ICG) in saline. Immediately after intradermal administration, ICG is taken up by functional initial lymphatics and transits through collecting and conducting lymphatic vessels. Skin is illuminated with dim near-infrared (NIR) light that penetrates tissues and excites ICG, resulting in near-infrared fluorescence (NIRF) that is collected with a custom intensified camera system [79, 92, 99] (**Figure 1.7**). As illustrated in **Figures 2.1B-D** healthy lymphatics are typically linear and well-defined, without lymphatic abnormalities such as dermal backflow, hyperplastic lymphatic capillaries radiating from injection sites, dilated vessels, or tortuous lymphatics typically observed in diseased subjects as previously shown in **Figures 1.7-1.8**. We conducted lower extremity NIRFLI from a nucleus family of four (**Figure 2.1E-2J**) harboring two probands, sisters aged 32 (Subject #2) and 37 (Subject #1) years old at the time of imaging, who were diagnosed with congenital lymphedema of the lower extremities and with *praecox* lymphedema of the left lower extremity, respectively. Their 58 year old father (Subject #3) had no reports of swelling or any other clinical signs of lymphedema. NIRFLI revealed that his lymphatics appeared normal, with the exception of abnormal lymphatic capillaries radiating from the injection sites on the left foot (**Figure 2.1E**) and medial calf. At the time of study, the 59 year old mother (Subject #4) had not been diagnosed but presented with edema of both ankles, self-reported to initially occur following a minor sprain on her left ankle at 54 years old thus swelling on her right ankle was spontaneous. Upon NIRF imaging and medical examination, her clinical diagnosis was classified as acquired (secondary) lymphedema on the right leg and *en tarda*

lymphedema on the left leg. NIRFLI revealed some additional abnormalities including fluorescent lymphatic capillaries radiating from the injection sites of the left foot (**Figure 2.1F**), dermal backflow on the medial left ankle (**Figure 2.1G**) and tortuosity on the right foot and right medial knee. She also possessed a few varicose veins.

The 37 year old daughter (Subject #1) had been diagnosed with Grade I unilateral lymphedema *praecox* at 14 years of age and possessed generally well-defined lymphatics in the right leg, with the exception of several fluorescent lymphatic capillaries radiating from the injection sites on the foot with some retrograde flow towards the toes. Her right "unaffected" shin also exhibited a lymphatic vessel crossing over just below the knee, indicating abnormality. However, her left edematous foot exhibited dermal backflow (**Figure 2.1H**) with fluorescent lymphatic capillaries radiating from the injection sites on the medial ankle and calf. The 32 year old daughter (Subject #2) had been diagnosed with Grade II bilateral lower extremity, congenital lymphedema at 1 year of age. NIRFLI revealed extensive dermal backflow in both legs as shown in the right foot (**Figure 2.1I**), the right ankle and the left lateral calf (**Figure 2.1J**). In summary, the sister diagnosed with congenital lymphedema (Subject #2) had few, if any, functional lymphatics resulting in extravascular deposition of ICG. In both subjects, other than edema and minimal toe fibrosis and skin cellulitis, there were no additional remarkable clinical signs such as varicose veins, distichiasis, limb hypertrophy, or vascular malformations.

Figure 2.1 Aberrant lymphatic phenotype of familial lymphedema imaged with NIRFLI. **(A)** Schematic illustrating the typical location of the intradermal injections administered in each subject. NIRF images of normal lymphatic vasculature in the (**B**) foot, (**C**) medial ankle, and (**D**) shin as outlined with the dotted lines**. (E-J)** Lymphatic vasculature observed in the nucleus family. The father (Subject #3; unaffected) had well-defined lymphatics in both legs except some lymphatic capillaries radiated from injection sites on the left foot (arrow) (**E**). The mother (Subject #4; *en tarda* in left leg and acquired lymphedema in right leg) had tortuous, lymphatic capillaries (arrows) radiating from injection sites in the left foot (**F**) and an area of dermal backflow (arrow) in the medial ankle (**G**). The older daughter (Subject #1; left unilateral lymphedema *praecox*) had dermal backflow in the left foot (**H**). The younger daughter (Subject #2; bilateral congenital lymphedema) had extensive dermal backflow in both limbs as shown in the right foot (**I**) and left lateral calf (**J**). Injection sites are covered with round adhesive bandages and/or black vinyl tape to avoid camera oversaturation. Scale bar = 1cm. *(Clinical lymphatic imaging conducted under an FDA-approved study (NCT#00833599: "Imaging lymphatic function in normal subjects and in persons with lymphatic disorders") by Germaine D. Agollah, Drs. John C. Rasmussen, I-Chih Tan, Melissa B. Aldrich and Chinmay Darne and clinical investigations conducted by Drs. Caroline E. Fife, Renie Guilliod and Erik A. Maus at Memorial Hermann Hospital Center for Lymphedema Management)*.

Figure 2.1 Aberrant lymphatic phenotype of familial lymphedema imaged with NIRFLI.

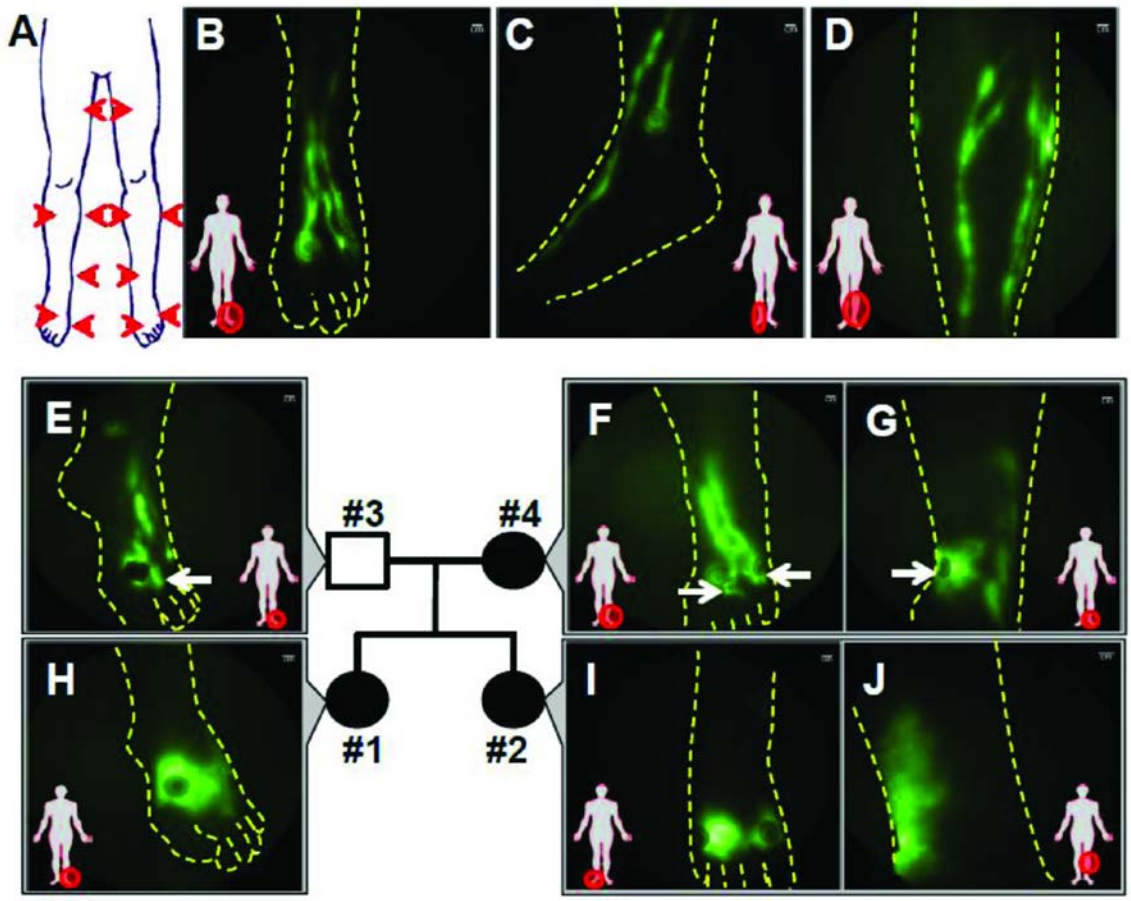

2.2.2: NIRF phenotype in a second family

In a second family (**Figure 2.2A-H**), the 73 year old mother (Subject# 17) presented with severe and disfiguring swelling in her left leg as shown in **Figure 2.2A**. NIRFLI revealed extensive dermal backflow throughout her left leg, as shown in **Figure 2.2B** and **2.2C**. While the conducting lymphatics were observed to be intact in the right leg, fluorescent initial lymphatic capillaries radiated from the injection site on the medial ankle, as shown in **Figure 2.2D**. The mother's 50 year old daughter (Subject #16) also presented with pronounced edema of her left leg, although less severe than her mother's (**Figure 2.2E**), with NIRFLI evidencing extensive dermal backflow throughout the leg (**Figure 2.2F-H**). The lymphatics in her right leg were well-defined, with the exception of fluorescent lymphatic capillaries which radiated from an injection site on the foot. The mother self-reported lymphedema onset at 15 years of age during pregnancy, and was clinically diagnosed at 58 years of age, while the daughter was diagnosed at 46 years of age.

Figure 2.2. Abnormal NIRF phenotype in second nucleus family with lymphedema

Shown clockwise from top left are (**A**) severe swelling in the left leg of mother (Subject #17) with dermal back flow in the left foot (**B**) and shin (**C**). A skin tone color chart is shown in (**A**). Lymphatics in the right leg were better-defined, but abnormalities including (**D**) lymphatic capillaries (arrow) radiating from injection sites were observed. The daughter (Subject #16) presented with less severe swelling in the left leg (**E**), but had dermal backflow in the left foot (**F**) and shin (**G**). The lymphatics in the right leg were well-defined, though lymphatic capillaries (arrow) were observed near injection sites as shown in the right foot (**H**). Injection sites are covered with round adhesive bandages and/or black vinyl tape. Scale bar = 1cm. *(Clinical lymphatic imaging conducted under an FDA-approved study (NCT#00833599: "Imaging lymphatic function in normal subjects and in persons with lymphatic disorders") by Drs. John C. Rasmussen, I-Chih Tan, Melissa B. Aldrich and Chinmay Darne and clinical investigations conducted by Drs. Caroline E. Fife, Renie Guilliod and Erik A. Maus at Memorial Hermann Hospital Center for Lymphedema Management).*

Figure 2.2. Abnormal NIRF phenotype in second nucleus family with lymphedema

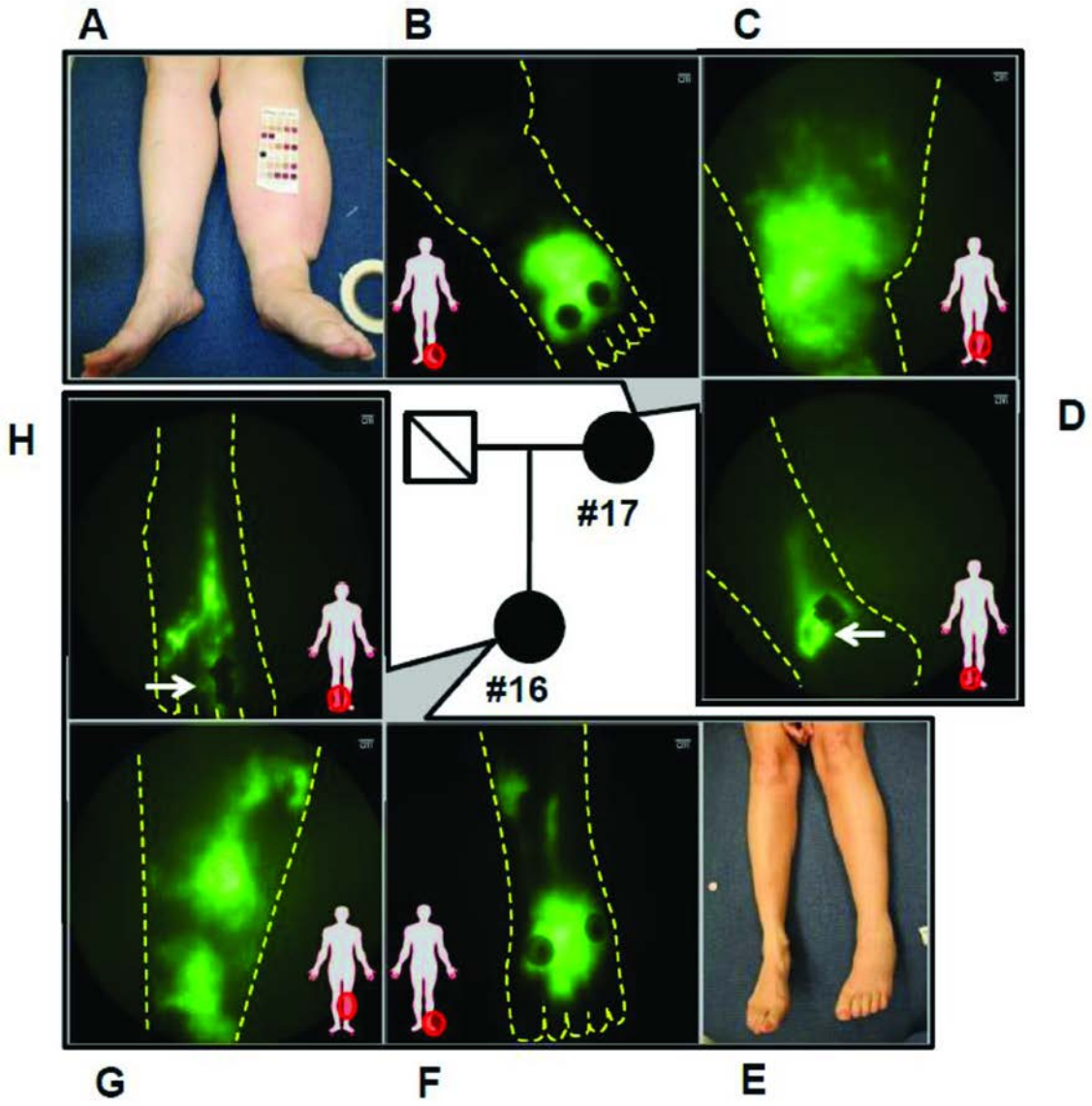

2.3: Identification of *INPPL1* mutations in subjects within two families with variable lymphedema phenotypes

2.3.1: Current strategies in identifying genes involved in lymphatic anomalies

The conventional approach to find genotypes of Mendelian disorders relies on interrogating exons (i.e. protein encoding) and adjacent intron regions by polymerase chain reaction (PCR) amplification techniques such as Sanger sequencing. This requires knowledge of target gene(s) or narrowing down the gene candidates to a manageable number for locus discovery. Following the identification of the *FLT4* gene that encodes VEGFR3; and *VEGFC* gene that encodes VEGFR3 ligand, VEGFC [11, 100], Ferrell *et al*., published the first study that identified *FLT4* as causal for familial lymphedema [101]. In that 1998 study, the authors used traditional genetic linkage analysis, which maps the chromosomal location of disease-causing genes based on the association of co-inherited genes on the same chromosome during meiosis. Subsequently, PCR-based Sanger sequencing was carried out to further identify *FLT4* mutations in familial lymphedema subjects [102, 103]. Further identification of genes important in embryonic development (**Table 1.1**) resulted in linkage analysis and Sanger sequencing used in identification of mutations in *FOXC2, SOX18, CCBE1, GJC2, GATA2, KIF11*, and *PTPN14* in subjects with lymphedema. However, majority of lymphedema patients do not harbor these mutations, and indeed, a recent screening study found that these genes, most which involve VEGFR3 signaling pathway, explain only one third of familial and only 8% of sporadic primary lymphedema [96].

For discovery research, whole exome sequencing (WES) provides a method to sequence all exons (estimated to be ~200,000) to find causal variants without the bias present in candidate gene studies. In addition, variable penetrance and expressivity of known causal genes such as *FLT4* could suggest the participation of otherwise unknown

modifier genes. The diploid human genome consists of 6 billion base pairs of which 90 million base pairs encode for proteins. Whole genome sequencing (WGS) accesses the entire genome including protein encoding regions (or exons) and non-protein encoding regions (or introns) and represents the most comprehensive approach to human genetic study. In contrast, mutations in protein encoding portions of the genome, called the exome, are most likely to cause gain or loss of functions that are responsible for ~95% of diseases, yet represents only ~2% of the entire genome. Consequently, WES currently represents the most cost-efficient manner to make new gene discoveries that, as opposed to WGS, can be translated into pharmacologic strategies.

WES involves probe-specific exon capture of targeted sequences from genomic DNA, followed by deep sequencing on commercially available next-generation sequencing platforms, greatly expanding the capacity of traditional targeted sequencing. Following bioinformatics analysis to identify potential candidate genes, their presence can be further validated by traditional Sanger sequencing. Furthermore, pathway analysis can be used to identify key signaling pathways that are affected by these identified candidate genes. Recently, the use of WES has been proposed as a more efficient method to identify genetic variants for lymphedema [96, 104].

2.3.2: Identification of T180A SHIP2 mutation in first nucleus family

There were no other siblings in the first nucleus family depicted in **Figure 2.1**, but with next generation sequencing (NGS) and cosegregation bioinformatics analyses, as little as four members are needed to discover new disease causative gene variants [97], provided accurate phenotyping with NIRFLI could identify affected family members. We collected blood and extracted DNA from this nucleus family (Subjects #1-4) and conducted WES. Our results showed both probands from the nucleus family possessed

a rare, heterozygous, damaging SNP (i.e. likely to alter the normal function of the gene or the encoded protein) within the alpha-chain of *HGF* (81359017 Hg19 resulting in C >A; p.G315V), but not in any other gene previously associated with lymphatic dysfunction. In their gene candidate studies, Finegold and coworkers [63] found *HGF* and *cMET* mutations in subjects with primary lymphedema, lymphangiectasia, and breast cancer-related lymphedema (BCRL) subjects that were not polymorphic in control populations. They concluded that *HGF* and *cMET* mutations were likely causal for primary lymphedema and/or susceptibility genes for acquired lymphedema, an affliction that impacts an estimated 15% of all cancer survivors [67]. HGF and cMET are both important for lymphatic vessel formation [105]. Additionally, because Saito *et al* [106] showed that HGF gene therapy reduced lymphedema volume in the rat tail lymphedema model created by lymphatic vessel disruption, we expected the mother in our study to harbor the *HGF* gene mutation, making her susceptible to her diagnosed acquired or *en tarda* form of lymphedema. However, she lacked the *HGF* gene variant. Surprisingly, the asymptomatic father who did not possess an abnormal NIRFLI phenotype had passed the *HGF* gene variant to his daughters.

As no other lymphedema-related genes were identified in this family, we conducted WES bioinformatics analyses to identify rare SNPs which could be likely causative or could increase susceptibility to lymphedema. Given that HGF could not explain lymphatic disease in the mother (Subject #4), and the varied penetrance of lymphedema in this family, we conducted pathway analysis with the goal of identifying potential HGF-modifier genes that could have been inherited from the mother that contribute to the probands' disease. We identified a rare, heterozygous missense mutation in *INPPL1*, which encodes SHIP2, in the probands (Subjects #1 and #2) and in their mother (Subject #4), but not in their father (Subject #3). This *SHIP2* mutation

results in the conversion of threonine 180, located carboxyl to the SH2 domain, to alanine (p.T180A) (**Figure 2.3C**). The T180A *INPPL1* mutation was validated by Sanger sequencing (**Figure 2.3A**), but we did not confirm that mRNAs encoding T180A SHIP2 protein was produced in affected individuals, nor RNAseq since the tissue biopsy required for RNAseq is well-known to be associated with an increased risk for infection in lymphedema subjects. While an *INPPL1* SNP at 71940154 (C>G; Hg19) resulting in T180S has been previously reported (rs376749049), our identified SNP at 71940153 (A>G; Hg19) resulting in T180A, has not been reported in SNP databases. The genomic region that harbors the *INPPL1* gene is unique, in particular the area surrounding the T180A mutation. To verify this mutation was not in an intronic region, we performed a blast analysis ± 100 bp on each flanking region, and there was a single hit on *INPPL1*. NM_001567 is the single transcript for *INPPL1* and there are no alternative splice versions, in addition RNAseq experiments identify the correct exons described in the gene model. The mutation that we describe in Hg19 chr11:71940153 corresponds to the codon 180 of exon 5 of SHIP2. This particular region is evolutionary conserved, free of repeat elements and with no common SNPs reported, consequently we consider *INPPL1* an evolutionary conserved gene with low tolerance for mutations. An overview of SHIP2 is discussed below in **Section 2.4**.

2.3.3: Identification of L632I SHIP2 mutation in second nucleus family

In the second family, WES results identified two missense mutations in the lymphatic receptor, VEGFR3, encoded by *FLT4*. The mother (Subject# 17) and daughter (Subject #16) shared a rare and damaging D481E mutation and an H890Q mutation which is benign and likely a natural variant. Mutations were predicted as either benign or damaging based on potential functional impact by at least two of three software tools (See **Chapter 6** Materials and Methods for details). It is of note this D481E mutation is

the first identified *VEGFR3* mutation outside the intracellular kinase domain in subjects with lymphedema. Additionally, we found another rare heterozygous missense SHIP2 mutation in the mother with more severe lymphedema (**Figure 2.2A**) while the daughter, who has less severe disease (**Figure 2.2E**), did not possess the SHIP2 mutation. This SHIP2 mutation results in the substitution of leucine 632, located in the catalytic domain of SHIP2, by an isoleucine residue (p.L632I). Both T180A and L632I SHIP2 mutations were validated by Sanger sequencing (**Figure 2.3A-B**) and shown in **Figure 2.3C** are the location of these mutations within the SHIP2 protein**. Table 2.1** shows the summary of these two SHIP2 mutations and the mutations in lymphatic receptor tyrosine kinases (RTKs)-related genes, *HGF* and *FLT4*.

Figure 2.3. Validation of whole exome sequencing (WES) by Sanger sequencing showing chromatograms of SHIP2 SNPs. (**A**) Family 1 (Subjects #1-4) at position of interest (highlighted in yellow), both alleles in Subject #3 contain adenosine (A; green peak) while Subjects #1, #2, and #4 have heterozygous SNPs at the same position, one containing adenosine (A; green peak) and the 2nd containing guanosine (G; black peak). This SNP results in amino acid codon change from threonine to alanine at the 180 residue of SHIP2 protein. (**B**) In Family 2 (Subjects #16 and #17) at position of interest, the mother (Subject #17) has heterozygous SNP; one containing cytosine (C; blue peak) and the 2nd containing adenosine (A; green peak). This SNP results in amino acid codon change from leucine to isoleucine at the 632 residue of SHIP2 protein. The daughter (Subject #16) does not possess this SNP. Positive (forward) strands shown. (**C**) Schematic of the SHIP2 protein indicating its domains with the two identified mutations at T180A (Family #1) outside the src homology 2 (SH2) domain and L632I (Family #2) within the catalytic 5'-phosphatase domain. *(Dr. Manuel L.Gonzalez-Garay analyzed whole exome sequencing and bioinformatics data and Germaine D. Agollah and Otis Hall performed Sanger sequencing validation).*

Figure 2.3 Validation of whole exome sequencing (WES) by Sanger sequencing showing chromatograms of SHIP2 SNPs

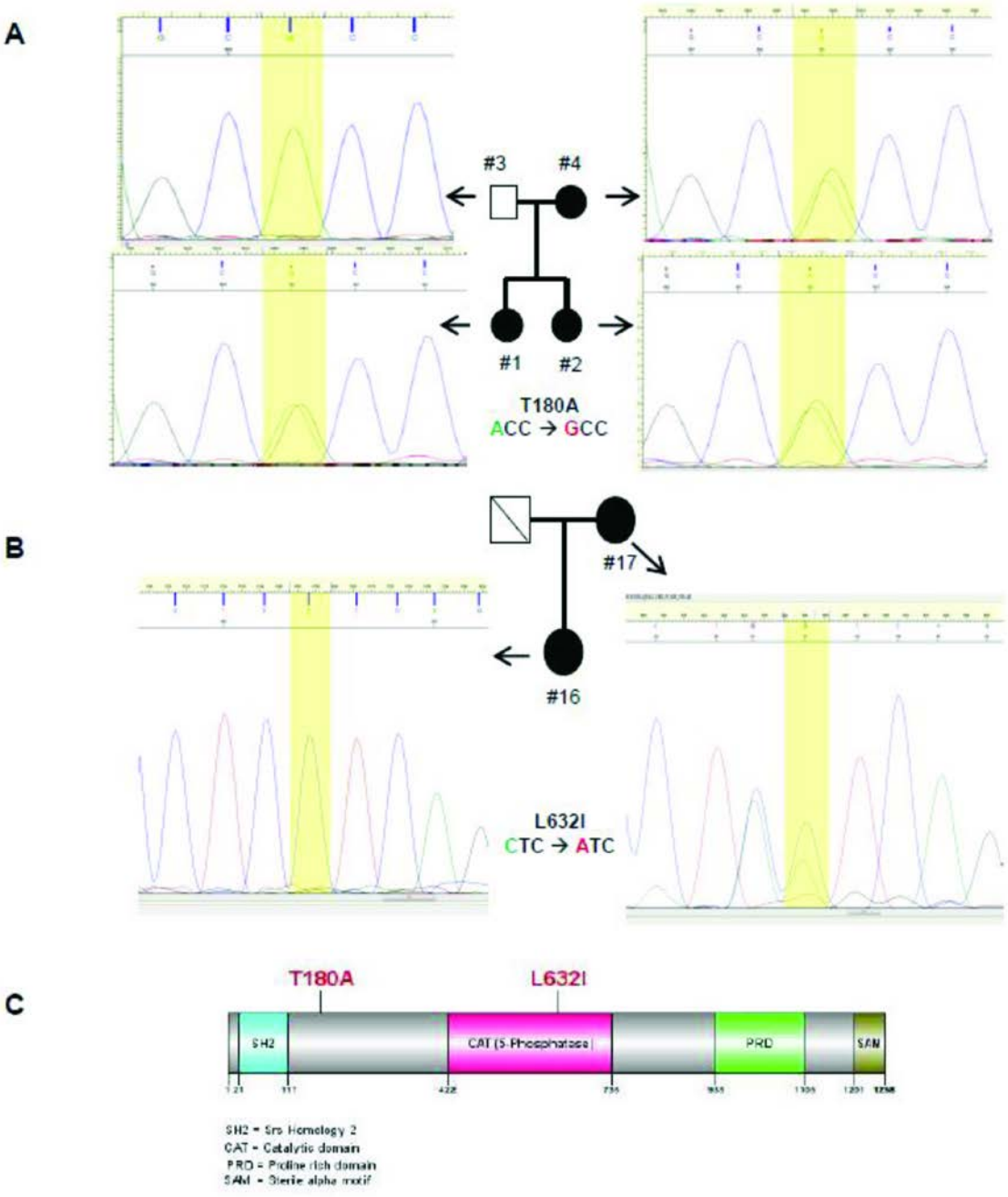

Table 2.1 List of SHIP2 (*INPPL1*) mutations and lymphatic-related RTK mutations identified by whole exome sequencing (WES) and validated by Sanger sequencing showing chromosomal location, nucleotide base change, zygosity and amino acid change.

Nucleus Family #1

Gene	Subject #1	Subject #2	Subject #3	Subject #4	Chromosome	Location (Hg 19)	Nucleotide change	Zygocity	Amino acid change
INPPL1	Yes	Yes	No	Yes	chr11	71940153	A -> G	Heterozygote	T180A
HGF	Yes	Yes	Yes	No	chr7	81359017	C -> A	Heterozygote	G315V

Nucleus Family #2

Gene	Subject #16	Subject #17	Chromosome	Location (Hg 19)	Nucleotide change	Zygocity	Amino acid change
INPPL1	No	Yes	chr11	72232917	C->A	Heterozygote	L632I
FLT4	Yes	Yes	chr5	180624040	G->T	Heterozygote	D481E
FLT4	Yes	Yes	chr5	180619344	G->C	Heterozygote	H890Q

2.3.4: Further identification of T180A SHIP2 within extended family

Clinical evaluation of the nucleus family depicted in **Figure 2.1** revealed that there were other extended family members with lymphedema. We therefore further conducted NIRFLI and/or WES studies on 11 additional maternal family members. Out of the eleven extended family subjects, excluding the nucleus family, five other subjects (Subjects #5, 6, 7, 11, and 13) were previously diagnosed with lymphedema (**Figure 2.4A**). Seven subjects (including nucleus family) were phenotyped with NIRFLI and genotyped with WES, of which five subjects harbored the T180A SHIP2 mutation, which was validated by Sanger sequencing. Of those five subjects, four subjects (Subjects #1,2, 4 and 6) were diagnosed with lymphedema and one subject (Subject #12) was unaffected but her NIRFLI phenotype revealed vessel tortuosity, small fluorescent vessels radiating from injection sites, and dilated vessels (**Figure 2.4D**). Her 30 year old daughter (Subject #13) was diagnosed with bilateral lower extremity *praecox* lymphedema at 13 years and also harbored T180A SHIP2. No clinical information was available for Subject #13's father. Subject #6 had swollen ankles and arms with venous insufficiency, and NIRF imaging revealed dermal backflow in her medial left ankle with diffuse dye uptake (**Figure 2.4B**), fluorescent vessels radiating from injection sites on thighs and limited lymphatic propulsion. The lymphatics of Subject #9 (unaffected) were mostly well defined but we observed slight tortuosity with fluorescent lymphatic capillaries radiating from injection site on medial ankle (**Figure 2.4C**). All 15 subjects were genotyped with WES, and no other lymphedema-related genes were identified, however a mutation of a gene encoding a protein within the MAPK/ERK pathway (*MAP3K7*) was identified in Subjects# 1, 2, 4, 7, 9, 12 and 13. Out of these seven subjects with *MAP3K7* mutation (Hg19 chr6:91229032; T > C) five of them were diagnosed with lymphedema (except Subjects #9 and 12) and also harbored the T180A SHIP2 mutation. The rare *MAP3K7* SNP, which results in p.N463S, has been reported in

SNP databases (rs375179983), but has not yet been associated with any human disease. The frequency of the *MAP3K7* mutation within 6500 exomes is very low (0.01%) and the resultant protein change is predicted to the functionally damaging by PolyPhen-2 software. Of the total 15 subjects, 8 subjects were not imaged and thus are incomplete phenotypes. Out of these eight subjects, four were diagnosed with lymphedema, of which three have T180A SHIP2. In Subjects #5 and #11, SHIP2 has no contributory role to their lymphedema but both subjects had later onset of symptoms (27yrs and 47yrs respectively) and additional lymphatic insults which either exacerbated (breast cancer surgery in Subject #5) or triggered edema (self-reported >14hour long flight in Subject #11). Two subjects (#8 and #14) were unaffected by symptoms, yet harbor the T180A SHIP2 mutation, however, it remains unknown whether these have any NIRFLI lymphatic phenotype or will encounter symptoms upon an injury, as did Subject #4. All subjects with lymphedema had lower extremity disease, except Subject #6 who had both upper and lower extremity lymphedema. There were no other lymphatic abnormalities such as chylous ascites or chylothorax reported in this family. While we did not estimate the mutation rate or penetrance of the T180A polymorphism in this family, 9 of 15 subjects harbored the SHIP2 mutation, and 6 of the 9 subjects diagnosed with lymphedema. Results of this nucleus and their extended family are summarized in **Table 2.2**.

Figure 2.4. Identification of T180A SHIP2 mutation in familial lymphedema. (**A**) Pedigree of the nucleus and extended family showing affected (filled) and unaffected (open) subjects with lymphedema, phenotyped by NIRF imaging and WES analysis revealing subjects who harbor T180A SHIP2, G315V HGF and N463S MAP3K7 mutations. NIRF imaging reveals (**B)** dermal backflow in medial left ankle of Subject #6 (bilateral lymphedema *praecox*) and also has abnormal lymphatic capillaries on thigh (not shown). (**C**) Abnormal lymphatic capillaries radiating from the injection site on the medial left ankle of Subject #9 which were also observed capillaries on the thigh on this unaffected subject. (**D**) Tortuous lymphatics draining the medial left ankle and lymphatic capillaries radiating from the left medial calf in Subject #12 (unaffected). All three subjects appeared to have dilated lymphatics also. *(Clinical lymphatic imaging conducted under an FDA-approved study (NCT#00833599: "Imaging lymphatic function in normal subjects and in persons with lymphatic disorders") by Germaine D. Agollah, Drs. John C. Rasmussen, I-Chih Tan, Melissa B. Aldrich and Chinmay Darne and clinical investigations conducted by Drs. Caroline E. Fife, Renie Guilliod and Erik A. Maus at Memorial Hermann Hospital Center for Lymphedema Management. Dr. Manuel L.Gonzalez-Garay analyzed whole exome sequencing and bioinformatics data and Germaine D. Agollah and Otis Hall performed Sanger sequencing validation).*

Figure 2.4. Identification of T180A SHIP2 mutation in familial lymphedema

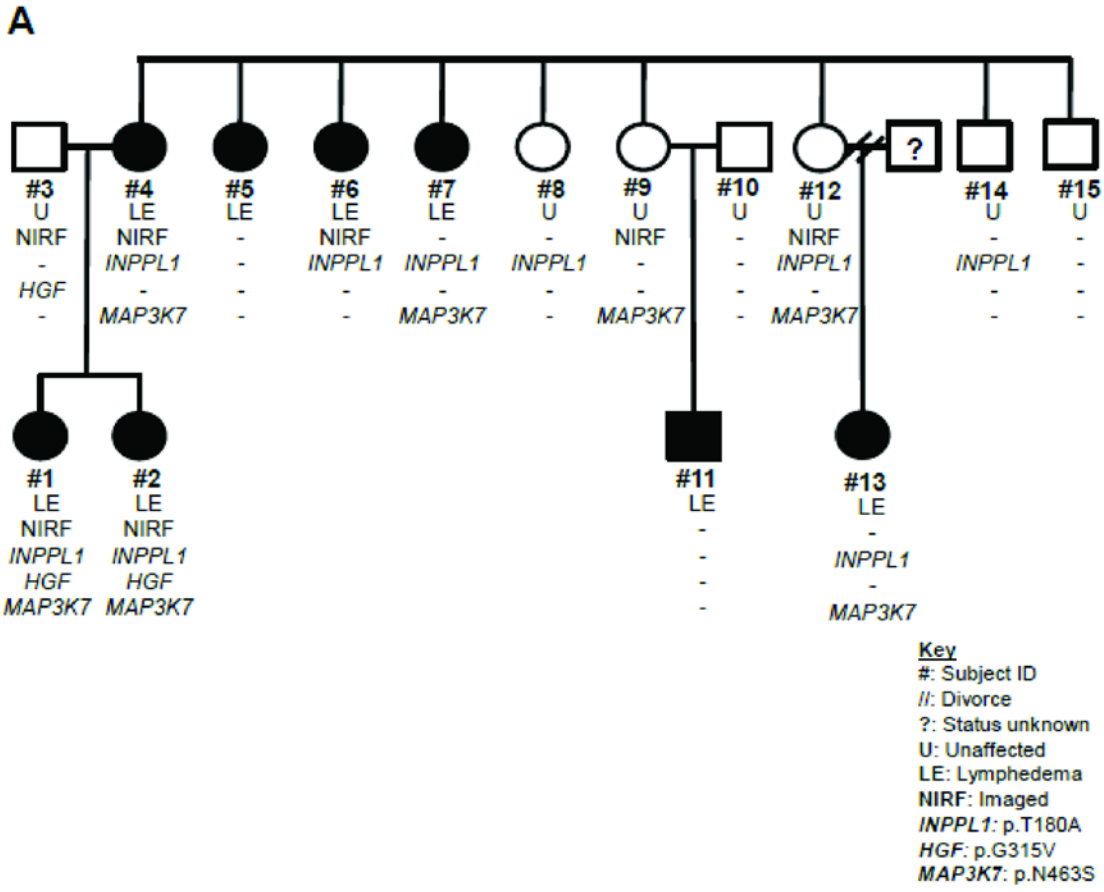

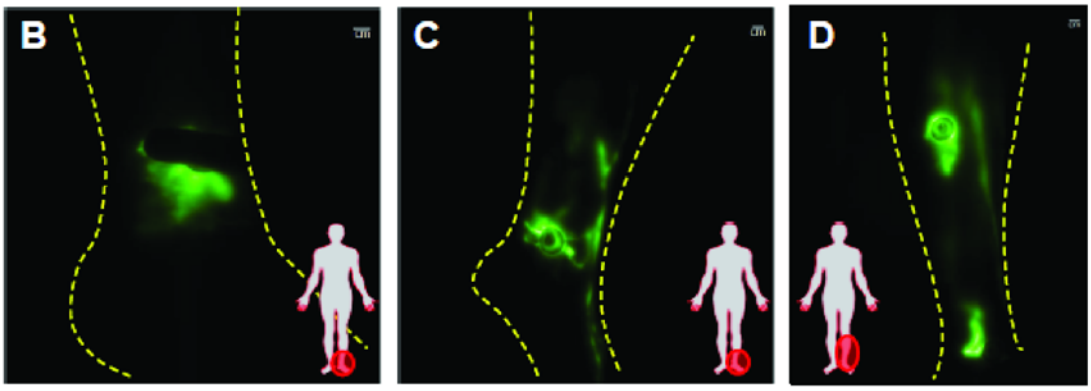

Table 2.2: Summary of lymphedema diagnosis and T180A SHIP2 status in nucleus (**Figure 2.1**) and their extended family

	Relation	Subject	*INPPL1* p.T180A	Lymphedema Diagnosis	Onset of Symptoms	Age at Study	NIRF Phenotype	Comments
Nucleus Family	Proband	#1	Yes	*Praecox*	14	37	Abnormal	Diagnosed Grade I left unilateral lower extremity LE on dorsum of left foot. Minimal fibrosis at base of toes
	Proband	#2	Yes	Congenital	1	32	Abnormal	Diagnosed Grade II bilateral lower extremity LE from knees down. Skin cellulitis.
	Father	#3	No	Unaffected	N/A	58	Normal	N/A
	Mother	#4	Yes	*en tarda (*left) Acquired (right)	54	59	Abnormal	Diagnosed Grade I right leg; Grade II left leg. Minor left ankle sprain preceded symptoms on both legs. Few varicose veins.
Extended Family	Maternal Aunt	#5	No	*Praecox*	27	58	N/A	Bilateral LE in both legs, ankles and feet. Mild edema in both arms following breast cancer bilateral lymph node dissection surgery. Venous insufficiency
	Maternal Aunt	#6	Yes	*Praecox*	8 (legs) 15(hands)	63	Abnormal	Bilateral LE in both legs, both hands and arms. Visible enlarged veins and telangiectasia. Venous insufficiency
	Maternal Aunt	#7	Yes	*Praecox*	20	61	N/A	Bilateral LE in both legs, feet and toes
	Maternal Aunt	#8	Yes	Unaffected	N/A	50	N/A	N/A
	Maternal Aunt	#9	No	Unaffected	N/A	69	Some abnormality	N/A
	Uncle (by marriage)	#10	No	Unaffected	N/A	77	N/A	N/A
	Maternal Male Cousin	#11	No	*en tarda*	47	50	N/A	Unilateral left foot LE; long >14hr flight preceded symptoms.
	Maternal Aunt	#12	Yes	Unaffected	N/A	54	Abnormal	N/A
	Maternal Female Cousin	#13	Yes	*Praecox*	13	30	N/A	Mild edema in both legs below the knee.
	Maternal Uncle	#14	Yes	Unaffected	N/A	48	N/A	N/A
	Maternal Uncle	#15	No	Unaffected	N/A	55	N/A	N/A

In summary of these clinical studies, the results of WES analysis combined with NIRFLI phenotyping suggested that T180A and L632I SHIP2 mutations may *contribute to but do not necessarily cause* lymphatic dysfunction. Furthermore, these analyses show that in these families, lymphatic abnormalities are more severe and of earlier onset in individuals with additional mutations in genes that have been associated with lymphatic disease previously, such as *HGF*, *FLT4* or within MAPK/ERK signaling pathway [44, 63, 81, 102] suggesting that SHIP2 may be a modifier of lymphatic dysfunction. Based on these clinical findings as well as previous reports that SHIP2 physically associates with cMET [107], we investigated a potential function for SHIP2 in lymphatic endothelial cells (LEC), which will be the focus of **Chapter 3**.

2.4: Overview of Src Homology 2- domain containing 5'-inositol phosphatase-2 (SHIP2)

2.4.1: Introduction

In response to external stimuli, cellular receptors become activated and recruit enzymes which generate second messengers. For example phosphatidylinositol-3,4,5-triphosphate (PI-3,4,5-P3 or PIP3) is a membrane lipid-derived second messenger that subsequently recruits pleckstrin homology (PH)-containing signaling molecules, such as protein kinase B or AKT, to the plasma membrane [108]. Upon activation, AKT translocates to the cytoplasm to further activate other downstream targets *via* phosphorylation. Consequences of this signaling include among others, cell proliferation, cell survival, and cytoskeletal reorganization. Cellular levels of PI-3,4,5-P3 are controlled in two ways: positive generation in response to growth factors and other external stimuli; and negative regulation by phosphoinositide (PI) phosphatase enzymes. Two pathways degrade PI-3,4,5-P3: (i) phosphatase and tensin homologue (PTEN) that hydrolyzes

PIP3 at the 3'-position of the inositol ring to produce PI-4,5-P2 and (ii) by 5'-inositol phosphatases to generate PI-3,4-P2. One such 5'-phosphatase is src homology 2-domain containing 5'-inositol phosphatase-2 (SHIP2), the focus of this dissertation.

2.4.2: Structure and functions of SHIP2

Inositol polyphosphate 5'-phosphatase-like protein 1 (*INPPL1*) on chromosome 11q23 (human), encodes SHIP2, a 142kD protein which contains an amino (N)-terminal SH2 domain, a central catalytic 5-phosphatase domain, a potential phosphotyrosine-binding (PTB) consensus sequences (NPXY), a proline-rich domain (PRD) and a sterile alpha motif (SAM) in the carboxy (C)-terminal (**Figure 2.3C**) [108, 109]. Mouse SHIP2 (on chromosome 7) shares 95% homology with human SHIP2 and 98% with rat SHIP2 (on chromosome 1) [110]. Beyond the catalytic function of SHIP2 which is mediated by the 5'-phosphatase domain, the other motifs of SHIP2 mediate interactions with various proteins to effect diverse cellular functions. The SH2 domain of SHIP2 interacts with p130CAS, src homology and collagen homology (Shc) and the HGF receptor, cMET to affect cell adhesion, cell scattering and cell spreading in various cellular contexts [107, 111, 112]. *Via* its PRD domain, SHIP2 interacts with filamin, c-Cbl, c-Cbl-associated protein (CAP), vinexin and JNK-interacting protein 1 and epidermal growth factor receptor (EGFR) [113-117]. The SAM domain of SHIP2 interacts with Arap3 and ephrin A2 (EphA2) receptor while the adaptor protein with a PH and SH2 domain (APS) binds the 5'-phosphatase domain of SHIP2 and enhances its catalytic activity [108]. These binding partners of SHIP2 are summarized in **Figure 2.5**. Recent evidence also shows that SHIP2 binds protein phosphatase 2A (PP2A), SH3 domain containing Ysc84-like 1 (SH3YL1) and the small GTPase, RhoA, to effect endocytosis, ruffle formation, cell polarity and migration [118-120].

In humans SHIP2 is widely expressed, with higher levels in the heart, placenta, brain and skeletal muscle but SHIP2 shows ubiquitous expression in most tissues in rodents [108, 110]. In quiescent cells, SHIP2 is in the cytosol and translocates to the plasma membrane following growth factor stimulation and to membrane ruffles during cell adhesion [109]. SHIP2 also undergoes tyrosine phosphorylation at its NPXY motif which contributes to its translocation and likely catalytic phosphatase function [108]. In all, both its catalytic and scaffolding capabilities allows SHIP2 to exert its influence on various cellular functions.

Figure 2.5. Binding partners of SHIP2. The 1258 amino acid protein comprises of a N-terminal SH2 domain, a central catalytic 5-phosphatase domain (5-CAT), a proline-rich domain (PRD) including NPXY sequences and a C-terminal sterile alpha-motif (SAM) domain. Also shown are binding partners of SHIP2.

Adapted from Suwa, A., Kurama, T., and Shimokawa, T., *SHIP2 and its involvement in various diseases.* Expert Opin Ther Targets, 2010. **14**(7): p. 727-37. [108].

Figure 2.5. Binding partners of SHIP2

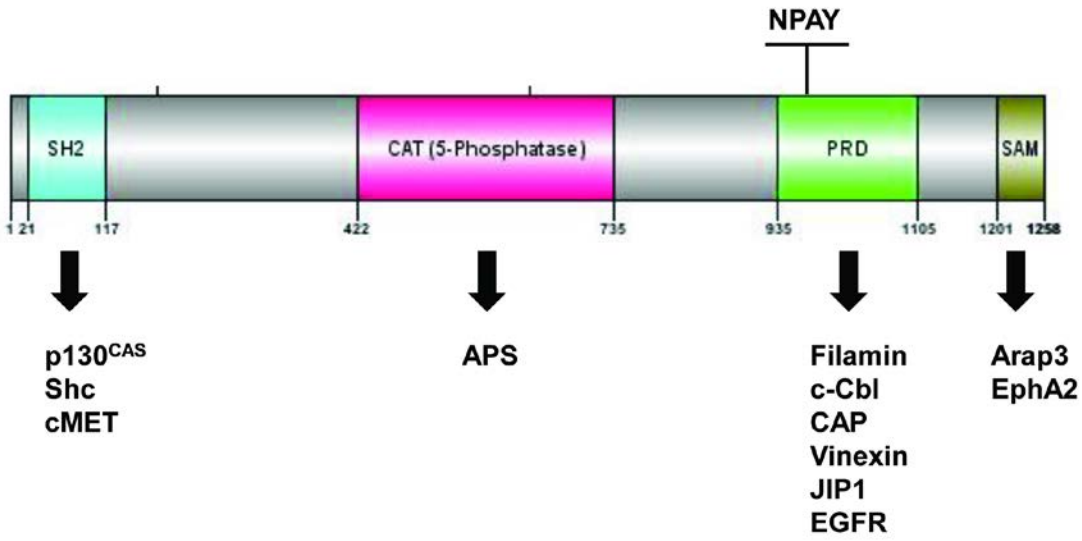

2.4.3: Role of SHIP2 in disease

SHIP2 in insulin signaling and Type 2 diabetes. Perhaps the most well studied role of SHIP2 in disease is its involvement in insulin signaling. SHIP2 negatively regulates PI3K-generated PIP3 in response to insulin stimulation and inhibits phosphorylation of AKT2, which is ultimately important in glucose uptake. Interestingly, SHIP2 does not regulate insulin-induced phosphorylation of AKT1 [108]. Genetic mouse models of *Ship2* exhibit disordered insulin signaling. In the first reported model by Clement *et al.* in which the first 18 exons covering SH2 and 5'-catalytic domains were left intact and last exons #19-28 deleted, *Ship2*$^{-/-}$ mice exhibited severe neonatal hypoglycemia and death within three days, while *Ship2*$^{+/-}$ mice showed enhanced insulin sensitivity [121]. However, in this model, a neighboring gene *Phox2a* was also inadvertently deleted. A second mouse model by Sleeman *et al*., addressed this problem by deleting the first 18 exons and replacing them with a gene reporter while exons 19-28 were left intact [122]. In this second model, *Ship2*$^{-/-}$ mice were viable with normal glucose and insulin levels, and interestingly, were resistant to weight gain even on high fat diets and also exhibited increased metabolic rates. A more recent mouse model by Dubois *et al*., in which *Ship2* is fully expressed but catalytically inactive, shows that homozygote mutant mice are viable with defects in lipid metabolism and insulin secretion but with no effect on glucose tolerance, insulin sensitivity nor insulin-induced Akt activation [123]. On the other hand, transgenic mice over-expressing *Ship2* show reduced insulin-induced Akt activation, gained more weight with increased insulin levels but normal glucose levels [124]. *Ship2* mutations have been identified in the Type 2 diabetic and hypertensive rat strain, Goto Kakizaki (GK), while the diabetic mouse strain *db/db* exhibits increased Ship2 protein levels [125]. Combined, these studies highlight the importance of SHIP2 in insulin signaling and in maintenance of glucose metabolism.

In humans, SHIP2 polymorphisms have been identified in metabolic syndrome, which is characterized by Type 2 diabetes, hypertension, abdominal obesity, and insulin resistance [125]. A study of Japanese subjects identified the L632I SHIP2 mutation in more control subjects than in diabetic subjects, and transfection of mutant L632I-SHIP2 into Chinese hamster ovary cells overexpressing human insulin receptors (CHO-IR) showed that L632I reduced SHIP2-mediated negative regulation of insulin signaling leading to the authors' conclusion that L632I is protective against insulin resistance in the Japanese population. However, the authors acknowledge that since Japanese Type 2 diabetes genetically differs from both North American and European Caucasians' disease, therefore the effect of this mutation and of SHIP2 in general, could differ depending on the studied ethnic group [126]. Nonetheless taken together, these rodent and human studies highlight the key role that SHIP2 plays in insulin signaling and obesity.

Role of SHIP2 in cancer. SHIP2 has been controversially implicated in cancer, suggested to play both proto-oncogenic and tumor-suppressive roles in human and murine models. As a proto-oncogene, SHIP2 expression has been found to be increased in breast cancer cell lines and in clinical specimens of breast cancer tissues, non-small cell lung cancer (NSCLC), and hepatocellular carcinoma (HCC), all of which correlate with poor prognosis [127-129]. Overexpression of SHIP2 in breast cancer cells increased their proliferation, while SHIP2 suppression reduced tumor growth and lung metastases in nude mice [117]. Recently, SHIP2 has been found to be overexpressed in breast cancer stem cells (BCSCs) with targeted SHIP2 silencing *via* RNAi and pharmacological inhibition resulting in reduced tumorigenicity, while SHIP2 overexpression enhanced epithelial-mesechymal transition (EMT) markers promoting breast cancer metastasis [130].

In contrast, SHIP2 has also been shown to have tumor-suppressive effects. As an inhibitor of PI3K/AKT signaling, a well-established oncogenic pathway that often increases cell growth, a positive oncogenic role for SHIP2 is understandably controversial. SHIP2 overexpression in glioblastoma brain cancer cells and in K562 erythroleukemia cells reduced their cell growth and proliferation [131, 132]. Of importance, miRNA-205 suppresses SHIP2 expression in squamous cell epithelium and squamous cell carcinoma (SCC) cells express elevated levels of miRNA-205 correlating with reduced SHIP2 expression and increased AKT phosphorylation [133]. Inhibition of miRNA-205 induces SHIP2 expression and expectedly decreased AKT phosphorylation. Since miRNA-205 is upregulated in kidney, bladder and ovarian cancers, but downregulated in breast and prostate cancers, it is likely that the contradictory role of SHIP2 as a proto-oncogene and a tumor-suppressor might be explained with expression of miRNA-205 in these cancers [108, 125].

SHIP2 in neurodegenerative disease and atherosclerosis. Other diseases in which SHIP2 plays a regulatory role are neurodegenerative diseases and atherosclerosis, both involving the capacity of SHIP2 to suppress PI3K/AKT signaling. Specifically, SHIP2 inhibits nerve growth factor (NGF)- and insulin growth factor 1 (IGF1)-induced PI3K/AKT activation leading to GSK-3β phosphorylation and activation of Tau, a microtubule-associated protein which is often hyperphosphorylated in Alzheimer's disease [134-137]. In atherosclerosis, SHIP2 inhibits platelet derived growth factor (PDGF)- and IGF1-induced PI3K/AKT activation leading to apoptosis of vascular smooth muscle cells (VSMCs), an event that leads to rupture of protective fibrous caps and deposition of a thrombus, followed by acute myocardial infarction. Additionally, following binding of the low density lipoprotein (LDL) receptor by apolipoprotein E4 (APOE4), SHIP2 can be recruited to the intracellular region of the LDL receptor resulting in

hydrolysis of PIP3 to inhibit AKT activation in umbilical vein endothelial cells, thus increasing the risk for atherosclerosis [138]. Interestingly, APOE4 is one of the major genetic risk factors for Alzheimer's disease, therefore it remains to be seen whether this novel APOE4-SHIP2 model applies to Alzheimer's disease as well [108].

In summary, the effects of SHIP2 seem to be context specific by being able to exert its influence depending on the specific cell and tissue type: for example SHIP2 can regulate AKT2 but not AKT1 during insulin signaling in skeletal muscle and adipose cells, and specifically regulate AKT1 signaling in cancer. With the involvement of PI3K/AKT pathway in various diseases, including lymphatic diseases (**Table 1.3**), it is not surprising that SHIP2, a negative regulator of this pathway is also involved in these pathologies.

2.5: Discussion

We report here two separate families with inherited lymphedema with distinct heterozygous non-synonymous rare mutations in the *INPPL1* gene that encodes the SHIP2 enzymatic and scaffolding protein. In addition, heterozygous damaging mutations in the *HGF* gene that encodes HGF or the *FLT4* gene that encodes VEGFR3 were identified in the two families. Mutations in *HGF* and *FLT4* have been associated with lymphedema beforehand [63, 102]. Of the two SHIP2 mutations that were identified in families, one (T180A) is located carboxy terminal to the SH2 domain whereas the other (L632I) is located within the catalytic domain (**Figure 2.3C**). Interestingly, individuals in these families that harbored mutations in both *INPPL1* and *HGF* or *INPPL1* and *VEGFR3* showed more severe lymphatic symptoms. Further WES analyses of the extended family from the first nucleus family identify this T180A SHIP2 mutation in 6

other subjects, 3 of whom have various diagnoses of lymphedema. This SHIP2 mutation also overlaps with a mutation of a gene within the MAPK/ERK signaling pathway, *MAP3K7*, in 5 individuals with lymphedema. However, while computationally predicted to be damaging, it remains to be biologically validated whether MAP3K7 specifically has a cellular functional role in LEC. Nonetheless, our findings implicate SHIP2 as a regulator of lymphatic function in humans and that inherited mutations in the *INPPL1* gene may act in concert with *HGF* and *VEGFR3,* and likely *MAP3K7*, mutations to exacerbate lymphatic phenotypes.

High penetrance genes associated with lymphedema, such as *VEGFR3*, exhibit the standard, rare Mendelian inheritance pattern in patients with an extreme phenotype. However, since lymphatic abnormalities most likely arise from the interplay between several genes and environmental factors as in the case of many other disorders, lymphedema likely cannot only be attributed to single, high penetrance genes. For the majority of the more common disorders such as stroke, hypertension, obesity, autism, schizophrenia, bipolar disorder, etc. a large number of genes are involved with each one contributing to the disorder. This situation may be expected in non-syndromic primary lymphedema, since only *VEGFC/VEGFR3* axis genes that have been identified as the sole source of the disorder (**Table 1.3**), yet 64% of patients with familial history and 92% of patients with sporadic non-syndromic lymphedema do not harbor these mutations [44, 96]. Inherited heterozygous mutations in *SHIP2* **<u>together</u>** with germline heterozygous mutations in other lymphatic-regulating genes may be sufficient for the development of lymphedema. Ideally, as evidenced by the variable phenotypes in our subjects, screening of families with syndromic lymphatic dysfunction for *INPPL1* mutations could be informative and substantiate the variable penetrance that is normally observed in

lymphatic disorders. Additonally, as suggested by NIRFLI phenotyping of aberrant lymphatic architecture and function in asymptomatic subjects, variations in normal physiologic challenges such as puberty, pregnancy, immune insults, or mechanical injury could provide physiologic and/or environmental second-hits that could account for the differences in disease expressivity and age of onset in subjects.

Recently both homozygous and heterozygous mutations in SHIP2 have been reported in a rare skeletal disorder, opsismodysplasia (OMIM: 258480) in both unrelated and consanguineous family members [139, 140]. Furthermore, while SHIP2 has been implicated in obesity, diabetes and insulin resistance in rodents [121-124] and in humans [126, 141, 142]; and has been suggested to have proto-oncogenic roles in human breast cancer, non-small cell lung cancer (NSCLC), and hepatocellular carcinoma (HCC) worsening patient outcomes [127-129], and paradoxically, a tumor-suppressive role in squamous cell carcinoma (SCC) [133], SHIP2 has not been associated with vascular disorders. However, PTEN, which similarly to SHIP2, is a negative regulator of PI3K/AKT signaling, has been implicated in lymphatic malformations specifically Proteus-like syndrome, exhibiting medium penetrance and loss-of-function phenotype [143]. Thus, it may be expected, but remains to be tested in genetic mouse models, whether SHIP2 plays a primary role in lymphangiogenesis and lymphatic vessel maintenance. To our knowledge, the only previous evidence suggesting a role of SHIP2 in lymphatic biology is a recent transcriptomic microarray study using paired punch biopsy samples of human lymphedema tissue versus normal samples. In that study, among ~8400 differentially expressed genes, *INPPL1* was found to have reduced expression in lymphedematous tissue samples suggesting a role for this protein in lymphatic function [71].

2.6: Significance

Discovery of variants responsible for inherited lymphatic abnormalities has been limited by candidate gene searches and inaccurate phenotyping which is often based on late-stage, overt symptomatic presentation. We address these two issues by (i) employing near-infrared fluorescence lymphatic imaging (NIRFLI) to accurately identify abnormal lymphatic phenotypes in two families, both symptomatic and asymptomatic members, who were diagnosed with congenital, praecox, en tarda, and secondary (acquired) lymphedema and (ii) through unbiased whole exome sequencing and analysis of rare SNPs with co-segregation analysis based on NIRFLI phenotyping, in order to discover gene variants. Using this approach, mutations in the inositol polyphosphate phosphatase-like 1(INPPL1) gene that encodes the src homology 2 domain containing 5'-inositol-phosphatase-2 (SHIP2) were identified. These imaging and genetics studies identify SHIP2 as a potential effector of lymphatic dysfunction in humans. However, the functional relevance of these INPPL1 mutations requires biological validation in lymphatic endothelial cell (LEC) culture studies, which is the focus of ***Chapter 3****.*

CHAPTER 3

DISRUPTION OF SHIP2 CONFERS AN *IN VITRO* LYMPHATIC PHENOTYPE

Portions of this chapter are based on: Agollah G.D., Gonzalez-Garay M.L, , Rasmussen JC., Tan I-C., Aldrich M.B., Darne C., Fife C.E., Guilliod R., Maus, E.A., King P.D., Sevick-Muraca E.M., *"Evidence for SH2 domain-containing 5-inositol phosphatase-2 (SHIP2) contributing to a lymphatic dysfunction"* PLoS ONE (2014) 9(11): e112548. doi:10.1371/journal.pone.0112548 [98]. *PLOS applies Creative Commons Attribution License (CCAL) and Open-Access License, wherein no permission is required from authors or publishers for reprints or reproduction of published works, except proper citation of original work*. *Germaine D. Agollah performed all experiments, unless otherwise noted in figure legends.*

3.1: Rationale

SHIP2 is a phosphatidylinositol (3,4,5) triphosphate (PIP3) 5'-phosphatase that negatively controls PIP3 levels in cells, thereby inhibiting the phosphatidylinositol-3-kinase (PI3K)/AKT signaling pathway. Recently, mutations within the PI3K/AKT pathway have been implicated in various lymphatic malformations and syndromic conditions that have a lymphatic involvement. CLOVES syndrome (OMIM: 612918) and Klippel-Trenaunay-Weber syndrome (KTWS, OMIM: 149000) are caused by gain-of-function mutations in *PI3KCA,* which encodes p110α, a catalytic subunit of PI3K, while *AKT1* mutations have been identified in Proteus syndrome (OMIM: 176920) [44, 144, 145]. In addition, targeted mutations of *Pik3r1*, *Pi3kca* and *Akt1* genes result in lymphatic abnormalities including lymphangiectasia, defective lymphatic sprouting and maturation, lymphatic vessel hypoplasia, and chylous ascites in mice [146-148]. SHIP2 is known to interact physically with receptor tyrosine kinases (RTKs), focal adhesion proteins, scaffold proteins, protein phosphatases, and cytoskeletal proteins to regulate cell proliferation, adhesion, migration, survival, and receptor internalization [108, 117, 149, 150]. Therefore, given the evidence that PI3K/AKT pathway plays a role in lymphatic malformation, one may hypothesize that SHIP2, a negative regulator of this pathway, could be involved in lymphatic disorders. Furthermore, as discussed in **Chapter 2**, with the identification of SHIP2 mutations in two families with varied diagnoses of lymphedema, we sought to investigate the functional role of SHIP2 in lymphatic endothelial cells (LECs).

3.2: Dysregulated HGF- and VEGFC-induced activation of AKT and MAPK in SHIP2-deficient LEC.

The role of SHIP2 has been previously evaluated in other cell types but not in LECs [107, 117, 127]. We confirmed the lymphatic lineage of primary human dermal lymphatic endothelial cells (HDLECs) and TIME (telomerase-immortalized microvascular endothelial) cells by flow cytometric analysis of lymphatic-specific podoplanin and pan-endothelial PECAM1 (CD31) antigen expression (**Figure 3.1A**). We found that SHIP2 was expressed in HDLECs (**Figure 3.1B**) and in TIME cells *via* immunofluorescence. Transfection of HDLECs and TIME cells with four different SHIP2 siRNA oligonucleotides resulted in effective knockdown of SHIP2 as revealed by Western blotting (**Figure 3.1C.D**), and RT-qPCR (**Figure 3.1E**). Subsequent SHIP2 siRNA transfections were carried out with the pool siRNA oligonucleotide comprising the four individual siRNA sequences to ensure effective knockdown. (*Note: general references to LECs imply both lymphatic cell lines, HDLECs and TIME cells*).

Figure 3.1 SHIP2 is expressed in lymphatic endothelial cells (LECs) (A) Confirmation of lymphatic lineage of primary HDLECs (passage 8) and TIME cells (passage 30) and expression of SHIP2 in HDLECs and TIME cells. Cells were grown to confluency and stained with pan-endothelial marker anti-human CD31 (top panels) and lymphatic marker anti-human podoplanin (bottom panels). Antigen markers are depicted in orange, isotype controls are in blue, and unstained in red. 50,000 events per experiment, N=3 independent experiments, 3 replicates per experiment. (**B**) Primary HDLECs (passage 5) were subjected to (pool) siRNA transfection for 48 hours then plated in chamber slides. LECs were allowed to adhere, fixed and permeabilized before staining with anti-human SHIP2 antibody followed by Alexa Fluor 546 antibody (green). Cells were counterstained with Alexa 488 phalloidin to detect actin (red) and nuclear stain DRAQ5 (blue). Scale bar = 25µm. (**C-D**) Western blot analysis of SHIP2 expression upon transfection with four different sequences of SHIP2 siRNA (#1-4 and pool, see **Chapter 6** Materials and Methods for oligonucleotide sequence information) in HDLEC and TIME cells. Equal loading was determined by Western blotting for actin. (**E**) RT-qPCR measurement of SHIP2 mRNA levels in HDLEC and TIME pool SHIP2 siRNA transfectants normalized to GAPDH expression levels; N=5 independent experiments, 3 replicates per experiment. Control = untransfected cells; Mock = transfection reagents only; NT = non-targeting control siRNA.

Figure 3.1 SHIP2 is expressed in lymphatic endothelial cells (LECs)

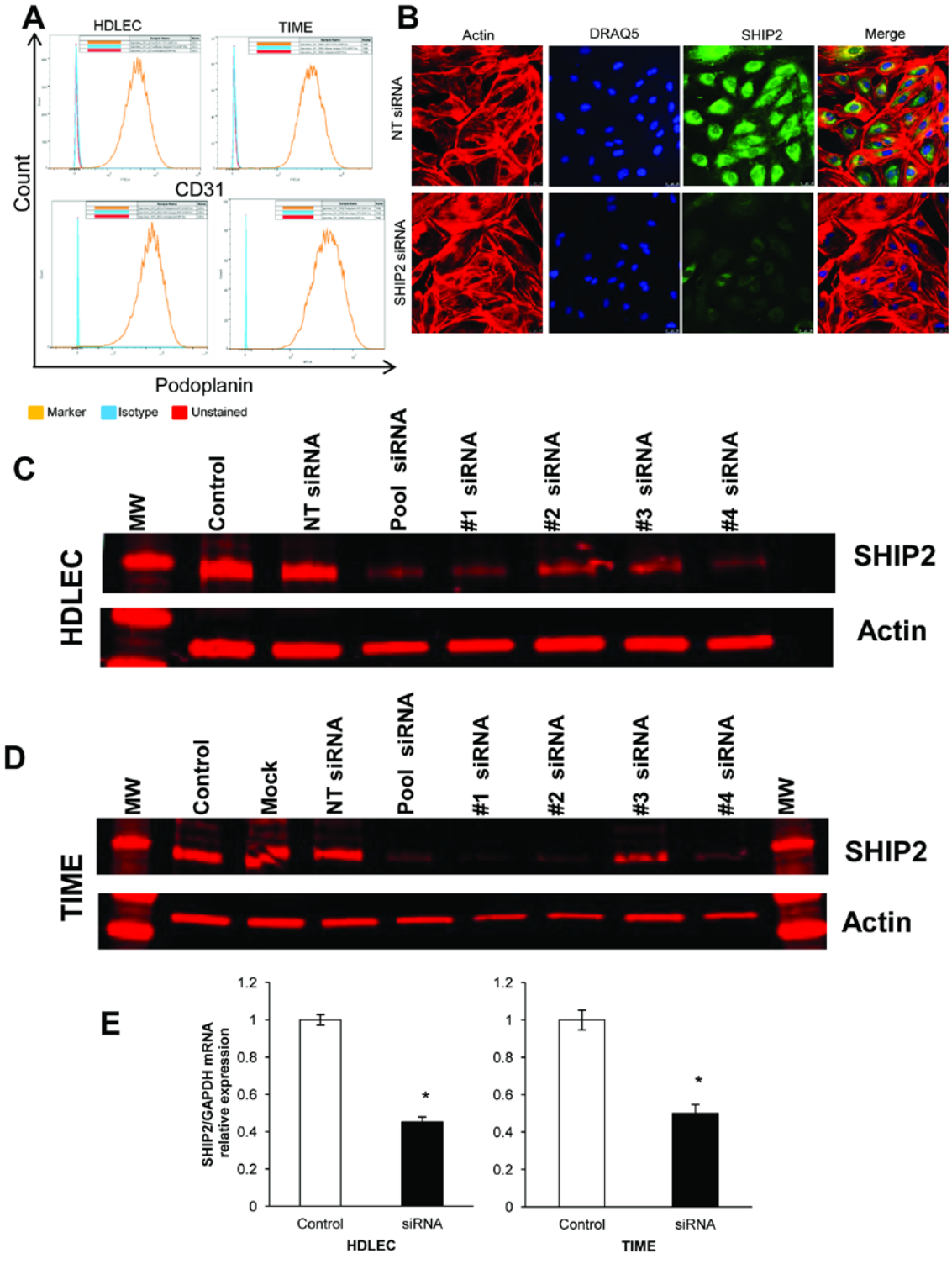

Given that the major reported function of SHIP2 is to dampen PI3K/AKT signaling, and that aberrant PI3K/AKT signaling results in lymphatic dysfunction in both mouse [146-148] and humans [144, 145] we examined the effect of SHIP2 knockdown upon HGF- and VEGFC-induced AKT activation in LEC. Activation of AKT in HDLECs and TIME cells was examined by Western blotting using phospho-specific anti-AKT antibodies (**Figures 3.2** and **3.3**). Stimulation of control HDLECs resulted in activation of AKT with the peak response evident between 10 and 15 minutes and 10 and 30 minutes after stimulation with HGF and VEGFC, respectively (**Figure 3.2A,C** and **Figure 3.3A,C**). After SHIP2 knockdown in HDLECs, the magnitude of AKT activation was modestly increased in response to HGF and substantially increased in response to VEGFC, although the kinetics of responses were not altered. Similar results were obtained in TIME cells after SHIP2 knockdown (**Figure 3.2B,C** and **Figure 3.3B,C**) These data are consistent with a function for SHIP2 as a negative regulator of the PI3K/AKT signaling pathway in LEC.

Recent studies have also identified mutations within the Ras/MAPK/ERK signaling network as responsible for lymphatic abnormalities [44, 81, 84, 85, 151, 152]. Given that we identified a mutation in *MAP3K7*, a Ras/MAPK/ERK-related gene, we also examined activation of MAPK in SHIP2 knockdown HDLEC using phospho-specific anti-ERK antibodies. In control HDLEC, HGF and VEGFC both induced activation of ERK with peak responses occurring at 15 and 10-15 minutes post-stimulation, respectively (**Figure 3.2A,D** and **Figure 3.3A,D)**. In SHIP2 knockdown HDLECs, substantial increases in the magnitude of ERK activation were evident in response to HGF and VEGFC stimulation. In both cases, activation of ERK occurred earlier and persisted for longer times after growth factor stimulation than in naïve HDLECs. These results were replicated in TIME cells in which we observed potent and protracted ERK activation

upon SHIP2 knockdown in response to both HGF and VEGFC stimulation (**Figure 3.2B,D** and **Figure 3.3B,D**). This data implicates SHIP2 as a negative regulator of MAPK signaling, as well as negative regulator of PI3K/AKT activation in LEC.

Figure 3.2 Dysregulated HGF-induced activation of AKT and ERK1/2 in SHIP2-deficient LECs. (**A**) HDLECs and (**B**) TIME cells were subjected to 48hr SHIP2 siRNA and stimulated with the HGF for the indicated times. Activation of AKT and ERK was determined by fluorescent double staining Western blotting of cell lysates with both phosphospecific antibodies and antibodies to total proteins. Phosphoantibodies were detected by IRDye680 (red signal) and total antibodies detected by IRDye800 (green signal) fluorescent secondary antibodies. Quantification of AKT (**C**) and ERK (**D**) activation in HDLECs and TIME cells by mean fluorescence intensity (MFI) and represented as a ratio of pAKT-S473 to total AKT and pERK1/2 to total ERK1/2, respectively. SHIP2 knockdown levels shown and COX IV used as loading control. MW=molecular weight marker.

Figure 3.2. Dysregulated HGF-induced activation of AKT and ERK1/2 in SHIP2-deficient LECs.

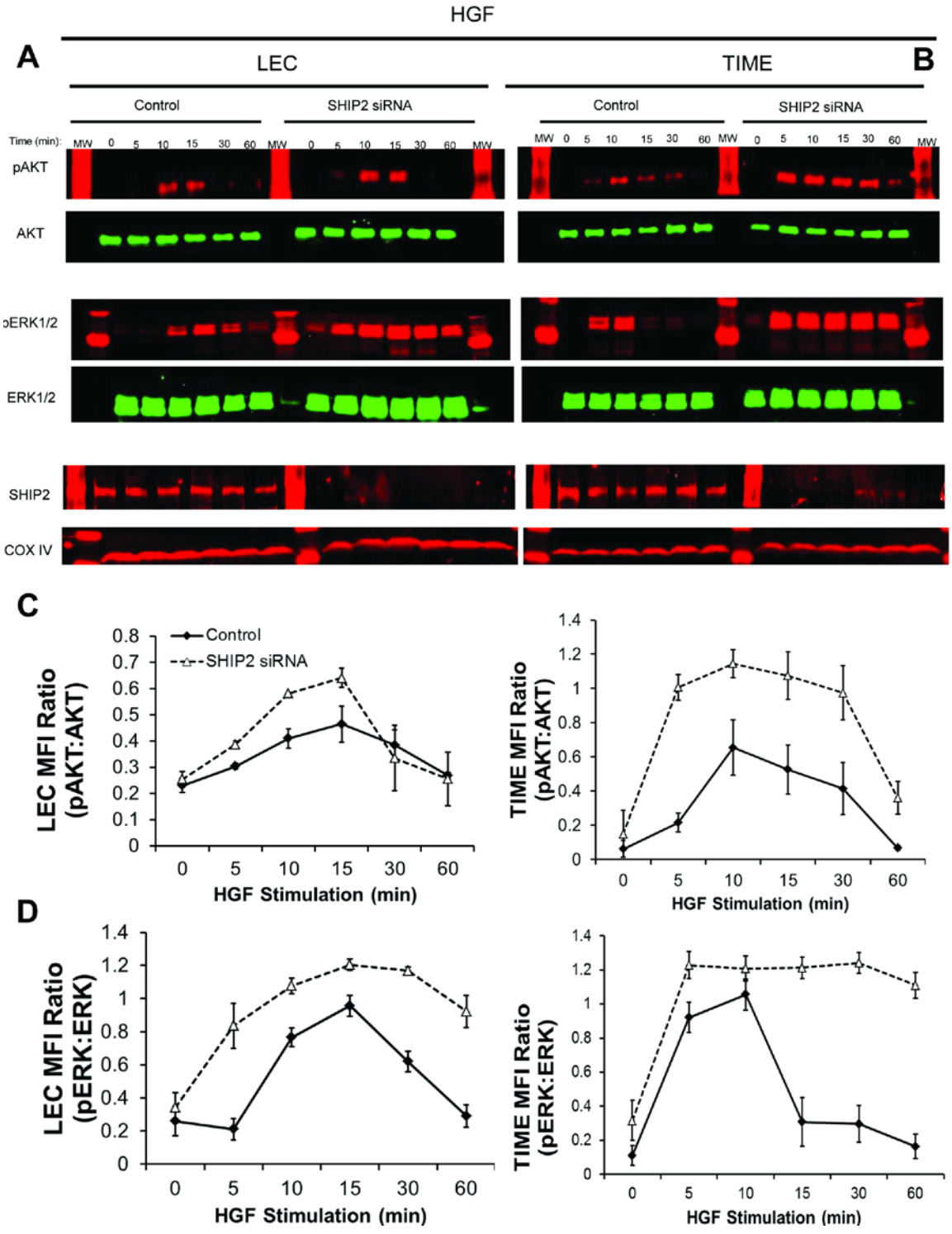

Figure 3.3 Dysregulated VEGFC-induced activation of AKT and ERK1/2 in SHIP2-deficient LECs. (**A**) HDLECs and (**B**) TIME cells were subjected to 48hr SHIP2 siRNA and stimulated with the VEGFC for the indicated times. Activation of AKT and ERK was determined by fluorescent double staining Western blotting of cell lysates with both phosphospecific antibodies and antibodies to total proteins. Phosphoantibodies were detected by IRDye 680 (red signal) and total antibodies detected by IRDye800 (green signal) fluorescent secondary antibodies. Quantification of AKT (**C**) and ERK (**D**) activation in HDLECs and TIME cells by mean fluorescence intensity (MFI) and represented as a ratio of pAKT-S473 to total AKT and pERK1/2 to total ERK1/2, respectively. SHIP2 knockdown levels are shown and COX IV used as loading control. MW=molecular weight marker.

Figure 3.3. Dysregulated VEGFC-induced activation of AKT and ERK1/2 in SHIP2-deficient LECs.

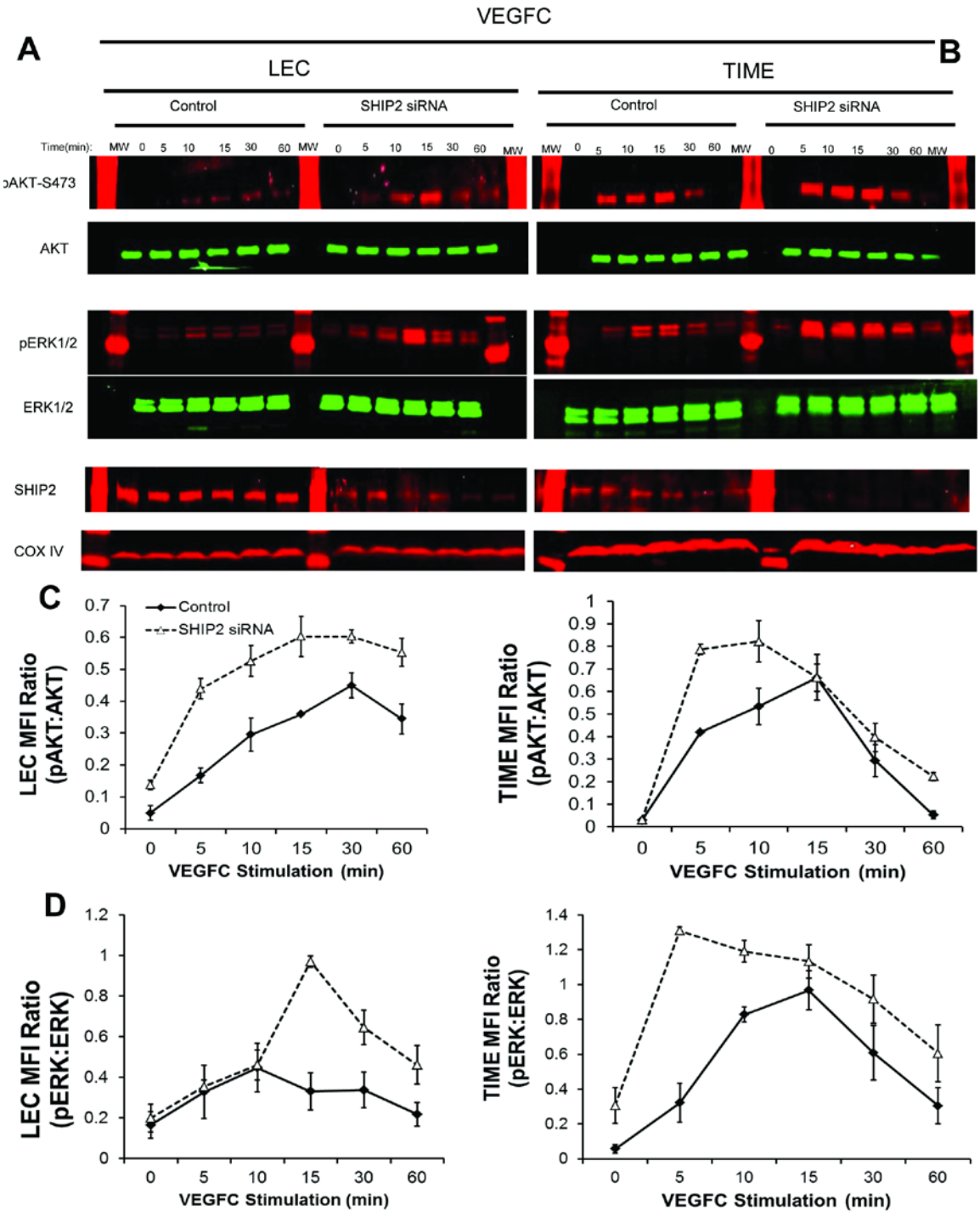

3.3: SHIP2 is required for HGF- and VEGFC-induced lymphangiogenesis *in vitro.*

We next sought to investigate the role of SHIP2 in LEC biology using *in vitro* assays of cell proliferation, adhesion, migration, and tubulogenesis that model different steps in lymphangiogenesis. Given the increases in AKT activation (**Figure 3.2 and 3.3**), we expected SHIP2 knockdown to result in increased LEC proliferation. However, we found reduced LECs proliferation both under basal conditions (1% FBS) and following HGF or VEGFC stimulation (**Figure 3.4A**). SHIP2-deficient LECs also exhibited a reduced capacity to adhere to extracellular matrix proteins, collagen, and fibronectin (**Figure 3.4B**) and showed reduced directed migration in scratch wound assays (**Figure 3.4C**). The ability of LECs to organize into tube-like structures was assessed using a 3D-Matrigel assay. SHIP2 knockdown resulted in significantly less tube formation after HGF and VEGFC stimulation (**Figure 3.4D**). However, contrary to the known pro-survival role of PI3K/AKT, we found increased apoptosis in SHIP2 knockdown LEC induced by overnight serum starvation or staurosporine treatment (**Figure 3.4E**). These results were also obtained in TIME cells in all functional assays (**Figure 3.5**).

Figure 3.4 SHIP2 is required for *in vitro* lymphangiogenesis in primary HDLECs. (**A**) MTS cell proliferation assay in response to growth factor stimulation for 48hrs, normalized to 1% FBS of non-targeting (NT) siRNA (N=3).(**B**) Cell adhesion assay of siRNA-transfected HDLECs onto BSA, collagen and fibronectin and quantification presented as area fraction of whole images (triplicates per experiment; 5 independent experiments). (**C**) Wound scratch cell migration assay of siRNA-transfected HDLEC immediately after injury, at 24hr and 48 hrs afterward. (**D**) 3D tube formation networks in response to growth factors imaged 24hrs post plating. (**E**) Annexin V apoptosis assay of siRNA-transfected HDLECs either untreated or following staurosporine treatment, quantification of total annexin v-positive cell populations and mean intensity of annexinV and propidium iodide of 3 independent experiments. Data presented as means±SEM. *$p<0.05$, ***$p<0.001$. Scale bar = 50μm. Control = untransfected cells; NT=non-targeting siRNA.

Figure 3.4 SHIP2 is required for *in vitro* lymphangiogenesis in primary HDLECs.

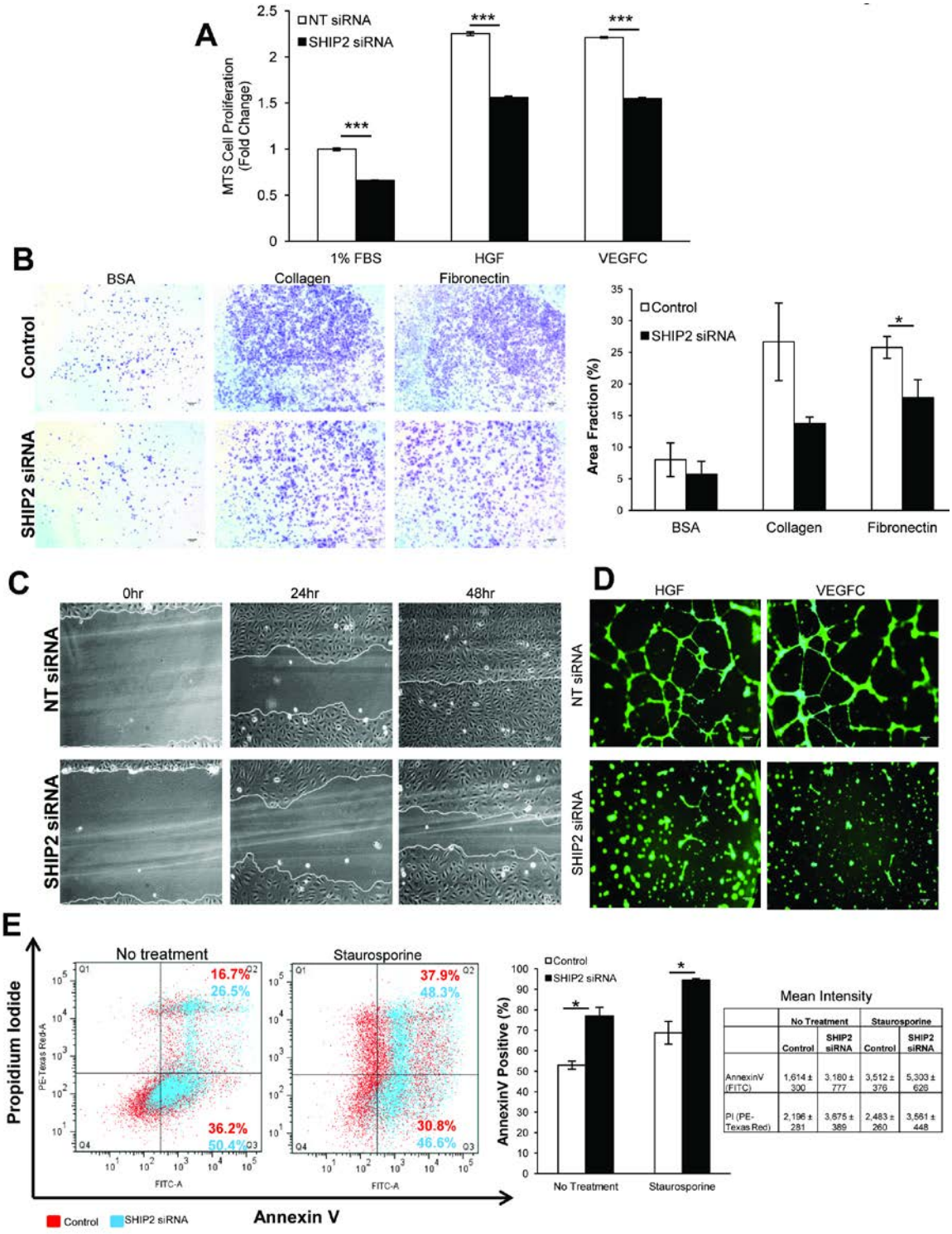

Figure 3.5 Phenotype of TIME cells upon SHIP2 knockdown. (**A**) MTS cell proliferation assay of 24hr-transfected TIME cells in response to 1% FBS over 48 hrs; N=3. (**B**) Representative images of cell adhesion assay of siRNA-transfected TIME onto BSA, collagen and fibronectin. (**C**) Wound scratch cell migration assay of siRNA-transfected TIME cells immediately after and at 24 and 48hrs after wounding. (**D**) 3D tube formation networks in response to growth factors imaged 24hrs post plating. (**E**) Annexin V apoptosis assay of siRNA-transfected TIME cells either untreated or following staurosporine treatment, quantification (N=3) of total annexin v-positive cell populations and mean intensity of annexinV and propidium iodide. Data presented as means±SEM. *p<0.05. Scale bar = 50µm. Control = untransfected cells; NT=non-targeting siRNA.

Figure 3.5 Phenotype of TIME cells upon SHIP2 knockdown.

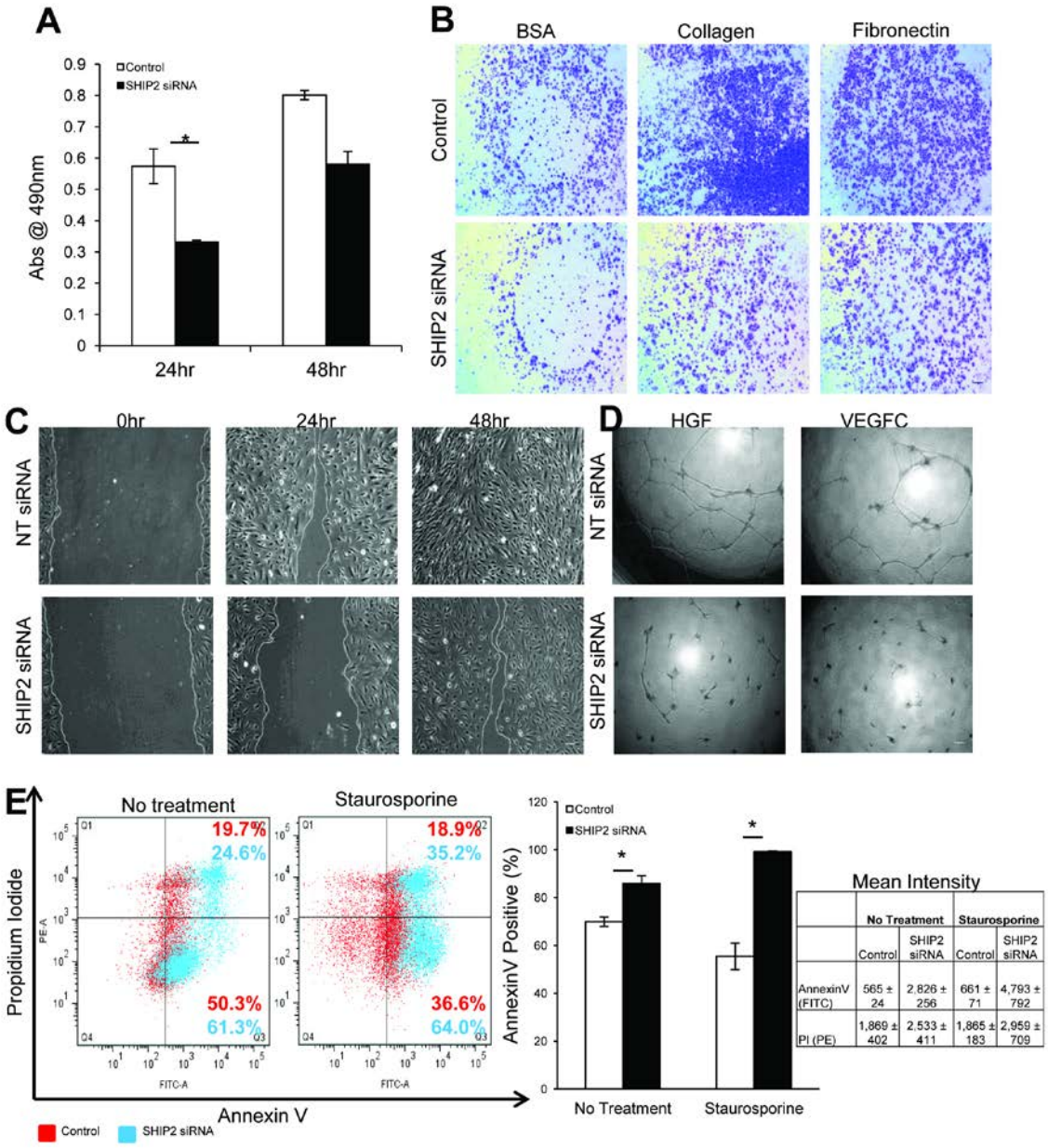

Taken together, these data suggest that while SHIP2 is necessary for *in vitro* lymphangiogenesis in HDLECs and TIME cells, the cellular phenotypes of reduced proliferation, adhesion, and migration may be secondary to increased apoptosis. Furthermore, the observed phenotypes were not as a result of reagent toxicity given that tube networks were stained with Calcein AM viability fluorescent dye (**Figure 3.4D**) and four SHIP2 RNAi with different targeting sequences were tested, including mock and non-targeting (NT) control transfections, and all four RNAi showed comparable levels of SHIP2 knockdown (**Figure 3.1C,D**). Why loss of SHIP2 would lead to increased AKT activation but increased apoptosis of LECs is unclear but may be explained by still greater increases in pro-apoptotic ERK activation (see **Section 3.10** Discussion).

3.4: SHIP2 is required for cytoskeletal reorganization in LECs

In addition to its catalytic 5'-phosphatase function, a major function of SHIP2 is to effect cell spreading, motility, and adhesion [117, 120]. We therefore assessed whether some of the loss-of-function phenotypes we had observed upon SHIP2 knockdown was due to altered cytoskeletal reorganization. Formation of lamellipodia, which are actin-rich projections at the leading edge of a mobile cell, was assessed in LECs plated onto collagen-coated slides for 1 hour. Starved cells (1% FBS) exhibited a spreading phenotype and reduced actin polymerization, with no obvious morphological differences observed between control and SHIP2-siRNA transfected LECs (**Figure 3.6A**). However following 10 minute VEGFC stimulation, control cells were polarized whereby lammellipodia localized to front end extending toward the direction of movement (line arrows) (**Figure 3.6B panels i-iii**). Control cells also exhibited increased fluorescent stress fibers indicative of actin polymerization (filled block arrows). On the other hand, SHIP2-siRNA transfected LECs retained the spreading phenotype, exhibited reduced actin fibers, while some cells had focal adhesions (open block arrows) and some had

radial protrusions that resemble peripheral lamellipodia (arrow head) (**Figure 3.6B panels iv-vi**). These experiments demonstrate an essential function of SHIP2 in maintaining intracellular actin organization which is necessary for LEC migration.

Figure 3.6 SHIP2 is necessary for cytoskeletal reorganization in LECs. Lamellipodia formation was assessed in LECs that had been subjected to 24 hour SHIP2 siRNA, starved overnight in 1%FBS, harvested, plated onto collagen-coated slides for 1 hour and then stimulated for 10 minutes using VEGFC. (**A**) Under starvation, both control and siRNA transfectants exhibit spreading phenotype. (**B**) Cytoskeletal reorganization in control LECs with lamellipodia formation at the leading edges of motile cells (line arrows) and bright regions of actin polymerization (filled block arrows) in response to VEGFC stimulation. Most SHIP2-siRNA transfected LECs have spreading phenotype (**B** panels **v-vi**), focal adhesion contacts (open block arrows) and some cells have peripheral polarizing lamellipodia (arrow head). Scale bar =20µm.

Figure 3.6 SHIP2 is necessary for cytoskeletal reorganization in LECs

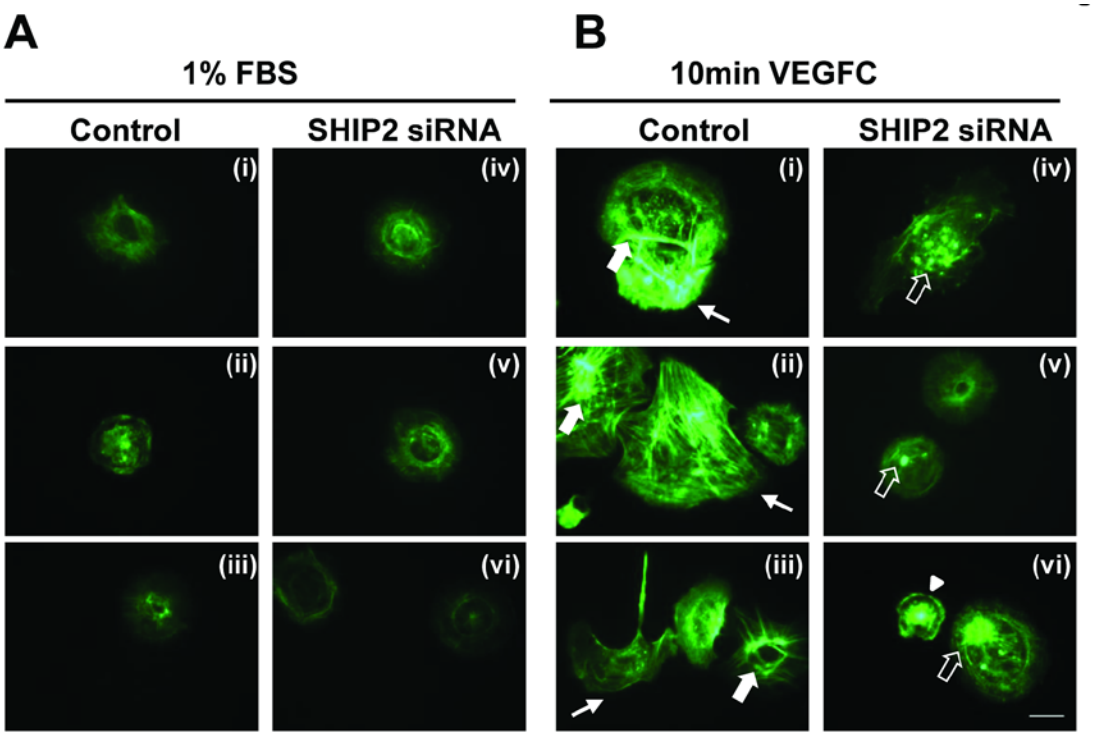

3.5: SHIP2 physically interacts with cMET and VEGFR3 in LECs.

SHIP2 interacts physically with cMET in epithelial cells to effect HGF-induced lammellipodia formation, spreading and spreading [107]. To confirm this interaction in LECs and investigate whether SHIP2 also interacts with VEGFR3 we used proximity ligation assays (PLAs) and traditional immunoprecipitation. PLA allows for *in situ* detection and quantification of protein-protein interactions in intact cells, whereby a fluorescent signal is generated when two PLA probes are present in close proximity within 30-40nm [153]. Through transfection of FLAG-tagged wild type (WT) SHIP2 into TIME cells, we confirmed that SHIP2 interacts with endogenous cMET upon HGF stimulation in PLA assays (**Figures 3.7A, C**). Additionally, we identified that SHIP2 associates with VEGFR3 following VEGFC stimulation in PLA assays (**Figures 3.7B, D**). Physical association between endogenous SHIP2 and cMET or VEGFR3 in response to growth factor stimulation was confirmed by co-immunoprecipitation (**Figure 3.7E**). Negative controls included the omission of one primary antibody during the PLA reaction (**Figure 3.7A**). The finding that SHIP2 physically interacts with cMET and VEGFR3 in LECs further substantiates the notion that SHIP2 mutations contribute to the lymphatic abnormalities in the studied families. Furthermore, a role for SHIP2 in cMET and VEGFR3 signaling pathways could provide an explanation for the occurrence of more serious disease in individuals with mutations in SHIP2 together with mutations in one or the other of these RTKs.

Figure 3.7. SHIP2 interacts with cMET and with VEGFR3. Proximity ligation assay (PLA) depicting interaction of (**A**) SHIP2-FLAG and cMET and (**B**) SHIP2-FLAG and VEGFR3 in Vector- and FLAG-tagged WT SHIP2-transfected TIME cells following (**A**) HGF stimulation and (**B**) VEGFC stimulation and respective quantification of PLA fluorescence signal (**C** and **D**) in 100 cells/experiment (N=3) quantified by ImageJ (NIH). (**E**) Co-immunoprecipitation depicting endogenous SHIP2 interacting with cMET and VEGFR3. Confluent naïve TIME cells were serum-starved overnight and subjected to HGF and VEGFC stimulation for 15 minutes before harvesting and lysates subjected to immunoprecipitation with anti-cMET and anti-VEGFR3 antibodies pre-absorbed with agarose beads. Immunocomplexes were subjected to immunoblotting, blots probed with anti-SHIP2 antibody, and GAPDH used to determine equal loading in whole cell lysates pre-IP. (**F,G**) PLA negative controls (**F**) SHIP2FLAG-cMET and **(G**) SHIP2FLAG-VEGFR3 interaction whereby a single primary antibody is used, the second primary antibody is omitted and both PLA probes added. Note lack of red PLA signal. Blue = DAPI, green = actin and red = PLA fluorescence with each red dot depicting *in situ* interaction site. Scale bar = 50μm, bottom right panel.

Figure 3.7. SHIP2 interacts with cMET and with VEGFR3

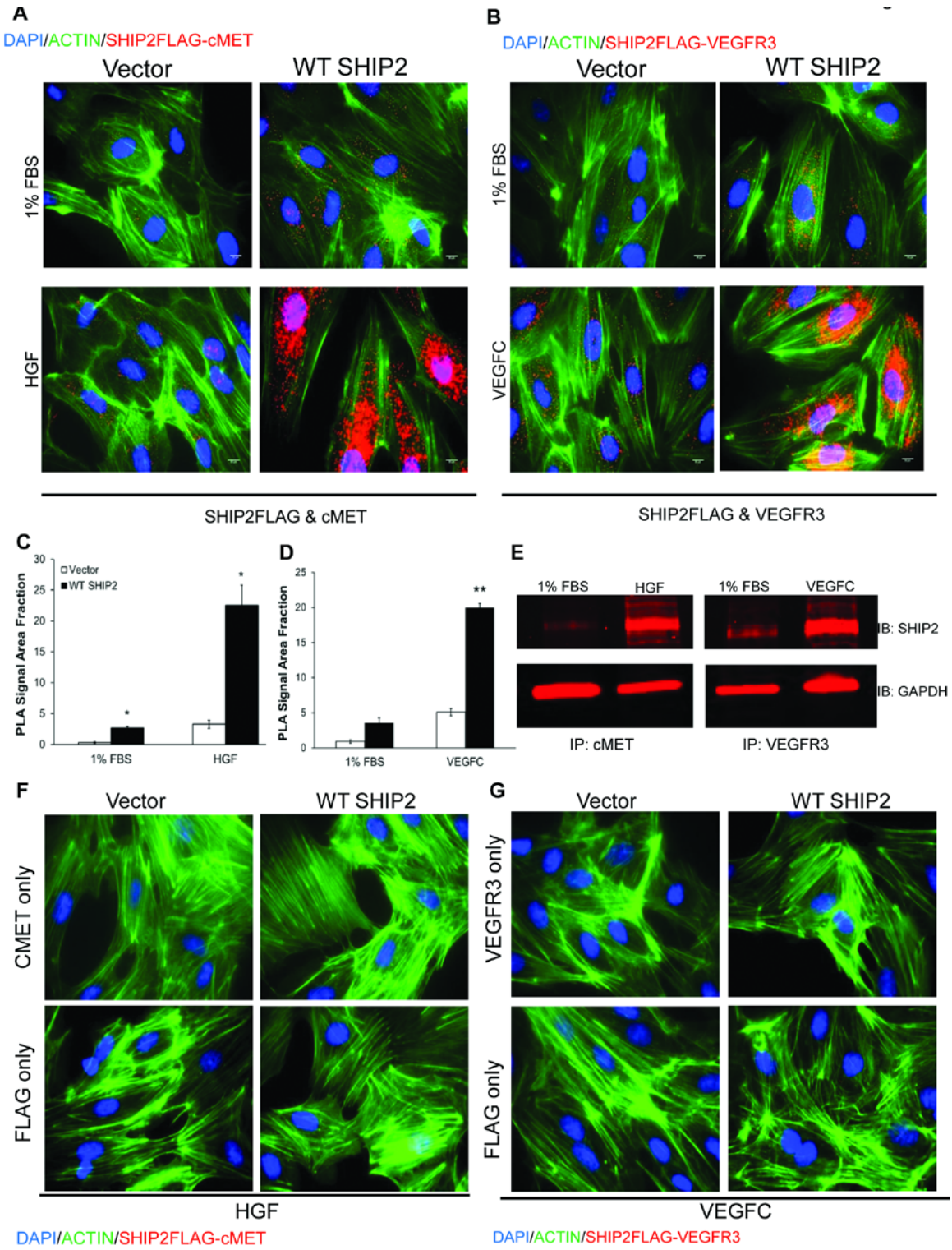

3.6: Influence of T180A and L632I SHIP2 mutations upon PIP3-directed phosphatase activity.

Given findings in SHIP2-deficient LECs, we next asked if T180A and L632I SHIP2 mutations might affect SHIP2 phosphatase activity. The T180A mutation resides between the SH2 and catalytic domains (**Figure 2.3C**). Because the entire crystal structure of the SHIP2 protein has not been solved, we were unable to model the potential impact of the T180A mutation on intramolecular interactions that could impact upon catalytic and non-catalytic (scaffolding) activity. In contrast, the L632I mutation lies within the catalytic domain, the three-dimensional structure of which has been elucidated [154]. Because recognition and binding of an enzyme to its substrate requires protein conformational changes which, among other factors, depend on the innate geometrical flexibility of the protein structure, we used rapid simulation methods [155] to access flexibility and provide valuable information on protein function [156]. We performed computational simulations to understand how L632I, could affect the PIP3 substrate binding site within SHIP2. We used rigidity analysis using FIRST [157] and explored flexible collective motions using FIRST/FRODA [158, 159] and El Nemo [160] software in combination [155]. We found that a highly flexible and mobile beta-hairpin loop (residues 674-683) exists above the substrate binding site and that this flexibility is likely to affect the binding site geometry. This almost entirely solvent-exposed beta-hairpin loop region appears to be structured only in a SHIP2 molecule that binds a synthetic lipid head group surrogate as determined by X-ray crystallography. Molecular modelling and dynamics studies suggested that this flexible loop might close over the ligand during binding [154]. Normally L632 is part of a pair of short helices (628-634 and 614-626) that are positioned above the main body of SHIP2 and L632 anchors the helices to I655 and W688 on one side, while W673 links the helices to the hairpin loop on the other side. The constraint network of hydrophobic tether interactions linking L632 through the two

helices to the hairpin loop is shown in **Figure 3.8A**. The flexible motion of SHIP2 involves motion of the hairpin loop affecting the binding site and coordinated motion of the hairpin loop and the two helices (**Figure 3.8B**). This suggests that this helical region is a “governor” affecting the flexible dynamics of the hairpin loop and the binding site, and therefore the L632I mutation affects the constraint network and disrupts the function of the governor.

To determine the potential impact of T180A and L632I mutations upon catalytic activity directly, we examined phosphatase activity toward PIP3 in *in vitro* phosphatase assays (**Figure 3.8C**). Following site-directed mutagenesis to generate point mutations that result in T180A and L632I, FLAG-tagged SHIP2 mutants were transfected in TIME cells. The WT and mutant SHIP2 proteins were eluted following immunoprecitations against FLAG antibody and the immunocomplexes subjected to Malachite green *in vitro* phosphatase assay against recombinant PIP3. The phosphatase activity of T180A SHIP2 was unaltered compared to WT SHIP2 in this assay. In contrast, the phosphatase activity of L632I SHIP2 was increased relative to WT SHIP2. This experimental finding correlates with the hypothesis suggested by our computational simulations: the conversion of leucine to isoleucine results in a gain of enzymatic function due to functional disruption of the helical (governor) region that ordinarily regulates the flexible hairpin loop and substrate-binding site within SHIP2.

Figure 3.8. Effect of T180A and L632I SHIP2 mutations on PIP3 catalysis. (**A**) Constraint network of hydrophobic tethers indicating location of L632 anchoring I655 and W688 on one side of the helices while W673 anchors the helices to the beta hairpin loop. (**B**) Depiction of flexible modes involving collective motion linking helices, hairpin loop and binding site of SHIP2 catalytic domain. (**C**) Malachite green *in vitro* phosphatase assay indicates increased phosphate released by L632I SHIP2 suggesting increased enzymatic activity against recombinant PIP3 substrate. *(Collaborator contributions: Dr. Stephen A. Wells and Prof. Barry V.L. Porter (University of Bath, U.K) performed computational simulations and data interpretation of flexible motions shown in Figure 3.8A-B).*

Figure 3.8. Effect of T180A and L632I SHIP2 mutations on PIP3 catalysis

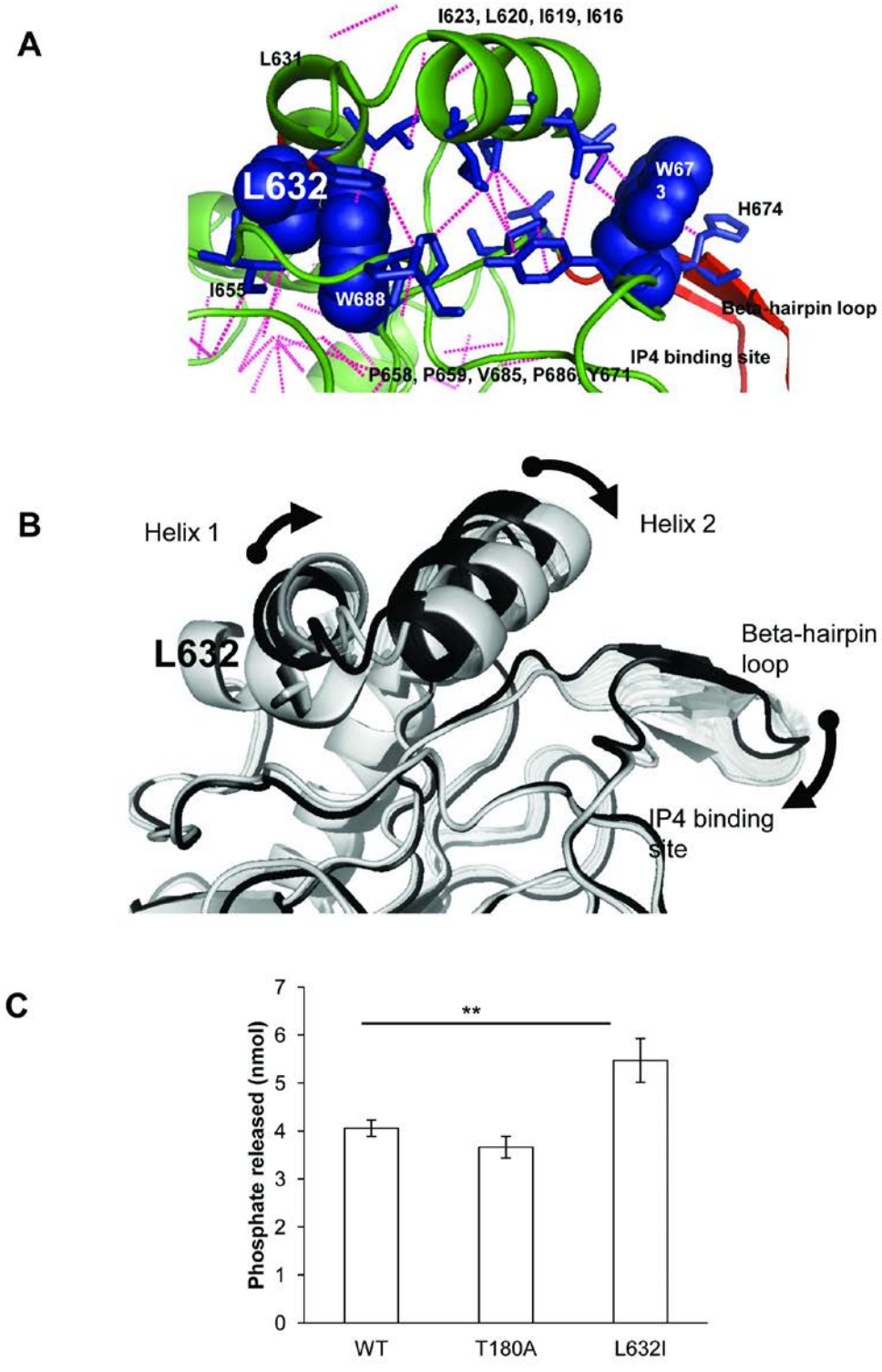

3.7: Effect of T180A and L632I SHIP2 mutations upon AKT and MAPK activation in LECs.

We next examined whether T180A and L632I mutations affected the function of SHIP2 in a cellular context. FLAG-tagged WT SHIP2 and SHIP2 mutants were stably expressed in TIME cells. As revealed by Western blotting using a FLAG antibody, WT and mutant SHIP2s were comparably expressed (**Figure 3.9A**). Consistent with its role as a negative regulator of PI3K/AKT signaling, over-expression of WT SHIP2 in TIME cells resulted in reduced HGF- and VEGFC–induced AKT activation compared to TIME cells that were transfected with vector alone (**Figure 3.9B**). However, this inhibitory effect of over-expressed WT SHIP2 upon HGF- and VEGFC–induced AKT activation was completely abrogated by the T180A and L632I SHIP2 mutations. We also assessed the effect of over-expressed WT and mutant SHIP2 upon ERK activation in TIME cells. In agreement with results obtained in SHIP2 knockdown experiments **(Figures 3.2** and **3.3**), over-expression of WT SHIP2 resulted in reduced HGF- and VEGFC-induced activation of ERK (**Figure 3.9C**). However, the T180A mutation abrogated the ability of over-expressed wild type SHIP2 to inhibit ERK activation in response to both growth factors. In contrast, the L632I SHIP2 mutation did not affect the ability of over-expressed WT SHIP2 to inhibit ERK activation in response to HGF and partially inhibited its ability to dampen ERK activation in response to VEGFC (**Figure 3.9C**).

3.8: Effect of T180A and L632I mutations upon SHIP2 interaction with cMET and VEGFR3

To provide insight into how T180A and L632I mutations result in loss of SHIP2 to inhibit AKT and ERK activation within LECs, we also examined the effect of mutations upon physical interaction with cMET and VEGFR3. Since T180 is in close proximity to the SHIP2 SH2 domain that is known to mediate interaction with cMET, we predicted a

reduced interaction with this RTK. However, as determined in PLA assays, the T180A mutation did not affect the ability of SHIP2 to bind cMET or VEGFR3 after stimulation of cells with their respective growth factors (**Figure 3.9D** and **E**). In contrast, and somewhat unexpectedly, the L632I mutation resulted in significantly reduced binding of SHIP2 to both growth factor receptors after ligand stimulation (**Figure 3.9D** and **E**). Reduced binding of L632I SHIP2 to these RTKs, therefore, could provide an explanation to the apparent paradox that the L632I mutation results in increased PIP3 phosphatase activity *in vitro* but loss of ability to inhibit AKT activation and partial loss of ability to inhibit ERK activation in transfected LECs. Thus, increased phosphatase activity afforded by the L632I mutation would be obviated by an impaired ability of SHIP2 to access PIP3 substrate at membrane locations.

Figure 3.9. Effect of T180A and L632I SHIP2 mutations on signal transduction and in interaction with cMET and VEGFR3. (**A**) Western blot analysis depicting expression of SHIP2 and DYKDDDDK (FLAG) tag epitope in SHIP2 TIME transfectants. COX IV used to determine equal protein loading. Activation of (**B**) AKT and (**C**) ERK was determined by Western blotting of cell lysates with phosphospecific antibodies. Blots were reprobed with total AKT and ERK antibodies to demonstrate equal loading. Initial phosho- and total-antibody reprobes were detected with IRDye680 secondary antibodies. Proximity ligation assay depicting decreased interaction of L632I-SHIP2 with (**D**) cMET and with (**E**) VEGFR3. Data expressed as % of PLA signal in at least 5 images, presented as mean±SEM *p<0.05 **p<0.01. Blue = DAPI green = actin and red = PLA fluorescence with each red dot depicting *in situ* interaction site. MW = molecular weight marker. Scale bar = 50 µm.

Figure 3.9. Effect of T180A and L632I SHIP2 mutations on signal transduction and in interaction with cMET and VEGFR3

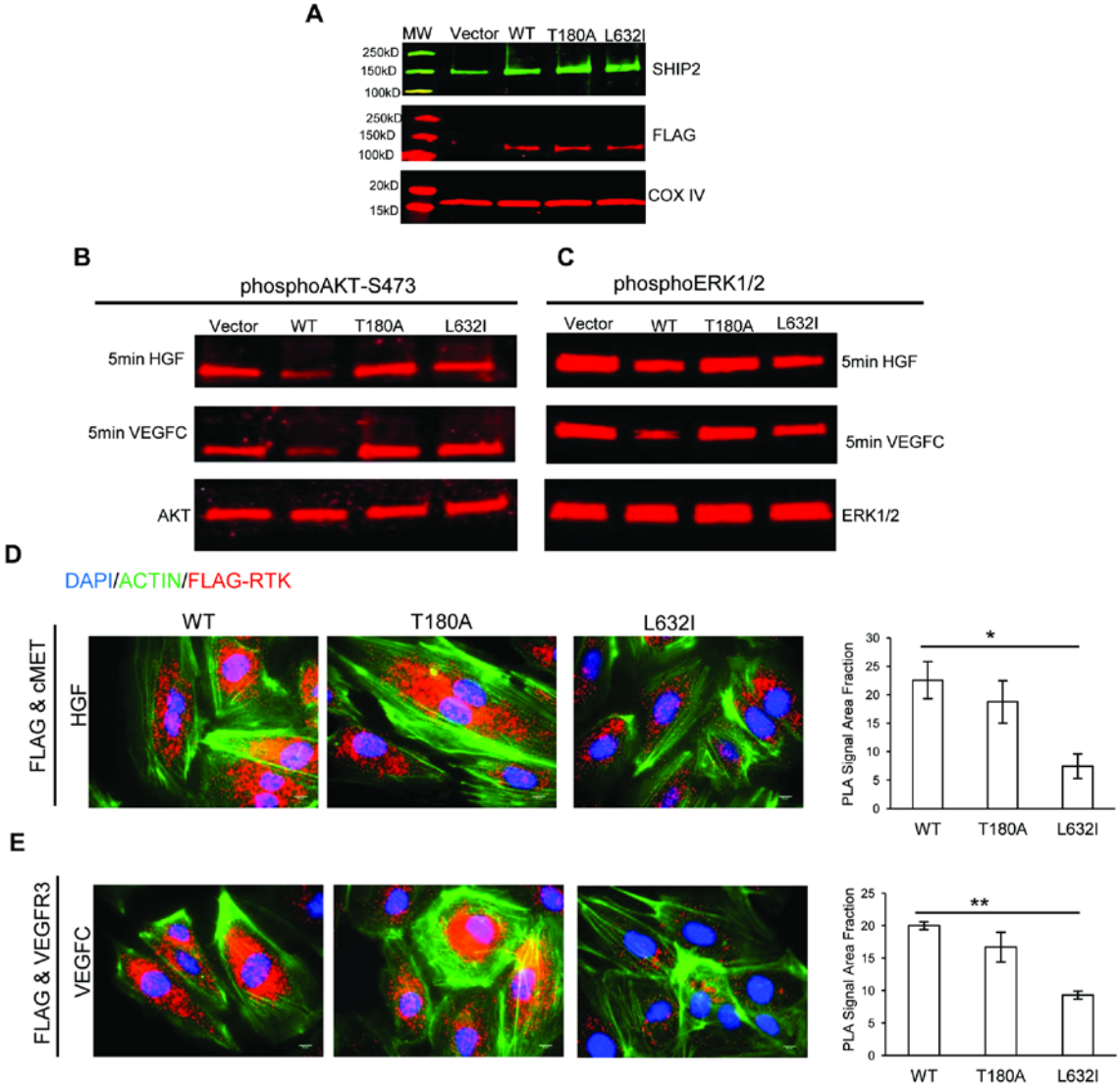

3.9: Influence of T180A and L632I SHIP2 mutations upon LEC functional responses.

We also examined the effect of T180A and L632I mutations upon LEC functional responses. As shown previously, SHIP2 knockdown resulted in reduced LEC proliferation, adhesion, directed migration, tube formation and survival (**Figure 3.4** and **3.5**). However, in comparison to vector controls, over-expressed WT SHIP2 did not influence LEC proliferation, directed migration, tube formation or survival, although it did result in increased LEC adhesion and increased chemotaxis in response to HGF (**Figure 3.10**). Increased chemotaxis to HGF and adhesion to collagen resulting from over-expression of SHIP2 was reduced by the T180A mutation, consistent with the loss of an ability of T180A SHIP2 to inhibit activation of AKT and MAPK (**Figures 3.9B, C**). On the other hand, the T180A mutation did not reduce the ability of over-expressed SHIP2 to increase adhesion to fibronectin. L632I SHIP2 transfectants behaved differently from WT SHIP2 and T180A SHIP2 transfectants in most regards. Thus, compared to WT SHIP2 LEC, L632I SHIP2 transfectants exhibited increased proliferation (**Figure 3.10A**), directed migration (**Figure 3.10B**), tube formation (**Figure 3.10D**) and survival (**Figure 3.10E**). They also demonstrated increased chemotaxis to HGF and VEGFC (**Figure 3.10C**) and increased adhesion to collagen and fibronectin (**Figure 3.10C**) compared to control cells, albeit the increases in adhesion were less than those observed in WT SHIP2 transfectants.

Summarized in **Table 3.1** are functional phenotypes of LECs upon SHIP2 siRNA knockdown and mutant overexpression.

Figure 3.10 Influence of T180A and L632I SHIP2 mutations upon LEC functional responses. (**A**) MTS cell proliferation rate is increased in L632I-SHIP2. (**B**) WT-SHIP2 exhibits increased chemotaxis compared to Vector (HGF ($p<0.05$) while chemotaxis towards VEGFC is N.S compared to Vector. T180A mutant has similar chemotaxis towards VEGFC and slightly reduced, but not significant, chemotaxis towards HGF, both compared to WT. L632I mutant has increased chemotaxis toward HGF (N.S) and VEGFC ($p<0.01$), both compared to WT. Data are presented as % of area covered by migrated cells on underside of transwell filters. (**C**) WT-SHIP2 exhibits increased adhesion over Vector on BSA, collagen and fibronectin. Both T180A and L632I mutants have decreased adhesion to collagen compared to WT. T180A mutant exhibits increased adhesion to fibronectin compared to WT. L632I exhibits decreased adhesion to BSA and similar adhesion to fibronectin compared to WT. (**B**) L632I mutant has increased cell migration and (**D**) enhanced tube formation. (**E**) Decreased apoptosis in L632I-SHIP2 transfectants as assessed by annexin v staining. All comparisons are between Vector *vs*. WT; WT *vs*. T180A and WT *vs*. L632I. *$p<0.05$, **$p<0.01$, *** $p<0.001$. Data presented as mean±SEM. Scale bar = 100μm. All experiments at least N=3.

Figure 3.10 Influence of T180A and L632I SHIP2 mutations upon LEC functional responses

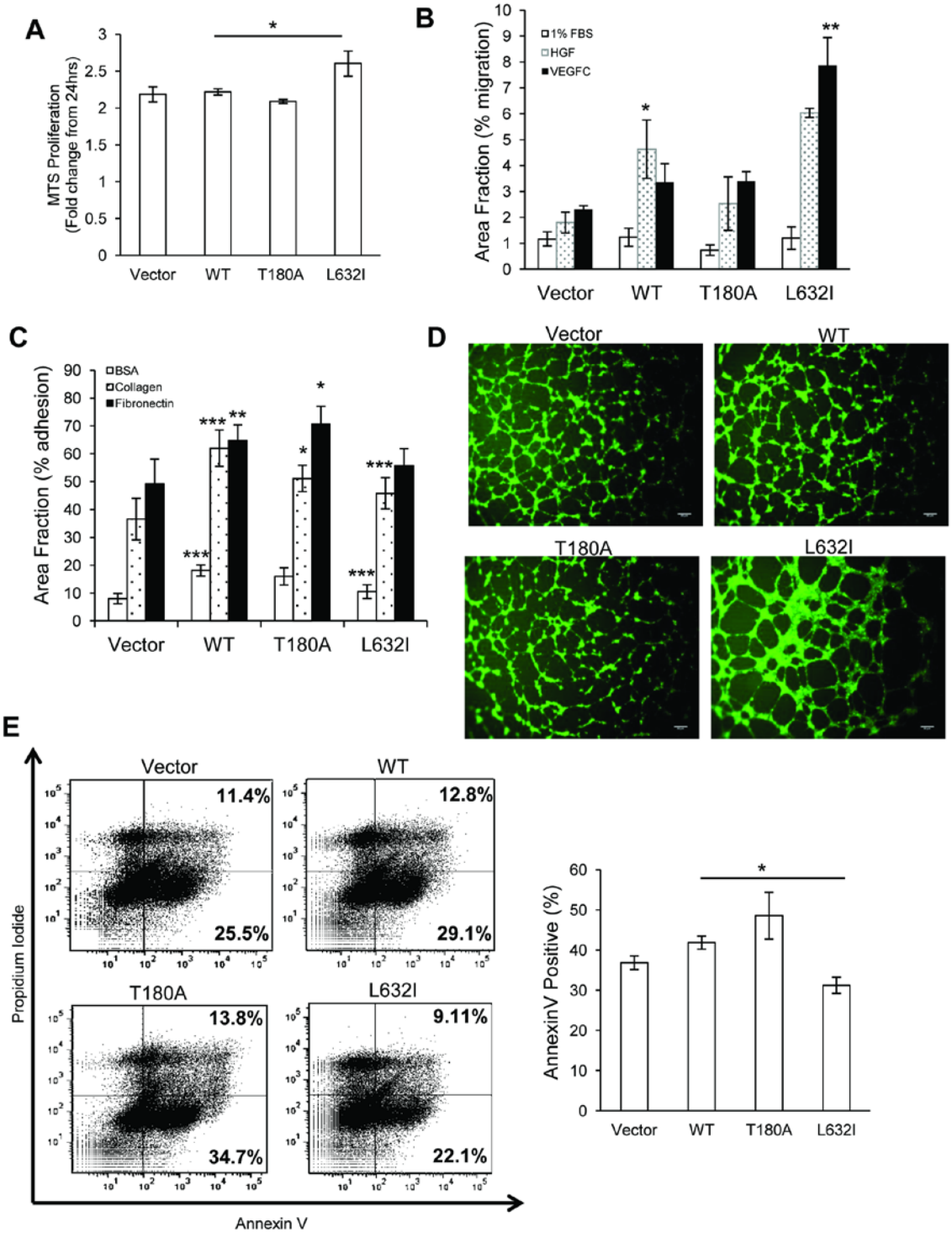

Table 3.1 Summary of functional phenotypes of LEC upon RNAi and mutant expression of SHIP2

	siRNA (HDLEC)	siRNA (TIME)	overexpressed WT SHIP2	T180A SHIP2 (Family 1)	L632I SHIP2 (Family 2)
Cell Proliferation	Reduced	Reduced	Similar to Vector	Similar to WT	Increased over WT
Cell Adhesion	Reduced	Reduced	Increased over Vector	Less than WT	Increased over WT
Cell Migration (wound healing)	Reduced	Reduced	Increased over Vector	Less than WT	Increased over WT
Cell Migration (chemotaxis)	Reduced	Reduced	Increased over Vector	Less than WT	Increased over WT
Tube Formation	Reduced	Reduced	Similar to Vector	Less than WT	Increased over WT
Apoptosis	Increased	Increased	Similar to Vector	Similar to WT	Less than WT
Interaction with cMET	N/A	N/A	Interaction	Less than WT (n.s)	Less than WT
Interaction with VEGFR3	N/A	N/A	Interaction	Less than WT (n.s)	Less than WT
Effect on cellular PIP3 levels	Increased over control	Increased over control	Less than Vector	Increased over WT	Increased over WT
Catalysis of recombinant PIP3	N/A	N/A	Catalysis	Similar to WT	Increased over WT
Activation of AKT	Increased activation over control	Increased over control	Reduced activation over Vector	Increased over WT	Increased over WT
Activation of ERK1/2	Increased and more sustained over control	Increased and more sustained over control	Reduced activation over Vector	Increased over WT	Increased over WT

In summary, although the T180A mutation in SHIP2 was found not to affect PIP3 phosphatase activity *in vitro* (**Figure 3.8C**), this mutation results in a complete loss-of-function of SHIP2 with regards to activation of AKT and ERK in a cellular context (**Figures 3.9** and **3.10**). In contrast, whereas the L632I mutation resulted in increased PIP3 phosphatase activity *in vitro* (**Figure 3.8C**), in a cellular context, the L632I mutant appears to behave as a partial loss-of-function SHIP2 that is unable to inhibit the activation of AKT but retains at least some activity as a negative regulator of ERK activation in HGF and VEGFC induced responses (**Figures 3.9 and 3.10**). Importantly, AKT and ERK activation in T180A or L632I transfected cells was not greater than that observed in vector control cells in response to either growth factor. This indicates that neither mutants function in a dominant negative capacity to regulate the activation of AKT and ERK in the respective growth factor induced signaling pathways.

3.10: Discussion

SHIP2 dephosphorylates PI(3,4,5)P3 at the 5' position of the inositol ring and thereby is a negative regulator of the PI3K/AKT signaling pathway. To verify this important role for SHIP2 in lymphatics, we performed SHIP2 knockdown studies in LECs. These studies confirmed that SHIP2 acts as a negative regulator of HGF- and VEGFC-induced PI3K/AKT signaling in LECs and further showed an important role for SHIP2 as a negative regulator of Ras-MAPK/ERK signaling in this cell type. SHIP2 has the potential to negatively regulate Ras-MAPK/ERK signaling through either catalytic or non-catalytic mechanisms. Non-catalytic mechanisms by which SHIP2 may inhibit MAPK activation are suggested by functional studies of SHIP1, which is homologous to SHIP2. For example in B cells, SHIP1 negatively regulates MAPK through inhibition of the binding of a Grb2/SOS Ras guanine nucleotide exchange factor complex to the Shc adapter protein, which is an event that is necessary for Ras activation [161]. In addition,

through physical interaction with the p62dok adapter protein, SHIP1 is thought to promote recruitment of the Ras GTPase-activating protein to membranes that inactivates Ras [162]. Additionally, over-expression of WT SHIP2 in the CHO cell line resulted in increased insulin-induced SHIP2/Shc association, reduced Shc/Grb2 association and, consequently, reduced MAPK activation, suggesting that SHIP2, like SHIP1, competes with Grb2 for Shc [126]. However our preliminary studies show that these observations do not extend to SHIP2 in LECs as SHIP2 does not seem to interfere with the Grb2/Shc complex in LECs (**Figure 3.11A**). Nonetheless we cannot rule out the possibility that SHIP2 could non-catalytically inhibit MAPK *via* the interaction of SHIP2 and protein phosphatase 2A (PP2A), a serine/threonine phosphatase that dephosphorylates and inactivates MEK1 and ERK-related kinases [163]. SHIP2 binds PP2A to inhibit epidermal growth factor receptor (EGFR)-signaling [118]. It is of note that we have recently identified a PP2A mutation in a separate family with lymphedema. Therefore, it remains to be validated whether SHIP2/PP2A complex could inhibit MAPK/ERK signaling, or even PI3K/AKT pathway for that matter given that PP2A can also inactivate AKT [164]. With regards to the catalytic regulation of MAPK by SHIP2, PIP3 could potentially lead to membrane recruitment of pleckstrin homology (PH) domain-containing proteins, other than AKT, that subsequently amplify growth factor induced activation of Ras, as reported previously for antigen receptor signaling in lymphocytes [165]. To this end, our preliminary results indicate that exogenous PIP3 is capable of activating MAPK in LECs (**Figure 3.11B**). To determine the extent to which PI3K and PIP3 are required for HGF- and VEGFC-induced MAPK activation in LECs, we further examined the effect of PI3K inhibition in these two pathways. PI3K inhibition substantially reduced but did not completely block HGF- and VEGFC-induced activation of MAPK (**Figure 3.11C**). While the exact mechanism needs to be further clarified in future studies, our initial finding is consistent with the possibility that SHIP2 can use a PIP3-dependent catalytic

mechanism, either directly or indirectly as a consequence of altered PI3K activity, to negatively regulate MAPK in LECs.

Figure 3.11. SHIP2 does not interfere with Shc/Grb2 complex in LEC and PIP3/PI3K influences MAPK activation in LECs. (**A**) TIME cells were transfected with WT SHIP2 (overexp SHIP2) or empty vector for 48 hours, serum-starved for 16 hours followed by HGF or VEGFC stimulation. Total lysates were harvested and subjected to Shc immunoprecipitation using anti-Shc antibody pre-absorbed with agarose beads. Immunocomplexes were probed for SHIP2, phosphoTyrosine (pTyr99), Grb2 and Shc using standard fluorescent immunoblotting techniques. The amount of SHIP2 associated with Shc was not increased over the amount of Grb2 associated with Shc. (**B**) Increasing concentrations of recombinant PI(3,4,5)P3 was delivered into TIME cells using Shuttle PIP kit (Echelon Biosciences) for 1 hour and cells subsequently lysed and subjected to immunoblotting against pAKT and pERK1/2 antibodies. (**C**) PI3K inhibition reduces HGF- and VEGFC-induced ERK activation in LECs. TIME cells were treated with LY294002 (PI3K inhibitor) and U0126 (MEK inhibitor) prior to 5 min growth-factor stimulation. Activation of ERK was determined by Western blotting of cell lysates with double staining of pERK1/2 antibody (red signal) and total ERK1/2 antibody (green signal) to demonstrate equal loading. MW = molecular weight marker. N=3.

Figure 3.11. SHIP2 does not interfere with Shc/Grb2 complex in LEC and PIP3/PI3K influences MAPK activation in LECs

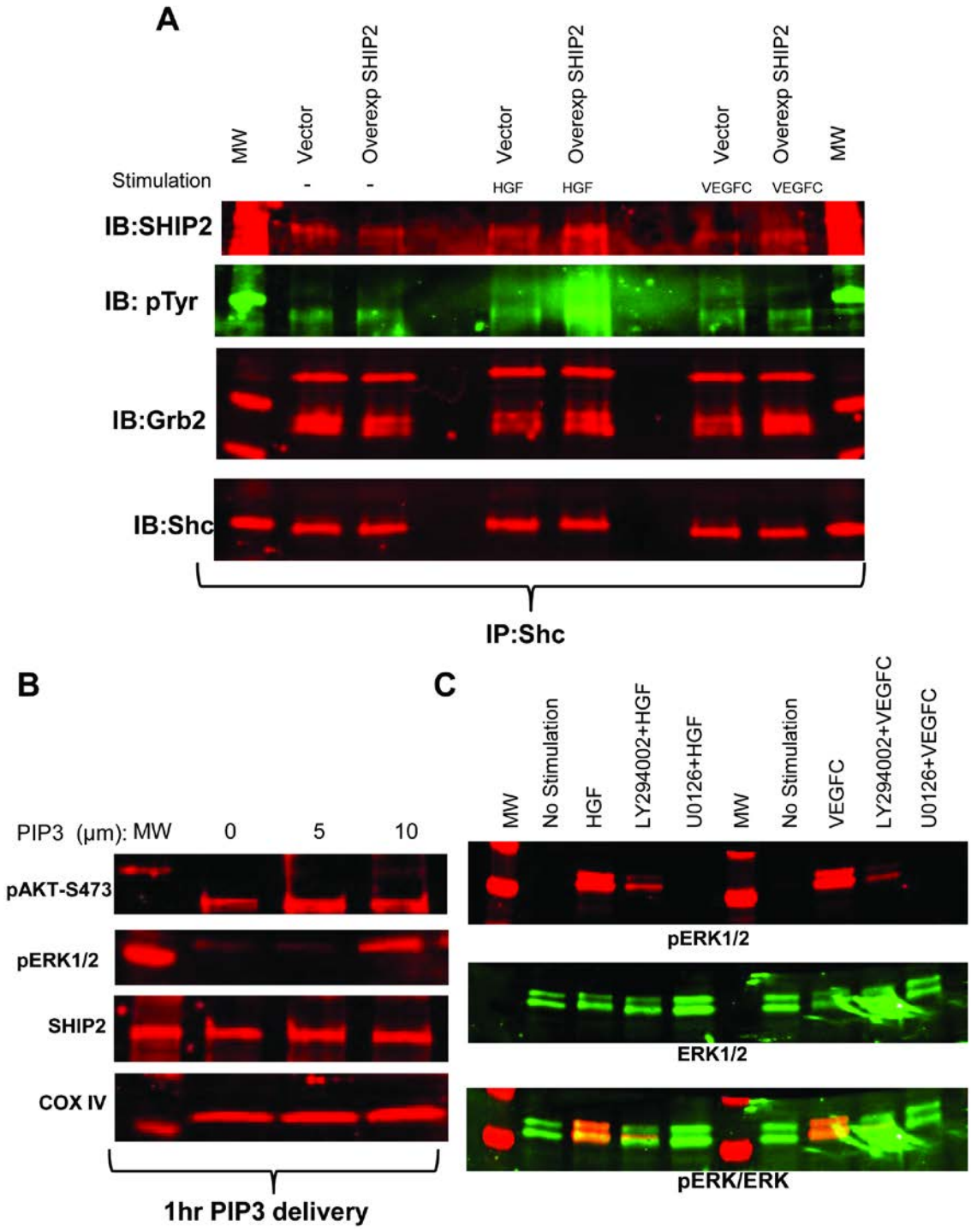

SHIP2 knockdown studies in LECs also showed that this phosphatase is necessary for optimal HGF- and VEGFC-induced proliferation, adhesion, migration, and tubulogenesis, which are all key processes in lymphangiogenesis. We also find that SHIP2 is required for cytoskeletal reorganization in LEC for the optimal polymerization of actin and in lammellipodia formation. As cytoskeletal reorganization is a foremost event that ultimately affects all our examined phenotypes, it is likely that this scaffolding feature of SHIP2 is the major contributing factor to the aberrant lymphangiogenic phenotype exhibited by SHIP2-deficient LEC. Surprisingly, we also found that knockdown of SHIP2 in LECs results in increased apoptosis, despite that PI3K/AKT signaling is recognized to promote cell survival. While the exact mechanisms responsible for this increased apoptosis remain to be studied, it is of note that sustained MAPK signaling, itself a mitogenic pathway, has paradoxically been shown to trigger cell death [166]. In this regard, the increase in MAPK signaling in SHIP2 knockdown LECs was substantially greater than the increase in PI3K/AKT signaling (**Figure 3.2 and 3.3**). Therefore, any increased survival resulting from augmented PI3K/AKT signaling may be counterbalanced and exceeded by increased apoptosis as a consequence of increased MAPK signaling. Mechanisms of ERK-mediated cell death include both intrinsic apoptosis activation characterized by mitochondrial release of cytochrome *c* and activation of caspase-9 and extrinsic apoptosis *via* activation of caspase-8 [166]. Potentially, increased apoptosis in SHIP2 knockdown cells could account for the impairment in the other LEC functional parameters that were examined. To confirm this hypothesis, future studies should evaluate the extent of apoptosis in SHIP2-deficient LEC treated with MAPK inhibitors. On the other hand, increased MAPK activation in other cell types has been shown to inhibit cell proliferation and migration directly [167, 168]. Accordingly, future studies are necessary to investigate whether these mechanisms are at play in the LEC context.

Of the two SHIP2 mutations that were identified in families, one (T180A) is located carboxy terminal to the SH2 domain whereas the other (L632I) is located within the catalytic domain. Molecular modeling studies predicted that the L632I mutation would affect SHIP2 catalytic activity directed toward PIP3. In line with this prediction, L632I SHIP2 showed increased phosphatase activity against PIP3 *in vitro*. Similar predictions could not be made for the T180A mutation since at the time of this writing, the entire three-dimensional crystal structure of SHIP2 has not yet been elucidated. Nonetheless, T180A SHIP2 showed similar levels of PIP3 phosphatase activity as WT SHIP2 *in vitro*. However, in transfected LECs, both of these mutations resulted in loss of an ability of SHIP2 to function as a negative regulator of AKT and MAPK. In contrast to WT SHIP2, T180A SHIP2 was completely unable to inhibit HGF- and VEGFC-induced activation of AKT and MAPK. Similarly, L632I SHIP2 was unable to inhibit HGF- and VEGFC-induced activation of AKT, although retained some activity as an inhibitor of ERK activation, particularly in response to HGF stimulation. Thus, at least with regards AKT and MAPK activation, T180A and L632I represent complete and partial loss-of-function SHIP2 mutations respectively. How the T180A mutation affects the inhibitory function of SHIP2 specifically *in vivo* is unclear at present but does not appear to relate to any impaired ability of SHIP2 to interact physically with cMET or VEGFR3. In contrast, the L632I mutation inhibited an ability of SHIP2 to interact with both receptors. Therefore, the partial loss-of-function of L632I SHIP2 can be explained on the basis of impaired SHIP2 localization to PIP3 which resides at membranes. How SHIP2 binds to VEGFR3 was not determined in this study, but interaction with cMET is known to be mediated by the SHIP2-SH2 domain [107]. As such, it is unclear how the L632I mutation, which is located in the catalytic domain, would affect this SH2 domain-mediated interaction. By analogy with SHP2 protein tyrosine phosphatase (encoded by

PTPN11), it is conceivable that L632 is involved in intermolecular interactions between the catalytic domain and SH2 domain that regulate an ability of the latter to recognize phosphotyrosine ligands [169, 170]. Further insight into how T180A and L632I mutations impair SHIP2 activity is likely to come from determination of the crystal structure of the full length SHIP2 protein. Additionally, while we cannot rule out what impact that endogenous SHIP2 has in the WT- and mutant overexpressing cells, we used vector-transfectants as a control to account for any experimental differences given that a stable SHIP2-null lymphatic cell line is not available.

Consistent with the finding that the magnitudes of AKT and MAPK activation in T180A SHIP2 transfected LECs were comparable to that observed in vector alone transfected LECs, functional responses of the two LEC types were similar. One exception was adhesion of LECs to fibronectin that was increased in T180A-SHIP2 transfected LECs to a similar extent as that observed in WT SHIP2 transfected LECs. This finding could indicate a role for SHIP2 in regulation of adhesion to fibronectin that is independent of its ability to regulate the activation of AKT and MAPK. The functional effects of L632I SHIP2 in LECs are more difficult to interpret. Thus, L632I SHIP2 transfected LECs showed increases in all examined LEC responses compared to control LEC and WT SHIP2 LEC with the exception of adhesion. Therefore, although the L632I mutation results in partial loss-of-function with respect to inactivation of AKT and MAPK, with regards to most functional parameters it has the capacity to behave as a gain-of-function mutation. Alterations in the balance between the extent of AKT *versus* MAPK activation observed in L632I SHIP2 transfected cells, compared to control and WT SHIP2 transfected cells, may underlie this apparent gain-of-function. In addition, unknown effects of the L632I mutation upon AKT- and MAPK-independent functions of SHIP2 may be a contributing factor.

Previous studies performed in epithelial cells have shown that SHIP2 binds HGF-activated cMET at Y1356 in the cMET cytoplasmic tail to effect cell scattering and spreading [107]. Here we show that SHIP2 also interacts with cMET in LECs (**Figure 3.7**). In addition, we show for the first time that SHIP2 interacts with VEGFR3 in LECs. cMET is known to couple to the PI3K signaling pathway through direct physical interaction with PI3K [171]. Similarly, VEGFR3 has recently been shown to trigger the PI3K pathway through physical interaction with PI3K [172]. Altogether, these studies reveal strong similarities in the mechanisms by which cMET and VEGFR3 activate and regulate the PI3K/AKT pathway. The finding that SHIP2 physically interacts with cMET and VEGFR3 in LECs further substantiates the notion that this SHIP2 mutation contributes to the lymphatic abnormalities in the studied families. Furthermore, a role for SHIP2 in cMET and VEGFR3 signaling pathways could provide an explanation for the occurrence of more serious disease in individuals with mutations in SHIP2 together with mutations in one or the other of these RTKs. Similar to mutations in *HGF* and *cMET* [63], it is still unclear why the SHIP2 mutations reported herein results in a lymphatic phenotype, given the relative ubiquitous expression of SHIP2. One possible explanation could be the rapid physiologic lymphatic responses to external triggers during developmental and adult lymphangiogenesis [81]. Compared to the blood vasculature, the lymphatic structure may better facilitate remodeling of capillaries, in which lymphatics' are thin-walled, lack tight junctions, and either lack or have incomplete basement membranes [21]. Another explanation may be the compounding effect of mutations in SHIP2, RTKs or their ligands, or in other components of PI3K/AKT and MAPK/ERK pathways, leading to abnormal LEC signal transduction and subsequently to lymphatic dysfunction.

3.11: Significance

As part of a clinical study to associate non-syndromic lymphatic phenotypes characterized by near-infrared fluorescence lymphatic imaging with genotypes found from unbiased next generation sequencing, we have uncovered two rare mutations in INPPL1. SHIP2 is a phosphatase that negatively regulates the PI3K/AKT signaling, a pathway implicated in syndromic human diseases and animal models of lymphatic dysfunction. With siRNA knockdown, we have shown that SHIP2 is required for the proliferation, adhesion, cytoskeletal reorganization, migration, tubulogenesis, and survival of human lymphatic endothelial cells (LECs), and regulates both PI3K/AKT and MAPK/ERK phosphorylation following stimulation by HGF and VEGFC. When overexpressed in immortalized LECs, mutant SHIP2 abrogated regulation of PI3K/AKT and MAPK/ERK pathways, associated with receptors important in lymphatic signaling, VEGFR3 and cMET, and resulted in impaired, migration, tubulogenesis, chemotaxis, and adhesion. These in vitro results contribute to growing evidence that balanced regulation of PI3K/AKT and MAPK/ERK is required for the development and maintenance of the lymphatic vasculature. However, further investigation into the role of SHIP2 in lymphatic pathophysiology requires in vivo studies, which is the focus of ***Chapter 4****.*

CHAPTER 4

SHIP2 IS REQUIRED FOR NORMAL BLOOD AND LYMPHATIC VASCULATURE FUNCTION IN MICE

This chapter is based on a manuscript that is currently under peer review, “Agollah G.D., Kwon, S., Robinson, H., Sevick-Muraca E.M., “Lymphatic and Vascular Responses to Pharmacological Inhibition of SH2 domain-containing 5-inositol phosphatase-2 (SHIP2)”. *Germaine D. Agollah performed all experiments, unless otherwise noted in figure legends.*

4.1: Rationale

Interruption of the lymphatic transport process caused by genetic defects, physical trauma during surgery, or infection can result in accumulation and stagnation of interstitial fluid and painful swelling leading to irresolvable edema known as lymphedema, a disfiguring and incurable condition [173]. Lymphedema can also be caused by excessive blood capillary filtration that (i) results from venous hypertension due to occlusion or vascular anomaly and (ii) exceeds the transport capacity of otherwise functional lymphatics. Thus it may not be surprising that tissue lymphedema can be part of syndromic disorders wherein the function of the blood vasculature is compromised, overwhelming the lymphatic system and giving rise to the aberrant lymphatics. Given that developmental biology shows that the lymphatic system embryonically arises from the cardinal vein, it is also not surprising that the two vascular systems may share key molecular regulators. With the identification of lymphatic-specific molecular regulators of lymphangiogenesis and embryonic lymphatic development, candidate gene studies have identified mutations in *FLT4* (*VEGFR3*) and *VEGFC* as well as other genes which interact with the vascular endothelial growth factor receptor 3 (VEGFR3)/VEGFC pathways in which they are associated, as being responsible for hereditary lymphatic anomalies, including lymphedema (**Table 1.3**) However, these putative genes that directly or indirectly involve VEGFR3 signaling are not causative in the majority of patients with familial primary lymphedema (64%), and an even higher percentage of those with sporadic lymphedema (92%), thus underscoring the need for identification of other genes directly responsible for lymphatic dysfunction, or contributing to edematous symptoms by mediating the permeability of the blood vasculature [96].

Recently, in an effort to associate lymphatic phenotypes with genetic causes, we conducted investigational non-invasive near-infrared fluorescence lymphatic imaging (NIRFLI) and unbiased gene search using whole exome sequencing (WES) on subjects with non-syndromic, familial lymphedema. We identified rare mutations in the inositol polyphosphate phosphatase-like 1 (*INPPL1*) gene that encodes src homology 2 domain containing 5'-inositol phosphatase-2 (SHIP2) in nine subjects. Six of these subjects have varied clinical diagnoses of lymphedema within a large extended family (**Figure 2.4; Table 2.2**) while two have subclinical disease as determined from aberrant lymphatic function detected from NIRFLI. A third subject with the SHIP2 mutation was not imaged by NIRFLI, therefore their lymphatic phenotype remains unknown. Three of these subjects exhibited varicose veins, two of whom had venous insufficiency showing visibly enlarged veins and telangiectasia. When the SHIP2 mutation was combined with a damaging mutation in hepatic growth factor (HGF), the ligand for the receptor tyrosine kinase (RTK) cMET, or with a mutation of a gene encoding a protein within the MAPK/ERK pathway (*MAP3K7*), family members suffered more severe clinical diagnoses of lymphedema than those who possessed the SHIP2 mutation alone, while no lymphatic abnormalities were associated with either the MAP3K7 or HGF mutation alone, even though mutations in HGF and cMET have been identified as likely causative for primary and secondary lymphedema in breast-cancer survivors [63]. In a second family we identified another SHIP2 mutation which was associated with more exaggerated forms of lymphedema resulting from mutations in *FLT4* that encodes VEGFR3 (**Figure 2.2; Table 2.1**). As discussed in **Chapters 2** and **3**, our clinical and lymphatic endothelial cell (LEC) studies suggest that SHIP2 contributes to, but does not necessarily cause, lymphedema.

Herein we further investigate the role of SHIP2 in lymphatic (patho-) physiology by employing AS1949490, the first discovered small molecule inhibitor of SHIP2 [174]. AS1949490 is a selective inhibitor of phosphatase function of SHIP2 that was recently identified via high throughput screening. AS1949490 is a competitive inhibitor of both mouse and human SHIP2, and was shown to increase phosphorylation of AKT, activate glucose metabolism, suppress gluconeogenesis and improve diabetic-related symptoms in *db/db* mice [174, 175].

4.2: Inhibition of SHIP2 *via* a small molecule inhibitor results in altered *in vitro* lymphangiogenic responses.

By employing RNAi, in **Chapter 3** we showed that SHIP2 is required for *in vitro* lymphangiogenesis in LECs. With the ultimate goal of investigating whether SHIP2 functional inhibition also alters lymphatic responses *in vitro*, we used AS1949490, a commercially available pharmacological inhibitor of SHIP2 [174, 175]. We therefore investigated the effect of AS1949490 on AKT and MAPK activation in HDLECs, to assess whether it had similar effects as we had previously observed with SHIP2-siRNA. We observed a dose-dependent, but modest, activation of AKT and ERK in response to HGF stimulation of HDLECs treated with AS1949490 for 1 hour (**Figure 4.1A** and **4.1B**) without affecting total SHIP2 protein levels. We next assessed the effect of AS1949490 on HDLEC functional responses. Treatment with AS1949490 for 24 hours resulted in reduced cell migration as assessed by wound scratch assay (**Figure 4.1C**) and reduced tube formation following 6 hours of drug treatment (**Figure 4.1D**). Taken together, our data evidences that perturbation of SHIP2, whether through reduced expression *via* siRNA (**Figure 3.2-3.4**) or functional inhibition *via* pharmacological inhibition of SHIP2,

results in reduced *in vitro* HDLEC lymphangiogenic responses and altered PI3K/AKT and MAPK ERK signaling in HDLEC.

Figure 4.1. AS1949490 results in altered *in vitro* lymphangiogenic responses. (**A**) AS1949490 results in a dose dependent modest activation of AKT and ERK1/2 in LECs following 1 hour inhibition followed by 10min HGF stimulation, with no effect on SHIP2 protein levels. Activation of AKT and ERK was determined by fluorescent double staining Western blotting of cell lysates with both phosphospecific antibodies and antibodies to total proteins. Phosphoantibodies were detected by IRDye 680 (red signal) and total antibodies detected by IRDye800 (green signal) fluorescent secondary antibodies. (**B**) Quantification of AKT and ERK activation in LECs by mean fluorescence intensity (MFI) and represented as a ratio of pAKT-S473 to total AKT and pERK1/2 to total ERK1/2, respectively. (**C**) Wound scratch cell migration assay of AS1949490-treated LECs immediately after injury and 24 hrs afterward. (**D**) 3D tube formation networks of AS1949490-treated LECs imaged 6 hrs post plating and treatment. Data presented as means±SEM. *p<0.05, **p<0.01, ***p<0.001. Scale bar = 100µm. N=3. MW=molecular weight marker.

Figure 4.1. AS1949490 results in altered *in vitro* lymphangiogenic responses

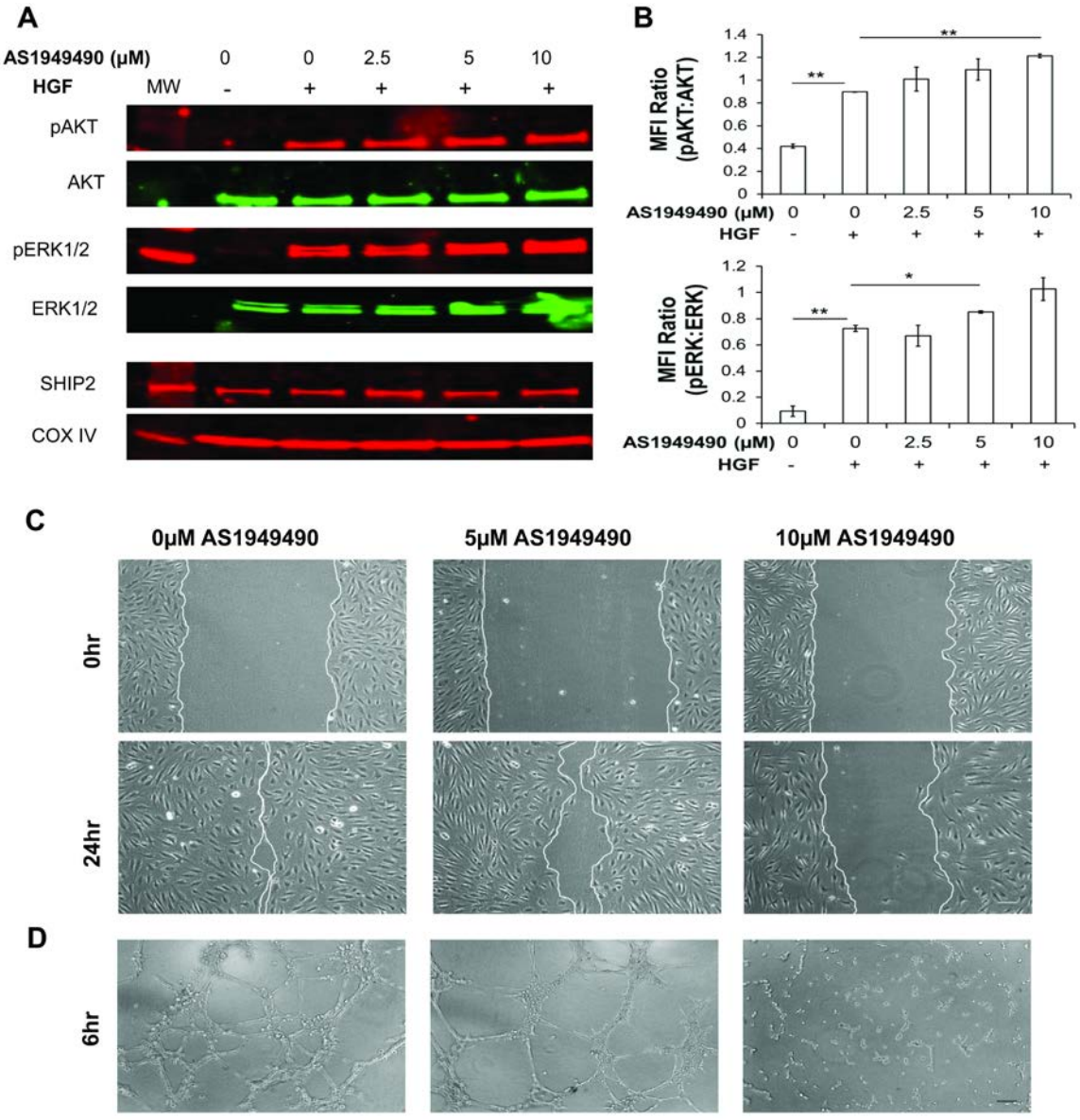

4.3: AS1949490 suppresses *in vivo* lymphatic contractile function.

To assess the effect of SHIP2 pharmacological inhibition on *in vivo* lymphatic function, we orally administered (*per os*; p.o) AS1949490 in normal C57BL/6 mice twice daily for 7 days at 300mg/kg. This chronic administration did not affect mice body weight, and thus was well tolerated as reported previously [174]. To evaluate changes in systemic lymphatic architecture and function in AS1949490-treated mice, non-invasive near infrared fluorescence (NIRF) lymphatic imaging was performed after intradermal (i.d.) injection of indocyanine green (ICG) in the base of tail (**Figure 4.2A**, arrow). ICG is quickly taken up by the lymphatic plexus at the injection site, trafficked to the inguinal lymph node (ILN; arrow head) and to the axillary lymph node (ALN; block arrow). Each mouse was imaged twice to establish normal (baseline) lymphatic architecture and function prior to drug treatment, at Day 3 and Day 7 p.o. Shown in **Figure 4.2A** are the overlay of white light and ICG NIRF images of two representative mice over the treatment period. We did not observe differences in *in vivo* lymphatic architectural between the two groups during treatment with AS1949490. In order to assess lymphatic contractile function, we selected three regions of interest (ROIs) along the fluorescent collecting vessel between the ILN and ALN. Using ImageJ (NIH), the number of ICG-laden lymph bolus contractions was counted between ~5-10 minutes post ICG injection, and the frequency of lymphatic contractions/minute was determined. The average propulsion frequency of two baseline imaging sessions in both control and AS1949490-treated mice was ~6.3/min (**Figure 4.2B**). Treatment with AS1949490 resulted in significantly reduced contractility to approximately ~3.5/min at day 3 p.o, which persisted to day 7 (T Test analysis p=0.002 Control *vs*. P.O Day 3; p=0.014 Control *vs.* P.O Day 7). We also confirmed that the retardation in contractility was not as a result of altered blood pressure. Furthermore, using Quansys cytokine array kit, we assessed whether

cytokine expression was affected by AS1949490 treatment. Of the four cytokines evaluated (interleukin -2 (IL-2), IL-4, IL-6 and tumor necrosis factor-alpha (TNF-α)), we found significantly increased expression of IL-6 and TNF-α in the skin (**Figure 4.2C**), and serum (**Figure 4.2D**), of AS1949490-treated mice. There were no differences in the levels of IL-2 and IL-4 of the skin or serum in the two groups (**Figure 4.2E-F**). Previously, it was found that certain cytokines, including IL-6 and TNF-α, mediate lymphatic contractility in response to acute inflammation [176]; thus, our data suggests that in response to AS1949490, lymphosuppressive cytokines such as IL-6 and TNF-α are upregulated, possibly resulting in reduced lymphatic propulsion. We also assessed activation of PI3K/AKT and MAPK/ERK pathways in homogenized skin of AS1949490-treated mice and found increased levels of pERK1/2, pAKT, pGSK3β, among others, indicating the activation of these pathways in response to SHIP2 inhibition which could contribute to reduced lymphatic function (**Figure 4.2G**).

Figure 4.2. Reduced *in vivo* lymphatic function following AS1949490 treatment. (**A**) Overlay of white light and fluorescent (green) images following ICG injection at base of tail (arrow) and trafficking to inguinal lymph node (ILN; arrowhead) onto the axillary LN (ALN, block arrow). No significant differences were seen in lymphatic architecture between control and AS1949490-treated mice over the treatment period. (**B**) Significantly reduced *in vivo* lymphatic contractility at day 3 with AS1949490 treatment which persists to day 7. N=4 Control, N=6 AS1949490. Data presented as means±SEM. Upregulation of lymphosuppressive cytokines IL-6 and TNF-α in skin (**C**) and serum (**D**), while no differences were observed in levels of IL-2 and IL-4 (**E-F**) in AS1949490-treated mice compared to Controls. (**G**) Analysis of skin homogenates using PathScan intracellular signaling array kit (Cell Signal) showing detection of 18 signaling molecules either phosphorylated or cleaved. (**B**) **p*<0.05, ***p*<0.01, ****p*<0.001 vs Control baseline; #*p*<0.05, ##*p*<0.01, ###*p*<0.001 vs. Control treatment at respective day; %*p*<0.05, %%*p*<0.01, %%%*p*<0.001 vs. AS1949490 baseline. (C and D) **p*<0.05, ***p*<0.01, ****p*<0.001 vs. Control. *(NIRF lymphatic imaging, as shown in Figure 4.2A, performed with assistance from Dr. SunKuk Kwon).*

Figure 4.2. Reduced *in vivo* lymphatic function following AS1949490 treatment

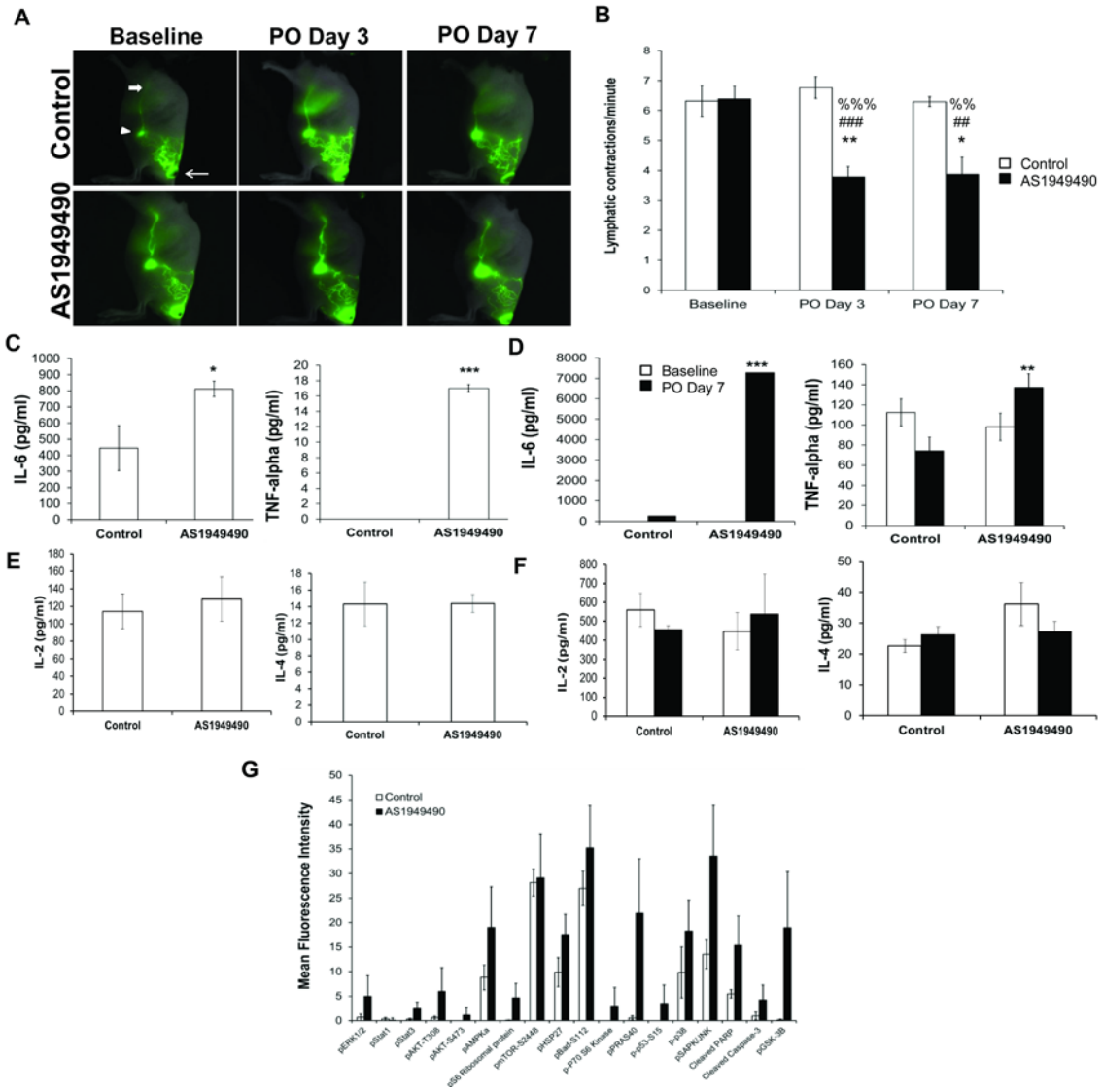

4.4: AS1949490 alters immune cell profiles in lymph nodes.

Given that AS1949490-treated mice had reduced lymphatic function, we next sought to determine whether the cellular composition in lymph nodes was altered due to AS1949490 treatment. Smaller lymph nodes were observed in AS1949490-treated mice in comparison to vehicle control-treated mice (**Figure 4.3A**). We performed flow cytometry on single cell suspensions harvested from axillary lymph nodes to analyze relative percentages of various immune cells as a function of total cells. This analysis revealed significantly reduced total leukocytes (CD45+) in mice treated with AS1949490 for 7 days, but no difference between control and 3-day treated mice (**Figure 4.3B**). This trend was also seen in percentages of B cells ($CD45^+CD19^+$), T helper cells($CD45^+CD4^+$), cytotoxic T cells ($CD45^+CD8^+$), macrophages ($CD45^+F4/80^+$), myeloid cells ($CD45^+CD11b^+$) and presumed neutrophils ($CD45^+Ly6g/Gr1^+CD11b^+$). Dendritic cells ($CD45^+CD11c^+$) were also reduced in day 7-treated mice, but the difference was not significant in comparison to either control or day 3. Interestingly, the frequency of presumed T regulatory cells ($CD45^+CD4^+CD25^+$) increased ~2-fold at day 3 compared to control levels, but then significantly decreased ~3 fold below control mice levels. On the other hand, the percentage of non-leukocytes ($CD45^-$) was significantly increased in day 7 mice in comparison to both control and day 3 mice. In summary, while the effect of AS1949490 on lymphatic function is evident by Day 3 (**Figure 4.2B**), immune cell profile is not altered until 7 days on treatment, and is accompanied by a shift to increased non-leukocyte populations in lymph nodes.

Figure 4.3 Altered immune cell profile in lymph nodes with prolonged AS1949490 treatment. (**A**) Smaller axillary LNs were observed in AS1949490 treated mice which also showed altered immune cell profiles compared to vehicle control and Day 3 treated mice (**B**). All data presented as means±SEM . *p<0.05, **p<0.01, ***p<0.001 vs Control; #p<0.05, ##p<0.01, ###p<0.001 vs AS1949490 PO Day 3. Scale bar = 1mm.

Figure 4.3. Altered immune cell profile in lymph nodes with prolonged AS1949490 treatment

A

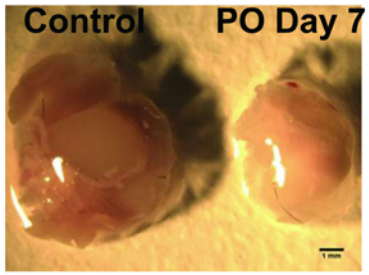

B

Cell Type	Gating	Control (n=6)	AS1949490 PO Day 3 (n=3)	AS1949490 PO Day 7 (n=4)
Leukocytes	CD45+	72.6 ± 2.98	72.8 ± 2.16	25.4 ± 3.38$^{***\#\#\#}$
Non-leukocytes	CD45-	25.0 ± 2.77	24.0 ± 2.01	71.9 ± 3.50$^{***\#\#\#}$
B cells	CD45+CD19+	26.9 ± 2.46	26.5 ± 1.93	10.3 ± 2.45$^{**\#\#}$
T helper cells	CD45+CD4+	29.1 ± 3.09	25.4 ± 3.12	9.4 ± 2.95$^{**\#}$
Cytotoxic T cells	CD45+CD8+	22.1 ± 1.85	26.1 ± 0.85	9.0 ± 1.95$^{***\#\#\#}$
T regulatory cells	CD45+CD4+CD25+	3.3 ± 0.30	7.0 ± 2.05*	1.2 ± 0.27$^{**\#}$
Dendritic Cells	CD45+CD11c+	6.7 ± 0.97	6.7 ± 0.80	4.1 ± 1.15
Macrophages	CD45+F480+	4.7 ± 0.68	12.9 ± 6.68	2.2 ± 0.67*
Myeloid Cells	CD45+CD11b+	7.8 ± 0.82	7.7 ± 2.06	3.4 ± 1.08**
Neutrophils	CD45+Ly6g/Gr1+CD11b+	10.1 ± 0.90	10.2 ± 1.78	4.4 ± 1.25$^{**\#}$

Data presented as mean±SEM
*p<0.05; **<0.01; ***<0.001 *vs.* Control
#p<0.05; ##<0.01; ###<0.001 *vs.* AS1949490 PO Day 3

4.5: AS1949490 alters wound healing responses in normal mice.

Wound healing is a complex process which requires coordination of angiogenesis, lymphangiogenesis, and inflammatory cell infiltration among other mechanisms, for complete tissue repair [177]. Given the anti-lymphangiogenic *in vitro* responses we observed following inhibition of SHIP2, we next investigated the effect of SHIP2 drug inhibition on *in vivo* lymphangiogenesis. Ear punch biopsy wounds were generated on normal C57BL/6 mice, and AS1949490 was administered twice daily for 7 days *via* oral gavage. Whole mount immunofluorescence staining for the lymphatic endothelial marker, LYVE-1 and blood vessel marker CD31 (also known as PECAM1 and exhibits higher expression in blood vessels) were used to visualize vessels at the wound edge on day 7 after wounding. Enlarged lymphatic vessels (arrow head) accompanied by more robust lymphatic sprouting (arrows) were seen in control animals (**Figure 4.4A**). In contrast, AS1949490-treated mice exhibited thinner lymphatic vessels (arrow head) and reduced vessel sprouting (**Figure 4.4B**). In control mice, we observed denser CD31-positive networks around the edge of the wound which appeared as increased CD31 staining at lower magnification (asterix), likely around the granulation tissue. Higher magnification images showed increased blood vessel density in control mice as compared to AS1949490-treated mice (arrows). Image analysis of vessels formed through lymphangiogenesis and angiogenesis carried out using AngioTool software [178] showed that AS1949490-treated mice had decreased lymphatic and blood vessel areas (**Figure 4.4C** and **4.4D**, respectively) in comparison to control animals. Assessment of non-wounded ears following AS1949490 treatment (**Figure 4.5A-D**) revealed a slight reduction (91495 *vs*. 93242µm^2) in total lymphatic vessel area of all analyzed animals, which was not statistically significant (**Figure 4.5C**) but significantly reduced blood vessel area (**Figure 4.5D**) compared to control treatment.

Figure 4.4. AS1949490 alters lymphangiogenic and angiogenic wound healing responses in normal mice. (**A, B**) Whole mount staining of the wound edge (white dashed line) on day 7 after wounding using lymphatic LYVE-1 (green) and blood vessel CD31 (PECAM1; red) of control-treated (**A**) and AS1949490-treated (**B)** mice. Note denser lymphatic networks with larger vessels (arrow head in LYVE1 inset panels and lymphatic sprouting (arrows) in control mice compared to AS1949490-treated mice. Denser blood vessels (asterix) and larger $CD31^+$ vessels (arrows) in control mice compared to AS1949490-treated mice (**C, D**) Graphical representation of lymphangiogenesis and angiogenesis analysis. N=7 Control, N=9 AS1949490. Scale bars = 400µm (top LYVE1 inset panel in **A** and **B**); 200µm (large double stained panels, middle and bottom LYVE1 inset panels and top CD31 inset panels in **A** and **B**); 100µm (middle CD31 inset panels in A and B); 50µm (middle and bottom CD31 inset panels in **A** and **B**).

Figure 4.4. AS1949490 alters lymphangiogenic and angiogenic wound healing responses in normal mice

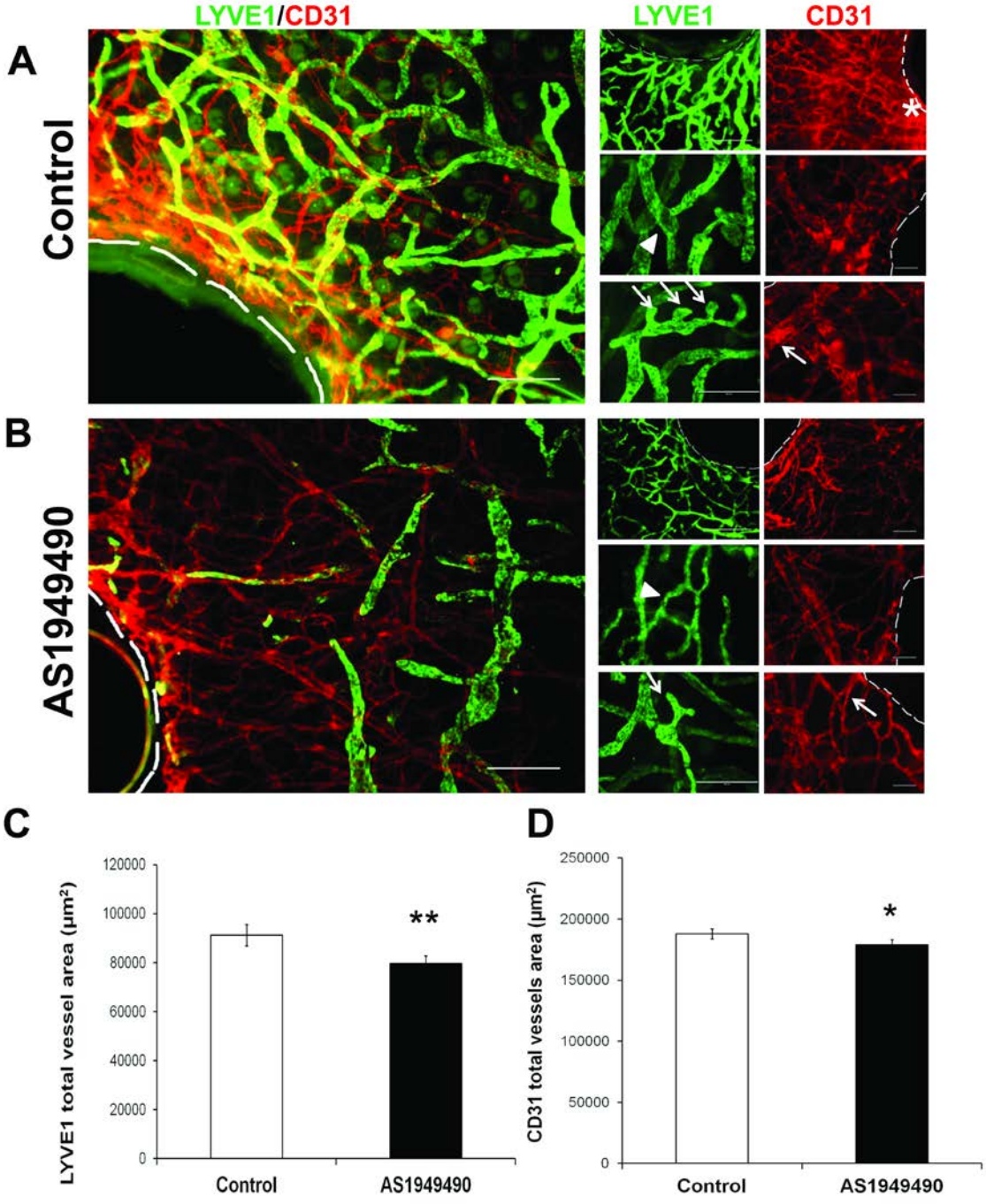

Figure 4.5 Effect of AS1949490 on lymphatic and blood vessels in unwounded ears. (**A, B**) Whole mount staining of contralateral (unwounded) ears on day 7 of lymphatic LYVE-1 (green) and blood vessel PECAM1 (CD31; red) of control-treated (**A**) and AS1949490-treated (**B)** mice. Difference in lymphatic vessel area is not significant between the two groups (**C**) while there is reduced blood vessel networks in AS1949490-treated mice (**D**) N=7 Control, N=9 AS1949490. *p<0.05, **p<0.01. Scale bar = 200µm.

Figure 4.5. Effect of AS1949490 on lymphatic and blood vessels in unwounded ears

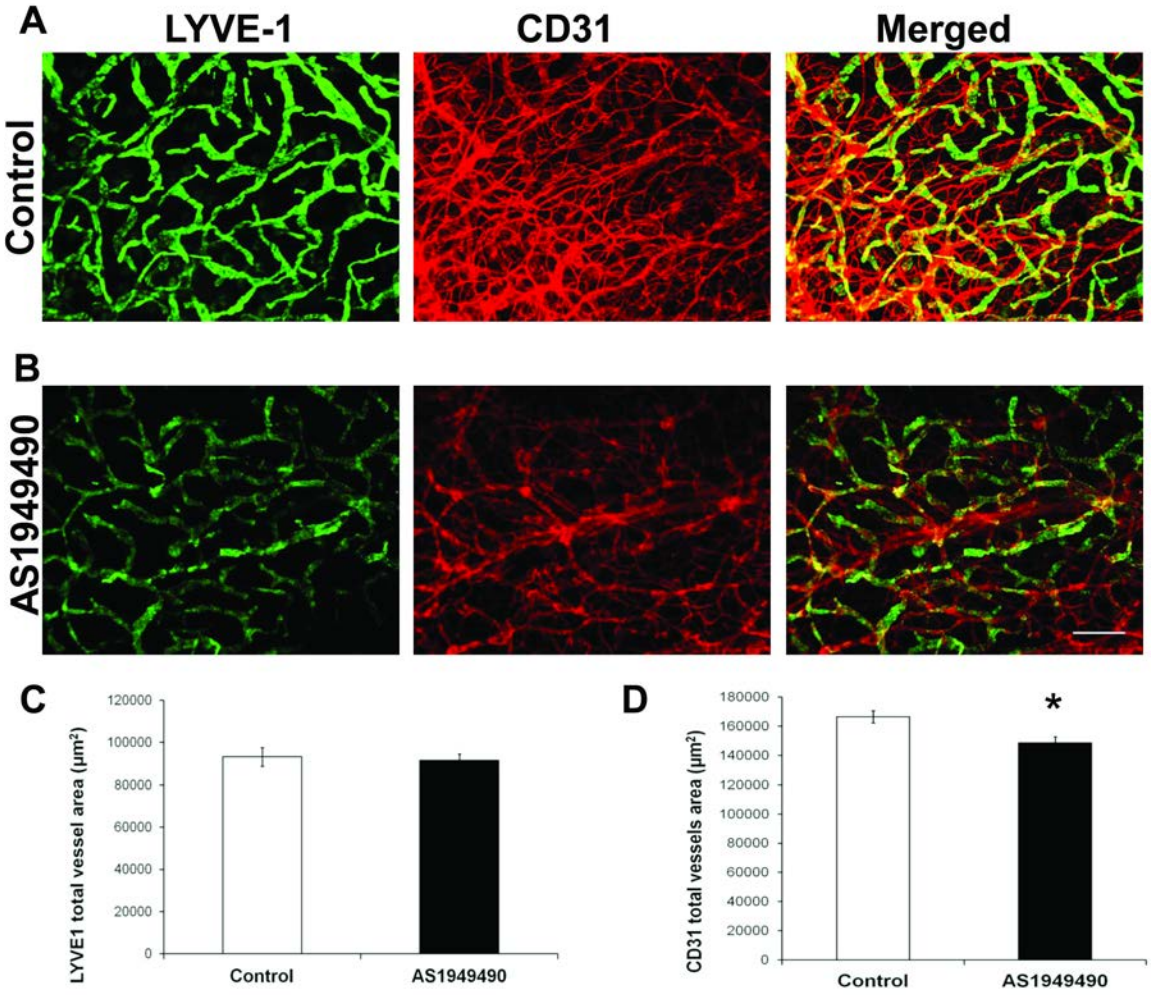

The wounds were costained with F4/80 to assess infiltration of macrophages to the wound bed (**Figure 4.6**). More macrophages were visualized in the wound edge in control mice compared to AS1949490-treated mice. Some of the $F4/80^+$ cells colocalized with $CD31^+$ (arrow head) and with $LYVE^+$ vessels (arrows) in control animals (**Figure 4.6A**), suggesting that endothelial vessels release chemoattractants of macrophages to the wound site. Quantification of macrophages in the wound edge shows a ~2-fold increase in the number of $F4/80^+$ cells in the wound edge in control animals compared to AS1949490-treated animals (**Figure 4.6C**). As macrophages respond to VEGFC signals and in turn themselves become a potent source of VEGFC thus inducing angiogenesis and lymphangiogenesis [31, 179], it is likely that AS1949490 hinders the initial production of lymph(angiogenic) growth factors such as VEGFC, leading to reduced macrophage infiltration at the wound site. In this study, VEGFC was not directly measured. In summary, chronic administration of AS1949490 significantly reduced macrophage infiltration, as well as suboptimal lymphangiogenic and angiogenic responses, all of which result in delayed wound healing in mice (**Figure 4.6D**).

Figure 4.6. AS1949490 alters macrophage infiltration during wound healing. (A) Increased F4/80^{+} macrophage infiltration at the wound edge of control animals, some of which colocalize with blood vessels (arrow head) and lymphatic vessels (arrows) compared to AS1949490-treated mice (**B**). (**C**) Macrophage cell counts in 400x images confirm reduced infiltration in AS1949490-treated mice. N=3 Control, N=3 AS1949490. (**D**) ImageJ analysis of area of wound at Day 7 shows smaller wounds in control-treated mice compared to AS1949490-treated mice. *p<0.05, **p<0.01. Scale bars = 100 (large panels in **A, B**) and 25μm (insets in **A, B**).

Figure 4.6. AS1949490 alters macrophage infiltration during wound healing

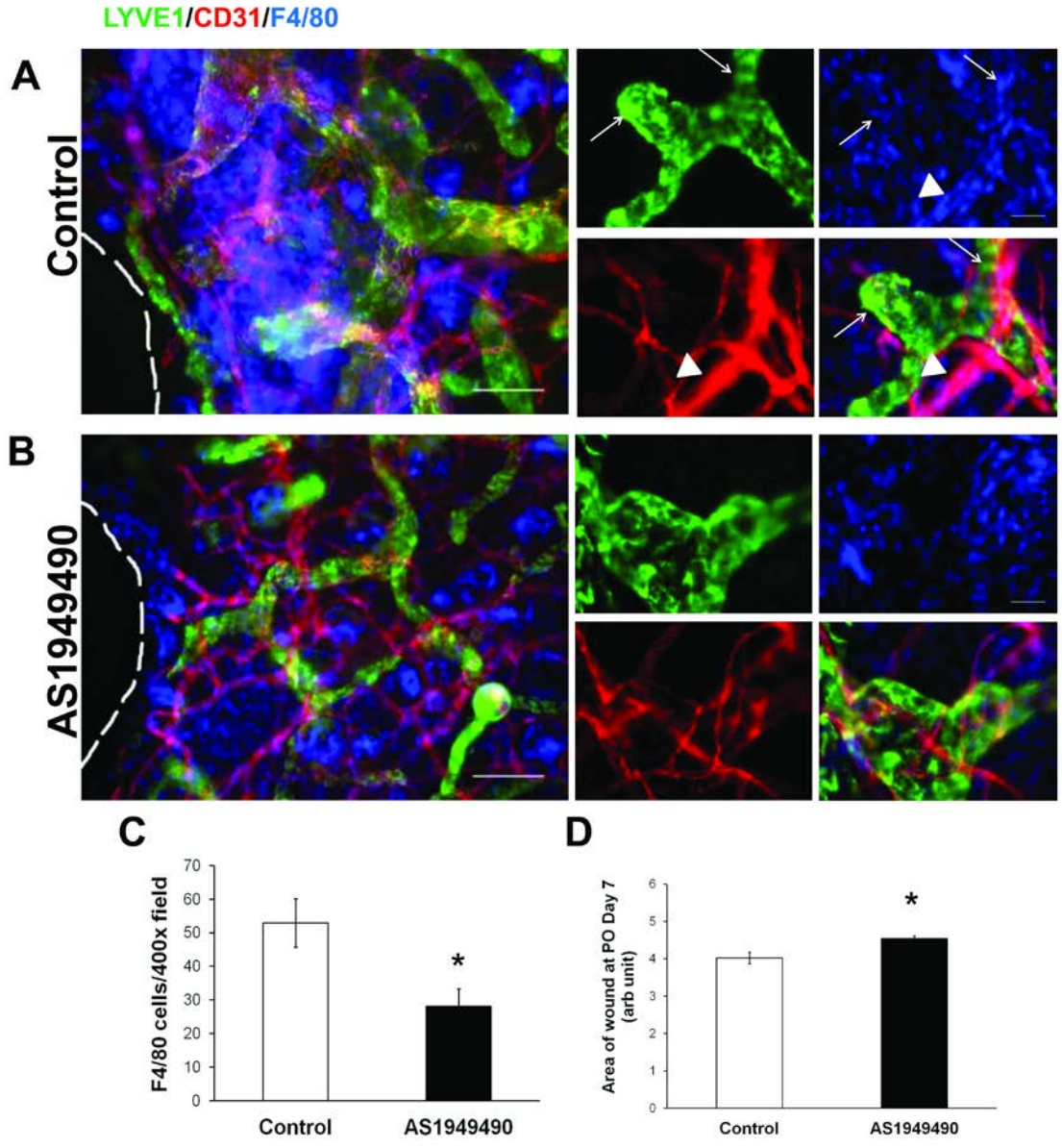

4.6: AS1949490 alters *in vitro* angiogenesis and MAPK activation in BEC.

Given the reduced angiogenic response in wound healing in AS1949490-treated mice, we next assessed whether SHIP2 directly plays a functional role in blood endothelial cells (BECs). We first confirmed the blood endothelial lineage of human umbilical vein/vascular endothelium cells (HUVECs) by flow cytometric analysis of lymphatic-expressing podoplanin and pan-endothelial CD31 antigen expression (**Figure 4.7A**). We found that SHIP2 was expressed in HUVECs, and transfection with SHIP2 siRNA resulted in effective knockdown as revealed by Western blotting (**Figure 4.7B**). The ability of HUVECs to organize into tube-like structures was assessed using a 3D-Matrigel angiogenesis assay. SHIP2 knockdown resulted in significantly less tube formation compared to control HUVECs (**Figure 4.7C, D**). Activation of AKT in HUVEC was examined by Western blotting using phospho-specific anti-AKT antibodies (**Figure 4.8A**). However, HGF-stimulation of control HUVECs showed no response in activation of AKT up to 60 minutes, a result also seen in SHIP2-siRNA transfectants. These results were also noted in response to VEGFA stimulation. We examined activation of MAPK after SHIP2 knockdown in HUVECs using phospho-specific anti-ERK antibodies. In control HUVECs, HGF induced activation of ERK, with peak responses occurring at 10 minutes, persisting to 15 minutes post-stimulation. In SHIP2 knockdown in HUVECs, substantial increases in the magnitude of ERK activation were evident in response to HGF and VEGFA, and similar kinetics were observed, but SHIP2-siRNA treatment increased ERK activation (**Figure 4.8A, C**). We also examined whether AS1949490 impacted activation of AKT and MAPK activation in HUVECs, as we had observed with HDLECs (**Figure 4.8B**). Similar to results seen with SHIP2-siRNA (**Figure 4.8A**), 1 hour SHIP2 inhibition *via* AS1949490 did not affect AKT activation, yet it significantly increased HGF-induced ERK activation in a dose-dependent manner. This effect was

also observed following VEGFA stimulation (**Figure 4.8B**). Combined, our data suggests that in HDLECs, SHIP2 exerts its influence *via* both the PI3K/AKT and MAPK/ERK pathways; but only *via* the MAPK/ERK pathway in HUVECs.

Figure 4.7 SHIP2 is necessary for *in vitro* angiogenesis in BECS. (**A**) Blood endothelial lineage of HUVECs was confirmed using lymphatic-specific marker anti-human podoplanin (left panel) and pan-endothelial marker anti-human CD31 (right panel). Markers are depicted in orange, isotype controls are in blue and unstained controls in red. HUVECs are Podoplanin^{-}CD31^{+}. 50,000 events per experiment, N=3. (**B**) Western blot analysis of SHIP2 in 3 independent transfections of SHIP2 siRNA in HUVECs. Equal loading was determined by Western blotting for COX IV. (**C**) 3D tube formation networks of SHIP2-siRNA HUVECs imaged 8 hrs post plating and quantification of percent vessel area (**D**) shows reduced tubulogenesis in SHIP2 siRNA transfectants. Cell viability confirmed with Calcein AM staining of tube networks. N=3. MW=molecular weight marker. Scale bar = 100µm.

Figure 4.7 SHIP2 is necessary for *in vitro* angiogenesis in BECs

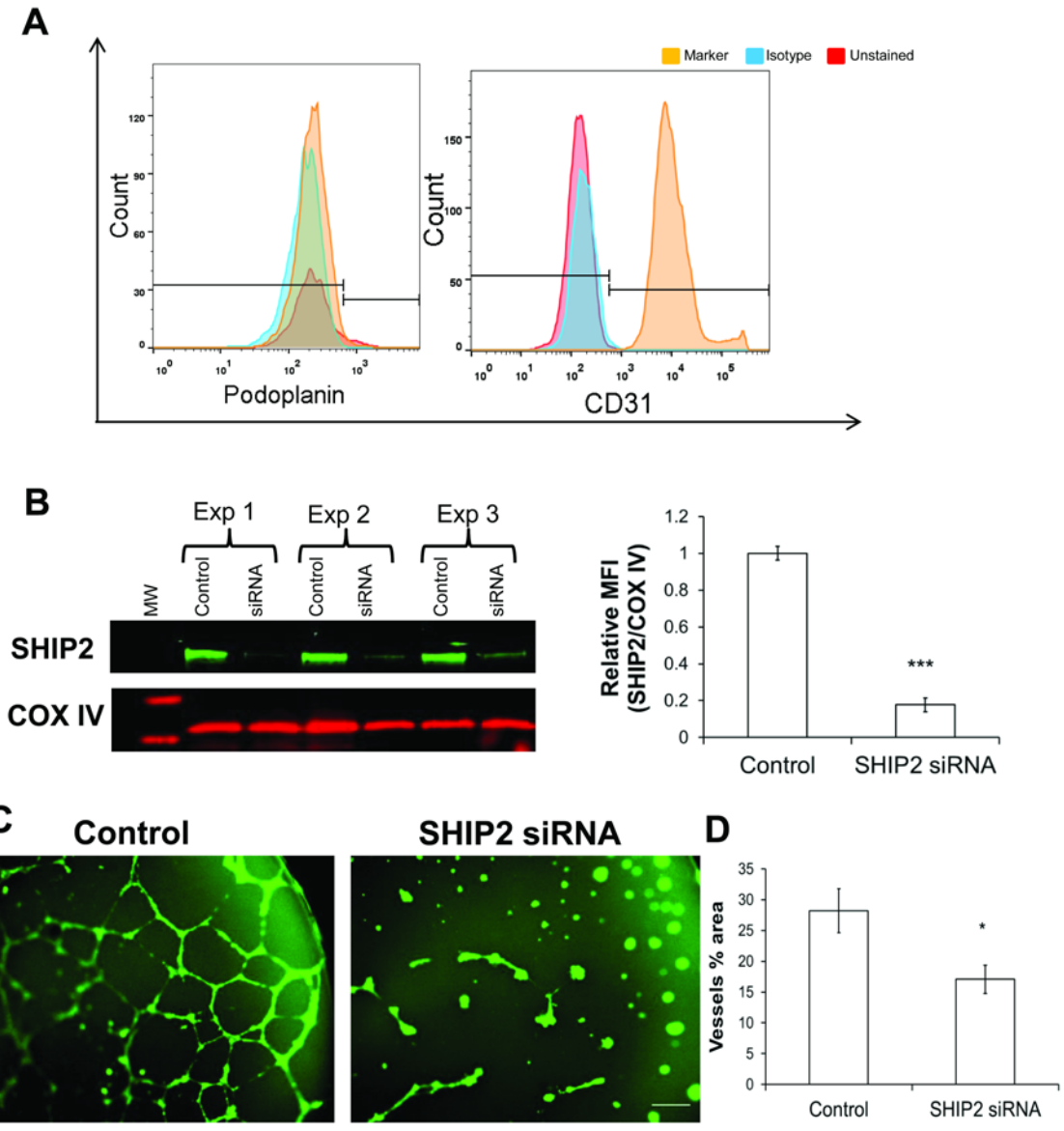

Figure 4.8 AS1949490 alters MAPK activation in BECs. (**A**) HUVECs were subjected to 48hr SHIP2 siRNA and stimulated with HGF and VEGFA for the indicated times. Activation of AKT and ERK was determined by fluorescent double staining Western blotting of cell lysates with both phosphospecific antibodies and antibodies to total proteins. Phospho-antibodies were detected by IRDye680 (red signal) and total antibodies detected by IRDye800 (green signal) fluorescent secondary antibodies. SHIP2 knockdown levels shown and COX IV used as loading control. (**B**) AS1949490 results in a dose dependent significant activation of ERK1/2 in HUVEC following 1 hour inhibition and 10min HGF and VEGFA stimulations, with no effect on AKT activation or SHIP2 protein levels. Quantification of ERK activation by mean fluorescence intensity (MFI) and represented as a ratio of pERK1/2 to total ERK1/2 following HGF stimulations of SHIP2 siRNA (**C**) and AS1949490 treatment (**D**). Data presented as means±SEM. **p*<0.05, ***p*<0.01, ****p*<0.001. N=3. MW=molecular weight marker. N.S=not significant.

Figure 4.8. AS1949490 alters MAPK activation in BECs

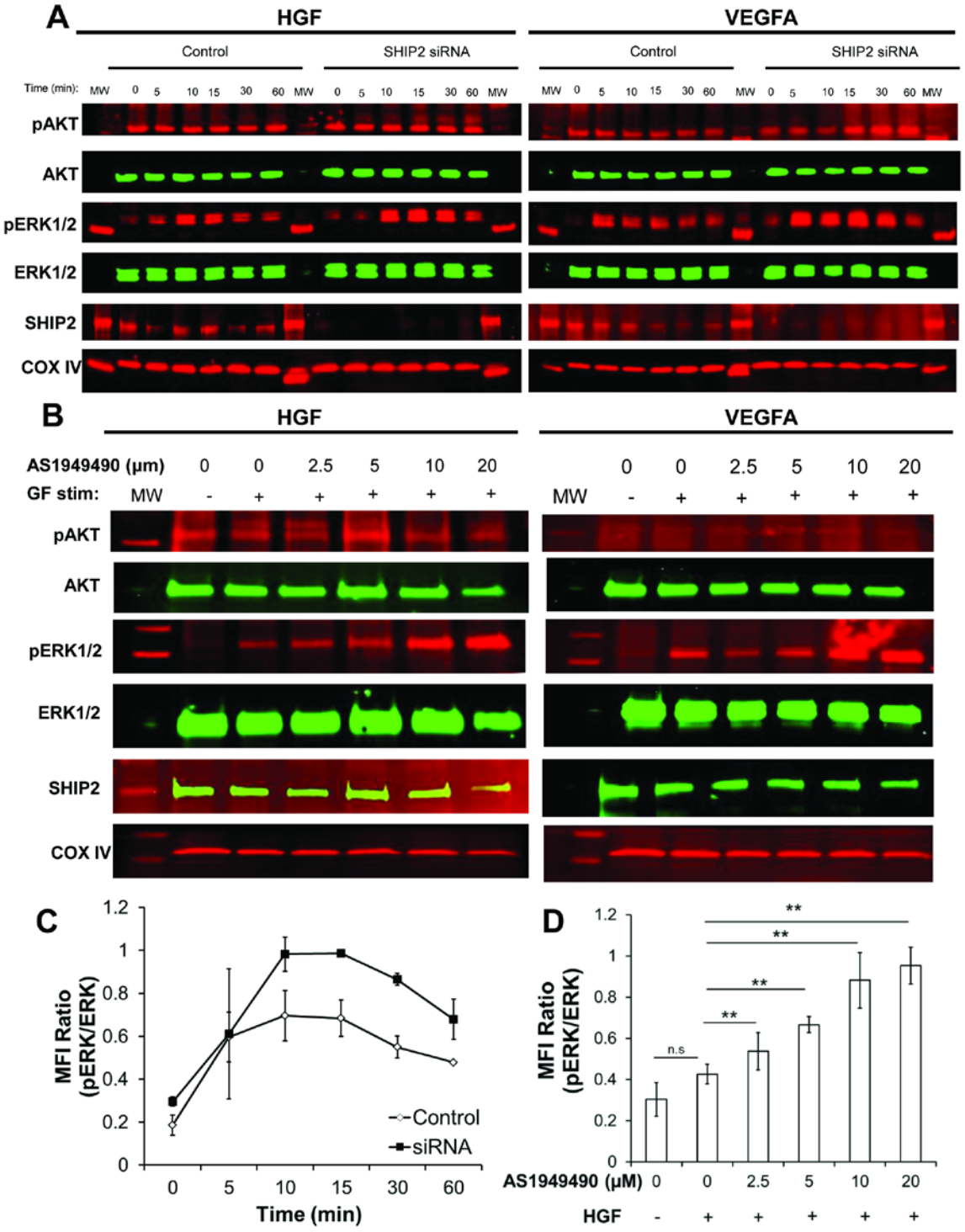

4.7: Discussion

Currently, known lymphedema-causing genes explain only one third of all familial primary lymphedema cases, thus WES techniques are necessary in identifying other currently unknown genes that contribute to lymphedema [96]. As part of a clinical study to associate non-syndromic lymphatic phenotypes characterized by NIRFLI with genotypes found from unbiased NGS, we uncovered SHIP2 mutations in families with lymphedema (Discussed in **Chapter 2** and **3**). In that study, *in vitro* analysis in LECs showed that mutant SHIP2 abrogated regulation of PI3K/AKT and MAPK/ERK pathways, resulted in impaired lymphangiogenesis, and SHIP2 associated with VEGFR3 and cMET, two RTKs important in lymphatic development and function. Enhanced ERK activation was associated with LEC apoptosis, consistent with reports from Cagnol *et al.* [166]. Herein, we further examine the potential effector role of SHIP2 in vascular function in HDLECs and HUVECs using AS1949490, a small molecule inhibitor of SHIP2, and RNAi transfections. In HDLEC, both AKT and ERK are activated in a dose-dependent manner in response to growth factor stimulation following AS1949490 treatment, while only ERK activation was observed in HUVECs (**Figure 4.1** and **4.8.)** In both HDLECs and HUVECs, AS1949490 resulted in reduced cell migration and tubulogenesis, consistent with dysregulated ERK activation which is likely due to apoptosis. These observations are also extended to effects of SHIP2 siRNA. Interestingly, our finding that neither HGF nor VEGFA induces AKT activation in HUVECs following SHIP2 knockdown or pharmacological inhibition, suggests that AKT and ERK have differing functions in LECs *versus* BECs, and that SHIP2 can exert its influence distinctly in either endothelial cell type, further highlighting the complexity of SHIP2 function in different cellular contexts (see **Chapter 2**, **Section 2.4.3**). Our results complement those by Tvorogov *et*

al. who showed that VEGFC strongly induces both AKT and ERK activation in LECs, but only ERK activation in BECs [180].

In this proof-of-concept study, we also showed that treatment with AS1949490 systemically suppressed *in vivo* lymphatic contractility as early as three days into treatment, suggesting that SHIP2 inhibition has a significant impact on systemic lymphatic function. While the exact mechanisms responsible for this AS1949490-induced retarded lymphatic contractility are currently unknown, they are likely not due to vessel dilation, as we observed no significant differences in *in vivo* lymphatic architecture as assessed by NIRF imaging. However, we assessed intracellular signaling molecules in the skin and found increased expression of pERK1/2, pAKT, pGSK3β, among others, indicating that AS1949490 also activates PI3K/AKT and MAPK/ERK signaling in the skin (**Figure 4.2E**). Moreover, we observed upregulation of lymphosuppressive cytokines in the skin and serum of AS1949490-treated mice. Previously it has been shown that during lipopolysaccharide (LPS)-induced acute inflammation, cytokines such as IL-1β, IL-6 and TNF-α are quickly upregulated within 4 hours, concurrent with stagnation of lymphatic flow. Additionally, local administrations of these cytokines impede systemic lymphatic function in normal mice in an inducible nitric oxide synthase (iNOS)-dependent manner [176]. These cytokines could directly impede lymphatic contractility, or induce LECs, BECs, macrophages, or other stromal cells to release additional factors that diminish lymphatic function. For example, a previous study showed that in response to TNF-α and interferon-γ (IFN-γ), macrophages secrete nitric oxide (NO), which induces mesenteric lymphatic vessel dilation and reduced contractility [181, 182]. During normal conditions, NO produced by endothelial nitric oxide synthase (eNOS) in LECs aids in maintenance of lymphatic contractility and NO produced by iNOS during inflammation overrides the normal eNOS-regulation [183-185];

thus, it is likely that increased levels of TNF-α lead to increased NO levels and reduced lymphatic contractility in response to AS1949490. Catalytic inhibition of SHIP2 *via* AS1949490 could also directly affect cytokine levels. Previous studies have shown that SHIP2 and its homologue SHIP1, negatively regulate IgE + antigen-induced cytokine production in mast cells, and specifically SHIP1 inhibits IL-6 and TNF-α by inhibiting calcium influx and phosphorylation of ERK [186, 187]. It remains to be elucidated whether similar mechanisms are at play in LECs and BECs following SHIP2 siRNA or AS1949490 treatment. Additionally, given that the lymphatics play a key role in immune response by providing a conduit for antigen presenting cells (APCs) and leukocyte migration, it may be expected that reduced lymphatic function could result in altered immune profiles in lymph nodes, and thus altered immune responses. Indeed, we found a significant decrease in all leukocyte subpopulations in lymph nodes with prolonged exposure to AS1949490. Our observations of no differences between control-treated and day 3 AS1949490-treated animals suggests that sustained stagnation of lymph flow may be required for altered immune cell profiles, and by day 7, the majority of cells in peripheral lymph nodes are non-leukocytes, which are likely stromal cells. While our studies ended seven days into treatment, these results raise the possibility of impaired immune surveillance upon prolonged SHIP2 inhibition.

Wound repair requires a coordinated effort requiring inflammation, granulation tissue formation, re-epithelization, angiogenesis and lymphangiogenesis [188]. During wound healing, macrophages are initially recruited by VEGFC secretion, and in turn, macrophages become the major source of growth factors, including VEGFC, that accelerate tissue repair [189]. Exogenous administration to wounds has shown that VEGFC enhances angiogenesis and lymphangiogenesis and accelerates wound healing [177, 188, 190]. In response to AS1949490, we observed reduced lymphatic and blood

vessel networks and macrophage infiltration to the wound bed. Given that SHIP2 is expressed by LECs, BECs, and other cell types that would affect the wound healing process, we cannot rule out the possibility that vascular changes we observe are directly reflective of lymphatic and blood vessel function, instead of secondary consequences of altered SHIP2 function in the different SHIP2-expressing cell types in the wound bed. Additionally, future studies are needed to assess whether AS1949490 alters local expression of VEGFR3 and cMET, and whether exogenous administration of HGF and VEGFC can overcome impaired wound healing in AS1949490-treated animals.

Known for its inhibitory role against PI3K/AKT signaling, a pathway that is often disordered in diabetes, SHIP2 has recently been investigated as a potential therapeutic target in Type 2 diabetes *via* development of small molecule inhibitors [174, 191, 192]. Of the published studies, AS1949490 is the only small-molecule inhibitor showing *in vivo* anti-diabetic effects [108, 174, 175]. However, wound healing is impaired in diabetes, and therefore our studies may suggest that inhibiting SHIP2 could potentially worsen diabetic wound healing. Strategies that stimulate lymph(angiogenesis) such as exogenous administration of VEGFC as shown by Saaristo *et al*. might be more beneficial in treating diabetic wounds [188]. Nevertheless, recent evidence suggests that SHIP2 also has a proto-oncogenic role in cancer, and pan-SHIP1 and SHIP2 inhibitors have been identified to have efficacy in killing multiple myeloma and SHIP2-overexpressing breast cancer cells [193]. The most recent *Ship2* genetic mouse model mimics the effect of systemic AS1949490, whereby Ship2 is expressed but catalytically inactive [123]. As there have been no reported NIRF-detected lymphatic defects in SHIP2 mouse models [121-123], it remains unknown whether lymphatic phenotypes would occur in response to inducible catalytic inactivation of *Ship2* in LECs. It is of note

that mouse knockouts of PTEN, which, similarly to SHIP2, is a negative regulator of PI3K/AKT signaling, do not exhibit lymphatic phenotypes [194-197]. However, PTEN has been implicated in human lymphatic malformations, specifically Proteus-like syndrome, exhibiting medium penetrance and loss-of-function phenotypes [143].

4.8: Significance

SHIP2 is a negative regulator of the PI3K/AKT pathway that has been implicated in syndromes involving lymphatic and blood vascular anomalies and more recently, in familial cases of non-syndromic lymphedema. We have shown that a selective, competitive inhibitor of SHIP2, AS1949490, significantly inhibits tubulogenesis and cell migration in both lymphatic and blood endothelial cell (LEC and BEC) assays, and results in enhanced phosphorylation of both AKT and ERK in LECs stimulated by HGF and VEGFC. In contrast, AS1949490 treatment of BECs has little or no impact on AKT phosphorylation but a strong dose-dependent ERK phosphorylation when stimulated by HGF and VEGFA as compared to control cells. These results may be consistent with the differential AKT driven responses of LECs and BECs recently reported by others. Furthermore, in animals with ear punch wounds that were administered vehicle as control and AS1949490 at therapeutic doses used in other studies, we further demonstrate that AS1949490 reduced in vivo lymphatic contractility assessed by dynamic NIRF lymphatic imaging, increased levels of serum and skin IL-6 and TNF-α, depressed the number of leukocytes in lymph nodes, and impaired wound repair processes of angiogenesis and lymphangiogenesis. Because SHIP2 is investigated as a therapeutic target against Type 2 diabetes in which patients are at risk for impaired wound healing, further work is required to understand the role of SHIP2 in the processes that mediate angiogenesis and lymphangiogenesis.

CHAPTER 5

CLINICAL SIGNIFICANCE AND FUTURE DIRECTIONS

While the main roles of the lymphatic circulatory system are to transport excess fluids and protein from interstitial tissue to lymph nodes for immune surveillance and to maintain hydrostatic fluid homeostasis, dysregulated lymphatics have been attributed to diverse pathological conditions including lymphedema, inflammation, tumor metastasis, and more recently to transplant rejection, cardiovascular disease and obesity [18, 22, 23, 29, 35, 38, 173, 198]. While the existence of the lymphatic system has been known since the early 20th century, the discoveries of molecular regulators of lymphatic development have only been identified within the last ~15 years. We are progressively gaining knowledge of biological mechanisms that underlie aberrant and normal lymphatic function, including associated genotypes and phenotypes. In this dissertation project, we have shown that the unique combination of NIRF, an emerging fluorescence lymphatic imaging modality, to accurately phenotype abnormal, yet asymptomatic lymphatics, and unbiased NGS techniques, can lead to gene discovery of polymorphisms that contribute to lymphatic disease.

Herein, in **Section 5.1**, we will summarize the major findings of this dissertation and highlight the potential clinical impact that this multidisciplinary project will have on the ever increasing population of cancer survivors, currently with lymphedema, or at risk for developing this incurable and highly disfiguring disease. In **Section 5.2**, we will discuss both short and long term research efforts that are necessary to address gaps in this field that are essential to maximize patient benefit. Namely, development of more stable and brighter dyes than ICG is necessary, which will aid in delineation of lymphatic architecture, and thus improve diagnosis and phenotypic characterization of subjects with lymphedema. Additionally, as discoveries of genes that contribute to lymphedema continue to be made, the simplistic classification of lymphedema that has remained in place for over 50 years that are based on age of onset rather than pathophysiology,

need be revised accordingly. Efforts should also be made to treat underlying specific pathology of lymphedema by development of molecular therapies.

Finally, in **Section 5.3**, we explore an emerging concept in lymphatic research: the likely reciprocal relationship between lymphedema and obesity, and whether SHIP2 could bridge these two fields.

5.1: Summary and Significance

5.1.1: Summary

Specifically, in this dissertation the following were accomplished:

1. Using indocyanine green (ICG)-based investigational NIRF lymphatic imaging, we non-invasively visualized lymphatic architecture and dynamic pumping function in symptomatic and asymptomatic in human subjects in two families with varied rare, primary and common, acquired (secondary) diagnoses of lymphedema.
2. We conducted unbiased WES on the subjects' collected DNA with the aim of linking genotypes with the associated abnormal phenotypes. We discovered two mutations in inositol polyphosphate phosphatase-like 1 (*INPPL1*) gene that encodes src homology 2 domain-containing 5'-inositol phosphatase 2 (SHIP2). We also identified mutations in *HGF* and *VEGFR3*, both of which are known to affect lymphatic development and function. When *SHIP2* mutations were combined with mutations in *HGF* or *VEGFR3*, family members suffered more severe forms of lymphedema, thus forming the basis of our hypothesis: *SHIP2 is a modulator of lymphatic function which could contribute to the varied expressivity and penetrance seen in lymphatic disorders, including lymphedema*.

3. We investigated the functional role of SHIP2 in lymphatic biology and identified that SHIP2 is expressed in LECs. Knockdown of SHIP2 using RNA interference expectedly resulted in activation of PI3K/AKT signaling, a pathway that has been implicated in lymphatic disease and that SHIP2 is known to inhibit *via* hydrolysis of PIP3. Interestingly, we identify that SHIP2 also inhibits MAPK/ERK signaling, a pathway that has recently been recognized in lymphatic malformations. Phenotypically, we showed that knockdown of SHIP2 altered all major aspects of *in vitro* lymphangiogenesis including LEC proliferation, adhesion, cytoskeletal reorganization, migration, microtubule morphogenesis and LEC survival, thus highlighting the importance of this enzymatic adaptor protein in optimal LEC function.
4. Overexpression of the SHIP2 mutants identified in human subjects in immortalized LECs revealed aberrant activation of PI3K/AKT and MAPK/ERK pathways and altered *in vitro* lymphangiogenesis in LEC, with T180A exhibiting a complete loss-of-function phenotype and L632I showing a partial loss-of-function phenotype.
5. Finally, we find that pharmacological inhibition of SHIP2 using AS1949490, a competitive small molecule inhibitor, resulted in similar loss-of-function *in vitro* functional phenotypes and activation of PI3K/AKT and MAPK/ERK pathways seen in RNAi and mutant SHIP2 LEC studies, further confirming the role of SHIP2 in LEC biology. Chronic administration of AS1949490 in normal mice resulted in suppressed *in vivo* lymphatic contractile function assessed by NIRFLI, concurrent with upregulation of cytokines previously recognized to impede lymphatic pumping. Prolonged treatment with AS1949490 also resulted in altered immune cell profiles in lymph nodes suggesting that SHIP2 is necessary for normal immunological responses. We find that the normal wound healing

responses of angiogenesis; lymphangiogenesis and inflammatory cell infiltration were altered in AS1949490-treated mice. Studies in blood endothelial cells (BECs) also show that SHIP2 is required for *in vitro* angiogenesis and regulates activation of MAPK/ERK, yet does not impact PI3K/AKT activation. In all, these studies suggest that SHIP2 is intricately involved in blood and lymphatic function, two circulatory systems that must cooperate in fluid homeostasis, thus could explain how SHIP2 contributes to lymphatic disease seen in human subjects.

5.1.2 Significance: Improving Cancer Survivorship through NIRF and Gene Discovery

In the Western world, secondary (or acquired) lymphedema (LE) following cancer treatment is the most common type of lymphatic disease. While personalized medicine strategies such as targeted molecular therapies are being developed, surgery and radiation remain the major treatment options for cancer. Lymph node dissection (LND) enables regional control of disease and staging to curtail metastases, as majority of epithelial cancers develop metastatic growth *via* lymphatic vessels to the tumor draining LN (TdLN) [198]. Unfortunately, while essential, LND damages and/or obstructs normal lymphatic flow thus increasing the risk for LE. The exact prevalence of cancer-related lymphedema (CRL) is unknown due to inconsistent diagnostic methods, which could be improved by imaging techniques such as NIRFLI. A study estimated that 43%-94% of all breast cancer survivors developed LE in the arm within 5 years post-surgery [199]. That such a huge variation exists in estimating BCRL further highlights the lack of consensus in diagnosing lymphedema. CRL is also prevalent in other cancers. 20% of cervical cancer survivors; up to 64% of melanoma prostate and bladder cancer survivors and 50% of all head and neck cancer survivors will develop LE as a direct result of their treatment [67, 200-205]. As of 2012, an estimated 3-5 million of the total 12 million

cancer survivors suffer from LE and more are at risk for the incurable disease [206, 207]. With increased cancer survivorship, the incidence of CRL is also expected to rise accordingly. While primary lymphedema is a rare disease with an estimated incidence of 1/6000 [208], secondary lymphedema is becoming increasingly common given the rise in cancer survivors. As diagnosis of primary LE is typically based on genetic causes and no prior trauma or surgery, molecular understanding of the rare primary disease, could enable our understanding of the more common secondary LE whose etiology is varied.

It remains unknown why some cancer survivors encounter lymphedema after minimally invasive sentinel LND, while others who have more extensive LNDs and radiation do not develop LE. Recent evidence suggests that an explanation for this CRL disparity might be genetically based. We posit that both primary and secondary LE are diagnoses within the same genetic spectrum, for example primary LE might be caused by ablative mutations that completely alter genetic function of the encoded proteins, while secondary LE may be predisposed by genetic variations that do not result in critical loss of function (first hit) but upon surgery or trauma such as during LND (second hit) there is onset of LE. Indeed, four clinical studies, summarized in **Table 5.1**, have thus far identified various genetic mutations as potential susceptibility genes for breast cancer related lymphedema (BCRL), lending credence to our hypothesis [63, 70, 209, 210].

Table 5.1 Identified mutations that increase risk for breast cancer-related lymphedema (BCRL)

Study	Study population	LE Candidate Genes Analyzed	BCRL Susceptibility Genes
Finegold *et al.*, 2008	Cases: 59 participants with BCRL; 21 participants with LE and intestinal lymphangiectasia Controls: 159 unrelated ethnically matched subjects	*VEGFR3, SOX18, FOXC2, HGF, cMET*	*HGF, cMET*
Finegold *et al.*, 2012	Cases: 80 participants with BCRL Controls: 108 BrCa survivors without LE	*VEGFR3, FOXC2, HGF, cMET, GJC2*	*GJC2 (Connexin 47)*
Newman *et al.*, 2012	Cases: 22 participants who developed LE within 18 months of BrCa diagnosis Controls: 98 BrCa survivors without LE	*VEGFR3, SOX18, VEGFC, VEGFD, VEGFR2, RORC, FOXC2, LYVE1, ADM, PROX1*	*VEGFR3, VEGFR2, RORC*
Miaskowski *et al.*, 2013	Cases: 155 participants with BCRL Controls: 387 BrCa survivors without LE	*ANGPT2, FOXC2, HGF, LCP2, LYVE1, cMET, NRP2, PROX1, RORC, SOX17, SYK, VCAM1, VEGFB, VEGFC, VEGFD, VEGFR2, VEGFR3*	*LCP2, NRP2, SYK, VCAM1, FOXC2, VEGFC*

LE, Lymphedema; BCRL, Breast cancer related lymphedema; BrCa, breast cancer

If there is indeed a genetic link between primary and secondary LE, as we believe, phenotypic characterization using non-invasive NIRF imaging and genetic techniques such as whole exome sequencing (WES), of cancer survivors and their family members could provide a method for gene discovery. The identification of lymphatic biomarkers could affect disease management, for example in a growing cancer-survivorship population where an unmet clinical need with huge economical potential and quality-of-life impact exists. For example, identification and biological validation of a biomarker, such as SHIP2, as a potential therapeutic target to treat and/or prevent CRL could ultimately influence cancer treatment in the following ways: (i) enable phenotypic characterization of lymphatic architecture and function prior to start of cancer treatment using NIRFLI; (ii) enable genetic screening of cancer patients to determine risk of developing CRL based on their biomarker status; and (iii) ameliorate the risk of LE by seeking alternate cancer treatment options for those patients who harbor a genetic predisposition for the disease.

5.2: Future Directions

In the short term, we can address the disparity in lymphedema diagnosis by improving the lymphatic imaging system; and reclassify lymphedema based on phenotype-genotype associations by incorporating NIRFLI and WES techniques, rather than age of onset. In the long term, molecular treatments should be developed that target the underlying pathology of lymphedema rather than management of symptoms.

5.2.1: Improving NIRF lymphatic imaging

Currently, NIRF imaging makes use of ICG, a fluorescent dye that has been used safely in humans for over 50 years in vascular and hepatic studies due to its dark green color and ability to bind serum and albumin proteins in blood [211-214]. ICG is the only

FDA-approved agent that can be used off-label as a NIR fluorophore used for interrogating lymphatics. However, ICG has poor fluorescent properties including short ~20-hour half-life once reconstituted and low quantum yield, necessitating development of brighter and stable NIR dyes. Owing to the poor stability and low quantum yield of ICG, we have recently developed an enhanced NIR peptide dye, cyclic albumin-binding domain peptide conjugated to IRDye800 (cABD-IRDye800). cABD-IRDye800 has high affinity for albumin and has superior optical properties and lymphatic retention compared to either ICG or IRDye800 alone. cABD-IRDye800 has a half-life of 20 days in solution and has been found to be 5-fold brighter than ICG in *in vivo* preclinical studies [215]. Regulatory efforts are currently being made towards translating cABD-IRDye800 for clinical use.

The use of fluorescent gene reporters in conjunction with ICG (or cABD-IRDye800) NIRF imaging is another option in increasing the utility of fluorescent lymphatic imaging. Gene reporter studies have traditionally involved expression of shorter wavelength visible fluorescent reporters such as green fluorescent protein (GFP) under control of lymphatic-specific markers such as *Prox1* promoter [216]. A recent study employed a dual fluorescence-luminescence reporter consisting of EGFP-LUC under control of *Vegfr3,* whereby low resolution non-invasive bioluminescence was used to longitudinally assess lymphatic responses and high resolution fluorescence microscopy performed at animal endpoint [177]. To our end, we are currently making use of far-red, longer wavelength fluorescent gene reporters in combination with near infrared longitudinal lymphatic imaging. For example, in a recent study [217] (**Appendix page 207**), we stably transfected infrared fluorescent protein (iRFP) gene reporter in human inflammatory breast cancer (IBC) cell line (SUM149) which was then inoculated in mice. Thus, a dual-wavelength analysis could assess tumor growth, progression and

metastasis using the iRFP spectra (excitation 690nm; emission 710nm) and associated lymphatic response using ICG spectra (excitation 785nm; emission 830nm). With development of other far-red fluorescent reporters currently underway, such dual imaging strategies will offer non-invasive methods to longitudinally monitor lymphatic response to tumor growth and could be extended to other pre-clinical applications, such as drug discovery.

5.2.2: Proposed classification of lymphedema based on phenotype-genotype associations

Historically, primary lymphedema has been classified based on the age of onset of disease. In 1934, Allen *et al.* introduced "lymphedema *congenita*" as primary lymphedema present at birth and "lymphedema *praecox"* as disease that presents shortly thereafter [218]. In 1957, Kinmoth *et al*. added "lymphedema *en tarda*" to the original classification if disease onset is >35yrs [219]. These simplistic classifications of primary lymphedema have since remained in place, and in 2010 Connell *et al*. proposed an algorithm based on clinical phenotype that took into account patient age, affected sites, and associated features, extent of lymphatic involvement and familial history [220]. In 2013, these authors updated this algorithm to include causative genes that had been discovered since 2010 and suggested genetic tests; a tool that has been useful in clinical diagnosis [221]. However, if this classification scheme were applied to our studies, subjects would be erroneously classified. For example Subjects #1, 4, 16 and 17 would be classified as having Meige disease with likely mutations in *GJC2*, which they do not possess; while Subject #2 would be classified as having Milroy's disease yet she does not harbor *VEGFR3* nor *VEGFC* mutations. Concurrent with the Connell 2013 study, Mendola *et al*. also proposed a scheme for genetic analysis of lymphedema [96]. With the accumulating evidence of a possible genetic link between primary and

secondary lymphedema, we build on both of these 2013 classification schemes and propose (i) the addition of accurate phenotyping such as that afforded by NIRF lymphatic imaging, (ii) inclusion of secondary lymphedema, both CRL and non-CRL such as filaria, (iii) whole exome analysis and subsequent pathway analysis to help identify potentially causative, yet currently unknown genes and finally, (iv) biological validation of potential genetic variants as we have attempted with SHIP2 in this dissertation project. This proposed classification scheme is shown in **Figure 5.1**. While we propose the use of WES, it is likely that as NGS techniques become more affordable, other analyses such as whole genome sequencing (WGS) that interrogate the entire genome including the protein-encoding exome and non-encoding intronic regions; and copy number variation (CNV) analysis that assesses regions that are deleted or amplified within chromosomes could be performed, which could potentially identify whether epigenetic and somatic changes have a role in lymphedema.

Figure 5.1 Proposed scheme for the phenotypic and genotypic analysis of lymphedema patients.

Adapted and modified from:

Mendola, A., Schlogel, M.J., Ghalamkarpour, A., Irrthum, A., Nguyen, H.L., Fastre, E., Bygum, A., van der Vleuten, C., Fagerberg, C., Baselga, E., Quere, I., Mulliken, J.B., Boon, L.M., Brouillard, P., and Vikkula, M., *Mutations in the VEGFR3 signaling pathway explain 36% of familial lymphedema.* Mol Syndromol, 2013. **4**(6): p. 257-66. [96].

Connell, F.C., Gordon, K., Brice, G., Keeley, V., Jeffery, S., Mortimer, P.S., Mansour, S., and Ostergaard, P., *The classification and diagnostic algorithm for primary lymphatic dysplasia: an update from 2010 to include molecular findings.* Clin Genet, 2013. **84**(4): p. 303-14. [221].

Figure 5.1 Proposed scheme for the phenotypic and genotypic analysis of lymphedema patients

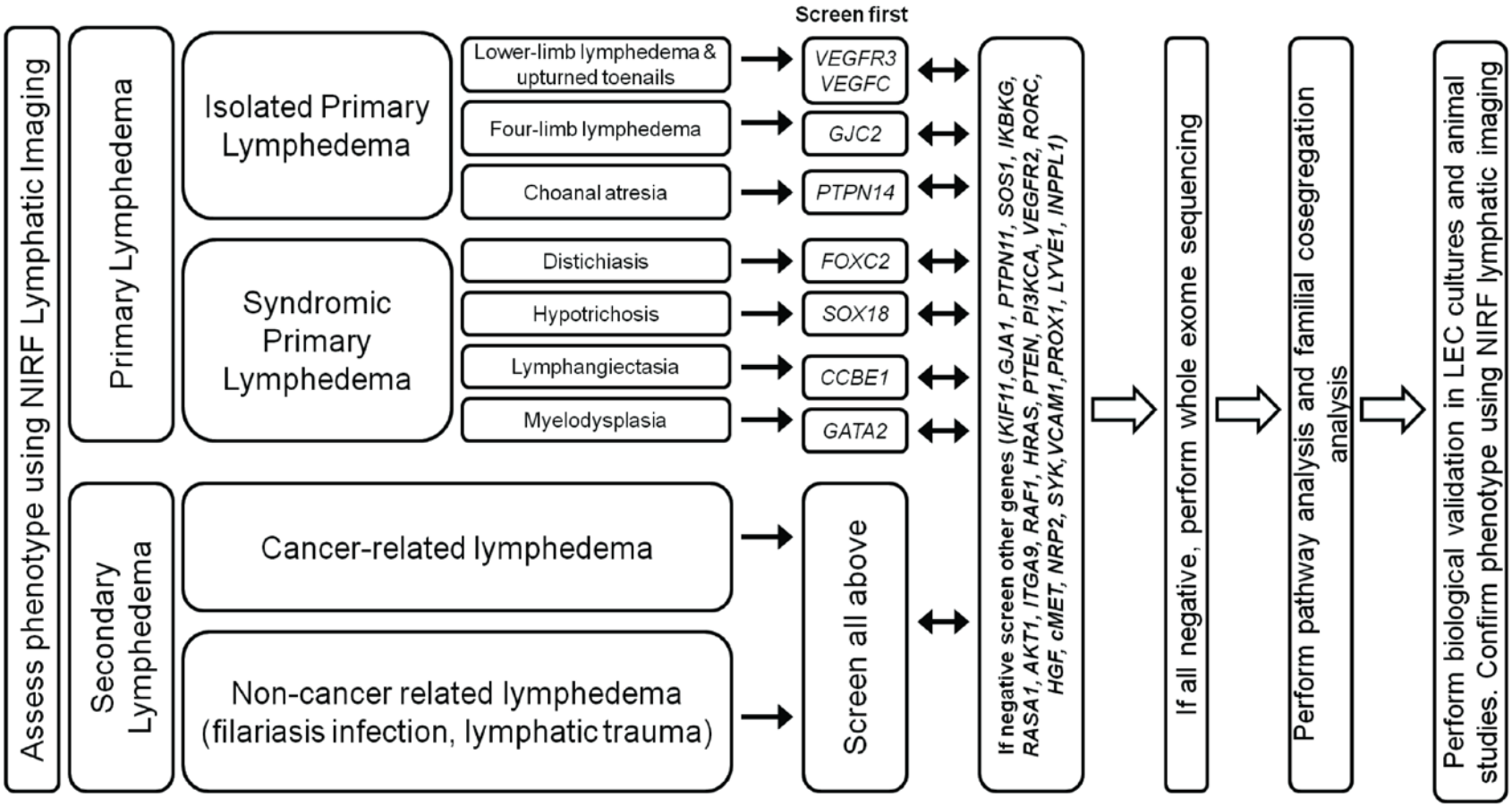

5.2.3: Treating Lymphedema: Beyond Manual Lymphatic Drainage (MLD)

Developed in the 1930's by Dr. Vodder, MLD therapeutic massage techniques still remain the standard of care for lymphedema treatment [222]. As discussed in **Chapter 1**, there are neither pharmacological treatments nor preventive strategies for lymphedema, and none of the current techniques reverse the underlying lymphatic pathophysiology of the disease. The basis of the MLD technique is two-fold: stimulation of lymphatic drainage from the receiving lymph node basins and subsequent stimulation of contractility of the superficial lymphatic vessels, with treatment outcomes measured through reduction of limb volume, often with varying success rates [223]. Additionally, patients are required to wear compression garments, which unfortunately are frequently uncomfortable and fraught with non-compliance. As a result, while incidence of lymphedema is rising and now among the most reimbursed therapeutic service by US Centers for Medicare and Medicaid Services (CMS), medical coverage is threatened as CMS recently reported that no study has demonstrated direct evidence of benefit of lymphedema MLD treatment (or lymphedema diagnosis using the current clinical "gold-standard" imaging technique of lymphoscintigraphy for that matter) [224]. Thus negative coverage decisions could impact the availability of the only clinically accepted treatment for lymphedema patients, including the growing number of cancer survivors [224]. Nonetheless, the recent identification of molecular regulators of lymphatic development and function provides an exciting new frontier for development of targeted, pharmacological therapies for lymphedema.

Lymphangiogenic growth factor therapy is the most promising molecular strategy in treating damaged or insufficient lymphatic vessels. Stimulation of VEGFR3 using VEGFC results in growth and survival of LECs and lymphangiogenesis. In mice, VEGFC therapy has been shown to result in lymphatic capillary growth, remodeling,

differentiation and maturation into functional vessels [225]. Various preclinical studies of primary and secondary lymphedema have shown effective reduction in lymphedema symptoms through VEGFC delivery either through adenoviruses, adeno-associated viruses, naked plasmids or recombinant protein soluble VEGFC to *Chy* (*Vegfr3* mutant) mice, rabbits and sheep [24, 226, 227]; (**Appendix page 210**). Other studies have included lymph node (LN) transplantation in conjunction with VEGFC therapy resulting in formation of afferent and efferent vessels around transferred LNs and their connection to pre-existing lymphatic networks, restoring lymphatic function [225, 228-230]. Ideally, treating human lymphedema will require long term delivery of VEGFC such as that afforded by adenoviral transfer, with or without LN transplantation, and following initial, active lymphangiogenesis, newly formed vessels would mature, with pericytes and intraluminal valves (**Figure 5.2**). This treatment strategy could be longitudinally monitored using NIRF lymphatic imaging.

Figure 5.2. VEGFC-induced regeneration of lymphatic vessels for treatment of lymphedema. Lymphedema develops following lymphatic injury such as during cancer treatment, surgery or infection. Adenoviral VEGFC with or without lymph node (LN) transfer at diseased site could be used. VEGFC expression increases with maximum levels at approximately two to three weeks. Following initial capillary sprouting and lymphangiogenesis, vessels mature, with smooth muscle cells (SMC; pericytes) development and formation of intraluminal valves, as levels of VEGFC reduce over time. NIRF lymphatic imaging can be used to noninvasively monitor effectiveness of treatment as newly-formed vessels become functional.

Modified and reproduced with permission from Zheng, W., Aspelund, A., and Alitalo, K., *Lymphangiogenic factors, mechanisms, and applications.* J Clin Invest, 2014. **124**(3): p. 878-87 [231].

Figure 5.2. VEGFC-induced regeneration of lymphatic vessels for treatment of lymphedema

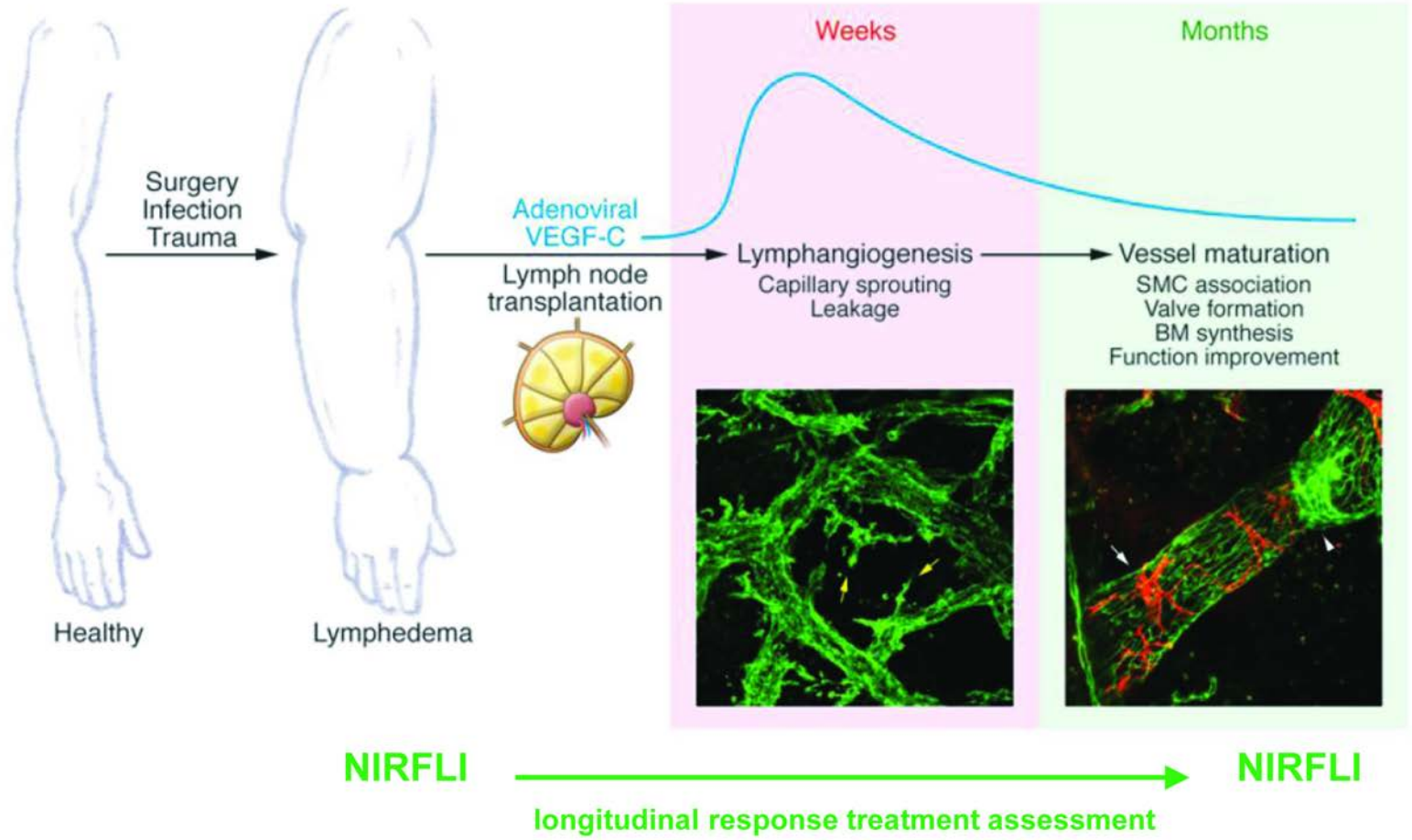

However, additional considerations should be made for cancer patients and cancer-related lymphedema. As most epithelial tumors metastasize *via* lymphatic vessels and produce lymphangiogenic growth factors which stimulate vessel growth to provide new routes for tumor progression, current cancer therapies are targeting tumor-induced lymphangiogenesis. Strategies of inhibiting VEGFR3 signaling include trapping VEGFC using soluble VEGFR3 (sVEGFR3), blocking ligand-receptor binding, inhibiting receptor dimerization using blocking antibodies or inhibiting the VEGFR3 tyrosine kinase activity, all of which have shown success in various tumor models in suppressing lymphangiogenesis [231]. Additionally, with activation of PI3K/AKT and MAPK/ERK pathways seen in many tumors, inhibitors of these pathways are successfully being used to suppress tumor growth. It remains to be seen whether these inhibitors have long-term anti-lymphangiogenic side effects which could ultimately result in lymphedema. Nonetheless, periorbital edema (lymphedema of the eye) is a common side effect to STI571 (imatinib mesylate), a selective inhibitor of the bcr-abl, c-KIT and platelet-derived growth factor receptor (PDGFR) kinases used in treating chronic myelogenous leukemia (CML) and gastrointestinal stromal tumors (GIST) [232, 233]. Given that lymphangiogenesis is usually active during development and decreases to low levels during adulthood unless reactivated during pathological conditions such as cancer, wound repair and inflammation, it is likely that in some patients anti-lymphangiogenic strategies would be initially used to control tumor growth and metastasis and if they develop lymphedema, pro-lymphangiogenic treatment such as that outlined in **Figure 5.2**, could be initiated during remission to treat secondary lymphedema. Additionally, if warranted by more studies, cytokine treatments such as anti-IL6 and anti-TNF-α can also be employed to offset lymphedema symptoms as a prophylactic therapy.

5.3: Lymphedema and Obesity: is SHIP2 the missing link?

An emerging concept in lymphatic research is whether a link exists between lymphedema and obesity. As lymphedema progresses, increased interstitial fluid accumulation leads to tissue fibrosis, unresolved inflammation and adipose tissue deposition. Clinical studies have shown that obesity increases the risk of secondary lymphedema following lymphatic damage [234]. Specifically, the 5-year incidence of lymphedema in breast cancer survivors with body mass index (BMI) >29 is 36%, in comparison to 12% risk of lymphedema in women with lower BMI. On the other hand, obesity increases the risk of lymphedema even without a preceding lymphatic injury, suggesting that obesity and lymphedema have a reciprocal relationship. Defects in lymphatic vasculature have been shown to promote obesity. Mice with heterozygous deletions in *Prox1*, the master regulator of lymphatic fate, have defective lymphatic vessel integrity causing fluid leakage and accumulation in the interstitial space, where lymph stimulates differentiation and growth of adipose cell precursors resulting in adult onset obesity [235]. Additionally, patients with Dercum's Disease, a rare adipose disorder suspected to be a lymphovascular disease and characterized by painful subcutaneous adipose tissue depositions, have dilated, sluggish, and tortuous lymphatics [236]. Given that the lymphatics play a major role in lipid absorption and cholesterol transport from peripheral tissues to blood vasculature *via* intestinal lymphatic vessels known as lacteals (**Figure 0.1**), aberrant lymphatics leads to accumulation of cholesterol and obesity-related diseases [23].

As discussed in **Chapter 2**, genetically modified *Ship2* mice exhibit defective lipid metabolism, with *Ship2* knockout mice being resistant to weight gain while conversely, transgenic mice, that overexpress *Ship2* gain weight; and SHIP2 has also been implicated in human metabolic syndrome, which is characterized by Type 2 diabetes,

hypertension, obesity, and insulin resistance [108, 125]. While a direct mechanism linking obesity and lymphedema has not been identified, SHIP2 could provide some insight. Hypercholesterolemia, the increase in low-density lipoproteins (LDL), commonly known as “bad cholesterol” is a major risk factor for obesity and cardiovascular disease (CVD). Mice deficient in the LDL apolipoprotein E (*apoE-/-*), exhibit defective and leaky lymphatic vessels [26]. A previous study by DeKroon *et al*. revealed a novel mechanism by which apoE4 inhibits high density lipoprotein (HDL; “good cholesterol”)-induced AKT activation by specifically recruiting and activating SHIP2 to inhibit PI3K/AKT signaling in endothelial cells, thus increasing risk for obesity and CVD [138]. Additionally, SHIP2 mutations have been recently identified in a rare disorder, opsismodysplasia, in which some subjects are reported pictorially to have distended abdomens at a young age, (which is consistent with chylous ascites) and other features suggestive of edema in lower extremities, although there are no reports in literature that they have chylous ascites or lymphedema. However, while the lymphatics of these rare subjects have not been evaluated, Type 2 diabetes patients exhibit increased dermal lymphatic vessels [25]. Therefore, our research showing SHIP2 having a previously unknown role in lymphatic dysfunction, could encourage clinical investigators to evaluate whether a dysfunctional lymphatic component is present in the rare disease of opsismodysplasia. Finally, as mentioned previously, SHIP2 is overexpressed in breast cancer, worsening patient prognosis and survival, and obesity is a known risk factor for breast cancer. Therefore it remains to be studied whether a direct correlation exists between SHIP2 overexpression, obesity, breast cancer incidence and prognosis and breast cancer-related lymphedema. Future studies will be necessary to explore this potential reciprocal link between lymphedema and obesity, and whether SHIP2 plays an effector role.

5.4: Conclusions.

Knowledge of the molecular regulation of the lymphatic system has exponentially grown in the last 15 years. During this period, gene modifiers of lymphatic function, lymphatic developmental events during embryogenesis, and lymphatic structural hierarchy have been identified. We anticipate that the next wave of lymphatic knowledge will be expanded by techniques such as (i) WES that will help identify new genetic modifiers of dysfunction, and sensitive imaging modalities such as (ii) NIRFLI that will be improved to allow for high resolution visualization of lymphatic architecture and function in real time. This new era of the lymphatic research has challenged the classic view that the lymphatics are merely passive conduits for fluid and immune cell trafficking, but actually an active circulatory system that modulates nearly all areas of human disease: inflammation, autoimmune disease, tumor immune response, transplant rejection, obesity and cardiovascular disease all have a lymphatic component. Finally, we are hopeful that by promoting understanding of the genetic basis of lymphatic failure, as we have aimed to do in this dissertation, we will develop new pharmacological therapies that address the underlying pathological causes of lymphatic dysfunction and design strategies that stimulate lymphatic flow, as is necessary in lymphedema and in persons at risk for lymphedema.

CHAPTER 6

MATERIALS and METHODS

Portions of this chapter are based on:

"Agollah G.D., Gonzalez-Garay M.L, , Rasmussen JC., Tan I-C., Aldrich M.B., Darne C., Fife C.E., Guilliod R., Maus, E.A., King P.D., Sevick-Muraca E.M., *"Evidence for SH2 domain-containing 5-inositol phosphatase-2 (SHIP2) contributing to a lymphatic dysfunction"* PLoS ONE (2014) 9(11): e112548. doi:10.1371/journal.pone.0112548 [98]. *PLOS applies Creative Commons Attribution License (CCAL) and Open-Access License, wherein no permission is required from authors or publishers for reprints or reproduction of published works, except proper citation of original work.*

This chapter is also based on a manuscript that is currently under peer review, "Agollah G.D., Kwon, S., Robinson, H., Sevick-Muraca E.M., "Lymphatic and Vascular Responses to Pharmacological Inhibition of SH2 domain-containing 5-inositol phosphatase-2 (SHIP2)".

Human Lymphatic Imaging. The lymphatic phenotype of each subject was determined using near-infrared fluorescence lymphatic imaging (NIRFLI). As part of an ongoing, IRB and FDA-approved study of lymphatic disorders conducted under Food and Drug Administration IND# 102,827 clinical study and funded by the National Heart Lung and Blood Institute of the National Institutes of Health (Clinical Trials No. NCT00833599: "Imaging lymphatic function in normal subjects and in persons with lymphatic disorders," www.clinical trials.gov), human subjects were imaged following intradermal injection of indocyanine green (ICG). All clinical investigation was conducted according to Declaration of Helsinki principles. Written informed consent was obtained from all participants prior to NIRFL imaging.

Each subject received a total of 12 intradermal injections of 25 µg of ICG in 0.1 mL saline, with a total dose of 300 µg, for uptake into the peripheral lymphatics. Injection sites were consistent between subjects and each limb received two injections on the dorsum of the foot, one injection on the medial ankle, one injection each on the lateral and medial calf, and one injection on the anterior thigh (see **Figure 2.1A**). Immediately following ICG administration and as described previously [99] each leg, starting at the foot and working upward, was illuminated by the diffuse output of a 785nm laser diode, and images of the resultant fluorescent signal emanating from the peripheral lymphatics were optically filtered and acquired using a custom intensified charge coupled device (ICCD) camera. Exposure times of 200ms permitted the acquisition of movies of lymphatic contractile function. Vital signs were measured for two hours following injection, and a follow-up phone call was made at 24 hours. Blood was obtained from each subject and whole exome sequencing (WES) performed. No adverse events were reported. Images were analyzed to assess lymphatic uptake at the injection site and the presence of abnormal lymphatic architecture such as dense

networks of lymphatic capillaries with extravascular fluorescence frequently known as dermal backflow, lymphatic capillaries radiating from the intradermal injection sites, as well as tortuous and/or dilated lymphatics. The brightness and contrast levels of the NIRFLI images presented herein were adjusted to increase the overall dynamic range observable in the image (i.e. to enable the visualization of both the dim and the bright signals within the lymphatics). The NIRF images are presented in pseudo-color.

Whole Exome Sequencing (WES). DNA was extracted from either blood using Paxgene Blood DNA Kit (PreAnalytix, Switzerland) or saliva using Promega's wizard genomic DNA purification kit according to both vendors' instructions. At least 2µg of genomic DNA were submitted to Axeq Technologies for human exome capture sequencing using TrueSeq 62-Mb target enrichment (Illumina, San Diego, CA). Approximately 63,000,000 reads of an average size of 107 bp per sample was returned to us as two fastq files (one file per orientation).

Genetic Sequencing Analysis. Each pair of fastq files was aligned to human genome (hg19) using Novoalign (Novocraft Technologies; www.novocraft.com), keeping parameters at the default settings, as recommended by Novocraft Technologies. Novoalign, SAMtools (http://samtools.sourceforge.net) was used to sort the SAM files, create BAM files, and generate their index files. Picard (SourceForge; http://picard.sourceforge.net) was used to remove all of the PCR duplicates from the BAM files. For local realignments, base quality recalibration, and variant calling, we used Genome Analysis Toolkit (GATK) Version 2.2. Finally, for variant annotation, we used SnpEff (http://snpeff.sourceforge.net/), variant tools and ANNOVAR using multiple

databases from UCSC Genome bioinformatics. Functional effects of each non-synonymous coding variant were evaluated using three different functional prediction algorithms: (1) Polyphen 2.0 Prediction of functional effects of human nsSNPs (http://genetics.bwh.harvard.edu/pph2), (2) SIFT and (3) MutationTaster (www.mutationtaster.org) using the dbNSFP database. Filtration of common polymorphisms was accomplished using frequencies from the NHLBI Exome sequencing project (ESP) (http://evs.gs.washington.edu/EVS) 1,000 Genomes Project (VCF Version 4; www.1000genomes.org/wiki/Analysis/Variant%20Call%20Format/vcf-variant-call-format-version-41)

Validation of Exome Sequencing Variants through Sanger Sequencing. Primers were designed using Oligo 7 and Primer3 softwares for exome sequencing variants that were considered potentially relevant to the lymphedema phenotype. Polymerase chain reactions (PCRs) were performed using the Kapa HiFi HotStart ReadyMix DNA Polymerase (KapaBiosystems #KK2602) as per manufacturer's instruction. To visualize DNA fragments, 5µL of the PCR product was loaded on a 1% agarose gel (or Lonza 1.2% agarose Flash Gel); ethidium bromide was used for the staining. Purification of the DNA was done utilizing Qiagen Gel Extraction Kit (#28706) following manufacturer's instruction. Purified PCR products were sequenced at the University of Texas MD Anderson genetic sequencing facility using a 3730XL DNAnalyzer (AppliedBiosystems, Foster City, California, USA). The following primers were used to validate mutations in *INPPL1* (Protein ID O15357); *HGF* (Protein ID P14210) and *FLT4* (Protein ID P35916):

Gene	Mutation	Forward (5'→3')	Reverse (5'→3')
INPPL1	p.T180A	GAGGCCTTCTAAGACCCCAC	GGTGTAATACATGGGGCTGG
INPPL1	p.L632I	TACCGCCTGGACATGGATATCCAGG	TGCCAGGCATATGTGTCCCGG
HGF	p.G315V	TGATCAGAAATCCACCTAGGGAT	ACATGTGGAGGTAAAATGCAT

			TTAA
FLT4	p.D481EQ	CTTGCAGAACTCCACGATCA	TACAGCTCACCTGCAACTGG
FLT4	p.H890Q	TGCATGTCAGCTTCCTTGTC	GGAGTTCGAGACCAGCTGAC

Animals. Sixteen female C57BL/6 mice (Charles River, Wilmington, MA), aged 6-8 weeks, were utilized in this study. Mice were housed and handled in compliance with the Association for Assessment and Accreditation of Laboratory Animal Care and protocols approved by The University of Texas Health Science Center at Houston Animal Welfare Committee (UTHSC-H AWC). 2-mm circular penetrating punch biopsy wounds were made in the left ear of all mice. A cohort of mice (N=9) was given 300mg/kg of AS1949490 (3-[(4-chlorobenzyl)oxy]-N-[(1S)-1-phenylethyl]-2-thiophenecarboxamide; R&D/Tocris Biosiences) suspended in 0.5% methylcellulose (Sigma Aldrich) twice daily by oral gavage. Seven control mice received 0.5% methylcellulose. Mice were sacrificed on either Day 3 or Day 7 p.o.

In vivo **functional NIRF lymphatic imaging** Mice were imaged twice for baseline assessment prior to beginning AS1949490 treatment (See treatment scheme **Supplementary Fig 1A**). Mice were anesthetized with isoflurane and maintained at 37°C on a warming pad. A volume of 10µl of 645µM of ICG (Akorn, Inc.) dissolved in mixture of distilled water and 0.9 % sodium chloride in a volume ratio of 1:9 was injected intradermally at the base of the tail using 31 gauge needles (BD Ultra-FineTM II Short Needle, Becton and Dickinson Medical). Fluorescence images were acquired immediately before and for up to 20 min after i.d. injection using a custom-built NIRF imaging system as described previously [88].

Lymphatic function analysis. The data was analyzed with ImageJ (National Institutes of Health). To reveal contractile activity resulting in propulsive lymph flow, the same size

of fixed regions of interest (ROIs) in fluorescent lymphatic vessels was defined on fluorescence images. The averaged fluorescence intensity within each ROI in each fluorescence image was plotted as a function of imaging time. The number of "pulses" of ICG-laden lymph is an indication of lymphatic contractile activity and termed as "contractions."

Cell Culture. Primary human dermal lymphatic endothelial cells (HDLEC) were obtained from Science Cell (Carlsbad, CA) at passage 2 and cultured in complete endothelial cell media (ECM) supplemented with 5% fetal bovine serum (FBS), penicillin/streptomycin, and growth supplements (ECGS), from Science Cell. Human telomerase-immortalized dermal microvascular endothelial cells (TIME) were obtained from American Type Culture Collection (ATCC, Mannassas, VA) at passage 25 and cultured in complete endothelial growth medium, EGM-2MV, from Clonetics-Lonza (Walkersville, MD) supplemented with 5% FBS, EGF, VEGF, hFGF-B, R3-IGF-1, ascorbic acid, hydrocortisone and blasticin S HCl. Human umbilical vein/vascular endothelium cells (HUVEC) were obtained from ATCC at passage 14 and cultured in complete ECM media used for HDLEC and supplemented with 0.1mg/ml heparin and 10% FBS. Confirmation of lymphatic and blood endothelial cell lineage was performed using flow cytometry analysis using anti-human podoplanin and CD31-fluorophore conjugated antibodies (eBioscience) and FACS data analyzed using FlowJo software (Treestar).

Whole mount staining: Ears were fixed in 4% paraformaldehyde (PFA) overnight at 4°C. Cartilage was removed under a dissecting microscope and tissues washed with 0.3% TritonX-PBS at least 10 times over 4 hours. Samples were blocked with 0.2%

BSA, 5% goat serum in 0.3% TritonX-PBS for 2 hours at room temperature before staining with rabbit-anti mouse LYVE1 antibody (1:100; Angiobio); rat anti-mouse PECAM (CD31; 1:100 Thermo Fisher) at 4°C overnight with shaking. Tissues were washed for at least 6 hours with 0.3% TritonX-PBS before being incubated at 4°C overnight with secondary antibody (Alexa-Flour 488nm; goat anti-rabbit; Alexa-Fluor goat anti-rat; 1:500 in 0.3% TritonX-PBS) with shaking. Some tissues were further stained with allophycocyanin- conjugated F4/80 (1:100; eBiosciences). Tissues were washed at least 10 times over 6 hours with 0.3% TritonX-PBS before 10 min fixation with 4% PFA. Final wash was performed with PBS 5 times over 30 mins before tissues were mounted with Vectashield (Vector Labs). Fluorescent images were analyzed using EVOS FL microscope (Invitrogen). Lymphatic and blood vessel networks were quantified using AngioTool software (NCI) [178] and F4/80 cell count of x40 images was performed by CellProfiler cell image analysis software (Broad Institute) [237, 238].

RNAi transfections. Double-stranded ON-TARGET Plus human siRNA SHIP2-specific sequences (#1-UCAAGGAGCUUACGGAUCU; #2-GUCAGUACGUCCAGUGUGA; #3-CCAAGAAAGGGCUCUCAAA; #4-GCACACGUAUCGCAUUCUG and SmartPool of these 4-(Catalog# L-004152-00-005)) and ON-TARGETplus Non-targeting (NT) Control (D-001810-01-05) were obtained from Dharmacon-Thermo Fisher (Lafayette, CO). Transfection was performed using Lipofectin reagent (Invitrogen) according to manufacturer's instructions at a final concentration of 100nM siRNA. To confirm transfection efficiency, Alexa Block-iT oligonucleotide (Invitrogen) was used. Mock transfection consisted of lipofectin reagent and Alexa Block iT oligonucleuotide only. Gene expression transcript and protein levels were determined using standard RT-qPCR and immunoblotting techniques.

Site-directed mutagenesis. Human *INPPL1* TrueORF^{TM} cDNA Myc-DDK clone was obtained from OriGene. SHIP2 T180A and L632I mutants in pCMV6-Entry-AC-MycDDK were made using QuickChange® site-directed mutagenesis kit (Stratagene). Single nucleotides were changed at 71617801 of A→G (forward sequence) and T→C (reverse) resulting in T180A and at 71621609 of C→A (forward) and G→T (reverse), resulting in L632I. Mutant plasmids were Sanger-sequenced to confirm the introduction of point mutations before transfection into TIME cells. Stably transfected cells were selected for neomycin resistance by 400µg/ml Geneticin (G418)

MTS Cell Proliferation Assay. $5x10^3$ cells/well were plated in 96-well plates and allowed to adhere overnight. For stimulation experiments, cells were starved 4 hours in 1% FBS, before growth factors were added. Cell proliferation was evaluated using tetrazolium salt colormetric assay (MTS) using CellTiter 96 AQeous One Solution (Promega) according to manufacturer's instructions at 24, 48 hr and 72 hrs post plating.

Cell Adhesion Assay. 96-wells plates were coated with 1% BSA, 10µg/cm^2 collagen or 10µg/ml bovine plasma fibronectin (Sigma) diluted in calcium/magnesium-free PBS overnight. Excess collagen and fibronectin was aspirated and all wells were blocked with 1% BSA for 2 hours, and then rinsed with PBS. $2x10^4$ cells/well were plated and allowed to adhere for 2 hours. Plates were washed 5 times with PBS to remove unattached cells, and adhered cells were then fixed using 4% paraformaldehyde, followed by permeabilization with 1% (w/v) Triton-X in PBS. Adhered cells were stained with 0.1% crystal violet in 2% ethanol and images acquired at 40x magnification.

Wound-Healing Cell Migration Assay. Cells were plated in either 6-well plates or rectangular culture plates and when approximately 80-90% confluent and then perpendicular scratches created using either sterile P1000 pipette tips or cell combs (Millipore). Cells were rinsed with PBS, and incubated over 48hrs, during which they were imaged using a Leica DM microscope (Leica Microsystems,) to assess the migration in closing the wound. Some cells were stained with 1µM CellTracker Green Fluorescent Probe (Lonza) prior to wounding, and fluorescent microscope images taken using the GFP filter. Wound area was calculated using ImageJ software (NIH) as percentage of 0hr coverage at wounding site.

Tubulogenesis Assay. Matrigel matrix (Becton-Dickson) was liquefied overnight on ice at 4°C. 50µl of the matrix was aliquoted in 96-well plates and incubated at 37°C for 30-60 min prior to plating $5x10^4$ cells per well. Cells were cultured for 24hrs and tube formation monitored by inspection by phase contrast microscopy (Leica Microsystems). At the end of the 24hr incubation, cells were labeled with 1µM Calcein AM (Trevigen) and cell viability assessed using a fluorescent inverted microscope with a 485nm excitation filter. For PI3K inhibition experiments, cells were treated for 2 hours with 50µm LY294002 before seeding into Matrigel.

Annexin V Apoptosis Assay. Cells were plated in 6-well dishes, subjected to siRNA transfection for 48hours then serum-starved overnight. Cells were treated with 1µM staurosporine (Cell Signal) for 3 hours. Cells were harvested, washed in cold PBS, counted and apoptosis quantified using Alexa Fluor 488 Annexin V/Propidium Iodide

dead cell kit (Invitrogen) following manufacturer's instructions. Cells were analyzed by flow cytometry BD FACS Aria II using FITC and Texas Red filters and 50,000 events used for each sample. Data was analyzed using FlowJo Software (Treestar) and data presented as total AnnexinV positive % (sum of AnnexinV population representative of early apoptotic cells and double positive PI+AnnxV representing late apoptotic cells). Fluorescence mean intensity of FITC (Annexin V) and phycoerythrin (PE) or PE-Texas Red (propidium iodide) is also presented.

Proximity Ligation Assay (PLA) and Immunofluorescence. Carefully following Duolink II instructions, cells were plated in chamber slides, allowed to adhere overnight, starved for 4 hours and stimulated with appropriate growth factors. Cells were then fixed using 4% paraformaldehyde (VWR) followed by permeabalization with 1% (w/v) Triton-X in PBS. Anti-DDK mouse monoclonal antibody (Origene) was combined with either rabbit polyclonals cMET or VEGFR3 (C28 and C20, SCBT). Following PLA, cells were counterstained with DAPI and Alexa-Flour Phalloidin. Fluorescence spots were quantified using ImageJ software (NIH). For immunofluorescence, cells were serum-starved, stimulated, fixed and permeabilized as described above. Immunofluorescence cytochemistry was done using rabbit anti-SHIP2 antibody (Cell Signal) for determining expression of SHIP2 in LEC and anti-PIP3 IgG antibody (Echelon Biosciences) to determine cellular levels of PtdIns(3,4,5)P3. For cytoskeletal reorganization experiments, cells were starved overnight in 1%FBS media, harvested and plated onto 10µg/cm2 collagen–coated chamber slide for lamellipodia assay for 1 hour prior to stimulation with VEGFC and stained with Alexa-488 phalloidin. Cells were counterstained with either Alexa Flour 488 or 594 phalloidin (Invitrogen) to show actin localization and either DRAQ5 (Biostatus) or DAPI (Invitrogen) to show cell nucleus. Cells were visualized

using either confocal laser microscope (Leica), epifluorescence inverted microscope (Leica) or EVOS FL microscope (Invitrogen).

Malachite Green Phosphatase Assay. Cells were serum-starved overnight then lysed using a nondenaturing buffer (10mM sodium phosphate pH 7.5, 150 mM NaCl, 1 mM PMSF and 1X Halt Protease and Phosphatase inhibitors cocktail). FLAG antibody was preabsorbed overnight with Protein A/G sepharose beads (SantaCruz Biotechnology) and immunocomplexed with precleared 500µg lysates. Immunocomplexes were washed and FLAG-tagged protein eluted from agarose beads using 2M glycine buffer, pH 2.8, and protein concentration quantified using BCA assay (Pierce). Eluted SHIP2 (0.05µg) was combined with 120µM recombinant PI(3,4,5)P3 substrate (P-3908, Echelon Biosciences) at final concentrations of 0.025µg and 60µM, respectively and catalysis allowed to occur at 37°C for 30 mins. Reactions were stopped using BIOMOL GREEN (AK-111, Enzo Biosciences), incubated at room temperature for 15mins while shaking, and absorbance read at 620 nm. Phosphate standard curve was performed to estimate the concentration of released phosphate in the experimental samples. 0.05µg recombinant SHIP2 (Echelon Biosciences) was used as positive control and 120µM recombinant PIP3 was used as negative control (substrate only, no enzyme).

Immunoblotting, Immunoprecipitation and PIP3 delivery. Cells were grown to desired confluency and lysed in buffer (20mM Tris pH 9, 137mM NaCl, 5mM EDTA and 0.5% (w/v) SDS containing 1mM phenylmethylsulfonyl fluoride (PMSF) and 1X Halt Protease and Phosphatase inhibitors cocktail (Thermo Fisher). Protein concentration was measured using BCA assay kit (Pierce). 50µg total protein was loaded in 4-20%

TGX SDS-PAGE gels (BioRad), and Western blots probed with appropriate primary antibodies (goat polyclonal SHIP2 (I-20, SCBT); rabbit antibodies against SHIP2, DYKDDDDK, pAKT-S473, pAKT-T308, pP44/P42, AKT, P44/P42, COX IV, β-actin and GAPDH from Cell Signal) . For signaling studies, after 48hr siRNA transfections, cells were serum-starved for 4hrs and stimulated with 30ng/ml rmHGF or 100 ng/ml rhVEGFC (R&D Systems) in 1% FBS prior to lysis and immunoblotting. For inhibitor studies, cells were pretreated with 10μm U0126 for 1 hour or 50μm LY294002 for 2 hours prior to growth factor stimulations. For AS1949490 SHIP2 inhibitor studies, cells were serum-starved overnight then treated with increasing doses of AS1949490 in starvation media for 1 hour prior to growth factor stimulations. For immunoprecipitations, cells were serum starved overnight and stimulated with indicated growth factors and lysed with IP lysis buffer (25mM Tris-HCl pH 7.4, 150mM NaCl, 1mM EDTA, 1% NP-40 and 5% glycerol containing 1mM PMSF) followed by centrifugation to remove debris. 1μg IP antibody was pre-adsorbed with 20μl Protein A/G PLUS agarose beads (Santa Cruz) overnight and washed with PBS and blocked with 10% BSA. 500μg total lysates were complexed with pre-adbsorbed antibody-beads for 4 hours at 4°C and immunocomplexes washed with cold PBS before samples were denatured and subjected to electrophoresis and immunoblotting. For exogenous PIP3 delivery, cells were treated for 1 hour with increasing concentrations of recombinant PtdIns(3,4,5)P3 using Shuttle PIP kit (Echelon Biosciences) following manufacturer's instructions before proceeding with standard immunoblotting techniques. All blots were followed by IRDye-labeled secondary antibodies (LICOR), and blots were viewed using Odyssey Classic fluorescence viewer (LICOR).

Boyden Chamber Chemotaxis Assay. Boyden chamber assay was performed using ThinCerts (3µm pores, Grenier BioOne) precoated with 1ug/ml fibronectin before use. Cells were starved overnight before seeding into upper chambers ($2x10^5$/well) in 1% FBS and stimulant media added to the bottom wells. Chemotaxis was assessed after staining with DRAQ5 by measuring fluorescence of cells migrated to the lower chamber using EVOS FL microscope using filters set at 618/40nm excitation and 692/40nm emission. Number of migrated cells was quantified using ImageJ (NIH).

Flow cytometry analysis. Single cell suspensions were prepared from axillary lymph nodes by passing through 70µm nylon cell strainers (BD Falcon) with syringe plungers. Cells were counted and labeled with fluorophore-conjugated mouse monoclonal antibodies anti-CD45, anti-CD4, anti-F4/80 (eBioscience), anti-CD8a, anti-CD19, anti-CD11c, anti-CD11b, and anti-Gr1/CD38 (BD Biosciences). 300,000 to 500,000 events were collected and analyzed using BD FACs Aria II (BD Falcon) and data analysis performed using FlowJo vX.0.7.

Multiplex cytokine profiling. Animals were bled and following room temperature incubation of the blood, serum was collected. Skin samples were obtained from euthanized mice and subjected to homogenization using denaturing lysis buffer with protease and phosphatase inhibitors, centrifuged at 12,000RPM for 30 minutes at 4°C to remove debris, and supernatants collected and stored at -20°C until analysis. Serum was diluted 2-fold, and 250ug total protein from skin supernatants was diluted in blocking buffer and incubated with mouse cytokine 4 target array (Quansys). Subsequent incubations were performed following manufacturer's instructions. Fluorescence

detection was performed using IRDye800-Streptavidin and plates scanned using Odyssey 262 infrared imaging system (Licor). Fluorescence signal intensities were quantified using Quansys software, and spots in each blot normalized to positive control spots followed by comparison of analytes between the treatment groups.

Flexible motion simulations. Elastic network normal mode analysis was carried out using Elnemo on a one-site-per-residue model of the SHIP2 structure, placing springs between all sites lying within 12 Angstroms of each other, generating low-frequency normal mode eigenvectors for modes 7 to 16, the ten lowest-frequency nontrivial motions. Flexible motion of the all-atom SHIP2 structure along each mode direction was then explored using template-based geometric simulation with FIRST/FRODA. Key settings were: a directed step size of 0.01 Angstroms and a hydrogen bond inclusion energy cutoff of -2 kcal/mol. 1000 frames of motion for each direction were generated with every 100th frame saved for inspection.

Statistical analysis. Student t-test and one way ANOVA were used to evaluate the data. Data are expressed as means ± SEM. All *in vitro* experiments independently repeated at least 3 times. *P* values of <0.05 were considered statistically significant.

APPENDIX

PROJECT SUMMARIES OF SECONDARY PRECLINICAL NIRFLI STUDIES

Systemically impaired lymphatic function in mice with dextran-sulfate sodium-induced acute colitis

Agollah G.D., Wu, G., Sevick-Muraca, E.M., Kwon, S., *(manuscript under review; December 2014)*

Background and Aim: Recent data suggests that the lymphatic system plays an important role in the pathogenesis of inflammatory bowel disease (IBD) and extra-intestinal manifestations. However, it is unknown if, and how local inflammation in the gut systemically affects the lymphatics. The aim of our study was to investigate whether lymphatic function and architecture are systemically altered in dextran sulfate sodium (DSS)-induced acute colitis.

Methods: Mice were fed 4% DSS in the drinking water for 7 days and monitored to assess disease activity. Mice were also treated with both DSS and a NOS inhibitor, N^G-nitro-l-arginine methyl ester (L-NAME). Mesenteric lymphatic vessels were visualized after oral gavage of a fluorescently-labelled fatty acid analogue. Dermal lymphatic contractile function and vessel remodeling were longitudinally characterized using dynamic near-infrared fluorescence (NIRF) imaging following intradermal injection of indocyanine green (ICG) prior to, 4, and 7 days after DSS treatment. In addition, dendritic cell (DC) migration, lymph node (LN) architecture and cytokine expression in the skin were assessed.

Results: NIRF imaging data demonstrated dilated lymphatic vessels and reduced lymphatic contractility in the skin of mice with DSS-induced acute colitis. DSS-colitis mice with L-NAME treatment showed partial but not complete improvement of systemic lymphatic pump activity. Additionally, peripheral LNs of mice exposed to DSS showed altered architecture, and DC migration.

Conclusions: The lymphatics are locally and systemically altered in acute colitis, and functional NIRF imaging is useful for noninvasively monitoring of systemic lymphatic changes during inflammation.

"*In vivo* lymphatic imaging of a human inflammatory breast cancer model"

Agollah G.D., Wu, G., Sevick-Muraca, E.M., Kwon, S., (*J Cancer* 2014; 5(9):774-783. doi:10.7150/jca.9835) [217]

Background: Inflammatory breast cancer (IBC) remains the most aggressive type of breast cancer with the greatest potential for metastasis and as a result, the highest mortality rate. IBC cells invade and metastasize through dermal lymphatic vessels; however, it is unknown how lymphatic drainage patterns change during IBC growth and metastasis. Herein, we non-invasively and longitudinally imaged lymphatics in an animal model of IBC using near-infrared fluorescence (NIRF) imaging.

Materials and methods: Mice were imaged *in vivo* prior to, and up to 11 weeks after subcutaneous or orthotopic inoculation of human IBC SUM149 cells, which were stably transfected with infrared fluorescence protein (iRFP) gene reporter (SUM149-iRFP), following intradermal (i.d.) injection of indocyanine green (ICG).

Results: Fluorescence images showed well-defined lymphatic vessels prior to SUM149-iRFP inoculation. However, altered lymphatic drainage patterns including rerouting of lymphatic drainage were detected in mice with SUM149-iRFP, due to lymphatic obstruction of normal lymphatic drainages caused by tumor growth. In addition, we observed tortuous lymphatic vessels and extravasation of ICG-laden lymph in mice with SUM149-iRFP. We also observed increased and dilated fluorescent lymphatic vessels in the tumor periphery, which was confirmed by *ex vivo* immunohistochemical staining of lymphatic vessels.

Conclusions: Our pre-clinical studies demonstrate that non-invasive NIRF imaging can provide a method to assess changes in lymphatic drainage patterns during IBC growth and metastasis.

"Spatio-temporal changes of lymphatic contractility and drainage patterns following lymphadenectomy in mice"

Kwon, S., **Agollah G.D**., Wu, G., Chan, W., Sevick-Muraca, E.M., (*PLoS ONE* 9(8): e106034.doi:10.1371/journal.pone.0106034 (2014)) [239]

Objective: To investigate the redirection of lymphatic drainage post-lymphadenectomy using non-invasive near-infrared fluorescence (NIRF) imaging, and to subsequently assess impact on metastasis.

Background: Cancer-acquired lymphedema arises from dysfunctional fluid transport after lymph node dissection (lymphadenectomy) performed for staging and to disrupt drainage pathways for regional control of disease. However, little is known about the normal regenerative processes of the lymphatics in response to lymphadenectomy and how this response can be accelerated, delayed, or can impact metastasis.

Methods: Changes in lymphatic "pumping" function and drainage patterns were non-invasively and longitudinally imaged using NIRF lymphatic imaging after popliteal lymphadenectomy in mice. In a cohort of mice, B16F10 melanoma was inoculated on the dorsal aspect of the paw 27 days after lymphadenectomy to assess how drainage patterns impact metastasis.

Results: NIRF imaging demonstrates that, although lymphatic function and drainage patterns change significantly in early response to popliteal lymph node (PLN) removal in mice, these changes are transient and regress dramatically due to a high regenerative capacity of the lymphatics and the co-opting of collateral pathways around the site of obstruction. Metastases followed the pattern of collateral pathways and could be detected proximal to the site of lymphadenectomy.

Conclusions: Both lymphatic vessel regeneration and co-opting of contralateral vessels occur following lymphadenectomy, with contractile function restored within 13

days, providing a basis for preclinical and clinical investigations to hasten lymphatic repair and restore contractile lymphatic function after surgery to prevent cancer-acquired lymphedema. Patterns of cancer metastasis after lymphadenectomy were altered, consistent with patterns of re-directed lymphatic drainage.

"Response to adeno-associated virus VEGF-C therapy in the *Chy* mouse, a model of human Nonne-Milroy disease, assessed by near-infrared fluorescence imaging"

Davies-Venn, C.A, Aldrich M.B., Kwon, S., **Agollah G.D.,** Gonzalez-Garay M.L, Rasmussen JC., Robinson, H., Alitalo K, Sevick-Muraca, E.M. *(manuscript under review; December 2014)*

Abstract

Currently, there is no cure for lymphedema, a chronic, debilitating disorder of the lymphatics that can result from mutations in genes for molecular factors crucial to lymphangiogenesis, the process of new vessel growth. Emerging therapies that can provide missing lymphangiogenic factors, such as vascular endothelial growth factor C (VEGFC), *via* adeno-associated viral delivery, promise correction of deficient lymph removal. In this study, we track lymphangiogenesis in response to adeno-associated virus-expressed VEGFC (vascular endothelial growth factor C) and soluble VEGFC therapy in a mouse model of lymphatic insufficiency, the *Chy* mouse, deficient in VEGFR3, a VEGFC receptor, using near-infrared fluorescence lymphatic imaging (NIRFLI). We also present lymphatic imaging of corresponding mutations in humans with *VEGFR3* mutations that result in the limb and truncal swelling, cellulitis, and other symptoms of lymphedema. In the mouse experiments, lymphatic vessel growth was evident in ears, but not inguinal areas, of approximately half of the AAV-VEGFC- treated mice. Variation in responses may have occurred due to variable penetrance of the *Flt4/Vegfr3* (Fms-related tyrosine kinase 4/vascular endothelial growth factor receptor 3) mutation in the *Chy* mouse model or genetic variations in the background strain. Despite the nonuniformity of responses in this mouse model, NIRFLI promises noninvasive, temporal monitoring of lymphangiogenic therapy in mice and potentially in humans.

"Direct Visualization of Changes of Lymphatic Function and Drainage Pathways in Lymph Node Metastasis of B16F10 Melanoma Using Near-infrared Fluorescence Imaging"

Kwon, S., **Agollah G.D**., Wu, G., Chan, W., Sevick-Muraca, E.M., (*Biomedical Optics Express*, Vol. 4, Issue 6, pp. 967-977 (2013)) [91]

Abstract

The lymphatic system provides an initial route for cancer cell dissemination in many cancers including melanoma. However, it is largely unknown how the lymphatic system changes during tumor progression due in part to the lack of imaging techniques currently available. In this study, we non-invasively imaged changes of lymphatic function and drainage patterns using near-infrared fluorescence (NIRF) imaging. Dynamic NIRF imaging following intradermal injection of indocyanine green (ICG) was conducted in C57BL/6 mice prior to inoculation of B16F10 murine melanoma cells to the dorsal aspect of the left hindpaw for baseline data or directly to the popliteal lymph node (PLN) and until 21 days postimplantation (p.i.). A series of acquired fluorescent images were quantified to measure lymphatic contractile function. Computed tomography (CT) was also performed to measure the volume of tumor-draining lymph nodes (LNs). We observed significant reduction of lymphatic contractility from 7 days p.i. until 21 days p.i. Altered lymphatic drainage patterns were also detected at 21 days p.i. in mice with tumor in the paw and at 11 days p.i. in mice with tumor in the PLN, due to lymphatic obstruction of normal lymphatic drainages caused by extensive tumor invasion of draining LNs. Since lymphatic function and architecture were progressively altered during tumor growth and metastasis, non-invasive NIRF imaging may provide a new method to stage disease. In addition, this novel technique can be used as a diagnostic method to non-invasively assess lymphatic response as mechanism of therapeutic action.

"Altered Lymphatic Function and Architecture in Salt-Induced Hypertension Assessed by Near-Infrared Fluorescence Imaging"

Kwon, S., **Agollah, G.D**., Chan, W., Sevick-Muraca, E.M., *J Biomed Opt.* 2012 Aug;17(8):080504-1[90]

Abstract

The lymphatic system plays an important role in maintaining the fluid homeostasis between the blood vascular and interstitial tissue compartment and there is recent evidence that its transport capabilities may regulate blood pressure in salt-induced hypertension. Yet, there is little known how the lymphatic contractile function and architecture responds to dietary salt-intake. Thus, we longitudinally characterized lymphatic contractile function and vessel remodeling non-invasively using dynamic near-infrared fluorescence (NIRF) imaging in animal models of salt-induced hypertension. The lymphatics of mice and rats were imaged following intradermal (i.d.) injection of indocyanine green (ICG) to the ear tip or the base of the tail before and during two weeks of either a high salt diet (HSD) or normal chow. Our non-invasive imaging data demonstrated dilated lymphatic vessels in the skin of mice and rats on a HSD as compared to their baseline levels. In addition, our dynamic imaging results showed increased lymphatic contraction frequency in HSD-fed mice and rats. Lymphatic contractile function and vessel remodeling occurs in response to salt-induced hypertension suggesting a possible role for the lymphatics in the regulation of vascular blood pressure.

BIBLIOGRAPHY

1. Sevick-Muraca, E.M., Kwon, S., and Rasmussen, J.C., *Emerging lymphatic imaging technologies for mouse and man.* J Clin Invest, 2014. **124**(3): p. 905-14.
2. Sabin, F.R., *On the origin of the lymphatic system from the veins, and the development of the lymph hearts and thoracic duct in the pig.* Am. J. Anat, 1902. **1**: p. 367–389.
3. Sabin, F.R., *The Method of Growth of the Lymphatic System.* Science, 1916. **44**(1127): p. 145-58.
4. van der Putte, S.C., *The early development of the lymphatic system in mouse embryos.* Acta Morphol Neerl Scand, 1975. **13**(4): p. 245-86.
5. van der Putte, S.C., *The development of the lymphatic system in man.* Adv Anat Embryol Cell Biol, 1975. **51**(1): p. 3-60.
6. Srinivasan, R.S., Dillard, M.E., Lagutin, O.V., Lin, F.J., Tsai, S., Tsai, M.J., Samokhvalov, I.M., and Oliver, G., *Lineage tracing demonstrates the venous origin of the mammalian lymphatic vasculature.* Genes Dev, 2007. **21**(19): p. 2422-32.
7. Jackson, D.G., *Biology of the lymphatic marker LYVE-1 and applications in research into lymphatic trafficking and lymphangiogenesis.* APMIS, 2004. **112**(7-8): p. 526-38.
8. Wigle, J.T. and Oliver, G., *Prox1 function is required for the development of the murine lymphatic system.* Cell, 1999. **98**(6): p. 769-78.
9. Francois, M., Caprini, A., Hosking, B., Orsenigo, F., Wilhelm, D., Browne, C., Paavonen, K., Karnezis, T., Shayan, R., Downes, M., Davidson, T., Tutt, D., Cheah, K.S., Stacker, S.A., Muscat, G.E., Achen, M.G., Dejana, E., and

Koopman, P., *Sox18 induces development of the lymphatic vasculature in mice.* Nature, 2008. **456**(7222): p. 643-7.

10. Srinivasan, R.S., Geng, X., Yang, Y., Wang, Y., Mukatira, S., Studer, M., Porto, M.P., Lagutin, O., and Oliver, G., *The nuclear hormone receptor Coup-TFII is required for the initiation and early maintenance of Prox1 expression in lymphatic endothelial cells.* Genes Dev, 2010. **24**(7): p. 696-707.
11. Kaipainen, A., Korhonen, J., Mustonen, T., van Hinsbergh, V.W., Fang, G.H., Dumont, D., Breitman, M., and Alitalo, K., *Expression of the fms-like tyrosine kinase 4 gene becomes restricted to lymphatic endothelium during development.* Proc Natl Acad Sci U S A, 1995. **92**(8): p. 3566-70.
12. Karkkainen, M.J., Haiko, P., Sainio, K., Partanen, J., Taipale, J., Petrova, T.V., Jeltsch, M., Jackson, D.G., Talikka, M., Rauvala, H., Betsholtz, C., and Alitalo, K., *Vascular endothelial growth factor C is required for sprouting of the first lymphatic vessels from embryonic veins.* Nat Immunol, 2004. **5**(1): p. 74-80.
13. Yang, Y. and Oliver, G., *Development of the mammalian lymphatic vasculature.* J Clin Invest, 2014. **124**(3): p. 888-97.
14. Karpanen, T., Heckman, C.A., Keskitalo, S., Jeltsch, M., Ollila, H., Neufeld, G., Tamagnone, L., and Alitalo, K., *Functional interaction of VEGF-C and VEGF-D with neuropilin receptors.* FASEB J, 2006. **20**(9): p. 1462-72.
15. Abtahian, F., Guerriero, A., Sebzda, E., Lu, M.M., Zhou, R., Mocsai, A., Myers, E.E., Huang, B., Jackson, D.G., Ferrari, V.A., Tybulewicz, V., Lowell, C.A., Lepore, J.J., Koretzky, G.A., and Kahn, M.L., *Regulation of blood and lymphatic vascular separation by signaling proteins SLP-76 and Syk.* Science, 2003. **299**(5604): p. 247-51.
16. Carramolino, L., Fuentes, J., Garcia-Andres, C., Azcoitia, V., Riethmacher, D., and Torres, M., *Platelets play an essential role in separating the blood and*

lymphatic vasculatures during embryonic angiogenesis. Circ Res, 2010. **106**(7): p. 1197-201.

17. Bertozzi, C.C., Schmaier, A.A., Mericko, P., Hess, P.R., Zou, Z., Chen, M., Chen, C.Y., Xu, B., Lu, M.M., Zhou, D., Sebzda, E., Santore, M.T., Merianos, D.J., Stadtfeld, M., Flake, A.W., Graf, T., Skoda, R., Maltzman, J.S., Koretzky, G.A., and Kahn, M.L., *Platelets regulate lymphatic vascular development through CLEC-2-SLP-76 signaling.* Blood, 2010. **116**(4): p. 661-70.
18. Kerjaschki, D., *The lymphatic vasculature revisited.* J Clin Invest, 2014. **124**(3): p. 874-7.
19. Alitalo, K., Tammela, T., and Petrova, T.V., *Lymphangiogenesis in development and human disease.* Nature, 2005. **438**(7070): p. 946-53.
20. Petrova, T.V., Karpanen, T., Norrmen, C., Mellor, R., Tamakoshi, T., Finegold, D., Ferrell, R., Kerjaschki, D., Mortimer, P., Yla-Herttuala, S., Miura, N., and Alitalo, K., *Defective valves and abnormal mural cell recruitment underlie lymphatic vascular failure in lymphedema distichiasis.* Nat Med, 2004. **10**(9): p. 974-81.
21. Karpanen, T. and Alitalo, K., *Molecular biology and pathology of lymphangiogenesis.* Annu Rev Pathol, 2008. **3**: p. 367-97.
22. Alitalo, K., *The lymphatic vasculature in disease.* Nat Med, 2011. **17**(11): p. 1371-80.
23. Randolph, G.J. and Miller, N.E., *Lymphatic transport of high-density lipoproteins and chylomicrons.* J Clin Invest, 2014. **124**(3): p. 929-35.
24. Karkkainen, M.J., Saaristo, A., Jussila, L., Karila, K.A., Lawrence, E.C., Pajusola, K., Bueler, H., Eichmann, A., Kauppinen, R., Kettunen, M.I., Yla-Herttuala, S., Finegold, D.N., Ferrell, R.E., and Alitalo, K., *A model for gene therapy of human hereditary lymphedema.* Proc Natl Acad Sci U S A, 2001. **98**(22): p. 12677-82.

25. Haemmerle, M., Keller, T., Egger, G., Schachner, H., Steiner, C.W., Stokic, D., Neumayer, C., Brown, M.K., Kerjaschki, D., and Hantusch, B., *Enhanced lymph vessel density, remodeling, and inflammation are reflected by gene expression signatures in dermal lymphatic endothelial cells in type 2 diabetes.* Diabetes, 2013. **62**(7): p. 2509-29.

26. Lim, H.Y., Rutkowski, J.M., Helft, J., Reddy, S.T., Swartz, M.A., Randolph, G.J., and Angeli, V., *Hypercholesterolemic mice exhibit lymphatic vessel dysfunction and degeneration.* Am J Pathol, 2009. **175**(3): p. 1328-37.

27. Shields, J.D., *Lymphatics: at the interface of immunity, tolerance, and tumor metastasis.* Microcirculation, 2011. **18**(7): p. 517-31.

28. Kim, H., Kataru, R.P., and Koh, G.Y., *Inflammation-associated lymphangiogenesis: a double-edged sword?* J Clin Invest, 2014. **124**(3): p. 936-42.

29. Ruddle, N.H., *Lymphatic vessels and tertiary lymphoid organs.* J Clin Invest, 2014. **124**(3): p. 953-9.

30. Card, C.M., Yu, S.S., and Swartz, M.A., *Emerging roles of lymphatic endothelium in regulating adaptive immunity.* J Clin Invest, 2014. **124**(3): p. 943-52.

31. Kerjaschki, D., *The crucial role of macrophages in lymphangiogenesis.* J Clin Invest, 2005. **115**(9): p. 2316-9.

32. Maruyama, K., Ii, M., Cursiefen, C., Jackson, D.G., Keino, H., Tomita, M., Van Rooijen, N., Takenaka, H., D'Amore, P.A., Stein-Streilein, J., Losordo, D.W., and Streilein, J.W., *Inflammation-induced lymphangiogenesis in the cornea arises from CD11b-positive macrophages.* J Clin Invest, 2005. **115**(9): p. 2363-72.

33. Lund, A.W., Duraes, F.V., Hirosue, S., Raghavan, V.R., Nembrini, C., Thomas, S.N., Issa, A., Hugues, S., and Swartz, M.A., *VEGF-C promotes immune*

tolerance in B16 melanomas and cross-presentation of tumor antigen by lymph node lymphatics. Cell Rep, 2012. **1**(3): p. 191-9.

34. Podgrabinska, S., Braun, P., Velasco, P., Kloos, B., Pepper, M.S., and Skobe, M., *Molecular characterization of lymphatic endothelial cells.* Proc Natl Acad Sci U S A, 2002. **99**(25): p. 16069-74.

35. Choi, I., Lee, S., and Hong, Y.K., *The new era of the lymphatic system: no longer secondary to the blood vascular system.* Cold Spring Harb Perspect Med, 2012. **2**(4): p. a006445.

36. Warren, A.G., Brorson, H., Borud, L.J., and Slavin, S.A., *Lymphedema: a comprehensive review.* Ann Plast Surg, 2007. **59**(4): p. 464-72.

37. Wang, Y. and Oliver, G., *Current views on the function of the lymphatic vasculature in health and disease.* Genes Dev, 2010. **24**(19): p. 2115-26.

38. Mortimer, P.S. and Rockson, S.G., *New developments in clinical aspects of lymphatic disease.* J Clin Invest, 2014. **124**(3): p. 915-21.

39. Milroy, W.F., *An undescribed variety of hereditary oedema.* NY Med. J, 1892. **56**: p. 505-508.

40. Milroy, W.F., *Chronic Hereditary Edema: Milroy's Disease.* JAMA, 1928. **91**(16): p. 1172-1175.

41. Evans, A.L., Brice, G., Sotirova, V., Mortimer, P., Beninson, J., Burnand, K., Rosbotham, J., Child, A., and Sarfarazi, M., *Mapping of primary congenital lymphedema to the 5q35.3 region.* Am J Hum Genet, 1999. **64**(2): p. 547-55.

42. Irrthum, A., Karkkainen, M.J., Devriendt, K., Alitalo, K., and Vikkula, M., *Congenital hereditary lymphedema caused by a mutation that inactivates VEGFR3 tyrosine kinase.* Am J Hum Genet, 2000. **67**(2): p. 295-301.

43. Connell, F.C., Ostergaard, P., Carver, C., Brice, G., Williams, N., Mansour, S., Mortimer, P.S., and Jeffery, S., *Analysis of the coding regions of VEGFR3 and*

VEGFC in Milroy disease and other primary lymphoedemas. Hum Genet, 2009. **124**(6): p. 625-31.

44. Brouillard, P., Boon, L., and Vikkula, M., *Genetics of lymphatic anomalies.* J Clin Invest, 2014. **124**(3): p. 898-904.

45. Gordon, K., Schulte, D., Brice, G., Simpson, M.A., Roukens, M.G., van Impel, A., Connell, F., Kalidas, K., Jeffery, S., Mortimer, P.S., Mansour, S., Schulte-Merker, S., and Ostergaard, P., *Mutation in vascular endothelial growth factor-C, a ligand for vascular endothelial growth factor receptor-3, is associated with autosomal dominant milroy-like primary lymphedema.* Circ Res, 2013. **112**(6): p. 956-60.

46. Dellinger, M.T., Hunter, R.J., Bernas, M.J., Witte, M.H., and Erickson, R.P., *Chy-3 mice are Vegfc haploinsufficient and exhibit defective dermal superficial to deep lymphatic transition and dermal lymphatic hypoplasia.* Dev Dyn, 2007. **236**(8): p. 2346-55.

47. Wheeler, E.S., Chan, V., Wassman, R., Rimoin, D.L., and Lesavoy, M.A., *Familial lymphedema praecox: Meige's disease.* Plast Reconstr Surg, 1981. **67**(3): p. 362-4.

48. Fang, J., Dagenais, S.L., Erickson, R.P., Arlt, M.F., Glynn, M.W., Gorski, J.L., Seaver, L.H., and Glover, T.W., *Mutations in FOXC2 (MFH-1), a forkhead family transcription factor, are responsible for the hereditary lymphedema-distichiasis syndrome.* Am J Hum Genet, 2000. **67**(6): p. 1382-8.

49. Finegold, D.N., Kimak, M.A., Lawrence, E.C., Levinson, K.L., Cherniske, E.M., Pober, B.R., Dunlap, J.W., and Ferrell, R.E., *Truncating mutations in FOXC2 cause multiple lymphedema syndromes.* Hum Mol Genet, 2001. **10**(11): p. 1185-9.

50. Brice, G., Mansour, S., Bell, R., Collin, J.R., Child, A.H., Brady, A.F., Sarfarazi, M., Burnand, K.G., Jeffery, S., Mortimer, P., and Murday, V.A., *Analysis of the*

phenotypic abnormalities in lymphoedema-distichiasis syndrome in 74 patients with FOXC2 mutations or linkage to 16q24. J Med Genet, 2002. **39**(7): p. 478-83.

51. Irrthum, A., Devriendt, K., Chitayat, D., Matthijs, G., Glade, C., Steijlen, P.M., Fryns, J.P., Van Steensel, M.A., and Vikkula, M., *Mutations in the transcription factor gene SOX18 underlie recessive and dominant forms of hypotrichosis-lymphedema-telangiectasia.* Am J Hum Genet, 2003. **72**(6): p. 1470-8.
52. Van Balkom, I.D., Alders, M., Allanson, J., Bellini, C., Frank, U., De Jong, G., Kolbe, I., Lacombe, D., Rockson, S., Rowe, P., Wijburg, F., and Hennekam, R.C., *Lymphedema-lymphangiectasia-mental retardation (Hennekam) syndrome: a review.* Am J Med Genet, 2002. **112**(4): p. 412-21.
53. Alders, M., Hogan, B.M., Gjini, E., Salehi, F., Al-Gazali, L., Hennekam, E.A., Holmberg, E.E., Mannens, M.M., Mulder, M.F., Offerhaus, G.J., Prescott, T.E., Schroor, E.J., Verheij, J.B., Witte, M., Zwijnenburg, P.J., Vikkula, M., Schulte-Merker, S., and Hennekam, R.C., *Mutations in CCBE1 cause generalized lymph vessel dysplasia in humans.* Nat Genet, 2009. **41**(12): p. 1272-4.
54. Hogan, B.M., Bos, F.L., Bussmann, J., Witte, M., Chi, N.C., Duckers, H.J., and Schulte-Merker, S., *Ccbe1 is required for embryonic lymphangiogenesis and venous sprouting.* Nat Genet, 2009. **41**(4): p. 396-8.
55. Ohara, I. and Taneichi, N., *Lymphaticovenous anastomosis in a case with primary lymphedema tarda.* Angiology, 1973. **24**(11): p. 668-74.
56. Segal, J. and Turner, A.F., *Lymphedema tarda.* JAMA, 1976. **235**(18): p. 1996-7.
57. Vieras, F. and Boyd, C.M., *Letter: Lymphedema tarda.* JAMA, 1976. **236**(10): p. 1116-7.
58. Majeski, J., *Lymphedema tarda.* Cutis, 1986. **38**(2): p. 105-7.
59. Burgos, J.A. and Luginbuhl, A., *Images in clinical medicine. Lymphedema tarda.* N Engl J Med, 2009. **360**(10): p. 1015.

60. Ma, G.C., Liu, C.S., Chang, S.P., Yeh, K.T., Ke, Y.Y., Chen, T.H., Wang, B.B., Kuo, S.J., Shih, J.C., and Chen, M., *A recurrent ITGA9 missense mutation in human fetuses with severe chylothorax: possible correlation with poor response to fetal therapy.* Prenat Diagn, 2008. **28**(11): p. 1057-63.

61. Hong, S.E., Shugart, Y.Y., Huang, D.T., Shahwan, S.A., Grant, P.E., Hourihane, J.O., Martin, N.D., and Walsh, C.A., *Autosomal recessive lissencephaly with cerebellar hypoplasia is associated with human RELN mutations.* Nat Genet, 2000. **26**(1): p. 93-6.

62. Ferrell, R.E., Baty, C.J., Kimak, M.A., Karlsson, J.M., Lawrence, E.C., Franke-Snyder, M., Meriney, S.D., Feingold, E., and Finegold, D.N., *GJC2 missense mutations cause human lymphedema.* Am J Hum Genet, 2010. **86**(6): p. 943-8.

63. Finegold, D.N., Schacht, V., Kimak, M.A., Lawrence, E.C., Foeldi, E., Karlsson, J.M., Baty, C.J., and Ferrell, R.E., *HGF and MET mutations in primary and secondary lymphedema.* Lymphat Res Biol, 2008. **6**(2): p. 65-8.

64. Wynd, S., Melrose, W.D., Durrheim, D.N., Carron, J., and Gyapong, M., *Understanding the community impact of lymphatic filariasis: a review of the sociocultural literature.* Bull World Health Organ, 2007. **85**(6): p. 493-8.

65. Pfarr, K.M., Debrah, A.Y., Specht, S., and Hoerauf, A., *Filariasis and lymphoedema.* Parasite Immunol, 2009. **31**(11): p. 664-72.

66. Vignes, S., Arrault, M., Bonhomme, S., and Spielmann, M., *[Upper limb lymphedema revealing breast cancer].* Rev Med Interne, 2007. **28**(9): p. 631-4.

67. Cormier, J.N., Askew, R.L., Mungovan, K.S., Xing, Y., Ross, M.I., and Armer, J.M., *Lymphedema beyond breast cancer: a systematic review and meta-analysis of cancer-related secondary lymphedema.* Cancer, 2010. **116**(22): p. 5138-49.

68. Pain, S.J., Barber, R.W., Ballinger, J.R., Solanki, C.K., Mortimer, P.S., Purushotham, A.D., and Peters, A.M., *Local vascular access of radioprotein injected subcutaneously in healthy subjects and patients with breast cancer-related lymphedema.* J Nucl Med, 2004. **45**(5): p. 789-96.

69. Pain, S.J., Purushotham, A.D., Barber, R.W., Ballinger, J.R., Solanki, C.K., Mortimer, P.S., and Peters, A.M., *Variation in lymphatic function may predispose to development of breast cancer-related lymphoedema.* Eur J Surg Oncol, 2004. **30**(5): p. 508-14.

70. Newman, B., Lose, F., Kedda, M.A., Francois, M., Ferguson, K., Janda, M., Yates, P., Spurdle, A.B., and Hayes, S.C., *Possible genetic predisposition to lymphedema after breast cancer.* Lymphat Res Biol, 2012. **10**(1): p. 2-13.

71. Lin, S., Kim, J., Lee, M.J., Roche, L., Yang, N.L., Tsao, P.S., and Rockson, S.G., *Prospective transcriptomic pathway analysis of human lymphatic vascular insufficiency: identification and validation of a circulating biomarker panel.* PLoS One, 2012. **7**(12): p. e52021.

72. Rockson, S.G., *Diagnosis and management of lymphatic vascular disease.* J Am Coll Cardiol, 2008. **52**(10): p. 799-806.

73. Rockson, S.G., *Update on the biology and treatment of lymphedema.* Curr Treat Options Cardiovasc Med, 2012. **14**(2): p. 184-92.

74. Lu, Q., Delproposto, Z., Hu, A., Tran, C., Liu, N., Li, Y., Xu, J., Bui, D., and Hu, J., *MR lymphography of lymphatic vessels in lower extremity with gynecologic oncology-related lymphedema.* PLoS One, 2012. **7**(11): p. e50319.

75. Notohamiprodjo, M., Weiss, M., Baumeister, R.G., Sommer, W.H., Helck, A., Crispin, A., Reiser, M.F., and Herrmann, K.A., *MR lymphangiography at 3.0 T: correlation with lymphoscintigraphy.* Radiology, 2012. **264**(1): p. 78-87.

76. Lakowicz, J.R., *Principles of Fluorescence Spectroscopy*1983: Plenum Press, New York.

77. Lakowicz, J.R., Szmacinski, H., Nowaczyk, K., Berndt, K.W., and Johnson, M., *Fluorescence lifetime imaging.* Anal Biochem, 1992. **202**(2): p. 316-30.

78. Berezin, M.Y. and Achilefu, S., *Fluorescence lifetime measurements and biological imaging.* Chem Rev, 2010. **110**(5): p. 2641-84.

79. Sevick-Muraca, E.M., *Translation of near-infrared fluorescence imaging technologies: emerging clinical applications.* Annu Rev Med, 2012. **63**: p. 217-31.

80. Jameson, D., Hazlett, T., *Biophysical and biochemical aspects of fluorescence spectroscopy* 1991, Plenum Ppress, New York. p. 105-133.

81. Sevick-Muraca, E.M. and King, P.D., *Lymphatic vessel abnormalities arising from disorders of Ras signal transduction.* Trends Cardiovasc Med, 2013.

82. de Wijn, R.S., Oduber, C.E., Breugem, C.C., Alders, M., Hennekam, R.C., and van der Horst, C.M., *Phenotypic variability in a family with capillary malformations caused by a mutation in the RASA1 gene.* Eur J Med Genet, 2012. **55**(3): p. 191-5.

83. Revencu, N., Boon, L.M., Mulliken, J.B., Enjolras, O., Cordisco, M.R., Burrows, P.E., Clapuyt, P., Hammer, F., Dubois, J., Baselga, E., Brancati, F., Carder, R., Quintal, J.M., Dallapiccola, B., Fischer, G., Frieden, I.J., Garzon, M., Harper, J., Johnson-Patel, J., Labreze, C., Martorell, L., Paltiel, H.J., Pohl, A., Prendiville, J., Quere, I., Siegel, D.H., Valente, E.M., Van Hagen, A., Van Hest, L., Vaux, K.K., Vicente, A., Weibel, L., Chitayat, D., and Vikkula, M., *Parkes Weber syndrome, vein of Galen aneurysmal malformation, and other fast-flow vascular anomalies are caused by RASA1 mutations.* Hum Mutat, 2008. **29**(7): p. 959-65.

84. Burrows, P.E., Gonzalez-Garay, M.L., Rasmussen, J.C., Aldrich, M.B., Guilliod, R., Maus, E.A., Fife, C.E., Kwon, S., Lapinski, P.E., King, P.D., and Sevick-

Muraca, E.M., *Lymphatic abnormalities are associated with RASA1 gene mutations in mouse and man.* Proc Natl Acad Sci U S A, 2013. **110**(21): p. 8621-6.

85. Lapinski, P.E., Kwon, S., Lubeck, B.A., Wilkinson, J.E., Srinivasan, R.S., Sevick-Muraca, E., and King, P.D., *RASA1 maintains the lymphatic vasculature in a quiescent functional state in mice.* J Clin Invest, 2012. **122**(2): p. 733-47.

86. Richards-Kortum, R. and Sevick-Muraca, E., *Quantitative optical spectroscopy for tissue diagnosis.* Annu Rev Phys Chem, 1996. **47**: p. 555-606.

87. Sharma, R., Wang, W., Rasmussen, J.C., Joshi, A., Houston, J.P., Adams, K.E., Cameron, A., Ke, S., Kwon, S., Mawad, M.E., and Sevick-Muraca, E.M., *Quantitative imaging of lymph function.* Am J Physiol Heart Circ Physiol, 2007. **292**(6): p. H3109-18.

88. Kwon, S. and Sevick-Muraca, E.M., *Functional lymphatic imaging in tumor-bearing mice.* J Immunol Methods, 2010. **360**(1-2): p. 167-72.

89. Kwon, S. and Sevick-Muraca, E.M., *Mouse phenotyping with near-infrared fluorescence lymphatic imaging.* Biomed Opt Express, 2011. **2**(6): p. 1403-11.

90. Kwon, S., Agollah, G.D., Chan, W., and Sevick-Muraca, E.M., *Altered lymphatic function and architecture in salt-induced hypertension assessed by near-infrared fluorescence imaging.* J Biomed Opt, 2012. **17**(8): p. 080504-1.

91. Kwon, S., Agollah, G.D., Wu, G., Chan, W., and Sevick-Muraca, E.M., *Direct visualization of changes of lymphatic function and drainage pathways in lymph node metastasis of B16F10 melanoma using near-infrared fluorescence imaging.* Biomed Opt Express, 2013. **4**(6): p. 967-77.

92. Rasmussen, J.C., Tan, I.C., Marshall, M.V., Fife, C.E., and Sevick-Muraca, E.M., *Lymphatic imaging in humans with near-infrared fluorescence.* Curr Opin Biotechnol, 2009. **20**(1): p. 74-82.

93. Maus, E.A., Tan, I.C., Rasmussen, J.C., Marshall, M.V., Fife, C.E., Smith, L.A., Guilliod, R., and Sevick-Muraca, E.M., *Near-infrared fluorescence imaging of lymphatics in head and neck lymphedema.* Head Neck, 2012. **34**(3): p. 448-53.

94. Sevick-Muraca, E.M., Sharma, R., Rasmussen, J.C., Marshall, M.V., Wendt, J.A., Pham, H.Q., Bonefas, E., Houston, J.P., Sampath, L., Adams, K.E., Blanchard, D.K., Fisher, R.E., Chiang, S.B., Elledge, R., and Mawad, M.E., *Imaging of lymph flow in breast cancer patients after microdose administration of a near-infrared fluorophore: feasibility study.* Radiology, 2008. **246**(3): p. 734-41.

95. Tan, I.C., Maus, E.A., Rasmussen, J.C., Marshall, M.V., Adams, K.E., Fife, C.E., Smith, L.A., Chan, W., and Sevick-Muraca, E.M., *Assessment of lymphatic contractile function after manual lymphatic drainage using near-infrared fluorescence imaging.* Arch Phys Med Rehabil, 2011. **92**(5): p. 756-764 e1.

96. Mendola, A., Schlogel, M.J., Ghalamkarpour, A., Irrthum, A., Nguyen, H.L., Fastre, E., Bygum, A., van der Vleuten, C., Fagerberg, C., Baselga, E., Quere, I., Mulliken, J.B., Boon, L.M., Brouillard, P., and Vikkula, M., *Mutations in the VEGFR3 signaling pathway explain 36% of familial lymphedema.* Mol Syndromol, 2013. **4**(6): p. 257-66.

97. Roach, J.C., Glusman, G., Smit, A.F., Huff, C.D., Hubley, R., Shannon, P.T., Rowen, L., Pant, K.P., Goodman, N., Bamshad, M., Shendure, J., Drmanac, R., Jorde, L.B., Hood, L., and Galas, D.J., *Analysis of genetic inheritance in a family quartet by whole-genome sequencing.* Science, 2010. **328**(5978): p. 636-9.

98. Agollah, G.D., Gonzalez-Garay, M.L., Rasmussen, J.C., Tan, I.C., Aldrich, M.B., Darne, C., Fife, C.E., Guilliod, R., Maus, E.A., King, P.D., and Sevick-Muraca, E.M., *Evidence for SH2 Domain-Containing 5'-Inositol Phosphatase-2 (SHIP2) Contributing to a Lymphatic Dysfunction.* PLoS One, 2014. **9**(11): p. e112548.

99. Rasmussen, J.C., Tan, I.C., Marshall, M.V., Adams, K.E., Kwon, S., Fife, C.E., Maus, E.A., Smith, L.A., Covington, K.R., and Sevick-Muraca, E.M., *Human Lymphatic Architecture and Dynamic Transport Imaged Using Near-infrared Fluorescence.* Transl Oncol, 2010. **3**(6): p. 362-72.

100. Joukov, V., Pajusola, K., Kaipainen, A., Chilov, D., Lahtinen, I., Kukk, E., Saksela, O., Kalkkinen, N., and Alitalo, K., *A novel vascular endothelial growth factor, VEGF-C, is a ligand for the Flt4 (VEGFR-3) and KDR (VEGFR-2) receptor tyrosine kinases.* EMBO J, 1996. **15**(7): p. 1751.

101. Ferrell, R.E., Levinson, K.L., Esman, J.H., Kimak, M.A., Lawrence, E.C., Barmada, M.M., and Finegold, D.N., *Hereditary lymphedema: evidence for linkage and genetic heterogeneity.* Hum Mol Genet, 1998. **7**(13): p. 2073-8.

102. Karkkainen, M.J., Ferrell, R.E., Lawrence, E.C., Kimak, M.A., Levinson, K.L., McTigue, M.A., Alitalo, K., and Finegold, D.N., *Missense mutations interfere with VEGFR-3 signalling in primary lymphoedema.* Nat Genet, 2000. **25**(2): p. 153-9.

103. Evans, A.L., Bell, R., Brice, G., Comeglio, P., Lipede, C., Jeffery, S., Mortimer, P., Sarfarazi, M., and Child, A.H., *Identification of eight novel VEGFR-3 mutations in families with primary congenital lymphoedema.* J Med Genet, 2003. **40**(9): p. 697-703.

104. Ostergaard, P., Simpson, M.A., Brice, G., Mansour, S., Connell, F.C., Onoufriadis, A., Child, A.H., Hwang, J., Kalidas, K., Mortimer, P.S., Trembath, R., and Jeffery, S., *Rapid identification of mutations in GJC2 in primary lymphoedema using whole exome sequencing combined with linkage analysis with delineation of the phenotype.* J Med Genet, 2011. **48**(4): p. 251-5.

105. Kajiya, K., Hirakawa, S., Ma, B., Drinnenberg, I., and Detmar, M., *Hepatocyte growth factor promotes lymphatic vessel formation and function.* EMBO J, 2005. **24**(16): p. 2885-95.

106. Saito, Y., Nakagami, H., Morishita, R., Takami, Y., Kikuchi, Y., Hayashi, H., Nishikawa, T., Tamai, K., Azuma, N., Sasajima, T., and Kaneda, Y., *Transfection of human hepatocyte growth factor gene ameliorates secondary lymphedema via promotion of lymphangiogenesis.* Circulation, 2006. **114**(11): p. 1177-84.

107. Koch, A., Mancini, A., El Bounkari, O., and Tamura, T., *The SH2-domian-containing inositol 5-phosphatase (SHIP)-2 binds to c-Met directly via tyrosine residue 1356 and involves hepatocyte growth factor (HGF)-induced lamellipodium formation, cell scattering and cell spreading.* Oncogene, 2005. **24**(21): p. 3436-47.

108. Suwa, A., Kurama, T., and Shimokawa, T., *SHIP2 and its involvement in various diseases.* Expert Opin Ther Targets, 2010. **14**(7): p. 727-37.

109. Dyson, J.M., Kong, A.M., Wiradjaja, F., Astle, M.V., Gurung, R., and Mitchell, C.A., *The SH2 domain containing inositol polyphosphate 5-phosphatase-2: SHIP2.* Int J Biochem Cell Biol, 2005. **37**(11): p. 2260-5.

110. Schurmans, S., Carrio, R., Behrends, J., Pouillon, V., Merino, J., and Clement, S., *The mouse SHIP2 (Inppl1) gene: complementary DNA, genomic structure, promoter analysis, and gene expression in the embryo and adult mouse.* Genomics, 1999. **62**(2): p. 260-71.

111. Prasad, N., Topping, R.S., and Decker, S.J., *SH2-containing inositol 5'-phosphatase SHIP2 associates with the p130(Cas) adapter protein and regulates cellular adhesion and spreading.* Mol Cell Biol, 2001. **21**(4): p. 1416-28.

112. Wisniewski, D., Strife, A., Swendeman, S., Erdjument-Bromage, H., Geromanos, S., Kavanaugh, W.M., Tempst, P., and Clarkson, B., *A novel SH2-containing phosphatidylinositol 3,4,5-trisphosphate 5-phosphatase (SHIP2) is constitutively tyrosine phosphorylated and associated with src homologous and collagen gene*

(SHC) in chronic myelogenous leukemia progenitor cells. Blood, 1999. **93**(8): p. 2707-20.

113. Dyson, J.M., O'Malley, C.J., Becanovic, J., Munday, A.D., Berndt, M.C., Coghill, I.D., Nandurkar, H.H., Ooms, L.M., and Mitchell, C.A., *The SH2-containing inositol polyphosphate 5-phosphatase, SHIP-2, binds filamin and regulates submembraneous actin.* J Cell Biol, 2001. **155**(6): p. 1065-79.

114. Vandenbroere, I., Paternotte, N., Dumont, J.E., Erneux, C., and Pirson, I., *The c-Cbl-associated protein and c-Cbl are two new partners of the SH2-containing inositol polyphosphate 5-phosphatase SHIP2.* Biochem Biophys Res Commun, 2003. **300**(2): p. 494-500.

115. Paternotte, N., Zhang, J., Vandenbroere, I., Backers, K., Blero, D., Kioka, N., Vanderwinden, J.M., Pirson, I., and Erneux, C., *SHIP2 interaction with the cytoskeletal protein Vinexin.* FEBS J, 2005. **272**(23): p. 6052-66.

116. Xie, J., Onnockx, S., Vandenbroere, I., Degraef, C., Erneux, C., and Pirson, I., *The docking properties of SHIP2 influence both JIP1 tyrosine phosphorylation and JNK activity.* Cell Signal, 2008. **20**(8): p. 1432-41.

117. Prasad, N.K. and Decker, S.J., *SH2-containing 5'-inositol phosphatase, SHIP2, regulates cytoskeleton organization and ligand-dependent down-regulation of the epidermal growth factor receptor.* J Biol Chem, 2005. **280**(13): p. 13129-36.

118. Zwaenepoel, K., Goris, J., Erneux, C., Parker, P.J., and Janssens, V., *Protein phosphatase 2A PR130/B"alpha1 subunit binds to the SH2 domain-containing inositol polyphosphate 5-phosphatase 2 and prevents epidermal growth factor (EGF)-induced EGF receptor degradation sustaining EGF-mediated signaling.* FASEB J, 2010. **24**(2): p. 538-47.

119. Hasegawa, J., Tokuda, E., Tenno, T., Tsujita, K., Sawai, H., Hiroaki, H., Takenawa, T., and Itoh, T., *SH3YL1 regulates dorsal ruffle formation by a novel phosphoinositide-binding domain.* J Cell Biol, 2011. **193**(5): p. 901-16.

120. Kato, K., Yazawa, T., Taki, K., Mori, K., Wang, S., Nishioka, T., Hamaguchi, T., Itoh, T., Takenawa, T., Kataoka, C., Matsuura, Y., Amano, M., Murohara, T., and Kaibuchi, K., *The inositol 5-phosphatase SHIP2 is an effector of RhoA and is involved in cell polarity and migration.* Mol Biol Cell, 2012. **23**(13): p. 2593-604.

121. Clement, S., Krause, U., Desmedt, F., Tanti, J.F., Behrends, J., Pesesse, X., Sasaki, T., Penninger, J., Doherty, M., Malaisse, W., Dumont, J.E., Le Marchand-Brustel, Y., Erneux, C., Hue, L., and Schurmans, S., *The lipid phosphatase SHIP2 controls insulin sensitivity.* Nature, 2001. **409**(6816): p. 92-7.

122. Sleeman, M.W., Wortley, K.E., Lai, K.M., Gowen, L.C., Kintner, J., Kline, W.O., Garcia, K., Stitt, T.N., Yancopoulos, G.D., Wiegand, S.J., and Glass, D.J., *Absence of the lipid phosphatase SHIP2 confers resistance to dietary obesity.* Nat Med, 2005. **11**(2): p. 199-205.

123. Dubois, E., Jacoby, M., Blockmans, M., Pernot, E., Schiffmann, S.N., Foukas, L.C., Henquin, J.C., Vanhaesebroeck, B., Erneux, C., and Schurmans, S., *Developmental defects and rescue from glucose intolerance of a catalytically-inactive novel Ship2 mutant mouse.* Cell Signal, 2012. **24**(11): p. 1971-80.

124. Kagawa, S., Soeda, Y., Ishihara, H., Oya, T., Sasahara, M., Yaguchi, S., Oshita, R., Wada, T., Tsuneki, H., and Sasaoka, T., *Impact of transgenic overexpression of SH2-containing inositol 5'-phosphatase 2 on glucose metabolism and insulin signaling in mice.* Endocrinology, 2008. **149**(2): p. 642-50.

125. Hakim, S., Bertucci, M.C., Conduit, S.E., Vuong, D.L., and Mitchell, C.A., *Inositol polyphosphate phosphatases in human disease.* Curr Top Microbiol Immunol, 2012. **362**: p. 247-314.

126. Kagawa, S., Sasaoka, T., Yaguchi, S., Ishihara, H., Tsuneki, H., Murakami, S., Fukui, K., Wada, T., Kobayashi, S., Kimura, I., and Kobayashi, M., *Impact of SRC homology 2-containing inositol 5'-phosphatase 2 gene polymorphisms detected in a Japanese population on insulin signaling.* J Clin Endocrinol Metab, 2005. **90**(5): p. 2911-9.

127. Prasad, N.K., Tandon, M., Badve, S., Snyder, P.W., and Nakshatri, H., *Phosphoinositol phosphatase SHIP2 promotes cancer development and metastasis coupled with alterations in EGF receptor turnover.* Carcinogenesis, 2008. **29**(1): p. 25-34.

128. Fu, M., Fan, W., Pu, X., Ni, H., Zhang, W., Chang, F., Gong, L., Xiong, L., Wang, J., and Gu, X., *Elevated expression of SHIP2 correlates with poor prognosis in non-small cell lung cancer.* Int J Clin Exp Pathol, 2013. **6**(10): p. 2185-91.

129. Fu, M., Gu, X., Ni, H., Zhang, W., Chang, F., Gong, L., Chen, X., Li, J., Qiu, L., Shi, C., and Bao, J., *High expression of inositol polyphosphate phosphatase-like 1 associates with unfavorable survival in hepatocellular carcinoma.* Int J Clin Exp Pathol, 2013. **6**(11): p. 2515-22.

130. Fu, C.H., Lin, R.J., Yu, J., Chang, W.W., Liao, G.S., Chang, W.Y., Tseng, L.M., Tsai, Y.F., Yu, J.C., and Yu, A.L., *A novel oncogenic role of inositol phosphatase SHIP2 in ER-negative breast cancer stem cells: involvement of JNK/vimentin activation.* Stem Cells, 2014. **32**(8): p. 2048-60.

131. Wendel, H.G., De Stanchina, E., Fridman, J.S., Malina, A., Ray, S., Kogan, S., Cordon-Cardo, C., Pelletier, J., and Lowe, S.W., *Survival signalling by Akt and eIF4E in oncogenesis and cancer therapy.* Nature, 2004. **428**(6980): p. 332-7.

132. Giuriato, S., Blero, D., Robaye, B., Bruyns, C., Payrastre, B., and Erneux, C., *SHIP2 overexpression strongly reduces the proliferation rate of K562*

erythroleukemia cell line. Biochem Biophys Res Commun, 2002. **296**(1): p. 106-10.

133. Yu, J., Ryan, D.G., Getsios, S., Oliveira-Fernandes, M., Fatima, A., and Lavker, R.M., *MicroRNA-184 antagonizes microRNA-205 to maintain SHIP2 levels in epithelia.* Proc Natl Acad Sci U S A, 2008. **105**(49): p. 19300-5.

134. Sperber, B.R., Leight, S., Goedert, M., and Lee, V.M., *Glycogen synthase kinase-3 beta phosphorylates tau protein at multiple sites in intact cells.* Neurosci Lett, 1995. **197**(2): p. 149-53.

135. Lovestone, S., Reynolds, C.H., Latimer, D., Davis, D.R., Anderton, B.H., Gallo, J.M., Hanger, D., Mulot, S., Marquardt, B., Stabel, S., and et al., *Alzheimer's disease-like phosphorylation of the microtubule-associated protein tau by glycogen synthase kinase-3 in transfected mammalian cells.* Curr Biol, 1994. **4**(12): p. 1077-86.

136. Schubert, M., Gautam, D., Surjo, D., Ueki, K., Baudler, S., Schubert, D., Kondo, T., Alber, J., Galldiks, N., Kustermann, E., Arndt, S., Jacobs, A.H., Krone, W., Kahn, C.R., and Bruning, J.C., *Role for neuronal insulin resistance in neurodegenerative diseases.* Proc Natl Acad Sci U S A, 2004. **101**(9): p. 3100-5.

137. Plum, L., Schubert, M., and Bruning, J.C., *The role of insulin receptor signaling in the brain.* Trends Endocrinol Metab, 2005. **16**(2): p. 59-65.

138. DeKroon, R., Robinette, J.B., Hjelmeland, A.B., Wiggins, E., Blackwell, M., Mihovilovic, M., Fujii, M., York, J., Hart, J., Kontos, C., Rich, J., and Strittmatter, W.J., *APOE4-VLDL inhibits the HDL-activated phosphatidylinositol 3-kinase/Akt Pathway via the phosphoinositol phosphatase SHIP2.* Circ Res, 2006. **99**(8): p. 829-36.

139. Huber, C., Faqeih, E.A., Bartholdi, D., Bole-Feysot, C., Borochowitz, Z., Cavalcanti, D.P., Frigo, A., Nitschke, P., Roume, J., Santos, H.G., Shalev, S.A.,

Superti-Furga, A., Delezoide, A.L., Le Merrer, M., Munnich, A., and Cormier-Daire, V., *Exome sequencing identifies INPPL1 mutations as a cause of opsismodysplasia.* Am J Hum Genet, 2013. **92**(1): p. 144-9.

140. Below, J.E., Earl, D.L., Shively, K.M., McMillin, M.J., Smith, J.D., Turner, E.H., Stephan, M.J., Al-Gazali, L.I., Hertecant, J.L., Chitayat, D., Unger, S., Cohn, D.H., Krakow, D., Swanson, J.M., Faustman, E.M., Shendure, J., Nickerson, D.A., and Bamshad, M.J., *Whole-genome analysis reveals that mutations in inositol polyphosphate phosphatase-like 1 cause opsismodysplasia.* Am J Hum Genet, 2013. **92**(1): p. 137-43.

141. Ishida, S., Funakoshi, A., Miyasaka, K., Shimokata, H., Ando, F., and Takiguchi, S., *Association of SH-2 containing inositol 5'-phosphatase 2 gene polymorphisms and hyperglycemia.* Pancreas, 2006. **33**(1): p. 63-7.

142. Kaisaki, P.J., Delepine, M., Woon, P.Y., Sebag-Montefiore, L., Wilder, S.P., Menzel, S., Vionnet, N., Marion, E., Riveline, J.P., Charpentier, G., Schurmans, S., Levy, J.C., Lathrop, M., Farrall, M., and Gauguier, D., *Polymorphisms in type II SH2 domain-containing inositol 5-phosphatase (INPPL1, SHIP2) are associated with physiological abnormalities of the metabolic syndrome.* Diabetes, 2004. **53**(7): p. 1900-4.

143. Zhou, X.P., Marsh, D.J., Hampel, H., Mulliken, J.B., Gimm, O., and Eng, C., *Germline and germline mosaic PTEN mutations associated with a Proteus-like syndrome of hemihypertrophy, lower limb asymmetry, arteriovenous malformations and lipomatosis.* Hum Mol Genet, 2000. **9**(5): p. 765-8.

144. Kurek, K.C., Luks, V.L., Ayturk, U.M., Alomari, A.I., Fishman, S.J., Spencer, S.A., Mulliken, J.B., Bowen, M.E., Yamamoto, G.L., Kozakewich, H.P., and Warman, M.L., *Somatic mosaic activating mutations in PIK3CA cause CLOVES syndrome.* Am J Hum Genet, 2012. **90**(6): p. 1108-15.

145. Hoey, S.E., Eastwood, D., Monsell, F., Kangesu, L., Harper, J.I., and Sebire, N.J., *Histopathological features of Proteus syndrome.* Clin Exp Dermatol, 2008. **33**(3): p. 234-8.

146. Mouta-Bellum, C., Kirov, A., Miceli-Libby, L., Mancini, M.L., Petrova, T.V., Liaw, L., Prudovsky, I., Thorpe, P.E., Miura, N., Cantley, L.C., Alitalo, K., Fruman, D.A., and Vary, C.P., *Organ-specific lymphangiectasia, arrested lymphatic sprouting, and maturation defects resulting from gene-targeting of the PI3K regulatory isoforms p85alpha, p55alpha, and p50alpha.* Dev Dyn, 2009. **238**(10): p. 2670-9.

147. Gupta, S., Ramjaun, A.R., Haiko, P., Wang, Y., Warne, P.H., Nicke, B., Nye, E., Stamp, G., Alitalo, K., and Downward, J., *Binding of ras to phosphoinositide 3-kinase p110alpha is required for ras-driven tumorigenesis in mice.* Cell, 2007. **129**(5): p. 957-68.

148. Zhou, F., Chang, Z., Zhang, L., Hong, Y.K., Shen, B., Wang, B., Zhang, F., Lu, G., Tvorogov, D., Alitalo, K., Hemmings, B.A., Yang, Z., and He, Y., *Akt/Protein kinase B is required for lymphatic network formation, remodeling, and valve development.* Am J Pathol, 2010. **177**(4): p. 2124-33.

149. Giuriato, S., Pesesse, X., Bodin, S., Sasaki, T., Viala, C., Marion, E., Penninger, J., Schurmans, S., Erneux, C., and Payrastre, B., *SH2-containing inositol 5-phosphatases 1 and 2 in blood platelets: their interactions and roles in the control of phosphatidylinositol 3,4,5-trisphosphate levels.* Biochem J, 2003. **376**(Pt 1): p. 199-207.

150. Deneubourg, L., Vanderwinden, J.M., and Erneux, C., *Regulation of SHIP2 function through plasma membrane interaction.* Adv Enzyme Regul, 2010. **50**(1): p. 262-71.

151. Ichise, T., Yoshida, N., and Ichise, H., *H-, N- and Kras cooperatively regulate lymphatic vessel growth by modulating VEGFR3 expression in lymphatic endothelial cells in mice.* Development, 2010. **137**(6): p. 1003-13.

152. Deng, Y., Atri, D., Eichmann, A., and Simons, M., *Endothelial ERK signaling controls lymphatic fate specification.* J Clin Invest, 2013. **123**(3): p. 1202-15.

153. Soderberg, O., Gullberg, M., Jarvius, M., Ridderstrale, K., Leuchowius, K.J., Jarvius, J., Wester, K., Hydbring, P., Bahram, F., Larsson, L.G., and Landegren, U., *Direct observation of individual endogenous protein complexes in situ by proximity ligation.* Nat Methods, 2006. **3**(12): p. 995-1000.

154. Mills, S.J., Persson, C., Cozier, G., Thomas, M.P., Tresaugues, L., Erneux, C., Riley, A.M., Nordlund, P., and Potter, B.V., *A synthetic polyphosphoinositide headgroup surrogate in complex with SHIP2 provides a rationale for drug discovery.* ACS Chem Biol, 2012. **7**(5): p. 822-8.

155. Jimenez-Roldan, J.E., Freedman, R.B., Romer, R.A., and Wells, S.A., *Rapid simulation of protein motion: merging flexibility, rigidity and normal mode analyses.* Phys Biol, 2012. **9**(1): p. 016008.

156. Li, H., Wells, S.A., Jimenez-Roldan, J.E., Romer, R.A., Zhao, Y., Sadler, P.J., and O'Connor, P.B., *Protein flexibility is key to cisplatin crosslinking in calmodulin.* Protein Sci, 2012. **21**(9): p. 1269-79.

157. Jacobs, D.J., Rader, A.J., Kuhn, L.A., and Thorpe, M.F., *Protein flexibility predictions using graph theory.* Proteins, 2001. **44**(2): p. 150-65.

158. Wells, S., Menor, S., Hespenheide, B., and Thorpe, M.F., *Constrained geometric simulation of diffusive motion in proteins.* Phys Biol, 2005. **2**(4): p. S127-36.

159. Wells, S.A., Crennell, S.J., and Danson, M.J., *Structures of mesophilic and extremophilic citrate synthases reveal rigidity and flexibility for function.* Proteins, 2014. **82**(10): p. 2657-70.

160. Suhre, K. and Sanejouand, Y.H., *ElNemo: a normal mode web server for protein movement analysis and the generation of templates for molecular replacement.* Nucleic Acids Res, 2004. **32**(Web Server issue): p. W610-4.

161. Tridandapani, S., Kelley, T., Cooney, D., Pradhan, M., and Coggeshall, K.M., *Negative signaling in B cells: SHIP Grbs Shc.* Immunol Today, 1997. **18**(9): p. 424-7.

162. Tamir, I., Stolpa, J.C., Helgason, C.D., Nakamura, K., Bruhns, P., Daeron, M., and Cambier, J.C., *The RasGAP-binding protein p62dok is a mediator of inhibitory FcgammaRIIB signals in B cells.* Immunity, 2000. **12**(3): p. 347-58.

163. Millward, T.A., Zolnierowicz, S., and Hemmings, B.A., *Regulation of protein kinase cascades by protein phosphatase 2A.* Trends Biochem Sci, 1999. **24**(5): p. 186-91.

164. Ugi, S., Imamura, T., Maegawa, H., Egawa, K., Yoshizaki, T., Shi, K., Obata, T., Ebina, Y., Kashiwagi, A., and Olefsky, J.M., *Protein phosphatase 2A negatively regulates insulin's metabolic signaling pathway by inhibiting Akt (protein kinase B) activity in 3T3-L1 adipocytes.* Mol Cell Biol, 2004. **24**(19): p. 8778-89.

165. Readinger, J.A., Mueller, K.L., Venegas, A.M., Horai, R., and Schwartzberg, P.L., *Tec kinases regulate T-lymphocyte development and function: new insights into the roles of Itk and Rlk/Txk.* Immunol Rev, 2009. **228**(1): p. 93-114.

166. Cagnol, S. and Chambard, J.C., *ERK and cell death: mechanisms of ERK-induced cell death--apoptosis, autophagy and senescence.* FEBS J, 2010. **277**(1): p. 2-21.

167. Moro, L., Arbini, A.A., Marra, E., and Greco, M., *Constitutive activation of MAPK/ERK inhibits prostate cancer cell proliferation through upregulation of BRCA2.* Int J Oncol, 2007. **30**(1): p. 217-24.

168. Liu, X., Ma, B., Malik, A.B., Tang, H., Yang, T., Sun, B., Wang, G., Minshall, R.D., Li, Y., Zhao, Y., Ye, R.D., and Xu, J., *Bidirectional regulation of neutrophil migration by mitogen-activated protein kinases.* Nat Immunol, 2012. **13**(5): p. 457-64.

169. Fragale, A., Tartaglia, M., Wu, J., and Gelb, B.D., *Noonan syndrome-associated SHP2/PTPN11 mutants cause EGF-dependent prolonged GAB1 binding and sustained ERK2/MAPK1 activation.* Hum Mutat, 2004. **23**(3): p. 267-77.

170. Keilhack, H., David, F.S., McGregor, M., Cantley, L.C., and Neel, B.G., *Diverse biochemical properties of Shp2 mutants. Implications for disease phenotypes.* J Biol Chem, 2005. **280**(35): p. 30984-93.

171. Ponzetto, C., Bardelli, A., Zhen, Z., Maina, F., dalla Zonca, P., Giordano, S., Graziani, A., Panayotou, G., and Comoglio, P.M., *A multifunctional docking site mediates signaling and transformation by the hepatocyte growth factor/scatter factor receptor family.* Cell, 1994. **77**(2): p. 261-71.

172. Coso, S., Zeng, Y., Opeskin, K., and Williams, E.D., *Vascular endothelial growth factor receptor-3 directly interacts with phosphatidylinositol 3-kinase to regulate lymphangiogenesis.* PLoS One, 2012. **7**(6): p. e39558.

173. Oliver, G. and Alitalo, K., *The lymphatic vasculature: recent progress and paradigms.* Annu Rev Cell Dev Biol, 2005. **21**: p. 457-83.

174. Suwa, A., Yamamoto, T., Sawada, A., Minoura, K., Hosogai, N., Tahara, A., Kurama, T., Shimokawa, T., and Aramori, I., *Discovery and functional characterization of a novel small molecule inhibitor of the intracellular phosphatase, SHIP2.* Br J Pharmacol, 2009. **158**(3): p. 879-87.

175. Suwa, A., Kurama, T., Yamamoto, T., Sawada, A., Shimokawa, T., and Aramori, I., *Glucose metabolism activation by SHIP2 inhibitors via up-regulation of GLUT1 gene in L6 myotubes.* Eur J Pharmacol, 2010. **642**(1-3): p. 177-82.

176. Aldrich, M.B. and Sevick-Muraca, E.M., *Cytokines are systemic effectors of lymphatic function in acute inflammation.* Cytokine, 2013.

177. Martinez-Corral, I., Olmeda, D., Dieguez-Hurtado, R., Tammela, T., Alitalo, K., and Ortega, S., *In vivo imaging of lymphatic vessels in development, wound healing, inflammation, and tumor metastasis.* Proc Natl Acad Sci U S A, 2012. **109**(16): p. 6223-8.

178. Zudaire, E., Gambardella, L., Kurcz, C., and Vermeren, S., *A computational tool for quantitative analysis of vascular networks.* PLoS One, 2011. **6**(11): p. e27385.

179. Skobe, M., Hamberg, L.M., Hawighorst, T., Schirner, M., Wolf, G.L., Alitalo, K., and Detmar, M., *Concurrent induction of lymphangiogenesis, angiogenesis, and macrophage recruitment by vascular endothelial growth factor-C in melanoma.* Am J Pathol, 2001. **159**(3): p. 893-903.

180. Tvorogov, D., Anisimov, A., Zheng, W., Leppanen, V.M., Tammela, T., Laurinavicius, S., Holnthoner, W., Helotera, H., Holopainen, T., Jeltsch, M., Kalkkinen, N., Lankinen, H., Ojala, P.M., and Alitalo, K., *Effective suppression of vascular network formation by combination of antibodies blocking VEGFR ligand binding and receptor dimerization.* Cancer Cell, 2010. **18**(6): p. 630-40.

181. Muthuchamy, M. and Zawieja, D., *Molecular regulation of lymphatic contractility.* Ann N Y Acad Sci, 2008. **1131**: p. 89-99.

182. Lukacs-Kornek, V., Malhotra, D., Fletcher, A.L., Acton, S.E., Elpek, K.G., Tayalia, P., Collier, A.R., and Turley, S.J., *Regulated release of nitric oxide by nonhematopoietic stroma controls expansion of the activated T cell pool in lymph nodes.* Nat Immunol, 2011. **12**(11): p. 1096-104.

183. Liao, S., Cheng, G., Conner, D.A., Huang, Y., Kucherlapati, R.S., Munn, L.L., Ruddle, N.H., Jain, R.K., Fukumura, D., and Padera, T.P., *Impaired lymphatic*

contraction associated with immunosuppression. Proc Natl Acad Sci U S A, 2011. **108**(46): p. 18784-9.

184. Ribera, J., Pauta, M., Melgar-Lesmes, P., Tugues, S., Fernandez-Varo, G., Held, K.F., Soria, G., Tudela, R., Planas, A.M., Fernandez-Hernando, C., Arroyo, V., Jimenez, W., and Morales-Ruiz, M., *Increased nitric oxide production in lymphatic endothelial cells causes impairment of lymphatic drainage in cirrhotic rats.* Gut, 2013. **62**(1): p. 138-45.

185. Shirasawa, Y., Ikomi, F., and Ohhashi, T., *Physiological roles of endogenous nitric oxide in lymphatic pump activity of rat mesentery in vivo.* Am J Physiol Gastrointest Liver Physiol, 2000. **278**(4): p. G551-6.

186. Leung, W.H. and Bolland, S., *The inositol 5'-phosphatase SHIP-2 negatively regulates IgE-induced mast cell degranulation and cytokine production.* J Immunol, 2007. **179**(1): p. 95-102.

187. Kalesnikoff, J., Baur, N., Leitges, M., Hughes, M.R., Damen, J.E., Huber, M., and Krystal, G., *SHIP negatively regulates IgE + antigen-induced IL-6 production in mast cells by inhibiting NF-kappa B activity.* J Immunol, 2002. **168**(9): p. 4737-46.

188. Saaristo, A., Tammela, T., Farkkila, A., Karkkainen, M., Suominen, E., Yla-Herttuala, S., and Alitalo, K., *Vascular endothelial growth factor-C accelerates diabetic wound healing.* Am J Pathol, 2006. **169**(3): p. 1080-7.

189. Schoppmann, S.F., Birner, P., Stockl, J., Kalt, R., Ullrich, R., Caucig, C., Kriehuber, E., Nagy, K., Alitalo, K., and Kerjaschki, D., *Tumor-associated macrophages express lymphatic endothelial growth factors and are related to peritumoral lymphangiogenesis.* Am J Pathol, 2002. **161**(3): p. 947-56.

190. Hall, M.A., Robinson, H., Chan, W., and Sevick-Muraca, E.M., *Detection of lymphangiogenesis by near-infrared fluorescence imaging and responses to*

VEGF-C during healing in a mouse full-dermis thickness wound model. Wound Repair Regen, 2013. **21**(4): p. 604-15.

191. Ichihara, Y., Fujimura, R., Tsuneki, H., Wada, T., Okamoto, K., Gouda, H., Hirono, S., Sugimoto, K., Matsuya, Y., Sasaoka, T., and Toyooka, N., *Rational design and synthesis of 4-substituted 2-pyridin-2-ylamides with inhibitory effects on SH2 domain-containing inositol 5'-phosphatase 2 (SHIP2).* Eur J Med Chem, 2013. **62**: p. 649-60.

192. Annis, D.A., Cheng, C.C., Chuang, C.C., McCarter, J.D., Nash, H.M., Nazef, N., Rowe, T., Kurzeja, R.J., and Shipps, G.W., Jr., *Inhibitors of the lipid phosphatase SHIP2 discovered by high-throughput affinity selection-mass spectrometry screening of combinatorial libraries.* Comb Chem High Throughput Screen, 2009. **12**(8): p. 760-71.

193. Fuhler, G.M., Brooks, R., Toms, B., Iyer, S., Gengo, E.A., Park, M.Y., Gumbleton, M., Viernes, D.R., Chisholm, J.D., and Kerr, W.G., *Therapeutic potential of SH2 domain-containing inositol-5'-phosphatase 1 (SHIP1) and SHIP2 inhibition in cancer.* Mol Med, 2012. **18**: p. 65-75.

194. Di Cristofano, A., Pesce, B., Cordon-Cardo, C., and Pandolfi, P.P., *Pten is essential for embryonic development and tumour suppression.* Nat Genet, 1998. **19**(4): p. 348-55.

195. Suzuki, A., de la Pompa, J.L., Stambolic, V., Elia, A.J., Sasaki, T., del Barco Barrantes, I., Ho, A., Wakeham, A., Itie, A., Khoo, W., Fukumoto, M., and Mak, T.W., *High cancer susceptibility and embryonic lethality associated with mutation of the PTEN tumor suppressor gene in mice.* Curr Biol, 1998. **8**(21): p. 1169-78.

196. Podsypanina, K., Ellenson, L.H., Nemes, A., Gu, J., Tamura, M., Yamada, K.M., Cordon-Cardo, C., Catoretti, G., Fisher, P.E., and Parsons, R., *Mutation of*

Pten/Mmac1 in mice causes neoplasia in multiple organ systems. Proc Natl Acad Sci U S A, 1999. **96**(4): p. 1563-8.

197. Yamada, K.M. and Araki, M., *Tumor suppressor PTEN: modulator of cell signaling, growth, migration and apoptosis.* J Cell Sci, 2001. **114**(Pt 13): p. 2375-82.

198. Karaman, S. and Detmar, M., *Mechanisms of lymphatic metastasis.* J Clin Invest, 2014. **124**(3): p. 922-8.

199. Armer, J.M. and Stewart, B.R., *Post-breast cancer lymphedema: incidence increases from 12 to 30 to 60 months.* Lymphology, 2010. **43**(3): p. 118-27.

200. Ohba, Y., Todo, Y., Kobayashi, N., Kaneuchi, M., Watari, H., Takeda, M., Sudo, S., Kudo, M., Kato, H., and Sakuragi, N., *Risk factors for lower-limb lymphedema after surgery for cervical cancer.* Int J Clin Oncol, 2011. **16**(3): p. 238-43.

201. Kunos, C., Simpkins, F., Gibbons, H., Tian, C., and Homesley, H., *Radiation therapy compared with pelvic node resection for node-positive vulvar cancer: a randomized controlled trial.* Obstet Gynecol, 2009. **114**(3): p. 537-46.

202. Chang, S.B., Askew, R.L., Xing, Y., Weaver, S., Gershenwald, J.E., Lee, J.E., Royal, R., Lucci, A., Ross, M.I., and Cormier, J.N., *Prospective assessment of postoperative complications and associated costs following inguinal lymph node dissection (ILND) in melanoma patients.* Ann Surg Oncol, 2010. **17**(10): p. 2764-72.

203. Tada, H., Teramukai, S., Fukushima, M., and Sasaki, H., *Risk factors for lower limb lymphedema after lymph node dissection in patients with ovarian and uterine carcinoma.* BMC Cancer, 2009. **9**: p. 47.

204. Smith, B.G., Hutcheson, K.A., Little, L.G., Skoracki, R.J., Rosenthal, D.I., Lai, S.Y., and Lewin, J.S., *Lymphedema Outcomes in Patients with Head and Neck Cancer.* Otolaryngol Head Neck Surg, 2014.

205. Smith, B.G. and Lewin, J.S., *Lymphedema management in head and neck cancer.* Curr Opin Otolaryngol Head Neck Surg, 2010. **18**(3): p. 153-8.

206. Society, A.C., *Cancer Facts and Figures 2012*, 2012. p. 68.

207. Society, A.C., *Cancer Facts and Figures 2013*, 2013. p. 64.

208. Dale, R.F., *The inheritance of primary lymphoedema.* J Med Genet, 1985. **22**(4): p. 274-8.

209. Finegold, D.N., Baty, C.J., Knickelbein, K.Z., Perschke, S., Noon, S.E., Campbell, D., Karlsson, J.M., Huang, D., Kimak, M.A., Lawrence, E.C., Feingold, E., Meriney, S.D., Brufsky, A.M., and Ferrell, R.E., *Connexin 47 mutations increase risk for secondary lymphedema following breast cancer treatment.* Clin Cancer Res, 2012. **18**(8): p. 2382-90.

210. Miaskowski, C., Dodd, M., Paul, S.M., West, C., Hamolsky, D., Abrams, G., Cooper, B.A., Elboim, C., Neuhaus, J., Schmidt, B.L., Smoot, B., and Aouizerat, B.E., *Lymphatic and angiogenic candidate genes predict the development of secondary lymphedema following breast cancer surgery.* PLoS One, 2013. **8**(4): p. e60164.

211. Craandijk, A. and Van Beek, C.A., *Indocyanine green fluorescence angiography of the choroid.* Br J Ophthalmol, 1976. **60**(5): p. 377-85.

212. Cherrick, G.R., Stein, S.W., Leevy, C.M., and Davidson, C.S., *Indocyanine green: observations on its physical properties, plasma decay, and hepatic extraction.* J Clin Invest, 1960. **39**: p. 592-600.

213. Saxena, V., Sadoqi, M., and Shao, J., *Degradation kinetics of indocyanine green in aqueous solution.* J Pharm Sci, 2003. **92**(10): p. 2090-7.

214. Marshall, M.V., Rasmussen, J.C., Tan, I.C., Aldrich, M.B., Adams, K.E., Wang, X., Fife, C.E., Maus, E.A., Smith, L.A., and Sevick-Muraca, E.M., *Near-Infrared*

Fluorescence Imaging in Humans with Indocyanine Green: A Review and Update. Open Surg Oncol J, 2010. **2**(2): p. 12-25.

215. Davies-Venn, C.A., Angermiller, B., Wilganowski, N., Ghosh, P., Harvey, B.R., Wu, G., Kwon, S., Aldrich, M.B., and Sevick-Muraca, E.M., *Albumin-binding domain conjugate for near-infrared fluorescence lymphatic imaging.* Mol Imaging Biol, 2012. **14**(3): p. 301-14.

216. Choi, I., Chung, H.K., Ramu, S., Lee, H.N., Kim, K.E., Lee, S., Yoo, J., Choi, D., Lee, Y.S., Aguilar, B., and Hong, Y.K., *Visualization of lymphatic vessels by Prox1-promoter directed GFP reporter in a bacterial artificial chromosome-based transgenic mouse.* Blood, 2011. **117**(1): p. 362-5.

217. Agollah, G.D., Wu, G., Sevick-Muraca, E.M., and Kwon, S., *In vivo lymphatic imaging of a human inflammatory breast cancer model.* J Cancer, 2014. **5**(9): p. 774-83.

218. Allen, E.V., *Lymphedema of the Extremities.* Arch Intern Med (Chic), 1934. **54**(4): p. 606-624.

219. Kinmonth, J.B., Taylor, G.W., Tracy, G.D., and Marsh, J.D., *Primary lymphoedema; clinical and lymphangiographic studies of a series of 107 patients in which the lower limbs were affected.* Br J Surg, 1957. **45**(189): p. 1-9.

220. Connell, F., Brice, G., Jeffery, S., Keeley, V., Mortimer, P., and Mansour, S., *A new classification system for primary lymphatic dysplasias based on phenotype.* Clin Genet, 2010. **77**(5): p. 438-52.

221. Connell, F.C., Gordon, K., Brice, G., Keeley, V., Jeffery, S., Mortimer, P.S., Mansour, S., and Ostergaard, P., *The classification and diagnostic algorithm for primary lymphatic dysplasia: an update from 2010 to include molecular findings.* Clin Genet, 2013. **84**(4): p. 303-14.

222. Kasseroller, R.G., *The Vodder School: the Vodder method.* Cancer, 1998. **83**(12 Suppl American): p. 2840-2.

223. Foldi, E., Foldi, M., and Clodius, L., *The lymphedema chaos: a lancet.* Ann Plast Surg, 1989. **22**(6): p. 505-15.

224. Oresmus, M., Walker, K., Dayes, I., Raina, P., *Diagnosis and Treatment of Secondary Lymphedema*, M.U.E.-b.P. Center, Editor 2010. p. 178.

225. Tammela, T., Saaristo, A., Holopainen, T., Lyytikka, J., Kotronen, A., Pitkonen, M., Abo-Ramadan, U., Yla-Herttuala, S., Petrova, T.V., and Alitalo, K., *Therapeutic differentiation and maturation of lymphatic vessels after lymph node dissection and transplantation.* Nat Med, 2007. **13**(12): p. 1458-66.

226. Yoon, Y.S., Murayama, T., Gravereaux, E., Tkebuchava, T., Silver, M., Curry, C., Wecker, A., Kirchmair, R., Hu, C.S., Kearney, M., Ashare, A., Jackson, D.G., Kubo, H., Isner, J.M., and Losordo, D.W., *VEGF-C gene therapy augments postnatal lymphangiogenesis and ameliorates secondary lymphedema.* J Clin Invest, 2003. **111**(5): p. 717-25.

227. Baker, A., Kim, H., Semple, J.L., Dumont, D., Shoichet, M., Tobbia, D., and Johnston, M., *Experimental assessment of pro-lymphangiogenic growth factors in the treatment of post-surgical lymphedema following lymphadenectomy.* Breast Cancer Res, 2010. **12**(5): p. R70.

228. Hartiala, P. and Saaristo, A.M., *Growth factor therapy and autologous lymph node transfer in lymphedema.* Trends Cardiovasc Med, 2010. **20**(8): p. 249-53.

229. Lahteenvuo, M., Honkonen, K., Tervala, T., Tammela, T., Suominen, E., Lahteenvuo, J., Kholova, I., Alitalo, K., Yla-Herttuala, S., and Saaristo, A., *Growth factor therapy and autologous lymph node transfer in lymphedema.* Circulation, 2011. **123**(6): p. 613-20.

230. Honkonen, K.M., Visuri, M.T., Tervala, T.V., Halonen, P.J., Koivisto, M., Lahteenvuo, M.T., Alitalo, K.K., Yla-Herttuala, S., and Saaristo, A.M., *Lymph node transfer and perinodal lymphatic growth factor treatment for lymphedema.* Ann Surg, 2013. **257**(5): p. 961-7.

231. Zheng, W., Aspelund, A., and Alitalo, K., *Lymphangiogenic factors, mechanisms, and applications.* J Clin Invest, 2014. **124**(3): p. 878-87.

232. Esmaeli, B., Prieto, V.G., Butler, C.E., Kim, S.K., Ahmadi, M.A., Kantarjian, H.M., and Talpaz, M., *Severe periorbital edema secondary to STI571 (Gleevec).* Cancer, 2002. **95**(4): p. 881-7.

233. McClelland, C.M., Harocopos, G.J., and Custer, P.L., *Periorbital edema secondary to imatinib mesylate.* Clin Ophthalmol, 2010. **4**: p. 427-31.

234. Mehrara, B.J. and Greene, A.K., *Lymphedema and obesity: is there a link?* Plast Reconstr Surg, 2014. **134**(1): p. 154e-160e.

235. Harvey, N.L., Srinivasan, R.S., Dillard, M.E., Johnson, N.C., Witte, M.H., Boyd, K., Sleeman, M.W., and Oliver, G., *Lymphatic vascular defects promoted by Prox1 haploinsufficiency cause adult-onset obesity.* Nat Genet, 2005. **37**(10): p. 1072-81.

236. Rasmussen, J.C., Herbst, K.L., Aldrich, M.B., Darne, C.D., Tan, I.C., Zhu, B., Guilliod, R., Fife, C.E., Maus, E.A., and Sevick-Muraca, E.M., *An abnormal lymphatic phenotype is associated with subcutaneous adipose tissue deposits in Dercum's disease.* Obesity (Silver Spring), 2014. **22**(10): p. 2186-92.

237. Carpenter, A.E., Jones, T.R., Lamprecht, M.R., Clarke, C., Kang, I.H., Friman, O., Guertin, D.A., Chang, J.H., Lindquist, R.A., Moffat, J., Golland, P., and Sabatini, D.M., *CellProfiler: image analysis software for identifying and quantifying cell phenotypes.* Genome Biol, 2006. **7**(10): p. R100.

238. Kamentsky, L., Jones, T.R., Fraser, A., Bray, M.A., Logan, D.J., Madden, K.L., Ljosa, V., Rueden, C., Eliceiri, K.W., and Carpenter, A.E., *Improved structure, function and compatibility for CellProfiler: modular high-throughput image analysis software.* Bioinformatics, 2011. **27**(8): p. 1179-80.

239. Kwon, S., Agollah, G.D., Wu, G., and Sevick-Muraca, E.M., *Spatio-temporal changes of lymphatic contractility and drainage patterns following lymphadenectomy in mice.* PLoS One, 2014. **9**(8): p. e106034.

VITA

Germaine Dorah Agollah was born to Alphonce Mrieke Agollah (deceased) and Evelyn Chebet Ruto. She completed her undergraduate studies at Houston Community College and University of Houston, earning a Bachelor's of Science Degree in Biology with Honors. She was a nanotechnology research associate at Nanospectra Biosciences, Inc. for six years prior to admittance to University of Texas Graduate School of Biomedical Sciences at Houston in August 2010. She joined the laboratory of Dr. Eva M. Sevick-Muraca at the Center of Molecular Imaging within The Brown Foundation Institute of Molecular Medicine in March 2011, where she completed her dissertation work.